AD NUMBER
AD503092
CLASSIFICATION CHANGES

TO: **unclassified**

FROM: **confidential**

LIMITATION CHANGES

TO:

Approved for public release, distribution unlimited

FROM:

Distribution authorized to U.S. Gov't. agencies and their contractors; Critical Technology; 11 JUL 1969. Other requests shall be referred to AFRPL [RPOR/STINFO] Edwards, CA 93523.

AUTHORITY

09Nov1972 - AFRPL ltr and document markings.; C TO U AFRPL LTR 9 NOV 72, ST-A AFRPL LTR 5 FEB 86

The following notice applies to any unclassified (including originally classified and now declassified) technical reports released to "qualified U.S. contractors" under the provisions of DoD Directive 5230.25, Withholding of Unclassified Technical Data From Public Disclosure.

<u>NOTICE TO ACCOMPANY THE DISSEMINATION OF EXPORT-CONTROLLED TECHNICAL DATA</u>

1. Export of information contained herein, which includes, in some circumstances, release to foreign nationals within the United States, without first obtaining approval or license from the Department of State for items controlled by the International Traffic in Arms Regulations (ITAR), or the Department of Commerce for items controlled by the Export Administration Regulations (EAR), may constitute a violation of law.

2. Under 22 U.S.C. 2778 the penalty for unlawful export of items or information controlled under the ITAR is up to ten years imprisonment, or a fine of $1,000,000, or both. Under 50 U.S.C., Appendix 2410, the penalty for unlawful export of items or information controlled under the EAR is a fine of up to $1,000,000, or five times the value of the exports, whichever is greater; or for an individual, imprisonment of up to 10 years, or a fine of up to $250,000, or both.

3. In accordance with your certification that establishes you as a "qualified U.S. Contractor", unauthorized dissemination of this information is prohibited and may result in disqualification as a qualified U.S. contractor, and may be considered in determining your eligibility for future contracts with the Department of Defense.

4. The U.S. Government assumes no liability for direct patent infringement, or contributory patent infringement or misuse of technical data.

5. The U.S. Government does not warrant the adequacy, accuracy, currency, or completeness of the technical data.

6. The U.S. Government assumes no liability for loss, damage, or injury resulting from manufacture or use for any purpose of any product, article, system, or material involving reliance upon any or all technical data furnished in response to the request for technical data.

7. If the technical data furnished by the Government will be used for commercial manufacturing or other profit potential, a license for such use may be necessary. Any payments made in support of the request for data do not include or involve any license rights.

8. A copy of this notice shall be provided with any partial or complete reproduction of these data that are provided to qualified U.S. contractors.

<u>DESTRUCTION NOTICE</u>

For classified documents, follow the procedure in DoD 5220.22-M, National Industrial Security Program, Operating Manual, Chapter 5, Section 7, or DoD 5200.1-R, Information Security Program Regulation, Chapter 6, Section 7. For unclassified, limited documents, destroy by any method that will prevent disclosure of contents or reconstruction of the document.

UNCLASSIFIED

AD. *503 092*

UNCLASSIFIED

DISCLAIMER NOTICE

THIS DOCUMENT IS BEST QUALITY
PRACTICABLE. THE COPY FURNISHED
TO DTIC CONTAINED A SIGNIFICANT
NUMBER OF PAGES WHICH DO NOT
REPRODUCE LEGIBLY.

SECURITY

MARKING

The classified or limited status of this report applies
to each page, unless otherwise marked.
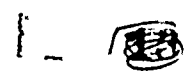Separate page printouts MUST be marked accordingly.

AFRPL-TR-69-122

DEVELOPMENT AND DEMONSTRATION OF A N_2O_4/N_2H_4 INJECTOR (U)

AD 503092

J. O. Hartsell
Aerojet-General Corporation

Technical Report AFRPL-TR-69-122

11 July 1969

DDC

AUG 4 1969

GROUP 4

DOWNGRADED AT 3-YEAR INTERVALS
DECLASSIFIED AFTER 12 YEARS

1211

Air Force Rocket Propulsion Laboratory
Air Force Systems Command
Liquid Systems Division
Edwards Air Force Base, California

CONFIDENTIAL

United States Patent Office Secrecy Order

CONFIDENTIAL
(This page is unclassified)

Final Demonstration Injector (u)

DEVELOPMENT AND DEMONSTRATION OF A N_2O_4/N_2H_4 INJECTOR (U)

J. O. Hartsell

GROUP 4

DOWNGRADED AT 3-YEAR INTERVALS
DECLASSIFIED AFTER 12 YEARS

FOREWORD

(U)   This is the final report of work performed under Contract F04611-68-C-0053, Program Structure 750G, AFSC Project 3058, for the Rocket Propulsion Laboratory at Edwards Air Force Base, California. It covers the period 1 April 1968 through 31 March 1969, and is submitted in accordance with the report requirements of Exhibit B of the contract.

(U)   The work was conducted under the cognizance of Thrust Chamber Engineering, Liquid Rocket Operations, Aerojet-General Corporation, Sacramento, California. The program was directed by Dr. C. B. McGough, program manager; Mr. J. F. Addoms was project manager; and Mr. J. O. Hartsell was the project engineer. Mr. M. V. Rogers was the Air Force project engineer, Rocket Propulsion Laboratory, Edwards Air Force Base, California.

(U)   The author wishes to acknowledge the contributions of Dr. R. J. LaBotz, who provided overall technical guidance in the areas of injector design and experimental data evaluation. The author also acknowledges the services of: Mr. K. Y. Wong, who performed all hardware design tasks; Mr. K. L. Gustafson, who provided technical assistance in the areas of braze technology and injector assembly; Mr. R. C. Keith, Mr. B. W. Cathroe, and Mr. B. F. Perkins, Jr., who, together with personnel of the Research Physics Laboratory, performed all the tests and contributed significantly to the resolution of associated problems; and Mr. K. R. Collins and Mr. R. E. Jones, Jr., who provided valuable technical assistance in the realm of engine application and overall system design.

(U)   This technical report has been reviewed and is approved.

Melvin V. Rogers
Reentry Propulsion Section

ii

UNCLASSIFIED ABSTRACT

(U)   A twelve-month program was conducted to develop and demonstrate an
advanced injector to be used with the propellants N_2O_4/N_2H_4 at a thrust level
of 3000 lbf. Five injectors were tested in 13 unique configurations to
establish the parameters necessary to the optimization of performance, dynamic
stability, chamber cooling capability, and injector/chamber compatibility.
Once established, the optimized parameters were incorporated into a final
injector. This last unit was employed in performance and stability demonstra-
tion tests and in long-duration durability tests. All contract design goals
were met or exceeded by the final optimized injector.

TABLE OF CONTENTS

TABLE LIST

FIGURE LIST

FIGURE LIST (cont.)

FIGURE LIST (cont.)

FIGURE LIST (cont.)

Report AFRPL-TR-69-122

LIST OF ABBREVIATIONS AND SYMBOLS

BLL	=	Boundary layer loss lbf-sec/lbm
DL	=	Divergence loss, lbf-sec/lbm
ERL	=	Energy release loss, lbf-sec/lbm
KL	=	Kinetic Losses, lbf-sec/lbm
I_{sp}	=	Vacuum specific impulse, lbf-sec/lbm
$\dot{m}$	=	Mass flow rate, lbm/sec
MRDL	=	Mixture ratio maldistribution loss, lbf-sec/lbm
O/F	=	Mixture ratio
ΔF_{BLL}	=	Boundary layer thrust decrement, lbf
ϵ	=	Area ratio
η_{DIV}	=	Nozzle curvature-divergence efficiency

Subscripts

del	=	delivered value
i	=	of "ith" stream tube
n	=	number of stream tubes
O/A	=	overall engine property
ODE	=	one dimensional equilibrium
ODK	=	one dimensional kinetic
T	=	total engine property
v	=	vaporized property

SECTION I

INTRODUCTION

A. GENERAL

(U)   Areas of technology which required further development for
possible application to an advanced post boost propulsion system were
recently defined. Among these areas was a requirement for a flight-type
N_2O_4/N_2H_4 rocket engine. This engine was to deliver good performance,
possess inherent and dynamic stability, and be capable of firing for long
cumulative durations with multiple hot restarts. In addition, the engine
had to possess reliability, ease of fabrication with a minimum of quality
control, low-cost per unit, and the ability to withstand vibration and
nuclear effects.

(U)   Little work has been done to develop injector-chamber assemblies
for this propellant combination at the levels of chamber pressure and thrust
which were required. Various agencies had worked on the development of
injectors for this propellant combination. However, many of these injectors
had not been developed in physical configurations suitable for application to
a system, and little work had been done to make these units capable of hot
restarts and compatible with state-of-the-art thrust chamber materials. As
a consequence, an intensive development program was conducted to demonstrate
the adequacy of a current injection technique to the stringent requirements
of the hydrazine engine. A major effort was directed toward establishing a
unit sufficiently qualified to be directly applicable to subsequent develop-
ment of a full-scale injector-chamber assembly.

(U)   This report presents the results of a twelve-month technical
program sponsored by the Air Force Rocket Propulsion Laboratory at Edwards
Air Force Base, California, under Contract F04611-68-C-0053.

I, Introduction (cont.)

B.   OBJECTIVES

(C)   The objective of this program was to demonstrate the applicability
of the HIPERTHIN* injector concept for use with the propellants N_2O_4/N_2H_4.
Specifically, the stability, performance, and injector/chamber compatibility
of the units were to be fully evaluated at a vacuum thrust level of 3000 lbf
and a chamber pressure of 300 psia. Design criteria and performance parameters
so obtained were to be incorporated into the fabrication and demonstration of
an optimized HIPERTHIN injector.

C.   TECHNICAL APPROACH

(C)   The objectives of this program were accomplished through a combined
theoretical-experimental effort directed towards defining and experimentally
evaluating the operational characteristics of the HIPERTHIN injector when
used with N_2O_4/N_2H_4. The program was conducted in two phases. The first
phase consisted of the initial analysis and design of two basic injector types
and of all workhorse chamber and propellant feed system hardware. The second
phase dealt with the experimental evaluation of the injector concepts resulting
from the design effort, and application of the experimental data to the pro-
duction and demonstration of a final optimized injector.

(U)   The work of Phase I was conducted in compliance with two criteria:
(1) to identify, through analysis, potential problem areas inherent to the
hardware concepts and desired range of operating conditions, and (2) to design
experimental hardware amenable to rapid modification should such problem areas
be encountered. In keeping with these criteria, the initial developmental
injectors were of two types, impinging and showerhead, and were multipurpose

---

(U)   *HIgh PERformance THrottlable INjector: A concept developed and owned
      by Aerojet-General Corporation on which Aerojet has patent No.
      3,413,704 and patents pending.

I, C, Technical Approach (cont.)

in that each unit had provisions for three unique injector configurations (see Section IV.B.1). It was thus possible to investigate, early in the program, several combinations of baffle pattern and flat-face area on two types of injection elements.

(U)   The design work of Phase I provided the nucleus of hardware about which Phase II was conducted. The first task of Phase II consisted of a thorough evaluation of injector type, baffle pattern, and boundary cooling parameters in terms of stability and overall performance. As each parameter was optimized, additional developmental injectors were fabricated which successively deleted the undesirable characteristics. The end result of Phase II, Task I was an injector of optimized injection element, baffle pattern, and zone cooling configuration. This final injector was then used to complete the contract. Task II of Phase II consisted of long-duration firings in which the inherent injector/chamber compatibility was demonstrated.

SECTION II

PROGRAM SUMMARY

(C)   A program was conducted to develop and demonstrate a HIPERTHIN injector for use with the propellants N_2O_4/N_2H_4. This injector, which was to operate at a thrust level of 3000-1bf and a chamber pressure of 300 psia, was to exhibit high performance over a mixture ratio range 0.95 to 1.40, dynamic stability and injector/chamber compatibility.

(U)   The program was conducted in two phases, the first of which was hardware design and pre-experimental analysis. The second phase consisted of hardware fabrication, experimentation, and design iteration based on experimental results. The work of these two phases produced two basic injector designs with four iterations: multipurpose impinging and showerhead injectors, single level impinging injectors, and a final optimized injector.

(U)   The first three injector-type iterations employed seven injectors, two of which were not tested due to inadequacies in the then-current fabrication techniques. The remaining five injectors were tested a total of 83 times. These tests were influential in allowing positive selection and identification of injector type, proper fabrication technique, performance capability, dynamic stability characteristics, and boundary cooling feasibility. The parameters so defined were incorporated into a final demonstration injector.

(U)   The final injector was tested 17 times, during which the required performance, stability, and cooling characteristics were demonstrated. The injector met or exceeded every applicable program goal. As a final demonstration, the injector was subjected to two 20 second duration tests to illustrate the high degree of thermal durability and structural integrity. The results of the entire program were then documented in this report.

SECTION III

FINAL INJECTOR OPERATING CHARACTERISTICS

(U)   The frontispiece of this report shows a pre-fire view of the final
injector produced during this program. This unit is the culmination of all
design, fabrication, and experimental data generated during the program.
The injector was fabricated and successfully tested in an eleven day period
following the completion of its conceptual design. It has been tested 17
times for a cumulative duration of approximately 75 seconds.

(U)   A comparison of the attained performance and the contract design goals
is presented in the following table. It is significant that the attained
values were achieved using a copper chamber of 6.5 inch characteristic length
(L*). This assembly had a 5 inch chamber length measured from injector-to-
throat, and a 1.67 contraction ratio. The injector diameter was 3.50 inches;
throat diameter was 2.70 inches.

(C)   HYDRAZINE INJECTOR PERFORMANCE (U)

	Contract Design Goals	Achieved
Thrust (vac.)	3000 lbf $\pm$ 5%	3000 lbf $\pm$ 2%
Chamber Pressure	300 psia $\pm$ 5%	300 psia $\pm$ 2%
Minimum I_{sp} (Vac at Opt. Mixture Ratio) (ε = 30:1)	300 sec	308 sec at MR = 0.9 309 sec at MR = 1.0 306 sec at MR = 1.2 304 sec at MR = 1.3 302 sec at MR = 1.4
Mixture Ratio Range	0.95 to 1.40	0.86 to 1.40
Dynamic Stability	40 millisecond recovery from 525 psi over pressure	20 to 40 millisecond recovery from 607 to 967 psi over pressure (tangential pulse and center bomb)
Cooling Capability	Unspecified	Less than 4500°F boundary recovery temperature

III, Final Injector Operating Characteristics (cont.)

(U)   It can be seen that every design goal was met or substantially exceeded. The boundary temperature achieved is not compatible with conventional phenolic chambers. It is, however, compatible with chambers containing liners made from refractory materials. Test data obtained on a company-sponsored program showed no pressure decay when refractory-lined chambers were tested.

(U)   The post-fire condition of the final injector, after approximately 75 seconds operation including two 20-second tests, is shown on page 188. This figure shows the high degree of durability attained with this unit. The heat marks seen on the face were in evidence after the first four short-duration tests. They remained substantially unchanged from that point. There was no metal removal on the active portion of the injector face.

(U)   There has also been no significant orifice deformation as a result of the transient and induced-pulse operation. This is a significant improvement over the earlier injectors of this type. As discussed in Section VIII, the initial program injectors degraded with accumulated test duration.

(U)   There has been no injector deterioration or variance in hydraulic characteristics during storage of the final unit. The longest continuous storage period accomplished with this injector to date has been two weeks. This period, which followed the final test, was preceded by a water flush and GN_2 purge. There was no attempt made to control the atmosphere during storage. Subsequent hydrotests and leak checks showed circuit resistances to be identical to the original pre-fire values.

(U)   The following sections detail the work conducted during the program which resulted in the final N_2O_4/N_2H_4 injector.

SECTION IV

DESIGN

A.   DESIGN ANALYSES

1.   General

(U)   This program had two phases; the first dealt exclusively with
the analytical evaluation and subsequent design of the test hardware.   The
purpose of the analytical effort was to provide as firm a basis as possible
for the initial design selections.   Potential problem areas were defined in
the areas of performance, stability, and heat transfer.   Consideration of
these potential problems was then incorporated into the initial designs to
provide versatile first-item hardware.   The techniques used in this early
design study are presented in the following subsections.

2.   Performance Analysis

a.   Objectives

(U)   The performance model employed during the design and
test phases of this program fulfilled three objectives.   These were:

(1)   Determination of the effects of significant design
and operation variables on performance.

(2)   Definition of the source and magnitude of various
performance losses.

(3)   Definition of high area ratio altitude performance
trends through extrapolation of low area ratio sea level test data.

IV, A, Design Analysis (cont.)

The first two of these goals apply either wholly or in part to the pre-test design phase. In analyzing the effect of potential design factors on overall performance, the performance model is extremely effective in first, deriving initial designs with a high probability of success, and second, in developing a test plan amenable to rapid parameter optimization. The model was used in this program to select the initial chamber sizes, contraction ratio, nozzle expansion ratio, and basic injector types. In addition, theoretical curves were generated which gave the effect of baffle pattern on overall performance. These curves were used in test planning relative to anticipated baffle modifications.

(U) Attainment of the second goal of the performance model - that of loss definition - was achieved theoretically before testing, and verified with the acquisition of experimental test data. The pre-test results were used in two ways. First, the values of predicted performance were used to detect obviously discrepant tests. The ability to recognize incongruous results immediately after a test prevented repetitive testing under conditions that could mask thrust chamber capabilities. As discussed later in the report, this capability was instrumental in detecting low engine performance due to contaminated propellant.

(U) The second way in which the pre-test analyses were employed was the use of the calculated losses during final data analysis. The prior determination of fixed losses such as divergence loss and boundary layer losses expedited analysis of the final data.

(U) Accurate prediction of the high area ratio altitude performance was the prime objective of the performance model as used during this program. To accomplish the objective, the calculable sea level and altitude performance losses were defined using the ICRPG-recommended procedures

IV, A, Design Analysis (cont.)

(Reference 1). Barrier cooling and energy release losses were analytically evaluated using a stream tube analysis (Reference 2) and a propellant vaporization analysis which is a modification of a technique developed by Priem (Reference 3). The incorporation of these analyses with the ICRPG programs in order to account for interaction effects is discussed in Reference 4. With the acquisition of test data, these analytically-derived losses were revised and new predictions made as required.

b. Model Description

(U)   The methodology of the performance model used in this program has been formulated in a manner similar to the ICRPG Standard Performance Evaluation Technique. Modifications have been made, however, to include performance loss interactions based on liquid propellant vaporization theory. Vaporization-limited combustion properties are used to calculate those losses due to incomplete energy release, finite-rate limited gas expansion, and boundary layer shear drag and heat transfer. This modified program is termed the "Vaporization Interaction Performance Model".

(U)   The technique employed for evaluation and prediction of performance considered the one-dimensional equilibrium (ODE) flow conditions to be the base case. As seen in the following equation, all performance losses are subtracted from this base:

$$I_{sp}(\text{delivered}) = I_{sp}(\text{ODE}) - \Sigma I_{sp}\text{ losses} \qquad (1)$$

(U)   One dimensional equilibrium performance was evaluated using Aerojet computer program #166. This documented program computes one-dimensional flow in chemical equilibrium and is the basis for all $\%I_{sp}$ and $\%C*$ quotations.

Report AFRPL-TR-69-122

IV, A, Design Analysis (cont.)

(U)   The losses which were considered during performance
analysis of the hydrazine engine are briefly described below along with the
basic relationships that incorporate the vaporized propellant parameters into
each performance loss definition. Each loss is defined independently from the
other performance losses in order to more clearly show how the vaporized
propellant parameters influence the loss analysis. The loss derivations are
developed without reference to any particular evaluation program; however, it
will be shown how both the ICRPG Standard and Simplified Reference Computer
Programs can be utilized with the final derived performance loss formulations.
A nomenclature list is included at the front of this report.

(1) The Energy Release Loss (ERL)

(U)   This loss accounts for the performance reduction
as a result of incomplete vaporization, mixing, and chemical reaction. This
loss is evaluated by determining the mass defect caused by unvaporized
propellant and the effect of the vaporized mixture ratio on the thermochemical
performance output. Using one dimensional equilibrium (ODE) conditions as the
baseline or maximum achievable performance, the energy release loss at any
nozzle expansion ratio can be found by subtracting the product of the total
percent mass of propellant vaporized and the ODE specific impulse at the
vaporized mixture ratio from the ODE specific impulse at the liquid propellant
mixture ratio. That is, in ODE notation;

$$ERL = I_{sp\ ODE\ (O/F)} - I_{sp\ ODE\ (O/F)_v} \frac{\dot{m}_v}{\dot{m}_T} \quad (2)$$

IV, A, Design Analysis (cont.)

(U)   For an engine with several "stream tubes" of
different mixture ratios or atomization/vaporization characteristics, this
process is used for each stream tube and the results are mass flow rate weight
summed to give the total loss. Therefore Equation (2) can be generalized to
the following notation:

$$ERL = \sum_{i}^{n} \left[I_{sp} \text{ ODE } (O/F) \ m_i - I_{sp} \text{ ODE } (O/F)_{vi} \ \dot{m}_{vi} \right] \ \frac{1}{\dot{m}_T} \tag{3}$$

(2)   The Mixture Ratio Maldistribution Loss (MRDL)

(U)   This loss accounts for the performance degradation
due to non-homogeneous combustion products on a macroscopic scale. The loss
may be intentionally induced, as with barrier or fuel film cooling or may be
unintentional as a result of non-uniform injector hydraulics. The mixture
ratio maldistribution loss is calculated using a stream tube technique. The
mass flow rate weighted sum of the ODE specific impulse for the individual
stream tubes at the stream tube mixture ratios are subtracted from the ODE
specific impulse at the overall mixture ratio to define this loss. This
performance loss definition is similar to the notation used in the present
ICRPG Performance Evaluation Procedures for MRDL calculations which are beyond
the two-stream tube capability of the reference computer program. Again using
ODE as the reference condition, the MRDL is defined by the following relationship:

$$MRDL = I_{sp} \text{ ODE } (O/F)_{O/A} - \sum_{i}^{n} (I_{sp} \text{ ODE } (O/F)_i \ . \ \frac{\dot{m}_i}{\dot{m}_T}) \tag{4}$$

where the "ith" stream tube refers to discrete zones of flow whose mixture
ratios are calculable by known injector hydraulic parameters.

IV, A, Design Analysis (cont.)

(3) The Kinetic Losses (KL)

(U)   This loss accounts for performance reduction from
the equilibrium condition due to finite chemical reaction and relaxation rates
of the species present in the exhaust gas during the nozzle expansion process.
The kinetic loss is defined by considering the mass flow rate-summed ODE per-
formance at the stream tube mixture ratios as the reference point. The one
dimensional kinetic (ODK) performance evaluated at the vaporized mixture ratio
for each of the individual stream tubes, and then summed over the "n" stream
tubes, is subtracted from the ODE performance to obtain the kinetic loss.
Again it is emphasized that both the kinetic and ODE performance must be evalu-
ated at the vaporized mixture ratio and mass flow rate rather than at the
liquid propellant mixture ratio, since the vaporized parameters represent the
actual composition of the exhaust gases. The unvaporized portion of the
propellants is actually in a non-gaseous state and cannot be considered in the
exhaust gas expansion process, other than the two phase flow velocity and
thermal lag effects which are beyond the scope of this report. Equation (5)
is a mathematic representation of this definition of kinetic loss.

$$ KL = \sum_{i}^{n} \left[I_{sp\ ODE\ (OF)_{vi}} - I_{sp\ ODK\ (O/F)_{vi}} \right] \frac{\dot{m}_{vi}}{\dot{m}_{T}} \qquad (5) $$

(4) The Boundary Layer Loss (BLL)

(U)   This loss accounts for the degradation of perfor-
mance due to shear drag and heat loss at the boundary of the thrust chamber.
The boundary layer loss is evaluated using the vaporized performance combustion
properties in the outer stream tube. Again, the vaporized composition is con-
sidered rather than the composition based on overall propellant flow rates.

IV, A, Design Analysis (cont.)

Using a suitable evaluation procedure, a ΔF_{BLL} is calculated and divided by the total propellant flow rate to determine the boundary layer loss.

$$BLL = \frac{(\Delta F_{BLL})(O/F)_v}{\dot{m}_T} \tag{6}$$

(5) The Nozzle Divergence Loss (DL)

(U)   This loss accounts for the decrease in thrust due to nonaxially directed momentum at the nozzle exit and the non-planar sonic surface. In most cases, this loss is not significantly affected by the variance of the vaporized mixture ratio from the overall liquid flow mixture ratio. Therefore, no vaporized mixture ratio notation is included in the definition of the divergence loss. This performance loss, when evaluated by itself, can usually be expressed in terms of a divergence efficiency, η_{DIV}, which modifies the delivered or actual thrust.

$$DL = \frac{I_{sp_{del}}}{\eta_{DIV}} - I_{sp_{del}} = I_{sp_{del}} \left[\frac{1 - \eta_{DIV}}{\eta_{DIV}} \right] \tag{7}$$

(U)   The analytically predicted specific impulse of a vaporization limited rocket engine can be evaluated by subtracting the above defined performance losses from the ODE theoretical condition.

$$I_{sp_{del}} = I_{sp_{ODE}} - \Sigma \ I_{sp \ losses}$$

$$= I_{sp_{ODE}} - \Sigma \ (ERL + MRDL + KL + BLL + DL) \tag{8}$$

IV, A, Design Analysis (cont.)

Substituting Equations (2) through (7) for the five performance loss terms of Equation (8) and cancelling like terms, the following final formulation is obtained.

$$I_{sp_{del}} = \sum_{i}^{n} \left[I_{sp_{ODK(O/F)_{vi}}} \cdot \frac{\dot{m}_{vi}}{\dot{m}_T} \right] n_{DIV} - \frac{\Delta F_{BLL}}{\dot{m}_T} \quad (9)$$

(U)   A more detailed description of the performance model and its component losses, along with a discussion of the application of the model to other engine programs, is given in Reference 2.

        c.   Application of Performance Program to Engine Design

(U)   The performance model described in the preceding section was employed during the design phase to ensure that the contractually required performance would be met. Injector, chamber, and nozzle parameters were recommended as a result of studies to determine a near optimum system in regard to performance. Injector design parameters which were considered during the design analysis included: channel size, injection velocity, number of elements, element spacing and element type. Chamber variables which were defined based on the performance analyses were: length, shape, contraction ratio, throat diameter and characteristic length. A low contraction ratio (CR = 1.67) conical chamber was selected as the best configuration with reference to performance potential. Chamber throat size was determined from thrust and I_{sp} requirements and the calculated combustion efficiency for the engine. The recommended chamber lengths of 5 and 10 inches were based on analyses which indicated that the longer length would permit required performance to be exceeded while the shorter length would allow definition of the "knee" of the combustion efficiency versus length curve. Nozzle design

IV, A, Design Analysis (cont.)

selections for sea level and altitude configurations were based on ease of
data analyses and optimum performance, respectively. The sea level test
nozzle had a 2:1 expansion ratio with a nozzle half angle of 15°. This
configuration was designed to provide under-expanded flow conditions at the
exit in order to yield thrust levels consistent with the load cell capability
of the test area. Also, the nozzle design for the sea level tests was selected
to facilitate the calculation of nozzle performance losses in order that thrust
based combustion efficiency could be easily determined. The altitude nozzle
selected for use with the N_2O_4/N_2H_4 injector and chamber was a 30:1 expansion
ratio minimum-length Rao contour. The expansion ratio of 30:1 was a contract
requirement; the minimum length Rao contour was used in order to provide
maximum performance within a given nozzle length.

(U)   During the course of the performance design studies,
predictions of altitude performance were made as functions of various design
and operating variables. The predicted effect of injector baffle area on
both the showerhead and the impinging stream injectors is shown in Figure 1
for chamber lengths of 5 and 10 inches. Test conditions are noted on the
figure. The steeper slope of the curves for the impinging stream injector
was a result of a predicted difference in efficiency between the showerhead
baffle elements and the impinging face elements. As the baffle area is
increased, the number of lower-efficiency baffle elements increases and
performance was predicted to decrease. With the showerhead injector, the
element efficiency was predicted to be essentially the same for the baffle
elements compared to the face elements, and the effect of percent baffle area
on performance was predicted to be negligible. Predicted values of altitude
specific impulse together with a performance loss analysis conducted during
the design phase is presented in Table I for various individual test conditions.

(C)   The data from the original design analysis presented in
Figure 1 and Table I were generated based on a predicted performance degradation
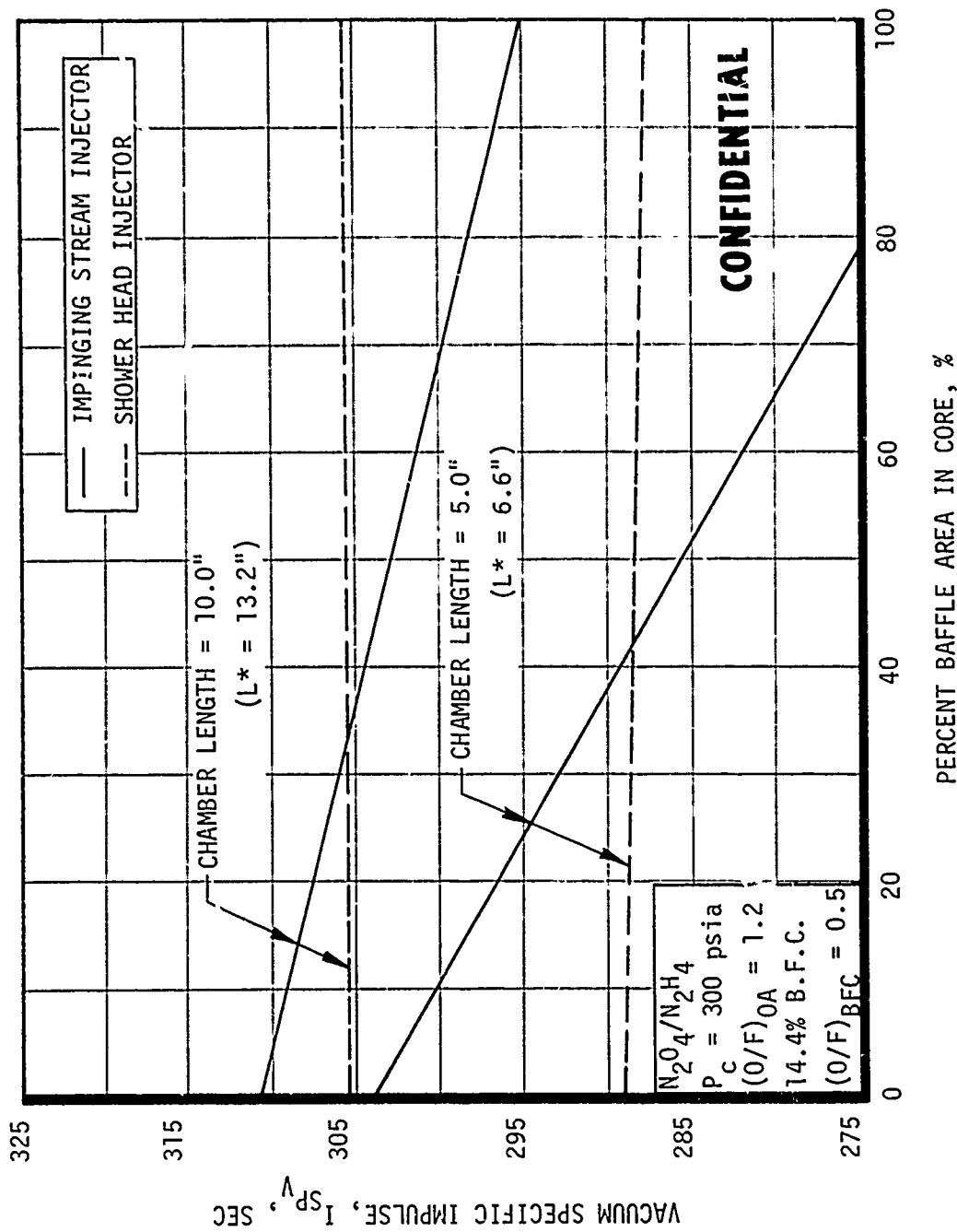
Figure 1. Effect of Baffle Area on Performance (u)

TABLE I

CALCULATED PERFORMANCE LOSSES - PRETEST VALUES (u)

Test Objective	Injector Type	Chamber Type	Chamber Length, in.	Engine O/F	Core O/F	Barrier O/F	Coolant Flow, %	Theo I, @ 30:1, sec	Boundary Layer, sec	Curvature-Divergence, sec	Losses Kinetics, sec	Mixture Ratio Distribution, sec	Energy Release, sec	Sum of Losses, sec	Predicted I, @30:1, sec	Energy Release Efficiency, %
Stability	Impinging	Steel	10	0.9	0.9	--	--	327.5	4.5	6.5	3.3	0	9.0	23.3	304.2	97.5
	Impinging	Steel	10	1.2	1.2	--	--	336.5	4.6	6.5	10.3	0	8.1	29.2	307.3	97.4
	Impinging	Steel	10	1.4	1.4	--	--	338.4	4.6	6.5	13.2	0	10.4	34.7	303.7	96.4
	Showerhead	Steel	10	0.9	0.9	--	--	327.5	4.5	6.5	3.2	0	7.4	21.6	305.9	97.7
	Showerhead	Steel	10	1.2	1.2	--	--	336.5	4.6	6.5	9.8	0	6.5	27.4	309.1	98.1
Stability	Showerhead	Steel	10	1.4	1.4	--	--	338.4	4.6	6.5	13.3	0	8.4	32.8	305.6	97.5
Cooling,L*	Showerhead	Copper	10	1.4	2.02	0.2	17.0	338.4	4.1	5.9	6.9	37.0	9.0	65.9	275.5	97.3
	Impinging	Copper	10	1.4	2.02	0.2	17.0	338.4	4.1	5.8	7.0	37.7	9.2	63.8	274.6	97.3
	Showerhead	Copper	10	1.4	1.97	0.3	18.4	338.4	4.1	5.9	7.0	32.9	9.1	59.0	279.4	97.3
	Impinging	Copper	10	1.4	1.97	0.3	18.4	338.4	4.1	5.9	7.0	33.1	9.8	59.9	278.0	97.2
	Showerhead	Copper	10	1.4	1.86	0.5	21.2	338.4	4.3	6.1	7.1	25.3	9.3	52.1	286.3	97.3
	Impinging	Copper	10	1.4	1.86	0.5	21.2	338.4	4.3	6.1	7.1	25.1	9.1	51.7	286.7	97.3
	Showerhead	Copper	10	1.4	1.82	0.4	17.4	338.4	4.3	6.1	7.6	24.8	9.9	52.7	285.7	97.1
	Showerhead	Copper	10	1.4	1.78	0.3	14.0	338.4	4.3	6.1	8.1	24.0	9.7	52.2	286.2	97.1
	Showerhead	Copper	10	1.4	1.76	0.2	11.6	338.4	4.4	6.1	8.5	23.9	9.9	52.8	285.6	97.1
	Showerhead	Copper	10	1.4	1.73	0.3	12.4	338.4	4.3	5.8	8.6	21.3	10.0	50.3	288.1	97.0
	Showerhead	Copper	5	1.4	1.73	0.3	12.4	338.4	4.1	6.2	7.5	21.2	27.5	66.1	272.3	91.9
	Showerhead	Copper	10	1.4	1.70	0.4	13.4	338.4	4.3	6.2	8.8	18.6	10.5	48.1	290.3	97.0
	Showerhead	Copper	5	1.4	1.70	0.4	13.4	338.4	4.1	5.8	7.5	28.7	17.0	63.8	274.6	91.8
	Showerhead	Copper	10	1.4	1.67	0.5	14.4	338.4	4.4	6.2	8.9	16.1	10.2	45.8	292.6	92.0
	Impinging	Copper	10	1.4	1.67	0.5	14.4	338.4	4.4	6.2	9.0	16.0	11.6	47.0	291.4	96.6
	Showerhead	Copper	5	1.4	1.67	0.5	14.4	338.4	4.1	5.9	7.6	16.2	27.3	61.1	277.3	91.5
Cooling,L*	Showerhead	Copper	5	1.4	1.63	0.5	12.5	338.4	4.2	5.9	8.0	13.5	27.8	59.4	279.0	91.8
	Showerhead	Copper	5	1.4	1.57	0.5	10.0	338.4	4.2	6.0	8.5	9.8	29.5	55.9	281.5	91.3

IV, A, Design Analysis (cont.)

due to baffle element efficiencies. Subsequent analysis of the test data indicates that the predicted inefficiency due to the baffle elements of the impinging stream injector was over estimated. As will be shown in the data results section, the energy release efficiency for the impinging stream injector is 99 - 100% at both the 5- and 10-inch chamber lengths.

3. Compatibility Analysis

(U)   Of primary importance in this program was an evaluation of the injector/chamber compatibility. In order for boundary cooling to be effective, it is necessary that strong outward radial gas dynamic forces at the injector face be eliminated. The initial designs were thus evaluated to determine the relative compatibility with various chambers. A discussion of the techniques used for injector/chamber compatibility evaluations is presented in the following paragraphs.

(U)   A compatible injector/chamber design requires flow at the chamber boundary to exhibit: (1) minimum thermal gradients, (2) compatible chemical properties, and (3) a minimal gas dynamic force component normal to the wall. The compatibility model used in this program graphically characterizes the element spray pattern, including its gross thermal and chemical composition, and the dynamic lateral movement of the resultant combustion gases. This is accomplished by application of three interrelated models: the Spray Overlap and Propellant Vaporization Models, and the Dynamic Force Model.

a.   Spray Overlap Model

(U)   The chemical and thermal environment of the flow at the wall of a combustion chamber is a function of the overall mixture ratio distribution and the spray-fan mixture ratio distribution from individual injector

IV, A, Design Analysis (cont.)

elements. The Spray Overlap Model allows evaluation of the intra-element gross mixture ratio distribution within each element stream tube. The gross mixture ratio gradient definitions within individual element spray boundaries have been correlated with empirical data.

(U)   The model assumes propellant vaporization is the rate controlling mechanism for combustion. Using this concept, the analysis was performed in the following sequence. First, the percent of vaporized propellant versus axial chamber length was calculated for each element as a function of its mass flow rate, operating mixture ratio, and atomization efficiency by using a procedure similar to that described in Reference 4. The combustion reactions produced by the vaporized propellants determined the energy release potential of that element. Next, the spray area of each element was assigned a value based on the energy release potential of that element. Since there is a delay time until sufficient quantities of the propellants vaporize, droplets from one element's spray pattern have time to intermix with droplets from adjacent element spray patterns. The complete spray pattern characterization was determined by placing the individual spray patterns on the injector face, or at some axial chamber plane, and evaluating the resultant overlapping zones of oxidizer-rich and fuel-rich spray.

(C)   Because the HIPERTHIN injector provides propellant flow through the baffle and injector walls as well as the injector face, the spray fan characterization was performed at two stations. The first station was near the injector face where the only elements are like-impinging doublets. The like-impinging doublet elements produce elliptical spray fans near the injector face with the major axis of the ellipse perpendicular to the plane passing through both orifices of the element. Interelement mixing is accomplished due to the closeness of elements. Therefore, each matrix section of the injector face was considered a stream tube of uniform mixture ratio. The energy release potential was then calculated as a function of axial length for the stream tube flow emanating from each matrix section.

A, A, Design Analysis (cont.)

(U)   The second axial station selected for a spray fan charac-
terization contains the stream tubes produced at the injector face plus stream
tubes formed by the intermixing of spray along the baffle and injector walls.
The baffle and injector wall stream tubes emanated from showerhead elements
that exist on the walls.

(U)   Because the propellant liquid was injected at different
axial planes, the vaporized mixture ratio at the injector/chamber interface
location was an integrated function of gases generated from the injector face
to that station. By extending the vaporization analysis, the vaporized mix-
ture ratio was determined at any axial station.

(U)   The results of applying this model are shown in Figure 2,
which displays the calculated vaporized mixture ratio of the stream tubes at
the chamber throat. The stream tube analysis illustrated in Figure 2 assumed
no diffusion or intermixing of gases between stream tubes and therefore repre-
sented the largest possible mixture ratio gradients. Based upon the results,
and an assumed heat transfer coefficient at the throat, it was predicted that
an unacceptable amount of throat erosion would occur in a phenolic chamber.
Actual thermal streaking was predicted at those points which exhibited boundary
mixture ratios in excess of 0.4.

                    b.   Gas Dynamic Force Model

(U)   This model examines radial gas movement at any axial
station through a relaxation technique (Reference 5). Application of the model
to this injector was accomplished using the stream tubes described above.
Characterization at two axial stations was made to determine the movement of
the combustion gases from one station to the next. The first station was just
above the baffle tips while the second station was just below the baffles.
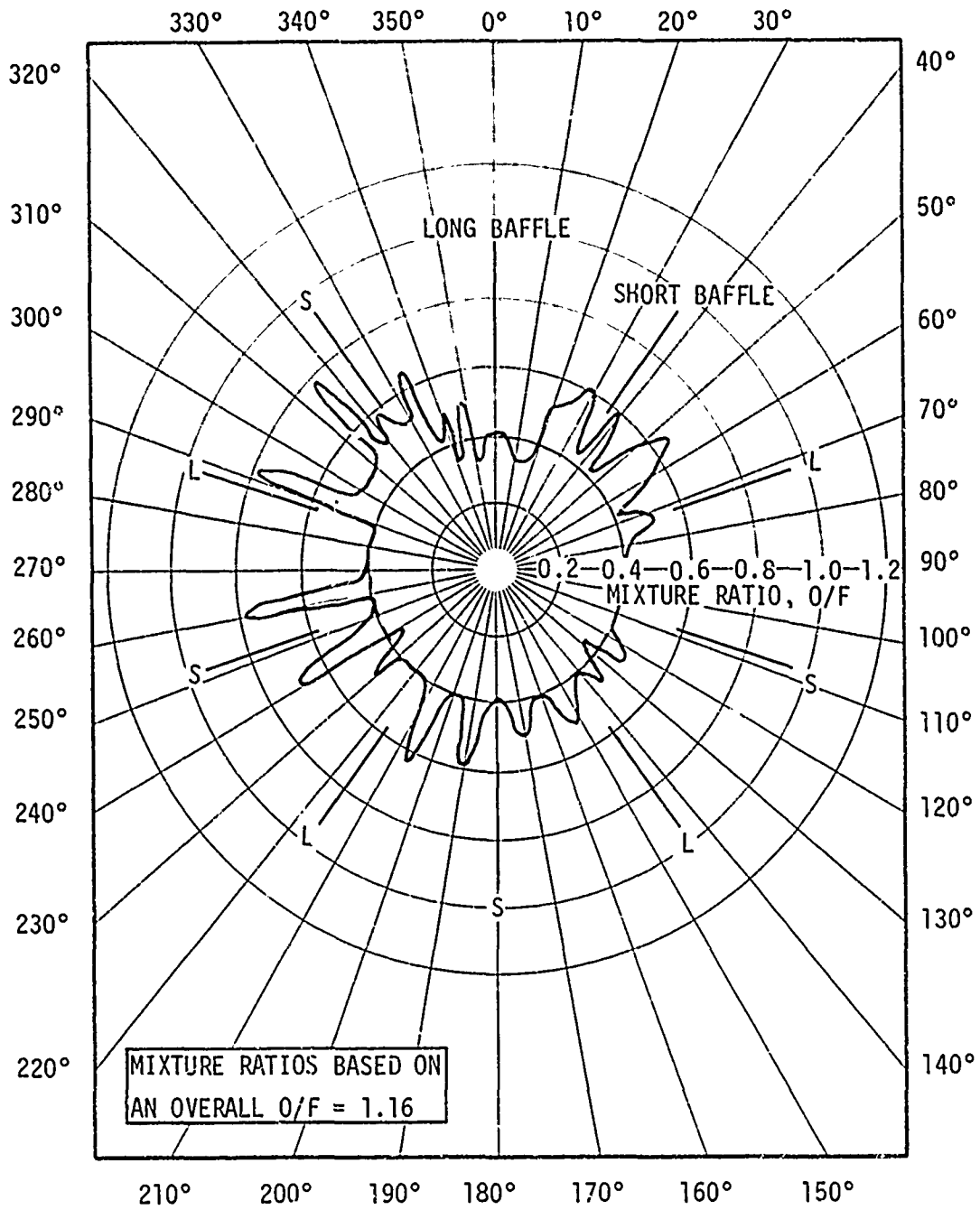
Figure 2. Stream Tube Mixture Ratios - Chamber Throat Station

IV, A, Design Analysis (cont.)

From experience with baffled injectors, lack of mass flow over the baffles usually allows large gas dynamic wind movement over the baffle tips. This increases the local heat transfer rates to the baffles and the chamber wall which in turn can be the cause of erosion.

(U)   Figure 3 illustrates the characterization at the above-mentioned stations. As shown in the figure, the stream tube was subdivided so that gas movement is more clearly shown. As would be expected from the difference in liquid injection planes, the baffle and injector wall flow have not had sufficient time to vaporize and combust in order to completely protect the chamber wall at the interface from the almost fully reacted propellant coming from the injector face. While this protection is superior to an equivalent conventional injector, it was expected that erosion with "soft" ablatives such as the silica-phenolics, would occur in-line with the major baffles due to increased heat transfer effects.

4. Thermal Analysis

(U)   The thermal analyses conducted prior to actual experimentation had two objectives. The first was a definition of the instrumentation to be applied to the chambers planned for use. The second task was the generation of a boundary cooling grid that could be used in hardware design and in experimental test planning.

      a.   Heat Sink Chamber Design and Thermal Instrumentation
          Techniques

      (1) Chamber Design Considerations

(U)   The objective of thermal instrumentation was to characterize injectors under various barrier flow conditions by providing a map of recovery temperatures and heat transfer coefficients within the chamber.
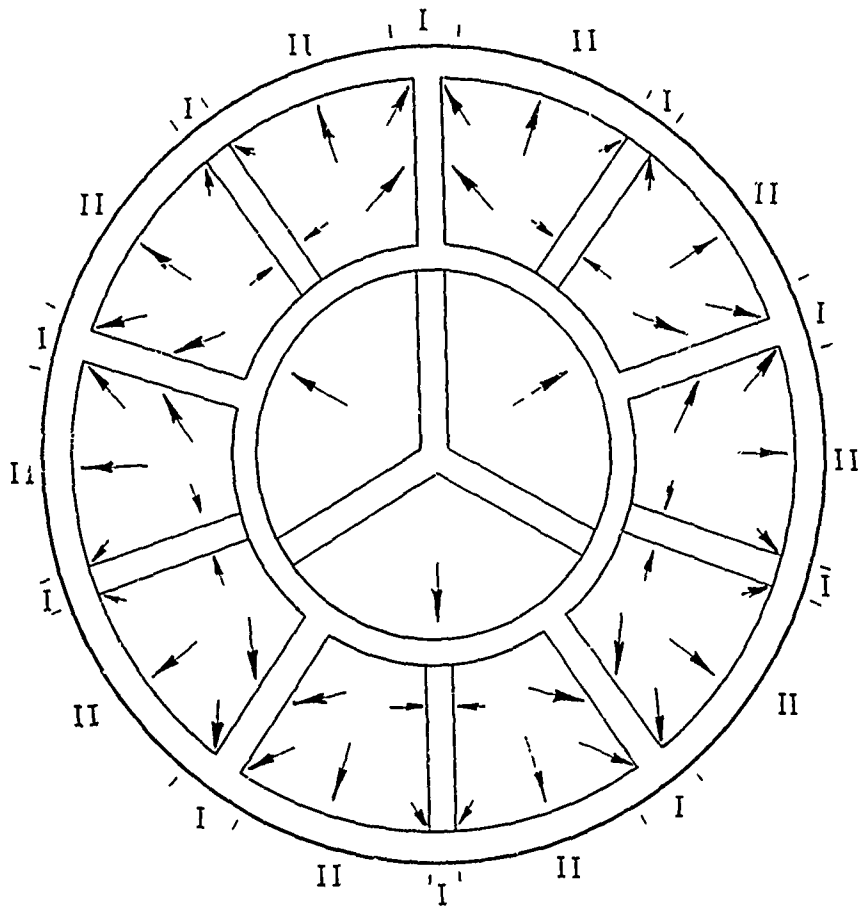
NOMENCLATURE

I.   REGION OF HIGH GAS DYNAMIC FORCE

II. REGION OF LOW GAS DYNAMIC FORCE

VECTOR REPRESENTS DIRECTION AND RELATIVE MAGNITUDE
OF GAS FLOW DURING FIRING

Figure 3.   Radial Gas Flow Characterization

Page 23

IV, A, Design Analysis (cont.)

The task of determining these parameters in a barrier cooled chamber is considerably more difficult because the local recovery temperature cannot be calculated from the c* performance parameter. There are two theoretical approaches to experimentally obtaining the local barrier recovery temperature, which is the parameter of greatest interest in design of a refractory-wall chamber. One is to calculate recovery temperature from heat flux measurements using the rate of change of flux with surface temperature extrapolated to zero flux. The other is to try to measure the barrier temperature directly, which in the chamber region approximates the recovery temperature.

(U)   The optimum method of obtaining the required data was to use thin wall (0.1 to 0.2 inch) metal chambers that could operate at temperatures approaching the gas barrier temperature. This approach, however, represented both a high-cost and high-risk means of checking out new injector designs. The optimum heat transfer chamber for these propellants would have required the use of columbium or molybdenum, both of which would have needed protective coatings to prevent chemical attack. It was thus decided to employ a thermally less optimum but physically more reliable instrumented chamber design. Accordingly, thick-walled, solid copper workhorse chambers were designed and instrumented to allow measurement of gas-side heat flux.

(2) Instrumentation Techniques

(U)   The selection of a heavy-wall copper chamber guaranteed data acquisition periods lasting up to 5 sec with minimum risk even under the most adverse conditions. However, since the wall temperatures on the copper were limited to about 1600°F, which is only 45 to 50% of the gas temperature, the data acquisition was compromised. In order to minimize the risk in thermal data acquisition, a second approach was also employed. This involved the direct measurement of the barrier gas temperature. Whereas the

IV, A, Design Analysis (cont.)

intent in the copper chamber design was to keep the wall cool as long as possible to enable heat flux to the wall to be inferred over a reasonably long fire period, the second objective was to elevate the surface temperature of the nozzle wall to the barrier temperature as rapidly as possible. Measurement of the final value would then approximate a direct measurement of the barrier temperature. This latter approach was accomplished through the use of insulated tantalum-tungsten type thermocouples of extremely rapid response.

(U)   The first goal was accomplished primarily through practical considerations of wall temperature versus baffle pattern. Thermocouple locations were specified in each chamber that would allow measurement of the heat flux as a function of pattern characteristic (i.e., pockets, minor blades, major blades). The thermocouples were arranged in five circumferential stations and five axial stations. All copper chamber instrumentation was specified to be of the calorimeter type. The 6.5-in. L* steel chamber employed insulated thermocouples capable of reading boundary temperature directly.

b. Boundary Cooling Analysis

(U)   The major task in this program phase was the definition of boundary flow parameters amenable to a thorough evaluation of the cooling effectiveness of localized off-mixture ratio conditions. Specifically, it was desired to establish the required percent off-MR flow and percent off-MR injection area for boundary mixture ratios ranging from 0.2 to 0.5. The following paragraphs describe the basic technique and present the results. A more detailed description of the analysis is presented in the appendix.

(U)   The analysis was performed assuming an overall injector mixture ratio of 1.4. In compliance with the injector design concept, a further assumption was made that only the oxidizer flow would be varied to

IV, A, Design Analysis (cont.)

provide an off-MR boundary condition. Under these assumptions, chemical composition data indicated densities of the barrier and of the core were reasonably close for the range of barrier mixture ratios being considered. It was thus appropriate to use existing barrier cooling data from air-to-air systems with small temperature differentials between flows. Data by Seban (Reference 6) were utilized in the analysis because of the wide range of velocity ratios investigated and the relatively short core flow development length provided during the experiments.

(U)   The physical system considered in this analysis is shown in Figure 4. In general, three axial regions can be identified in describing the boundary flow analysis: an initial core mixing region which is unaffected by the wall and boundary layer development along the wall; a transitional region in which the core mixing layer and the wall boundary layer interact and merge; and an asymptotic downstream region which follows the complete merger of these layers into a boundary layer type flow. The cooling effectiveness $(\eta = T_{core} - T_{adiabatic\ wall} / T_{core} - T_{initial\ barrier})$ is unity throughout the first region and decreases with increasing axial distance (X) in the other two. Of interest in this analysis was control of the transition region, since excessive barrier flows are required to maintain the initial region to the throat, and practical throat wall temperature (4000°F) precludes the ..ow effectiveness values of the asymptotic region.

(U)   Figure 5 shows the barrier flow design curves generated under the assumptions of constant fuel flow, acceleration-induced mixing com- mensurate with a conical chamber, and transition region effectiveness values as reported by Seban. The abscissa of the plot represents the percent of total propellant flow injected at off-MR boundary conditions. The ordinate represents the percent total face area over which the boundary is injected. The values for X (10, 14, and 20 in.) shown on the plot represent theoretical
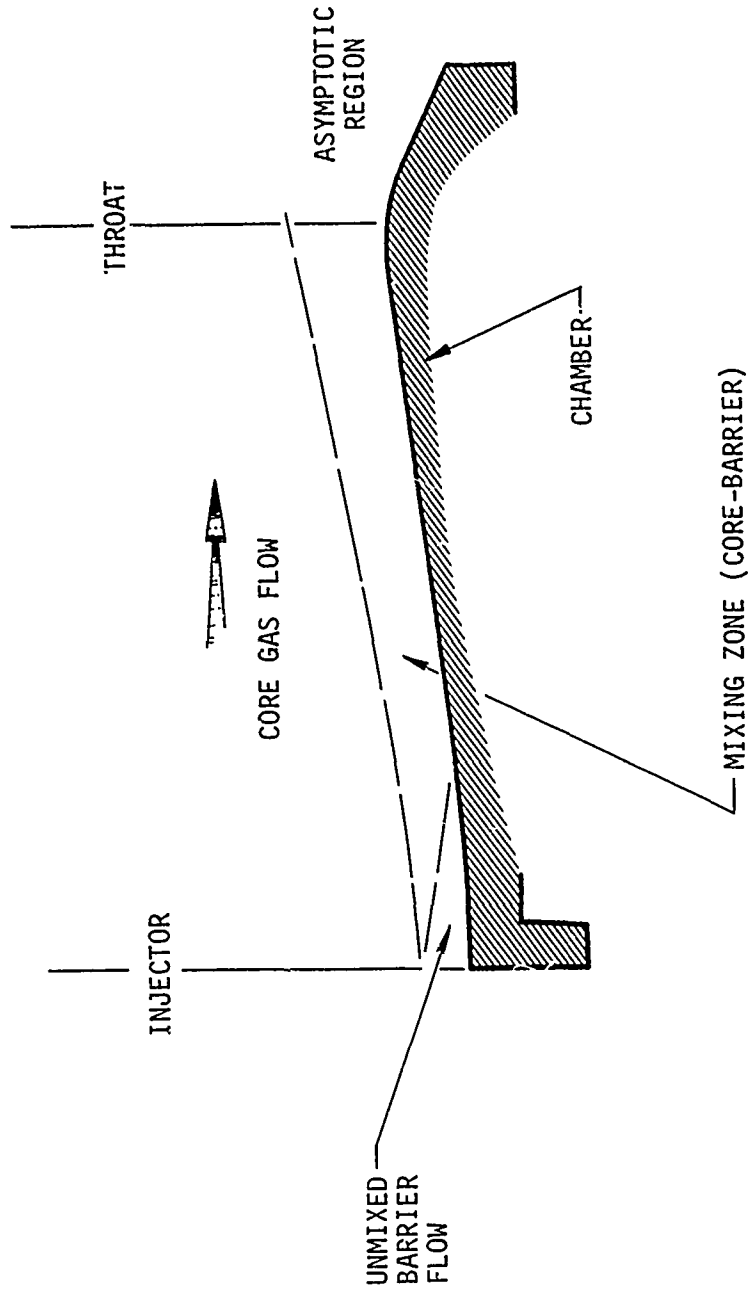
Figure 4. Definition of Thermal Zones - Boundary Flow Analysis
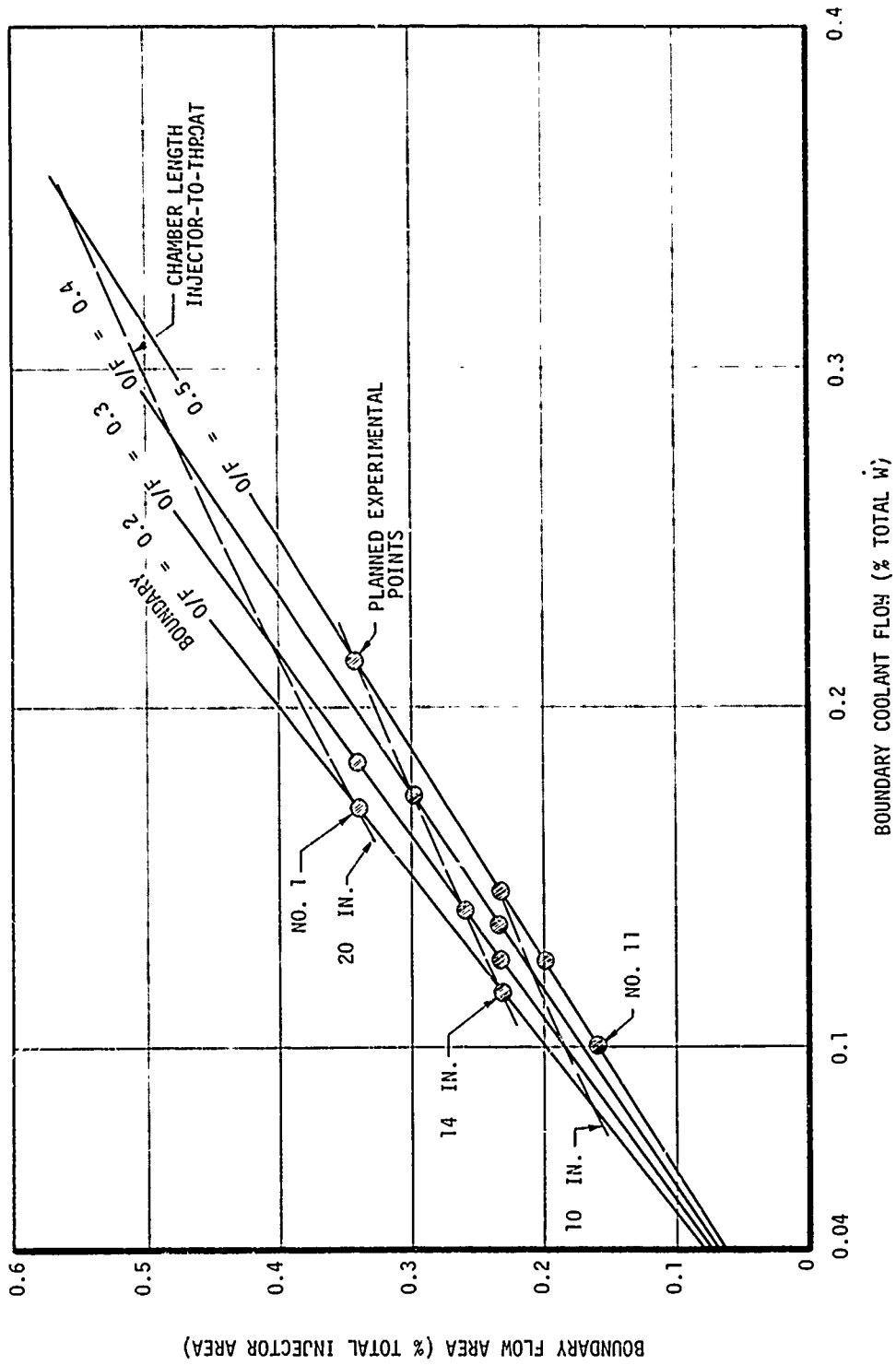
Figure 5. Barrier Flow Design Curves

IV, A, Design Analysis (cont.)

chamber lengths corresponding to cooling safety factors of approximately
0, 25, and 100% for an actual 10-in. chamber. The lines associated with each
theoretical length shown are lines of constant throat wall temperature.

The curves of Figure 5 were employed to derive a test
plan amenable to a complete evaluation of boundary cooling effectivenss in
both 10-in.- and 5-in.-long chambers. The circled points of Figure 5 illustrate
the points that were to be experimentally investigated. The required values
of boundary mixture ratio, percent off-MR flow, and boundary injection area
were then incorporated into the design of the injectors to be tested.

5. Stability Analysis

It is well known that the processes occurring within a liquid
rocket combustion chamber are never entirely smooth. Even when the mean
operating conditions are constant, fluctuations around these mean values occur
in all of the quantities that characterize the flow. The nature of the fluctu-
ations can vary widely from one combustor to another, and in a single combustor
for different operating conditions. If the fluctuations are random and of
small amplitude, this unsteadiness is referred to as "combustion noise". With
random fluctuations of large amplitude, the operation of the engine is said
to be "rough", and the functioning of the system of which the engine is a
part may be impaired.

Much more serious than rough operation is the problem of
combustion instability, also termed unstable combustion, oscillatory combustion,
or resonant combustion. Whereas rough combustion refers to random fluctuations,
combustion instability consists of organized oscillations that are maintained
and amplified by the combustion process itself. The various types of combus-
tion instability can be classified roughly into three categories: low fre-
quency, intermediate frequency, and high frequency. However, the classifica-

IV, A, Design Analysis (cont.)

tion is not based simply on frequency alone. Just as electrical and mechanical systems respond to specific frequencies depending on the type of coupling, so also liquid rocket systems exhibit representative frequency and amplitude patterns.

a. Low-Frequency

Low-frequency combustion instability, or chugging, and intermediate instability are due to an interaction between the combustion process and the dynamics of all, or a part of, the propellant feed system that is sufficient to sustain oscillation in a closed loop manner. Schematically, this interaction is described by the block diagram of Figure 6. For a sustained oscillation, a perturbation in the system must experience sufficient gain and proper phase shift to reinforce itself after traveling around the closed loop. Under resonant conditions, the gain is equal to the ratio of the mixture ratio weighting factor (a function of mixture ratio and characteristic velocity) to the flow resistance existing between the resonant dynamics and the combustion chamber.

(U) There are two dominant modes of coupling with the combustion process. The first is an interaction between the combustion and the propellant feed lines. The second is a coupling between the chamber and the dynamics of the injector itself. Both processes impact heavily upon the system design. In the former case, coupling may be avoided by providing sufficient pressure drop through the injector circuit. In the case of injector/chamber coupling, resonant gain can be lowered by increasing injector pressure drop and decreasing manifold volume.

Report AFRPL-TR-69-122

FUEL FEEDBACK LOOP —
TRANSFER FUNCTION

COMBUSTION PROCESS
TRANSFER FUNCTION
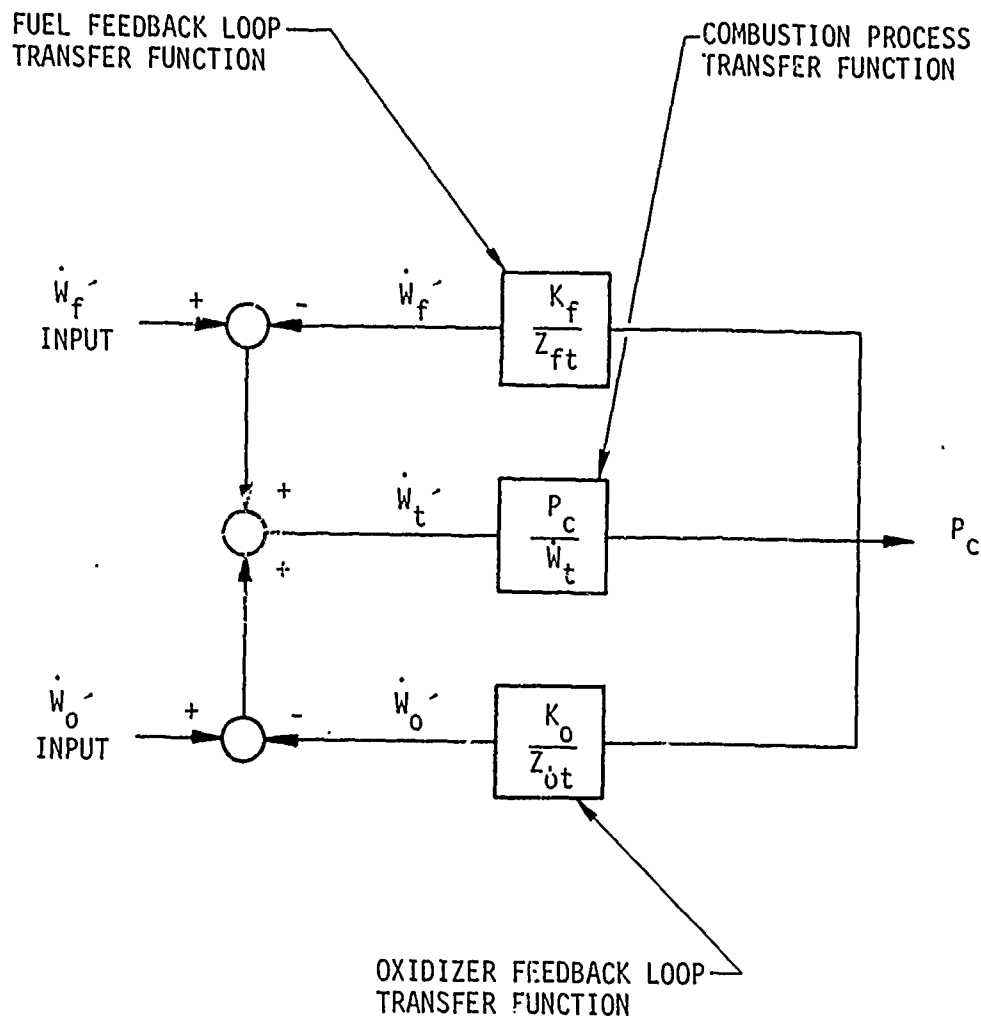
Figure 6. Schematic of Closed Loop Combustion/Feed System
Interaction

IV, A, Design Analysis (cont.)

(U)   During the initial design phase of the hydrazine injec-
tors, an analysis was conducted to define the dynamic low-frequency stability
characteristics of the worst-case injector/chamber/feed system combination.
The system considered included a three-level injector (greatest manifold vol-
ume), the largest chamber configuration (lowest resonant frequencies), and
no propellant line pressure drops. The results of this design-phase investiga-
tion are shown in Figure 7.

(U)   The objectives of the analysis were threefold. First,
it was desired to establish the frequency boundaries within which instability
could potentially occur. Secondly, it was desired to establish the lowest
natural frequencies of the injectors themselves. Finally, it was necessary to
determine the gain curve associated with each injector coupled to the combus-
tion process.

(U)   The zones of stable and potentially unstable operation
for each injector are shown in Figure 7. The crosshatched areas represent
zones of stable operation. The boundaries of these zones were established
through consideration of the equation:

$$\frac{Z_c}{Z_{FS}} = \left[\frac{c^*}{A_t g} \left(\frac{e^{-j\omega\tau_1}}{1 + j\omega\tau_2} \right) \right] \left[\frac{K_{Oxid}}{Z_{Oxid}} + \frac{K_{Fuel}}{Z_{Fuel}} \right]$$

where:

Z_c = Impedance of combustion process

Z_{FS} = Impedance of total propellant feed system

τ_1 = Time from propellant injection to combustion

τ_2 = Time from combustion plane to throat

ω = Frequence of oscillation

K = Constant (includes $\frac{\partial c^*}{\partial MR}$, etc.)
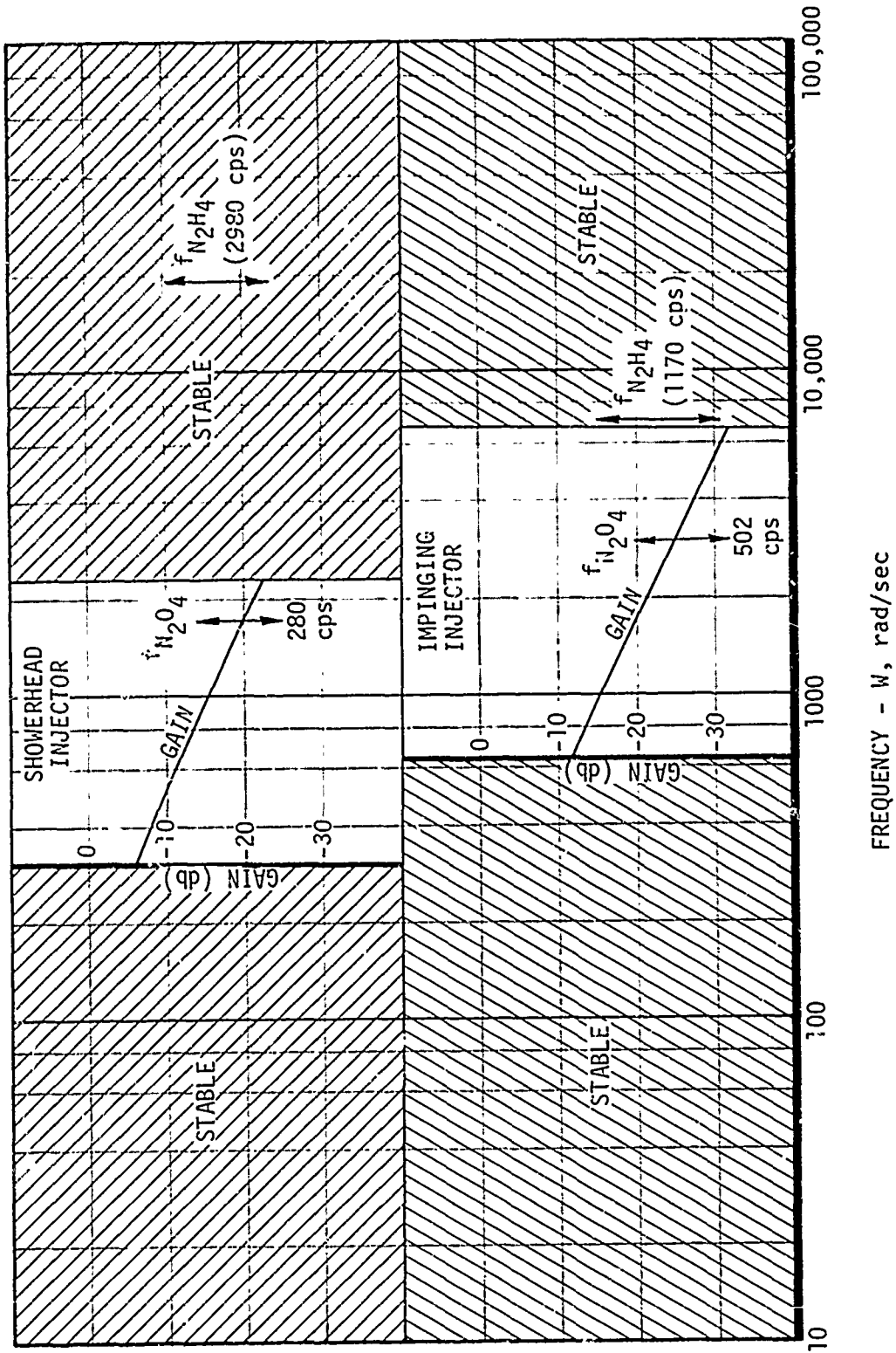
Figure 7. Low Frequency Stability Characteristics of Phase I
Injectors

IV, A, Design Analysis (cont.)

The assumption was made that no resistance existed in the propellant feed circuit, thus setting the feed circuit phase shift limits at a maximum of $\mp 90°$. By plotting the combustion process gain-phase curve (represented by the term

$$\frac{c^*}{A_t g} \quad \frac{e^{-j\omega\tau_1}}{1 + j\omega\tau_2})$$

for a range of frequencies and superimposing the feed system phase shift limits upon this curve, it was possible to define frequency limits below and above which the system would always be phase-stabilized (i.e., $\zeta_{combustion} + \emptyset_{feed\ system} \neq -180°$). The area between these limits represents a zone of potential instability. (The instability zones in Figure 7 will in actuality be narrower, since the addition of resistance to the feed circuit will reduce the maximum phase shift to a value less than 90°.)

(U) The second task was accomplished through a consideration of the capacitance and inertance inherent to the injectors themselves. Using the equation

$$f = \frac{1}{2\pi} \left[\frac{1}{LC}\right]^{1/2}$$

where:

f = frequency

L = circuit inertance

C = circuit capacitance

It was found that the natural frequency of both injector fuel circuits fell within the phase-stabilized zones of the system. The oxidizer circuits had natural frequencies of 280 cps and 502 cps for the showerhead and impinging injectors, respectively. In both cases, however, the gain, or ability of the circuit to amplify the oscillation, was found to be less than zero db. Thus,

Report AFRPL-TR-69-122

IV, A, Design Analysis (cont.)

injector-sustained oscillations of significant amplitude were not expected. Also, since the additive gain of the feed lines could have been reduced to insignificance by adding resistance to the circuit, no significant oscillations were expected from the injector/feed line combination.

b. High Frequency

(1) General.

(U)   In this section attention will be focused on the third type of combustion instability, namely, high-frequency instability. This type depends upon a coupling between the combustion processes and flow oscillations in the combustion chamber. Such coupling requires no input from the feed system. The frequencies to be expected are in the thousands Hertz range.

(U)   At the present time, the most completely developed theory of high frequency combustion instability is the Sensitive Time Lag Theory (Reference 7, 8, 9, 10, 11) developed by Crocco and his co-workers at Princeton University. The theory is based on the analysis of the stability of small perturbations from the mean operating conditions of the thrust chamber. For analytical simplicity, the gradual conversion of reactants to products is replaced by a step-function, thus defining a total combustion time lag associated with each element of propellant. It is further assumed that, during the time period between injection and combustion of a given element of propellant, there exists a period of time during which the rate controlling processes are sensitive to local combustion chamber conditions (such as pressure, temperature, gas velocity). This portion of the time lag is referred to as the sensitive time lag (τ). The degree of sensitivity is measured by the interaction indices, each index being associated with one of the local

Page 35

IV, A, Design Analysis (cont.)

perturbation quantities. The interaction index, n, measures the pressure
sensitivity of the combustion process. From the perturbed conservation
equations for flow with combustion in the thrust chamber, a characteristic
equation is developed which establishes the conditions for neutral stability
(i.e., the conditions for which a small perturbation will neither grow nor
decay). These stability limits are conveniently represented in the n,τ
plane. For a given thrust geometry and operation conditions, the n,τ zones
can be calculated. A typical set of limit curves for the 6.5-in. L* copper
chamber is shown in Figure 8. The curves represent the locus of n,τ points
at which the system would be neutrally stable. The region below the curves
represents the stable region; that above the curves represents the unstable
region.

(U) It is postulated that each injector has associated
with it a particular value of n and τ which, when located at the n,τ plane
relative to the calculated zones, can be used to determine the stability of
t^n system. Since the theory considers only small perturbations, the stability
predicted refers only to spontaneous instability. For pulse instability, only
semi-quantitative results are obtainable.

(a) Definition of Unstable Modes

(U) It has been observed through the study of
combustion instability that unstable pressure oscillations generally assume
the characteristics and frequencies of the resonant acoustic modes of the
combustion chamber. Therefore, it is desirable to understand the characteristics
of the acoustic oscillations in order to investigate the character of a com-
parable unstable combustion oscillation.
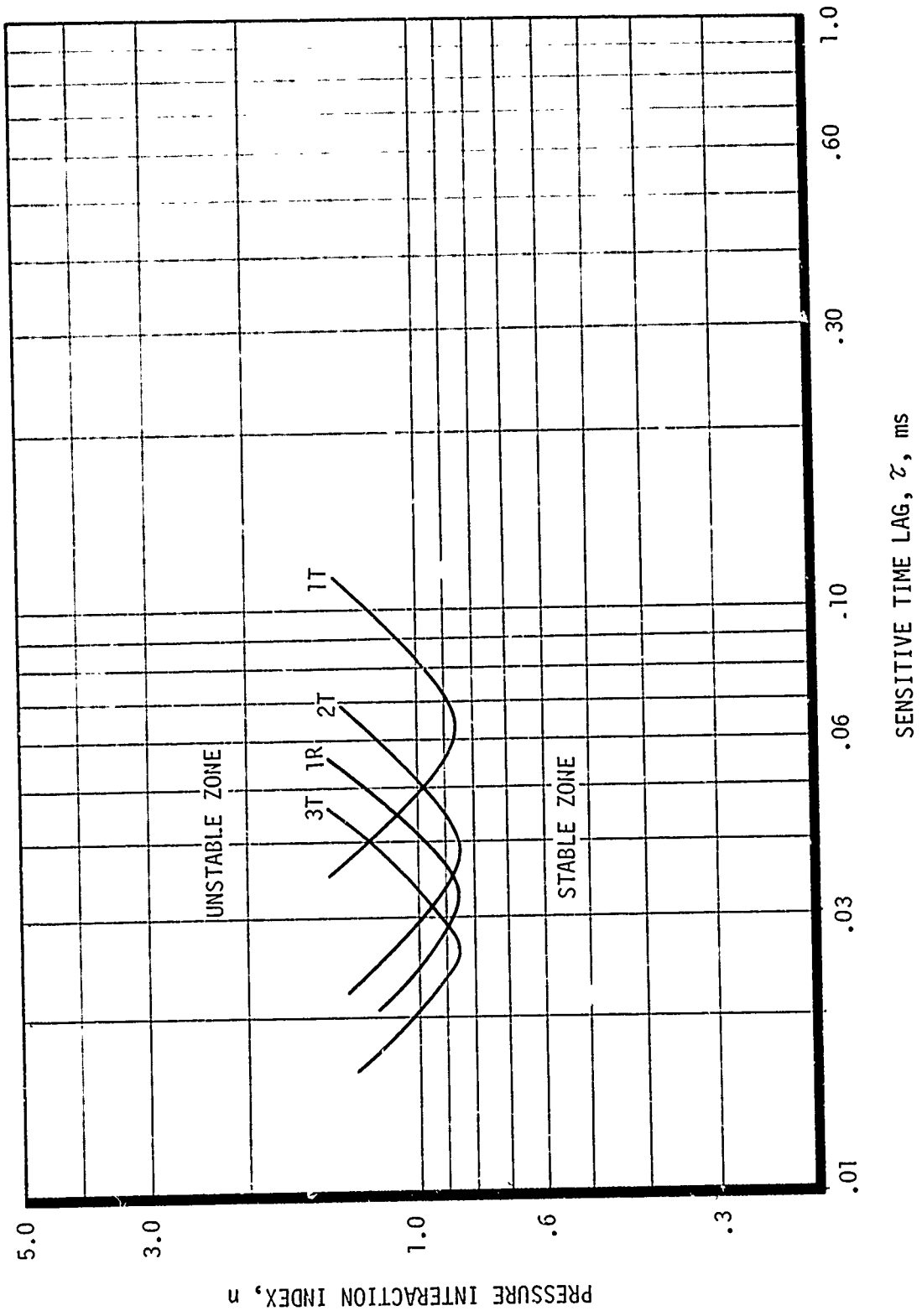
Figure 8. Instability Limit Curves for 6.5-in. L* Chamber

IV, A, Design Analysis (cont.)

(U)   Acoustic oscillatory modes can be separated
into three distinct categories: (1) transverse modes--those involving either
radial or tangential pressure variations in planes perpendicular to the
chamber axis; (2) longitudinal modes--those involving only pressure variations
parallel to the chamber axis; and (3) combined modes--those involving
characteristic pressure variations of both longitudinal and either transverse
mode, or of both of the transverse modes simultaneously.

(b) Transverse Modes

(U)   The frequencies of transverse modes approxi-
mate either the fundamental or higher harmonic frequencies of acoustic oscil-
lations in a circular cylinder. The frequencies can be computed from the
following equation:

$$f = \frac{a - S_{NH}}{2\pi r_c} \qquad\qquad (Eq\ 1)$$

where: a = speed of sound, ft/sec ($a = \sqrt{kgRT}$)

f = frequency, Hertz

r_c = chamber radius, ft

H = represents the Hth zero of the derivative of a Bessel
function

N = order of the Bessel function

S_{NH} = argument, x, at $J_N'(x) = 0$

$J_N(x)$ = Bessel function of the first kind of the order N

$J_N'(x)$ = slope of $J_N(x)$

θ = angular coordinate

IV, A, Design Analysis (cont.)

Further amplification of the term S_{NH} may be necessary to fully understand its usage in Equation 1. S_{NH} is the value of the argument, x, corresponding to maxima and minima of the Bessel function of the first kind, $J_N(x)$, or in other words, points where $J_N'(x) = 0$. The subscripts N and H are indices that assume distinct values for each particular mode of transverse oscillation.

(U)   The various pressure oscillations have frequencies associated with the acoustic oscillation frequencies calculated by Equation 1. The fact that there is a pressure oscillation implies that there is an associated oscillatory motion of the combustion gases. In the case of the fundamental transverse modes, the entire chamber cross-section planar area is associated with this oscillatory motion. Each succeeding fundamental mode divides the chamber cross-sectional area into smaller areas; e.g., the second tangential mode has two areas each of positive and negative pressure concentration, the third has three each, etc. Some sample pressure and velocity patterns for transverse modes are shown in Figure 9. By looking at these patterns and referring to the above discussion, pressure and velocity patterns for any harmonic of either a pure tangential or pure radial mode can be defined.

(U)   In this particular application, only the transverse mode was considered a possibility. Both longitudinal and combined modes are heavy damped by the nozzle relative to transverse modes. The assumption was thus made that the damped modes would not be experienced. The following sections present a brief review of the theoretical effects of baffles, injection distribution, and chamber geometry on the transverse modes. The last section presents the baffle patterns selected and the modes to which they would be effective.

IV, A, Design Analysis (cont.)

(c) Theoretical Effect of Baffles on Stability

(U)   Injector face baffles are intended as a damp-
ing device only for transverse modes of high-frequency instability. These
modes are characterized by acoustic pressure and velocity variations parallel
to the injector face. In general, the principles of design for baffles to
damp pure transverse modes apply equally well to the combined modes.

(U)   Of major concern in the design of an effective
baffle is the location of the baffle relative to the gas particle paths since
the baffles constitute an obstruction to particle motion. For example, with
the exception of the first tangential mode or combinations thereof, the trans-
verse velocity at the center of the injector is zero. In general, as tangential
modes become of higher order, the major gas particle motion and pressure varia-
tions are limited to the outer circumference of the chamber. This characteris-
tic becomes important in considering the placement of baffles to suppress the
higher order modes.

(U)   In the case of pure radial modes, the velocity
perturbations are limited to the radial direction and, as in the case of the
tangential modes of higher than the first order, no gas particle motion is
present at the injector center.

(U)   The mechanisms from which baffles have been
postulated to derive their damping effects fall into three categories: protec-
tion of the sensitive flame region, phase stabilization, and gain stabilization
or increasing damping. Protection of the sensitive flame region is postulated
to desensitize the precombustion processes (e.g., mixing and vaporization) to
perturbations. Phase stabilization results from significant changes in reson-
ant acoustic modes of the combustion chamber so that the sensitive frequencies
associated with the combustion process are no longer in the vicinity of the

IV, A, Design Analysis (cont.)

chamber resonances. Gain stabilization, or increased damping, is postulated to be the result of two possible mechanisms; increased damping due to additional viscous losses resulting from the increased surface area introduced by the baffles, and the scattering of energy into other modes that are easily damped. The former is considered a second order effect.

(U)   The optimum number of blades for any baffle configuration depends primarily on the mode of instability to which the system is most susceptible. For example, referring to Figure 9, the selection for a baffle configuration to damp a first tangential mode would be a three-bladed baffle. It is also apparent from Figure 9 that a one- or two-bladed baffle could, at the most, only cause the mode to stand in the baffle cavity with the velocity antinodes located 90° from the baffle. The same type of logic applied to a second tangential mode would indicate that a symmetrical three-bladed baffle would be effective and that the two- and one-bladed baffle would not. Also--not as obvious, but equally true--a symmetrical four-bladed baffle would have little or no effect because the mode can be set within the baffle cavity with the velocity antinodes located 45° from the baffle radial legs.

(U)   Extension of these considerations to the higher order tangential modes leads to the generalization that a radial baffle system having an odd number of blades (with the exception of a single blade) would offer protection from modes which are of the order less than the number of blades. Also, an odd number of blades would provide, to some degree, protection from modes of an order higher than the number of blades, provided the order of the mode divided by the number of blades is not equal to an integer.

(U)   The generalized description of a technique for selection of a minimum number of blades does not necessarily indicate the optimum number of blades to maximize chamber damping and/or change chamber

PURELY RADIAL MODES

$S_{02} = 3.8317$ $S_{03} = 7.0156$

P   V

FIRST (1R)   SECOND (2R)

PURELY TANGENTIAL MODES

$S_{11} = 1.84129$ $S_{21} = 3.0543$

P   V

FIRST (1T)   SECOND (2T)

COMBINED MODES

$S_{12} = 5.3313$ $S_{13} = 8.5263$ $S_{22} = 6.7060$

P   V

1T-1R   1T-2R   2T-1R

$$f = \frac{S\nu_h \, C_o}{2\pi r_c}$$

f = FREQUENCY
C_o = SOUND SPEED
r_c = CHAMBER RADIUS
$S\nu_h$ = CHARACTERISTIC EIGEN VALUE
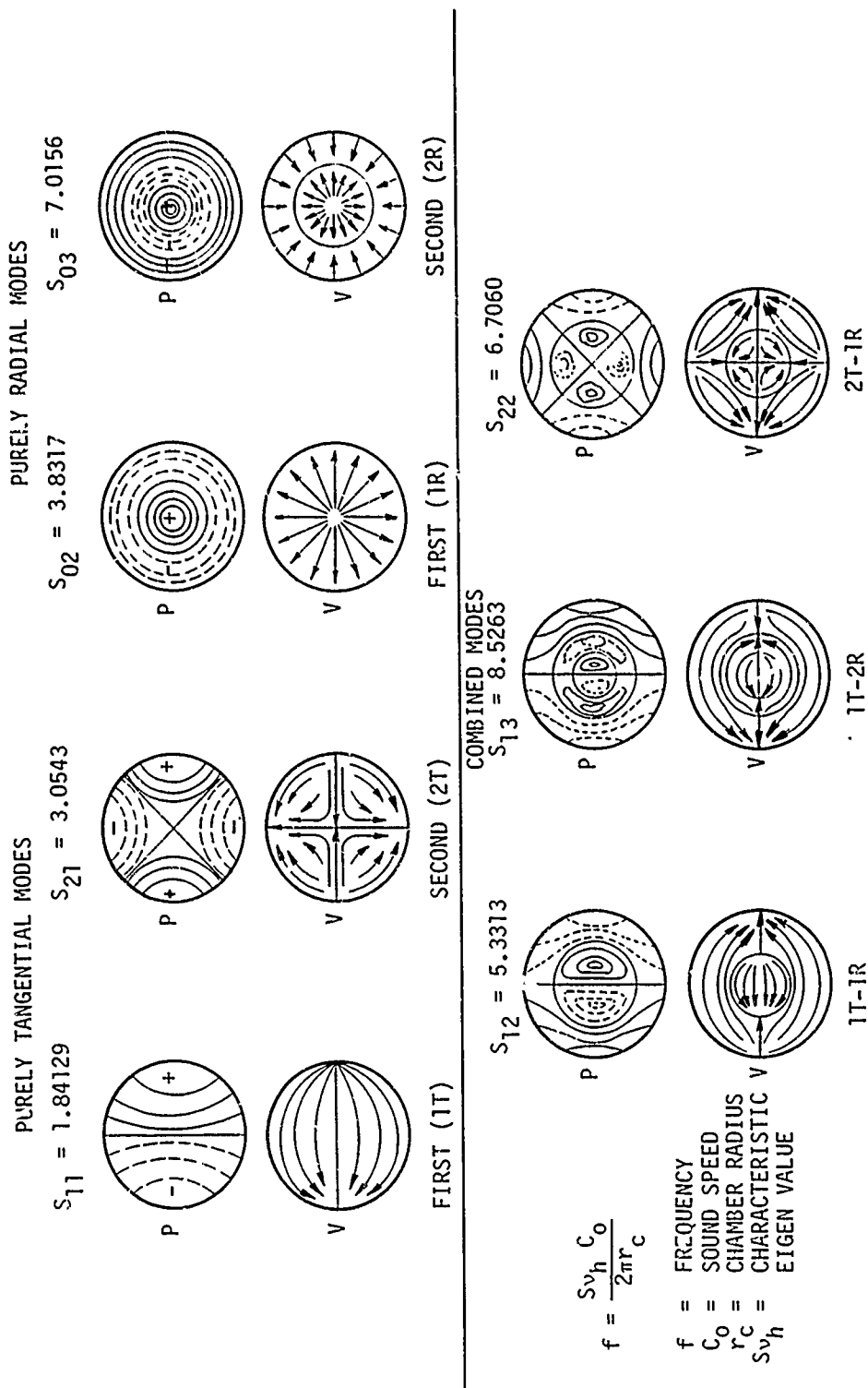
Figure 9. Pressure and Velocity Patterns for Transverse Modes

IV, A, Design Analysis (cont.)

resonant frequencies. Experimental results must be relied upon for this. Other design criteria may also be substantiated from experimental data. Some of the general rules applying to baffle design which have been experimentally verified are   follows:

> <u>1</u>   An odd number of baffle blades is best for the tangential modes, providing the order of the mode divided by the number of blades is not an integer.

> <u>2</u>   For the radial modes, hubs located at the velocity antinodes indicated in Figure 9 are best. The minimum number of hubs required are equal to the order of the mode (i.e., first radial requires one hub).

> <u>3</u>   Making the baffle compartments too small may be detrimental. A baffle characteristic cavity dimension (W) in the range $0.2 \leq \lambda \leq 0.4$, where $\lambda = \frac{C}{F}$, appears to be most desirable.

> <u>4</u>   Baffle length to chamber diameter ratios in the range of 0.2 to 0.3 appear to be optimum.

>> (d)   Theoretical Effect of Injection Distribution on Stability

(U)   The exact analysis of unsteady, two-phase turbulent flow with combustion distributed arbitrarily in three dimensions is quite a formidable problem. An approximate method has been developed (Reference 12) in which the nonuniform transverse injection distribution appears as a variation in the sensitivity of the combustion process as determined by the Sensitive Time Lag Theory. From the Sensitive Time Lag

IV, A, Design Analysis (cont.)

Theory, it is apparent that the greatest stability can be obtained by maximizing the interaction index required for neutral oscillations, i.e., by moving the unstable region upward on the n,τ plane. According to the approximate analysis of Reference 12, maximum stability is associated with minimum values of the distribution coefficients as calculated therein.

(U)   One of these coefficients is the pressure coefficient, A, which varies with injector radius as shown in Figure 10 for the first and second tangential modes and the first radial mode.

(U)   For the tangential modes, A reaches a maximum at the chamber wall (r_i = 1) and goes to zero at the center of the injector mode. Therefore, maximum stabilization for the tangential modes is achieved by injection of the propellants at the chamber wall. On the other hand, the first radial mode reaches its most destabilized condition with injection at the center because the center of the injector and the chamber wall represents pressure antinodes for that mode. Absolute stability of the radial mode is achieved at r_i = 0.627. Therefore, for the case of concentrated combustion, sensitive only to pressure effects, the first radial mode of instability could be expected with injection in the interval $0 < r_i < 0.42$, and the tangential modes of instability could be experienced for $0.61 < r_i < 1.0$. Stable operation could be expected in the central interval, $0.42 < r_i < 0.61$, since coefficients for both modes are relatively low.

(U)   It can be seen that an effective approach toward instability suppression would be to concentrate the combustion near pressure nodal points. This concept can be extended to suppress specific modes of transverse instabilities. The methods of Reference 12 show the methods used to apply this to the n,τ plots obtained from the Sensitive Time Lag Theory.
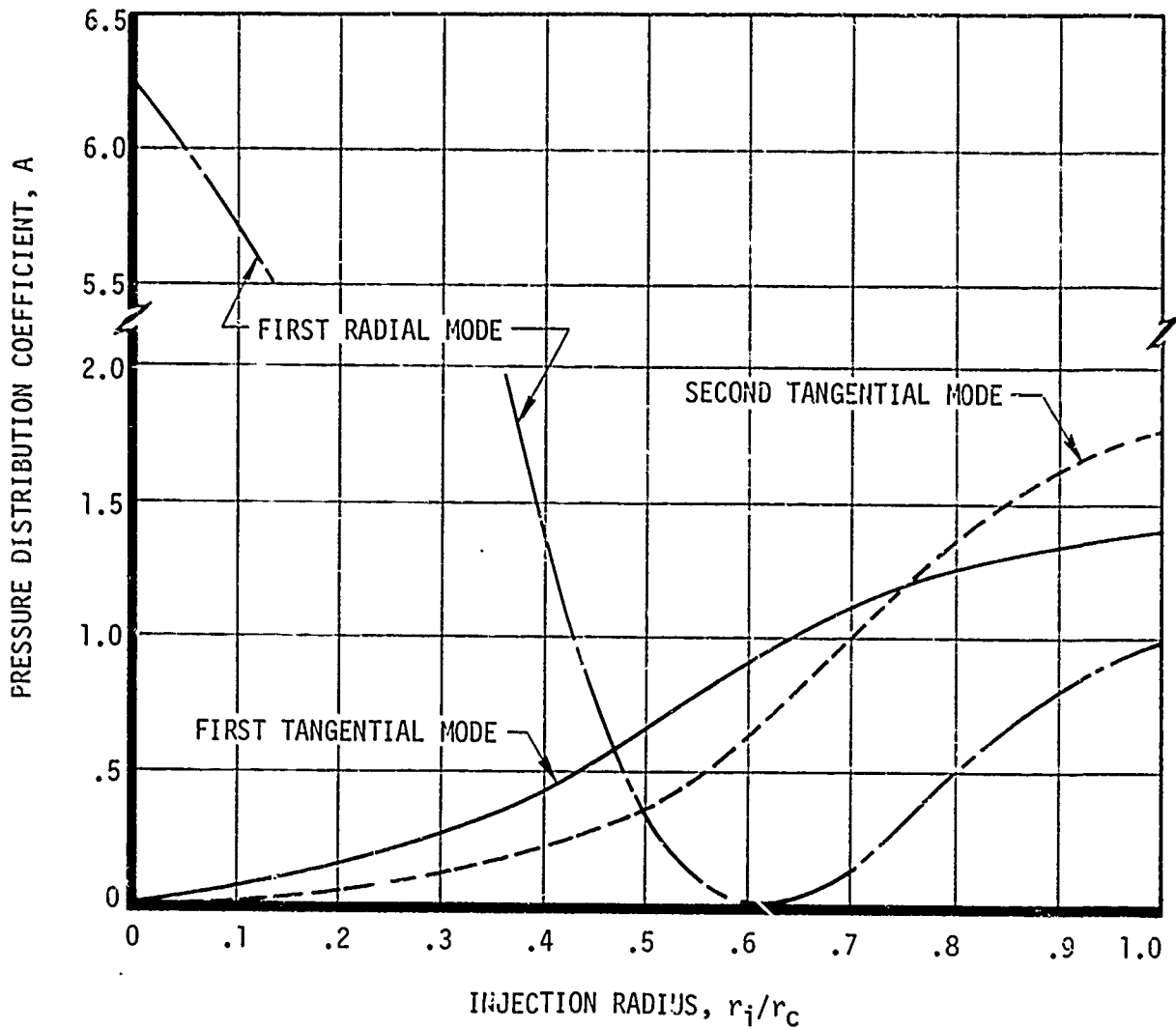
Figure 10. Pressure Distribution Coefficient for Radially
Concentrated Injection

CONFIDENTIAL

(This Page is Unclassified)

IV, A, Design Analysis (cont.)

(U)   In general, the effect of barrier cooling (the injection of a significant amount of low mixture ratio propellants) corresponds to a low injected mass flux near the chamber wall. The effect on the stabilization of the system by the barrier cooling is a beneficial one for the tangential acoustic modes but somewhat destabilizing to the radial modes.

(e) Theoretical Effect of Chamber Geometry

(U)   Theoretical basis exists for changes in instability behavior with chamber geometry. Priem's theory suggests that the use of a chamber with a low contraction ratio to increase the velocity difference between the injected liquid propellant and the surrounding gas will lead to increased stability in the transverse modes. This hypothesis was verified with earth-stable propellants (as reported in Reference 13) with a 15° half angle tapered chamber. Additionally, it is known from the Sensitive Time Lag Theory that a large L/D chamber will tend to provide a stabilizing influence on transverse modes. In this case, however, the longitudinal modes tend toward destabilization.

(f) Application of Theory to Engine Design

(C)   During the proposal phase of this program, a 4.0-in.-dia HIPERTHIN showerhead injector, tested using N_2O_4/N_2H_4 as propellants, proved to be unstable when fired without sufficient provision for damping the acoustic modes of the chamber. A sufficient provision for damping, based on these test results, proved to be seven radial baffles 0.7 in. long, a 0.2-in. hub baffle, and radial baffles that further divided each long baffle compartment (Figure 11).
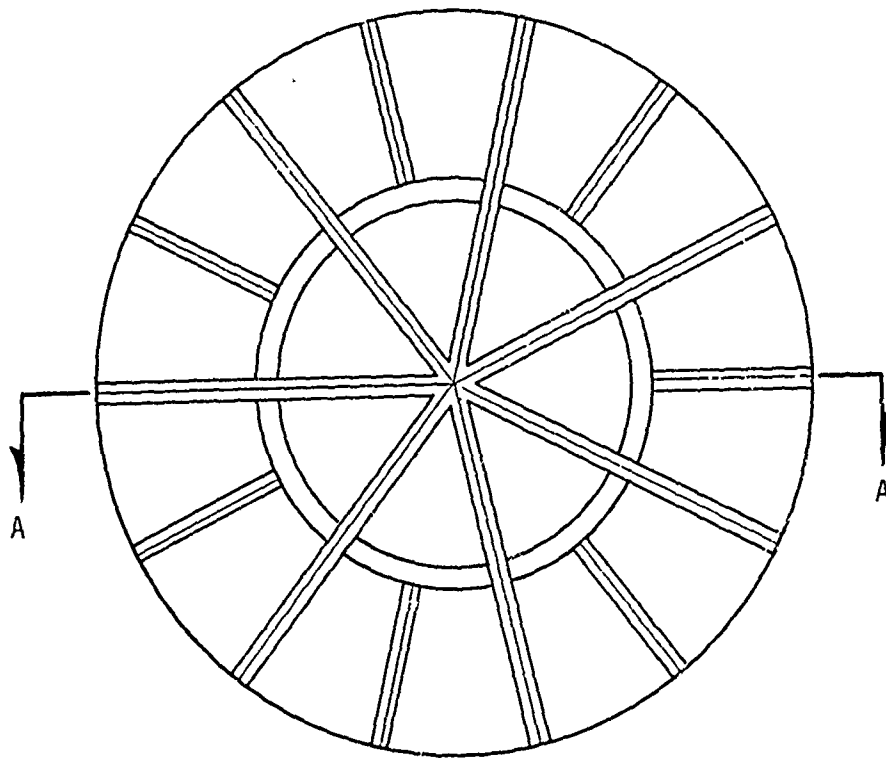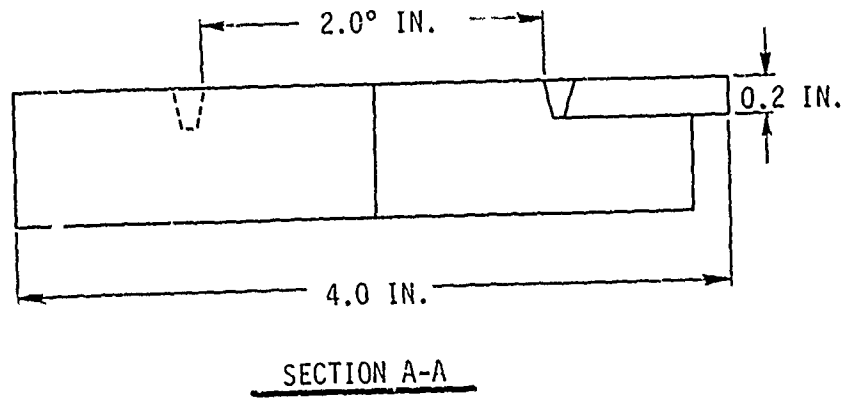
Report AFRPL-TR-69-122

SECTION A-A

Figure 11.   Prepoposal Injector Pattern

Page 47

IV, A, Design Analysis (cont.)

The results of the above program were reviewed, and, in light of these data and the theoretical considerations mentioned earlier, a stability analysis was completed. This program differed from the proposal effort in three major ways: (1) the presence of a significant amount of low mixture ratio (MR) barrier cooling, (2) an injector diameter decreased from 4.0 in. to 3.5 in., and (3) a contraction ratio (A_e/A_t) decreased from 2.34 to 1.67. The latter change corresponds to a theoretical increase in the chamber Mach number from 0.26 to 0.38.

The barrier cooling percent flow/percent area values correspond to an injected mass flux distribution near the chamber wall of only 0.5 and 0.67 as compared to a uniform injected mass flux distribution of 1.0. The 34% and 16% injector areas correspond to about 19% and 8% of the chamber radius, respectively. These are significant stabilizing influences for the first, second and third tangential acoustic modes but slightly destabilizing to the first radial mode.

As stated in Section IV,B, each phase one injector had provision for fabricating three unique baffle patterns, each 0.7 in. long from injector face to downstream baffle tip. Of the three baffle pattern designs, the first was based on the cylindrical coordinate system with radial baffles, a concentric ring or hub baffle, and two baffle lengths (Figure 12).

The second baffle design was based on the rectangular coordinate system and looked like an "egg crate". It was also composed of two different length baffles as is shown in Figure 12. Both the designs anticipate that the unstable modes for this injector would be the first, second, and third tangential (1T, 2T and 3T) and the first radial (1R). These two baffle designs were chosen to duplicate as much as possible the
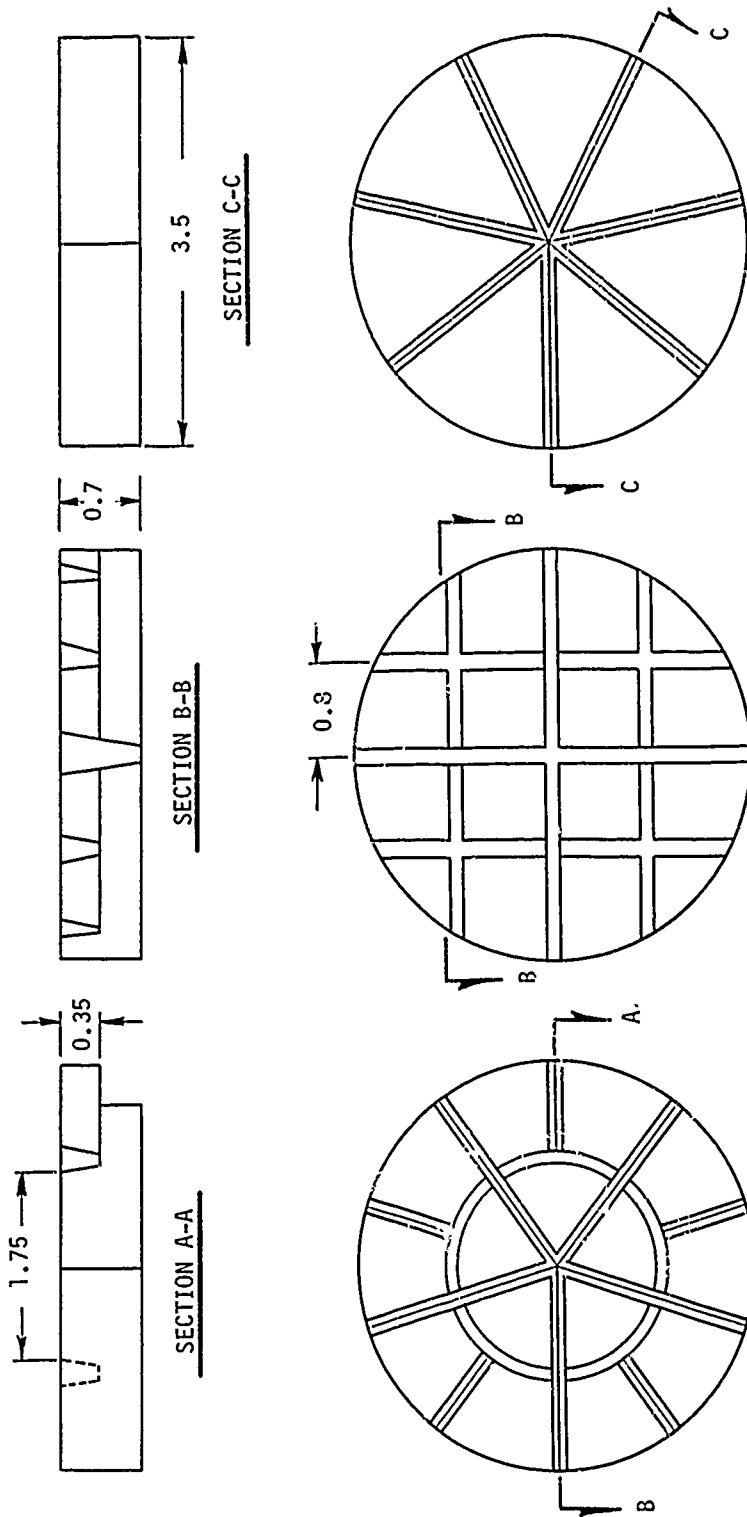
Figure 12. Pretest Baffle Pattern Selection

IV, A, Design Analysis (cont.)

4.0-in.-dia baffle pattern inasfar as the actual size of the baffle pockets
are concerned, while increasing the baffle lengths relative to the chamber
diameter to compensate for the loss in the number of baffles. The third baf-
fle design consisted of seven constant length radial blades only with no pro-
vision for the first radial mode (Figure 12).

(C)   The stability characteristics of the first two
baffle designs were expected to be very similar to that previously experienced
on the 3000-lb thrust HIPERTHIN injector tested with N_2O_4/N_2H_4 propellants.
This was despite the small improvement expected from the slightly reduced mass
flux per unit of injector area near the chamber wall due to the barrier cool-
ing and due to the higher chamber Mach number. The third baffle design was
expected to provide an evaluation of the first radial mode.

(U)   The frequencies of oscillation of the acoustic
modes expected were: first tangential at 8000 cps, second tangential at
13,000 cps, first radial at 16,000 cps, and third tangential mode at about
18,000 cps.

6. Fabrication Analysis

(C)   A degree of effort was expended in reviewing fabrication tech-
niques that had, in past programs employing platelet hardware, resulted in suc-
cessful component assembly. Specifically, fabrication procedures and tolerance
limits techniques were reviewed to ensure that anticipated problems due to
leakage between end plates and the platelet stack, and plugging of propellant
flow channels during the braze operation would be avoided.

(C)   The former problem had been encountered on those injectors
whose massive end plates doubled either as manifold casings or bolt flanges.
The problem of end plate separation is a result of unequal cooldown between the

IV, A, Design Analysis (cont.)

thick end plates and the platelet stack after brazing. Resulting thermal stresses cause the end plates to pull away from the stack, leaving voids through which propellants could leak externally. The use of thinner end plates, or end plates containing grooves to promote even cooldown have been proven effective; however, these techniques could not be applied in this program because of the need for bolt flange material.

(C)   The solution to the end plate problem was to use blank platelets between the platelet stack and the end plates. These blanks, first employed in the injectors of Contract NAS 8-21052 and in a hydrazine injector built during the proposal stage of this contract, consisted of unplated steel stock void of any active propellant channels. It was found that by placing one blank at each interface, propellant was restrained from leaking through any gaps formed at the end plate. In essence, the blank became the active end plate and the actual end plate served only as a flange.

(C)   Orifice plugging was solved by compiling a history of braze plugging as a function of braze alloy thickness tolerance. Spare platelets for injectors fabricated on prior programs were metallographically analyzed to determine the exact alloy thickness present on each. Plating thickness variations were correlated with braze success to define the absolute plating tolerances required. By defining the amount of plating required and the tolerances applicable to this thickness, it was possible to fabricate six injectors during this contract that were free of copper plugging.

IV, Design (cont.)

B.   MECHANICAL DESIGN

(U)   The second task of Phase I dealt with the actual design of the
experimental hardware. The results of the analyses previously described were
used to generate initial multi-purpose configurations. Subsequent test data
obtained with these injectors were then incorporated into the design of the
final demonstration unit. The following paragraphs describe the design of all
program hardware.

1.   Injector

(C)   The design selected for use with N_2O_4/N_2H_4 was of the HIPERTHIN
type. This concept is an Aerojet-General developed and owned design which
represents a new approach to the design and construction of liquid rocket engine
injectors. The injector face contains thousands of small slots several
thousandths-of-an-inch wide. Each slot is connected to either a fuel or an
oxidizer manifold by means of a precisely controlled flow passage that accurately
meters propellant flow to the slot. The small size of the feed slot and the
minimal spacing between slots gives this injector its unique properties of
excellent atomization and intimate mixing.

(C)   The key element in construction of this injector is the plate-
let; a thin sheet of metal (typically 0.001 to 0.020 in. thick) which has a
pattern of flow channels and holes etched into its surface. Two types of
platelets are used in an injector: fuel platelets and oxidizer platelets.
The primary differences between the fuel and oxidizer platelets are in the lay-
out of the flow passages. The outer contour of the two platelet types is the
same. The injector is formed by alternately stacking fuel and oxidizer plate-
lets and bonding the stacked platelets together to form a single integral unit.

IV, B, Mechanical Design (cont.)

(U)   The specific program injector designs were generated in three
phases. The first phase produced multi-purpose hardware amenable to rapid
modification. The second phase hardware incorporated only those character-
istics proved feasible with the original units. These injectors contained
provisions for relatively few baffle iterations. The final injector design
was the culmination of the phase one and two injector results. This last unit
essentially "froze" the injection type, baffle pattern, and manifolding design
applicable to the N_2O_4/N_2H_4 application.

a.   Phase One Injectors

(C)   The phase one injectors used in this program were
designed to one basic criterion: to allow a maximum number of iterations in
baffle configuration with a minimum amount of hardware. In compliance with
this criterion, the first injector types were designed to include multiple
face levels within a single unit. These levels are vividly demonstrated by
the platelet drawings shown in Figure 13. It may be seen that both metering
platelets contain three zones of narrow channels, followed by considerably
longer channels of greater width. The narrow channels provide a high injector
pressure drop, thus distributing the flow uniformly and preventing low-
frequency instability. The long, constant width channels provide zones into
which any stabilizing blade configuration can be machined. Because nearly all
of the injector ΔP is taken through the narrow channels, the differential
channel length resulting from face contouring does not appreciably change the
total ΔP, nor does it result in areas of high and low flow rate.

(C)   The platelets of Figure 13 are illustrative of an
impinging injector, one of two basic injector types which was designed and
subsequently evaluated. The operation of the impinging design is explained
with reference to the platelet drawings. Since the injectors are baffled to
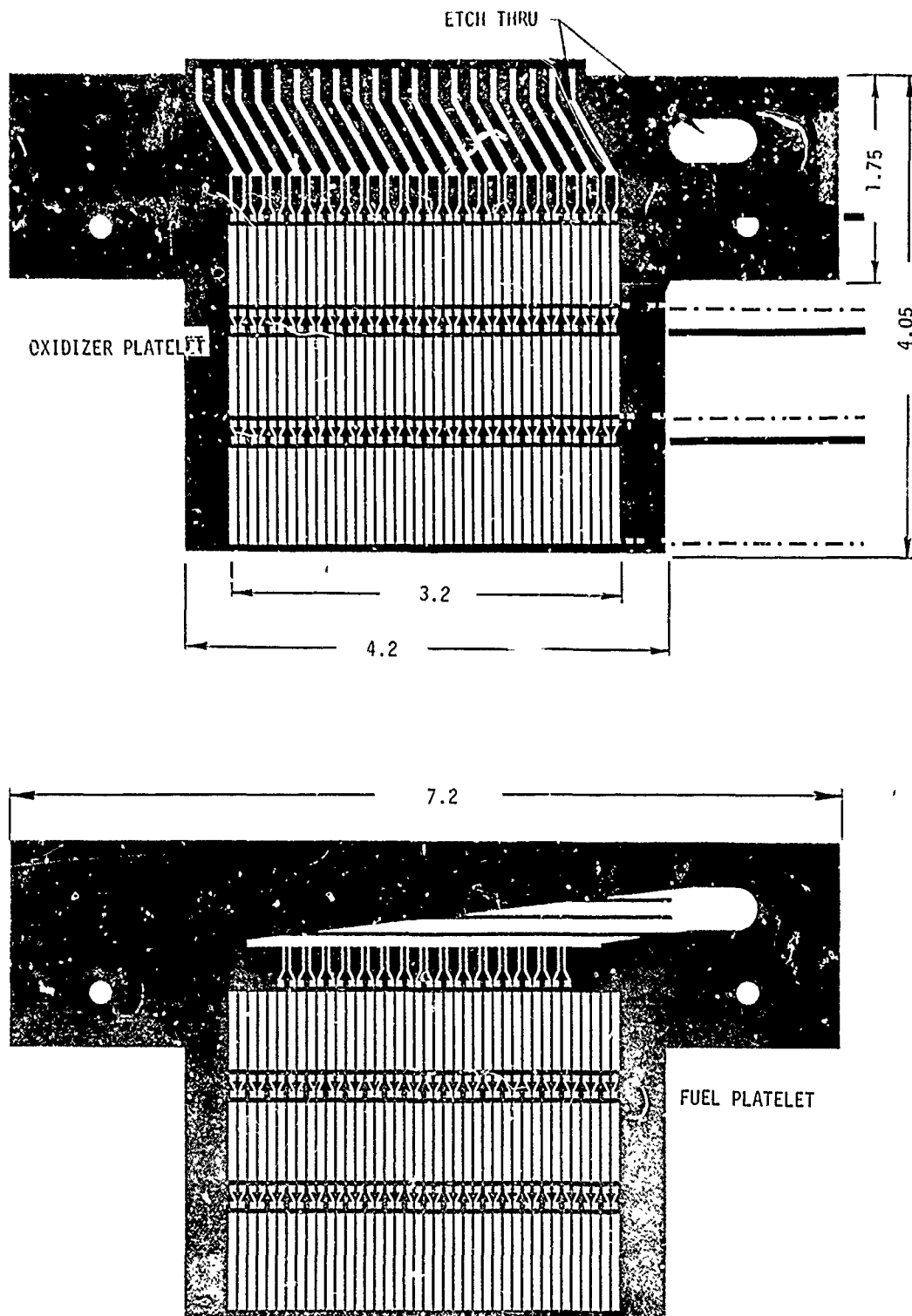
Figure 13. Impinging Injector Subcomponents - Phase I Design (u)

IV, B, Mechanical Design (cont.)

a contour similar to those of Figure 12, the injection elements do not all lie in a single plane but form a contoured surface of various elevations ranging from the baffle tips to the flat pockets between the baffles. These two extremes of the injector face elevation are indicated by the lines shown on the platelet drawing. Consider first the plane surfaces in the pockets between the baffles. These surfaces are formed by cutting the platelets back to any of three levels indicated by the solid lines. The channels at these points on the platelets form like-on-like impinging doublets.

(C) The pattern formed at the baffle tips is the result of cutting the platelets to the lower, or dashed, lines. The channels at these points are wider than at the impinging levels so that the injection velocities are lower. The pattern is essentially a showerhead pattern, as is the pattern at any point between the face level and the baffle tip level. By designing three impinging/showerhead levels into the platelets, it was possible to fabricate a single unit capable of demonstrating a minimum of three unique baffle configurations, or a greater number, depending on the number of minor iterations performed within each level.

(C) The separator platelets applicable to the phase one impinging injectors are shown in Figure 14. These platelets, which are placed between fuel and oxidizer metering platelets, contain noncritical flow passages only (see Section V). One item of significance in these platelets is the depth-etched pockets occurring at intervals down the platelet in the direction of propellant flow. Reference to the metering platelets of Figure 13 will show that the through-etched flow paths in the metering platelets were not continuous but stopped at the inlet and exit of each impinging pair. The etched pockets in the separators were used to channel the propellant flow past these metering platelet obstructions. This flow path was incorporated for two reasons. The first was to avoid the long, unsupported metering platelet
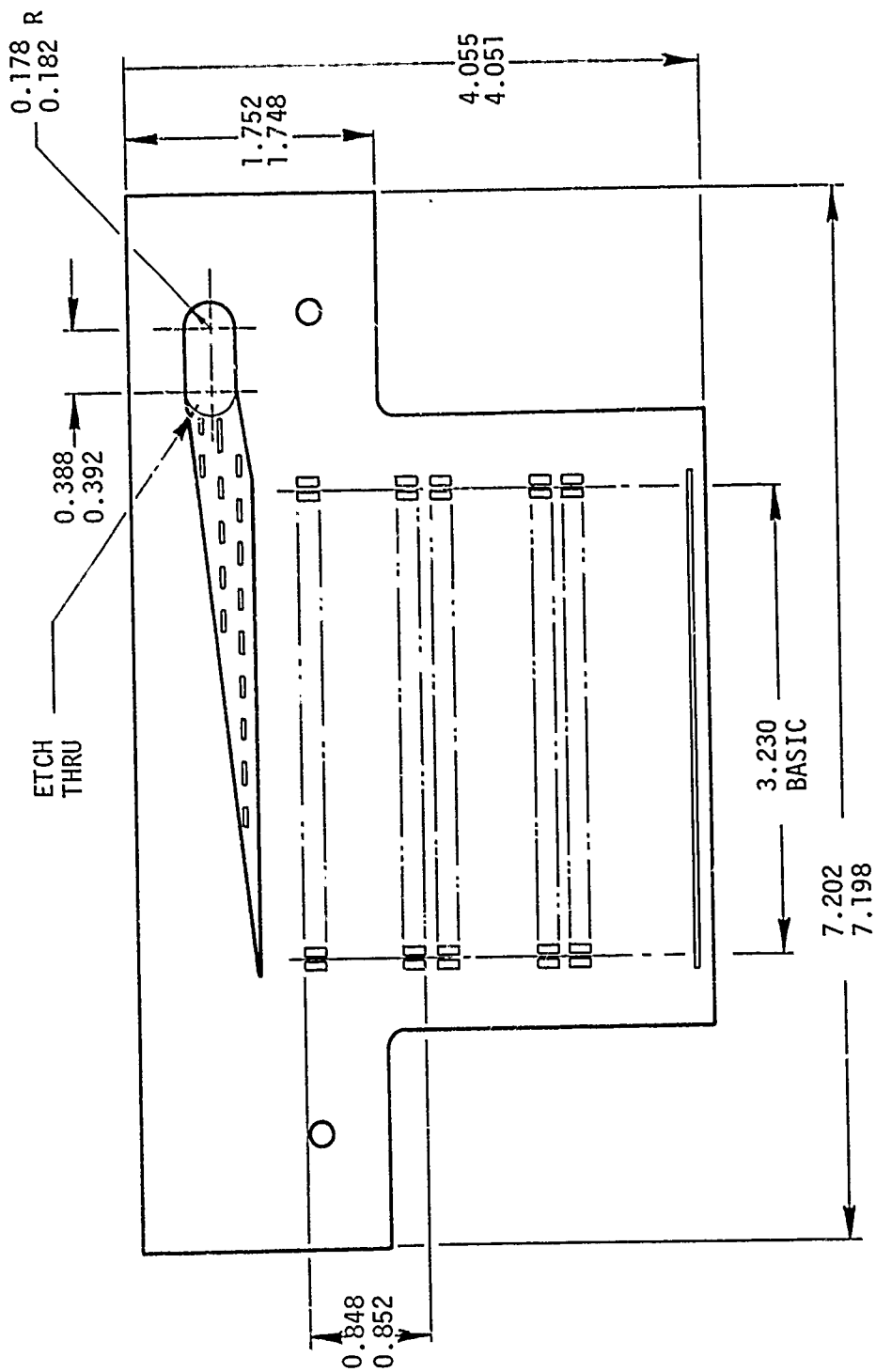
Figure 14. Impinging Injector Subcomponents - Phase I Design (u)

IV, B, Mechanical Design (cont.)

filaments that would have existed side by side had the through-etched flow paths been made continuous. The second reason for the pockets was to induce a degree of turbulence into the propellant flow as it left the impinging orifices and went into the showerhead zones. By forcing the propellant to turn as well as spread, the transition from high velocity impinging flow to low velocity showerhead flow was more rapidly achieved. As shall be discussed (Section V), these pockets posed severe fabrication difficulties and were subsequently deleted from the design.

(C)   The second type of injector designed during the phase one effort contained only showerhead injection elements. This unit, the metering platelets for which are shown in Figure 15, differs from the impinging injector in the method by which atomization and mixing are achieved. The impinging injector relies primarily upon stream impingement for mixing. The showerhead injector is dependent upon pattern fineness for its atomization and mixing. This fact is exemplified by a comparison of pertinent platelet data.

	Showerhead Injector	Impinging Injector
Thrust, lb	3000	3000
Total Number Platelets	530	281
Separator Platelet Thickness, in.	0.010	0.020
Maximum Slots/Platelet	50	40
Total Number Injection Slots	10,954	4336

	Oxidizer	Fuel	Oxidizer	Fuel
Flow Rate, lb/sec	5.46	4.54	5.46	4.54
Metering Platelet Thickness, in.	0.003	0.003	0.004	0.004
Injection Velocity @ Face, ft/sec	11.5	10.6	50	60
Injection Velocity @ Baffle, ft/sec	--	--	15.5	16.5
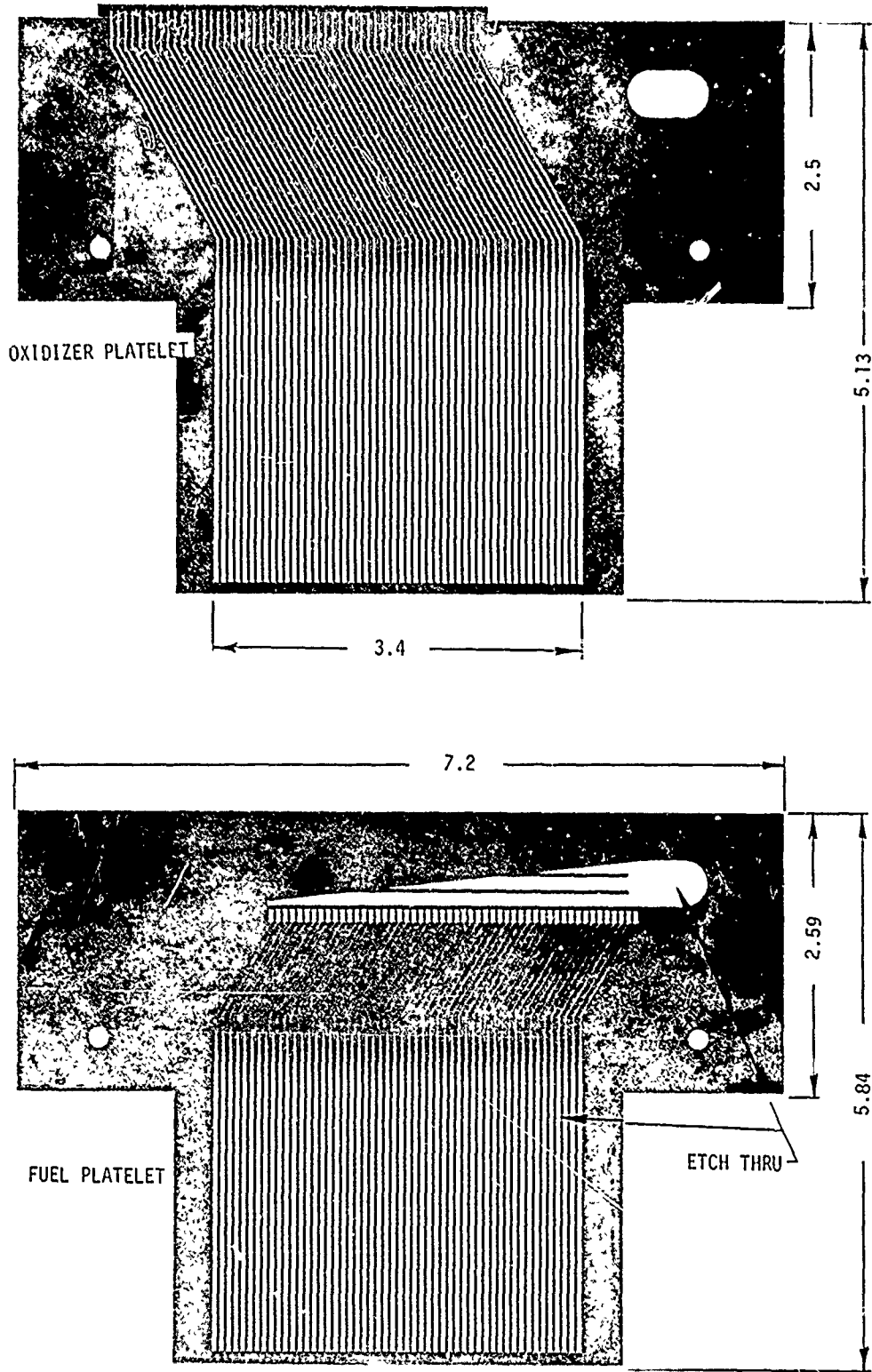
Figure 15. Showerhead Injector Subcomponents - Phase I Design (u)

IV, B, Mechanical Design (cont.)

It may be seen from the above table that the showerhead injector pattern is considerably less coarse than that of the impinging unit. Because of this pattern fineness, the showerhead injector was felt to potentially offer a more uniform, turbulence-free combustion gas. The platelets of Figure 15 were thus designed for incorporation into a showerhead unit.

(C)   It may be seen from Figure 15 that the showerhead plate-lets offer greater versatility for rework in that the face levels are not limited to specific positions. Each showerhead injector, as designed, is thus representative of many potential units.

(C)   The separator platelets applicable to the showerhead unit are shown in Figure 16. These platelets are essentially identical to those used in the impinging unit, with the exception that the showerhead plate-lets do not contain depth-etched pockets in the flow paths.

(C)   The fuel elements in both injectors were cross-fed from an internal fuel plenum located on one side of the injector (Figures 13 and 15). Fuel separators were depth-etched in the manifold region to allow low velocity and, thus, evenly distributed flow through the manifold area. Metering plate-let support strips, sandwiched between opposing lands in the separator manifold areas, prevented the fuel manifold inlets from collapsing either during brazing or actual operation.

(C)   The fuel platelets of both impinging and showerhead injectors differed from the oxidizer platelets in number of elements as well as in manifolding design. As shall be discussed in Section V, the circular injector face is machined from the square platelet stack after brazing. In the oxidizer circuit, where all platelets have an equal number of flow pas-sages, the circular machining leaves dead-ended orifices in the areas formed

Page 59
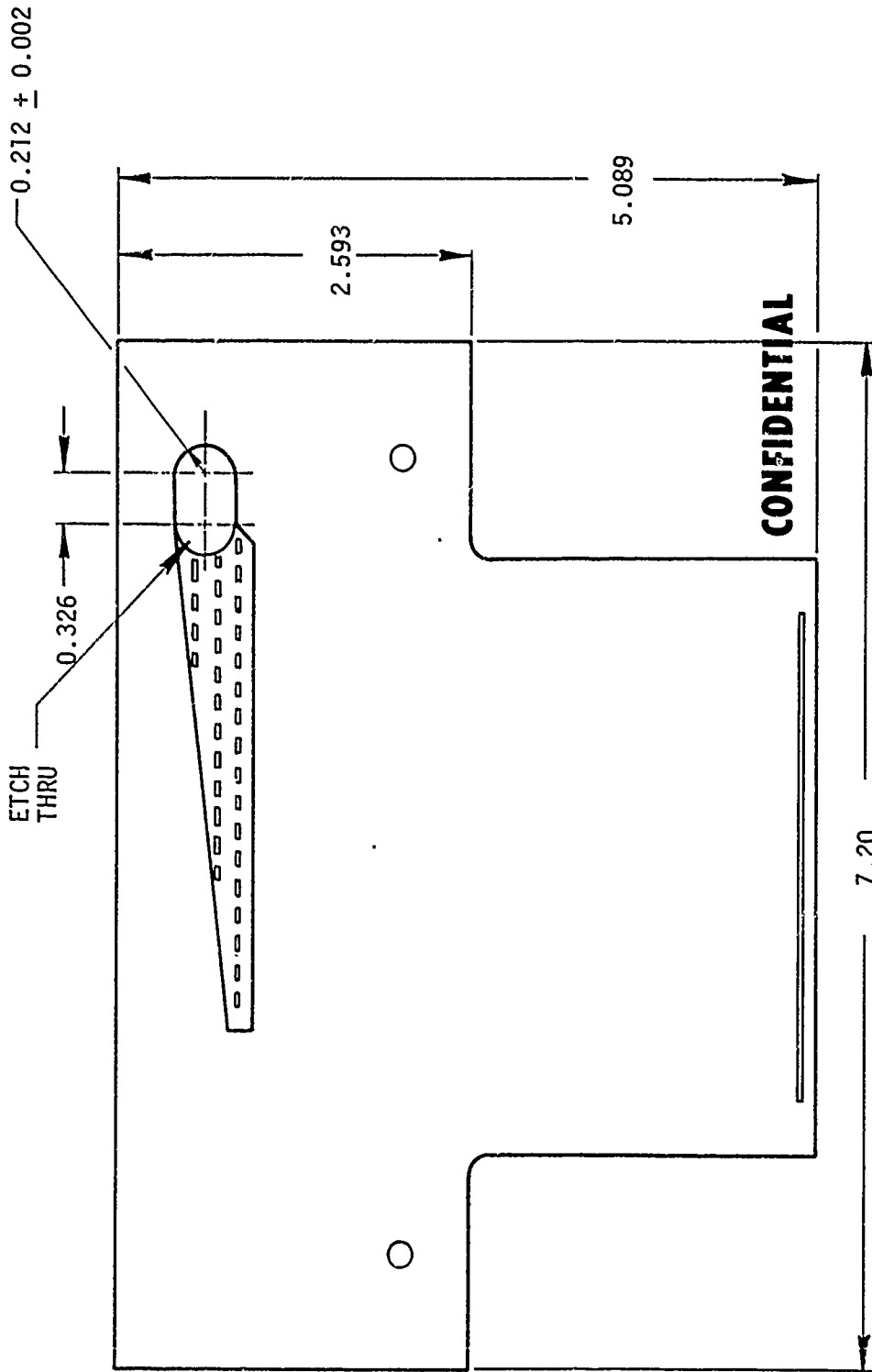
Figure 16. Showerhead Injector Subcomponents - Phase I Design (u)

IV, B, Mechanical Design (cont.)

by the corners of the original square stack. It is possible, in the oxidizer circuit, to prevent propellant filling of these orifices by sealing the external inlets at the back or manifold surface. The internal plenum of the fuel circuit prohibits such sealing. Passages not machined open during the circular face machining would be fed propellant nonetheless. This would result in hydrazine traps within the injector and, thus, possible detonation zones during injector operation.

(C)   To avoid the dead-ended hydrazine orifices, the fuel platelets were designed with "stepped" fuel orifices. The phase one injectors contained 18 unique fuel platelets, each of which had progressively fewer orifices. By stacking these platelets in sequence, it was possible to form a stack in which the outer periphery of active fuel elements simulated a circle. Circular face machining could then be accomplished on a diameter slightly exceeding the outer-element diameter with no intersection of active fuel orifices or formation of dead-ended passages.

(C)   The oxidizer channels were fed from an external plenum on the opposite side of the injector, as shown in Figure 17. This plenum was smaller in diameter than the active face area to block the outermost ring of oxidizer elements from impinging or spraying directly on the chamber wall. An external plenum was adopted to allow variation of the oxidizer inlet flow and generation of an off-mixture ratio boundary. As seen in Figure 18, a flow distribution ring was inserted inside the oxidizer circuit of the bolt-on manifold cover. These rings, designed to provide the wide variation in boundary mixture ratio discussed in Section IV,A,4, effectively split the incoming oxidizer flow between the main core and the boundary. By starving the oxidizer flow to the boundary, fuel-rich and, thus, cooler boundary combustion was achieved. Boundary mixture ratio variation was achieved by simply replacing the cooling ring. As shall be discussed, these methods of manifolding were
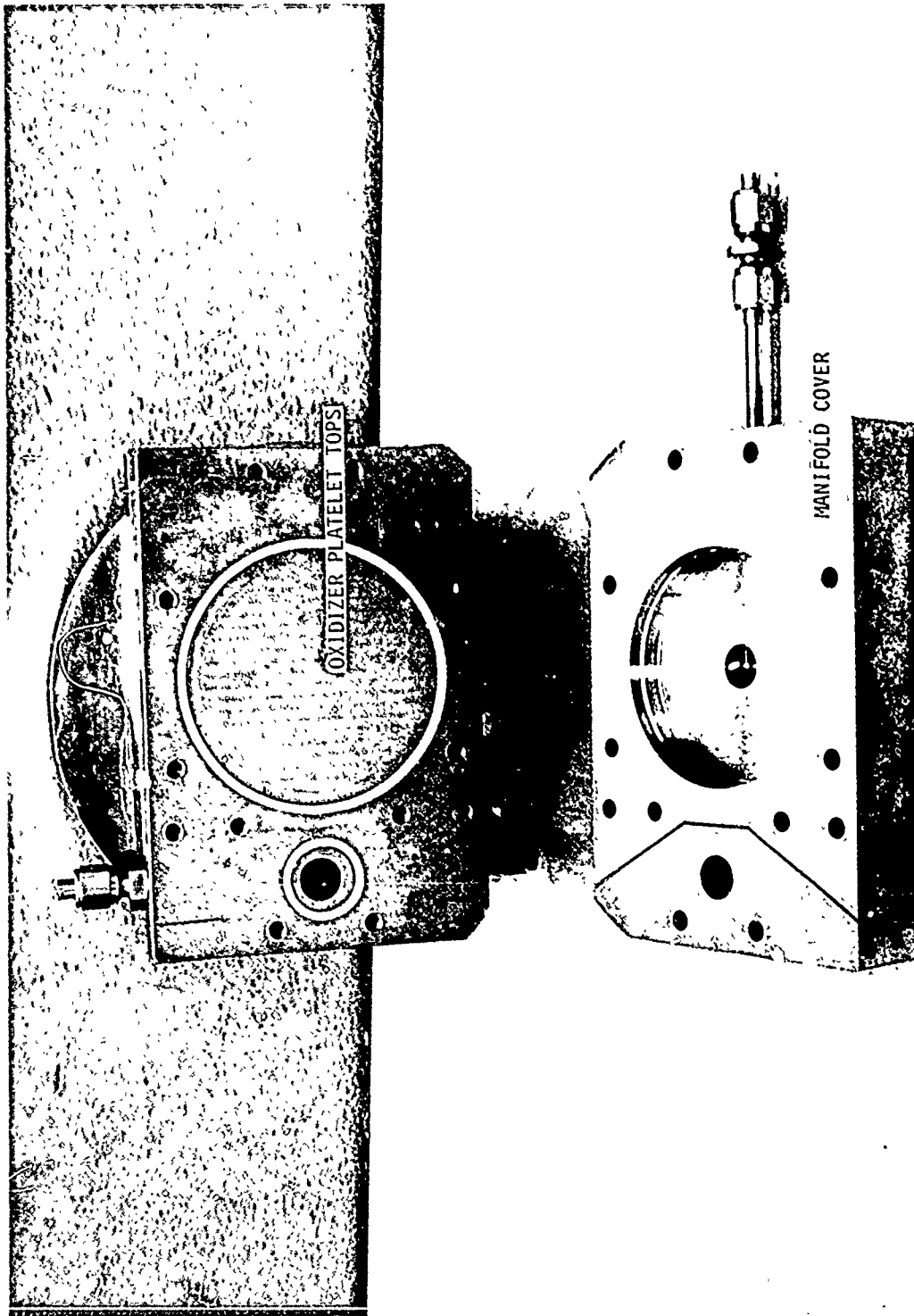
Figure 17. Phase I Injector Manifolding Technique (u)
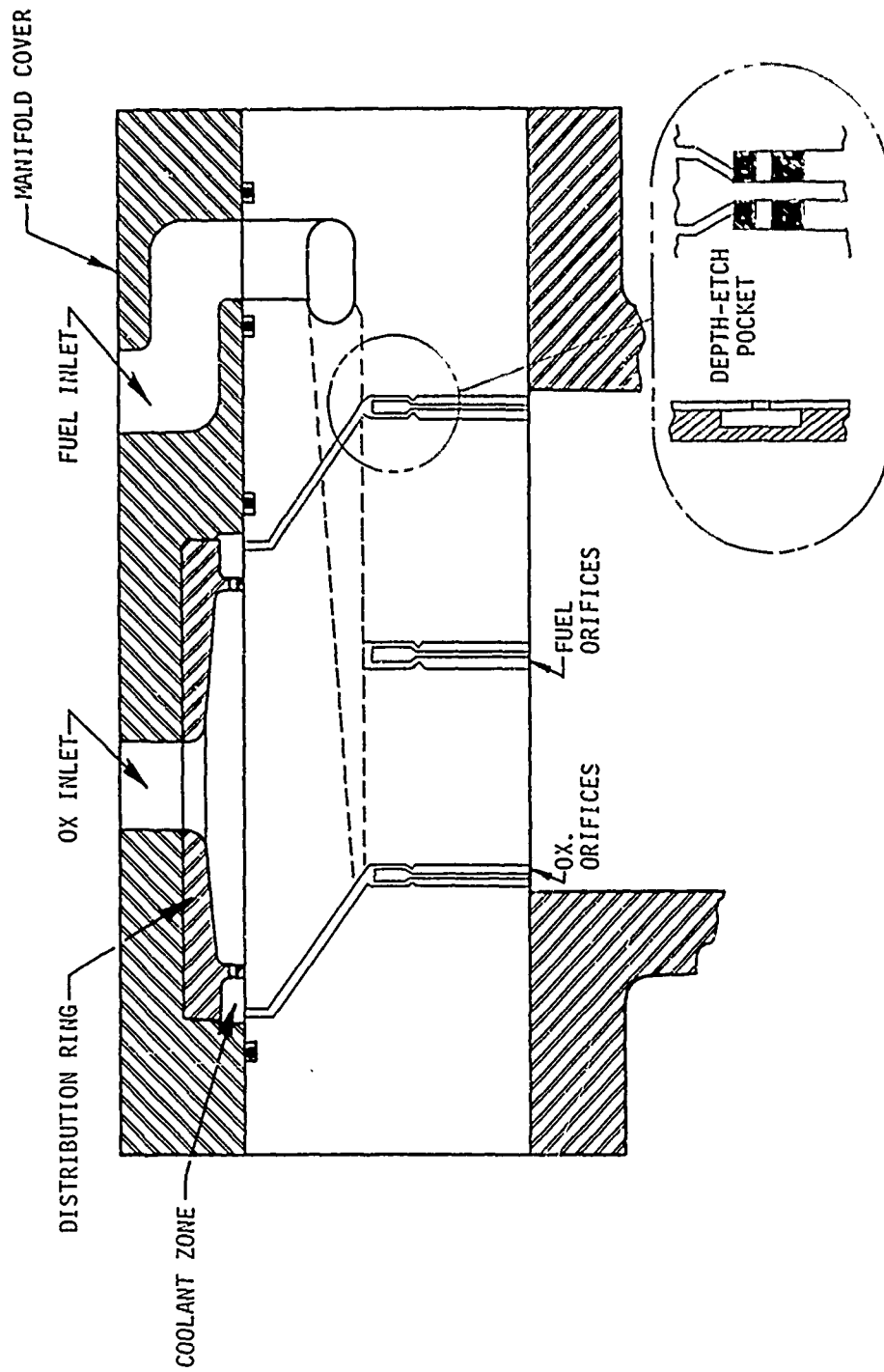
Figure 18. Oxidizer Manifold Flow Distribution Ring (u)

IV, B, Mechanical Design (cont.)

unchanged throughout the program. The use of a separate cooling ring was maintained until optimum cooling conditions had been established.

b. Phase Two Injectors

(C) A completed injector of the phase two design is shown in Figure 19. Corresponding platelets are shown in Figure 20. It is apparent that the greatest change effected in the phase two design was the elimination of the multipurpose component and adoption of a single-level design. This change was practical after test results generated on phase one hardware had allowed selection of near optimum baffle patterns. A second change in the phase two design effort was the elimination of the showerhead injector type. The test results presented in Section VII,A delineate the reasons for this change.

(U) The resulting phase two impinging injector was identical to that of phase one with three exceptions: elimination of the three-level design, elimination of the depth-etched flow transition pockets in the separators, and elimination of the stepped-fuel orifice technique. As shall be discussed in Section V, the former two design modifications were generated to aid in the fabricability of the units. The stepped-fuel orifice design was changed for economic reasons.

c. Final Injector

(C) The design of the final injector is reflected in the platelet drawings of Figure 21. The single-level design of phase two was retained, as was the impinging element and the method of propellant manifolding. The basic changes made in the design were twofold: first, the technique of stepping the fuel platelets to avoid trapped hydrazine was resumed; and second,
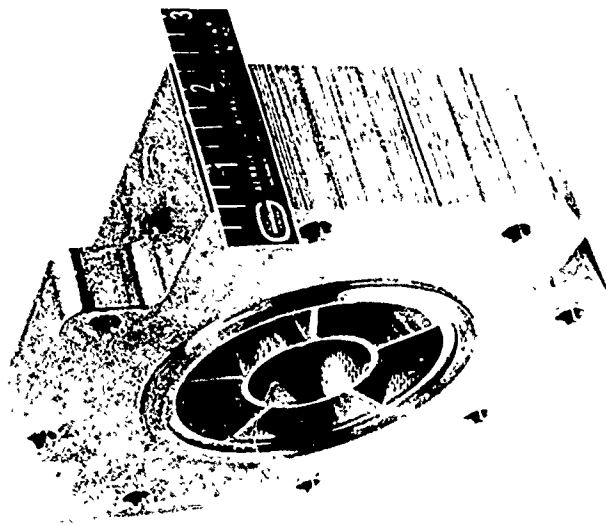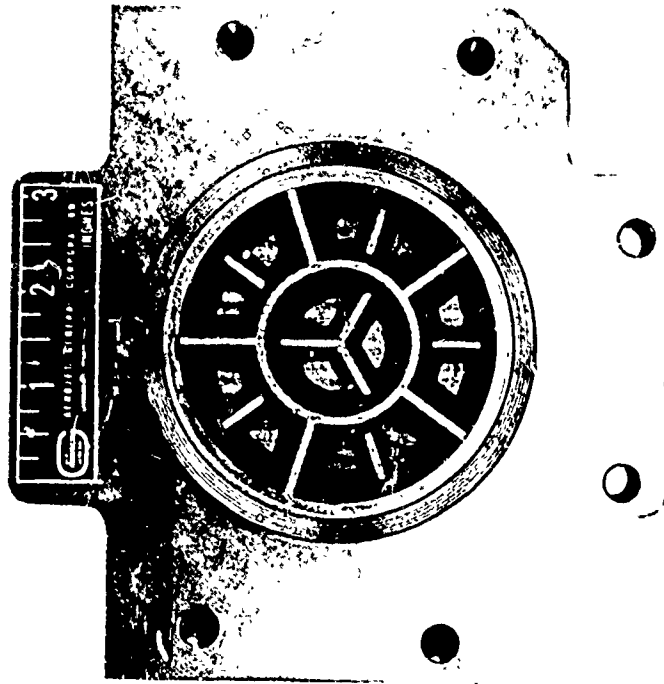
Figure 19. Injector 14-MO (u)
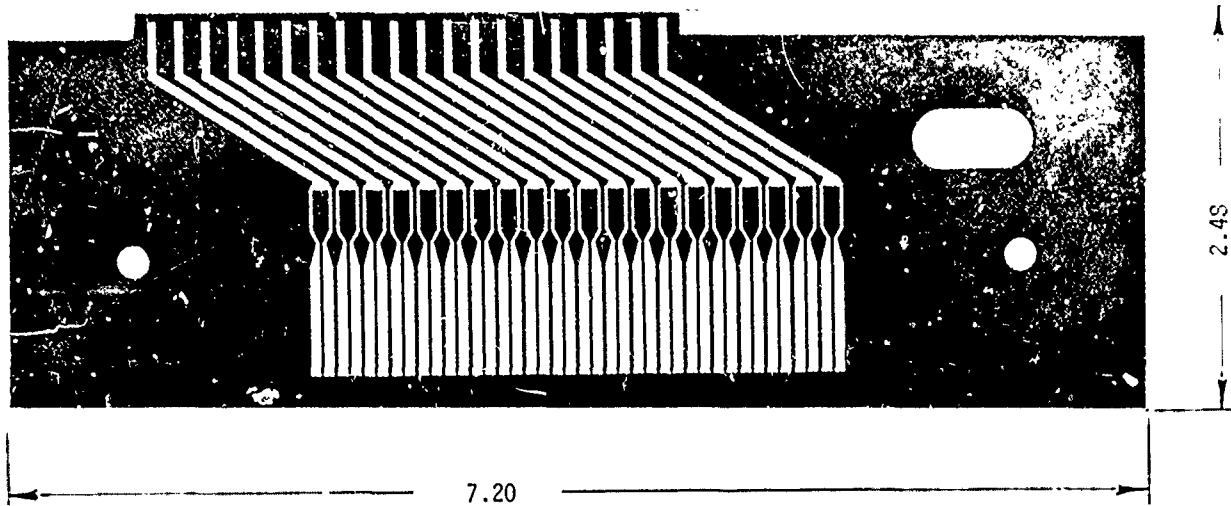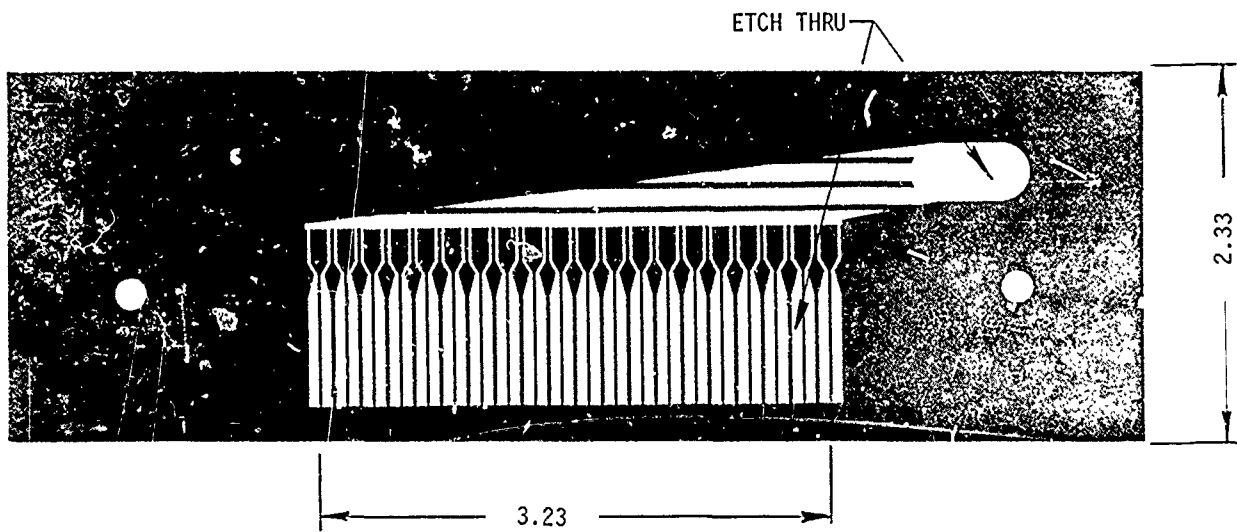
OXIDIZER PLATELET

FUEL PLATELET

Figure 20.   Impinging Injector Subcomponents – Phase II Design (u)
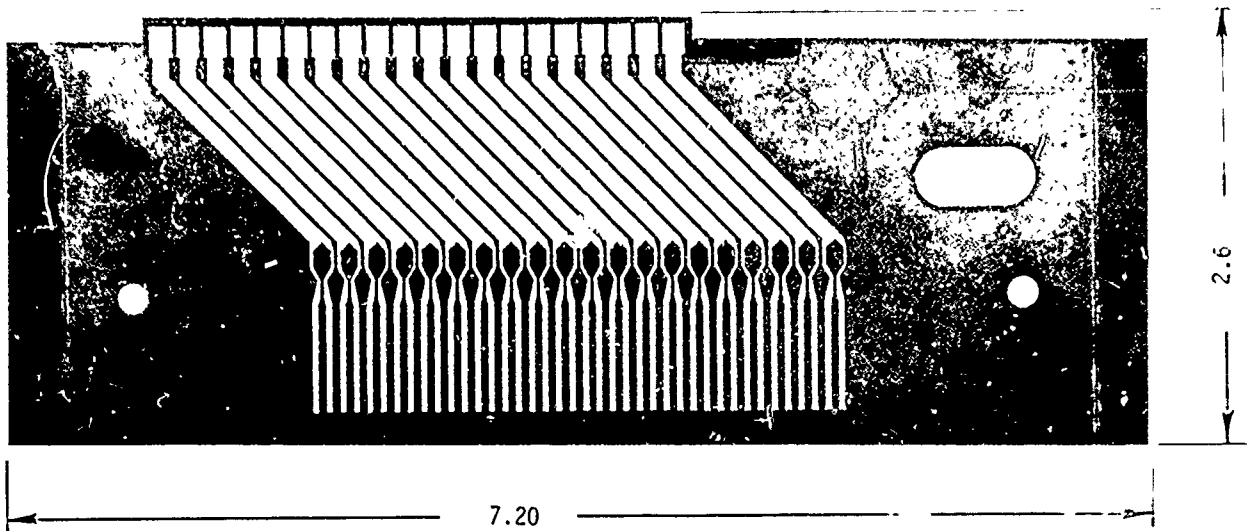
OXIDIZER PLATELET
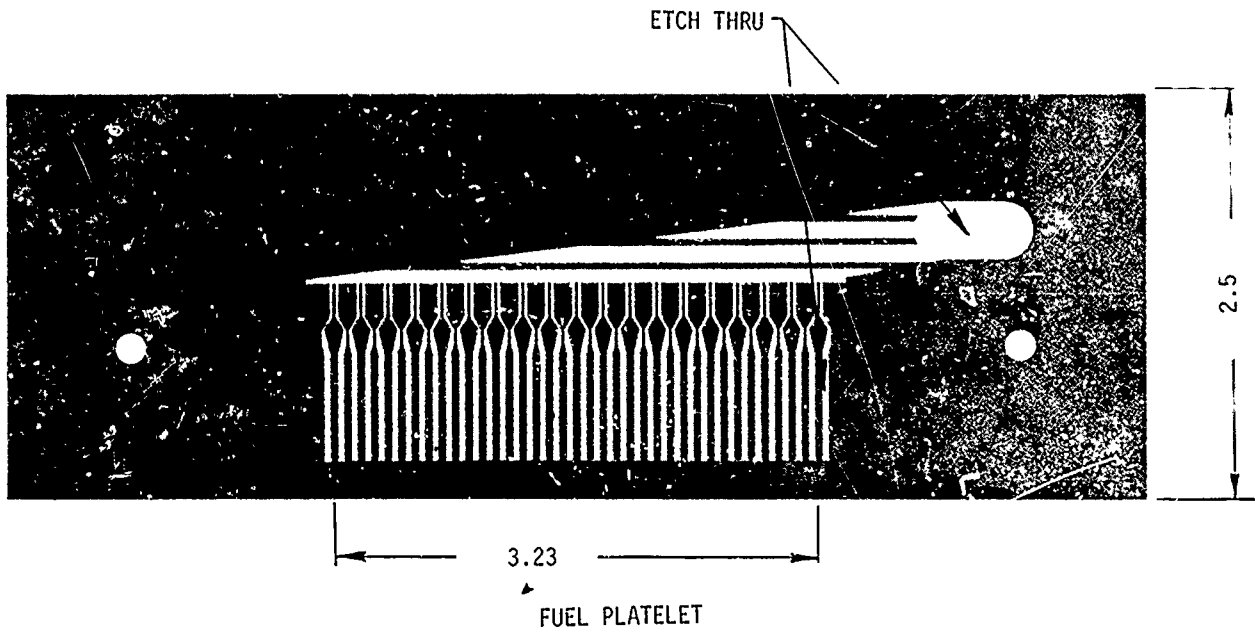
FUEL PLATELET

Figure 21. Impinging Injector Subcomponents - Final Design (u)

IV, B, Mechanical Design (cont.)

the orifice width in the showerhead region was reduced from 0.065 in. to
0.040 in. This latter change was effected to increase the injection velocity,
thus promoting more uniform mixing, and to decrease the unsupported orifice
area between supporting lands (see Section VIII,C). As a result of these
changes, orifice deformation and platelet splitting were eliminated.

(C)   A third change incorporated into the final injector was
in the oxidizer manifold flow distribution ring. Test data generated with
phase one and phase two hardware allowed parametric evaluation of performance
versus boundary cooling. The final injector benefited from this analysis in
that the optimum cooling requirements were known and a fixed cooling ring
could be built into the manifold cover. This change is shown in Figure 22. In
the final injector, sealing between the core and the boundary was obtained
with a knife-edge aluminum crush seal bearing directly on the tops of the
oxidizer platelets.

2. Ancillary Hardware

a. Chambers

(U)   The thrust chambers employed in this program were
designed in reference to specific tasks. Three analytical areas defined the
chamber requirements: stability, performance, and injector/chamber
compatibility. Major details of the chamber designs were unique, depending
upon the analytical task to which the chamber was to be applied. Common to
all chambers was a contraction ratio of 1.67:1 and a sea-level nozzle expan-
sion ratio of 2:1.

(U)   The chamber used during all dynamic stability evaluation
tests is shown in Figure 23. Its detailed design is shown in Figure 24.
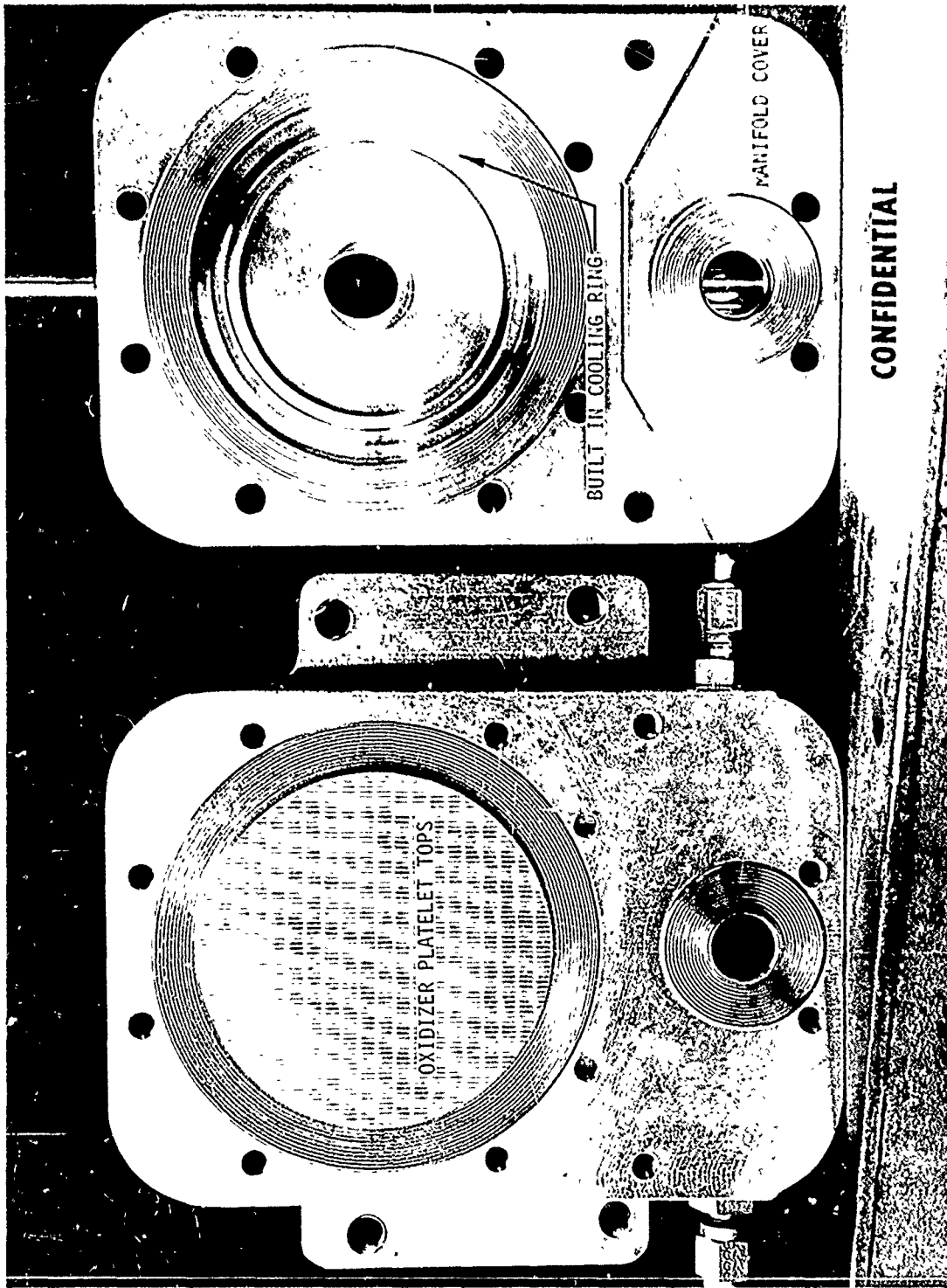
Figure 22. Final Injector Manifolding Technique (u)
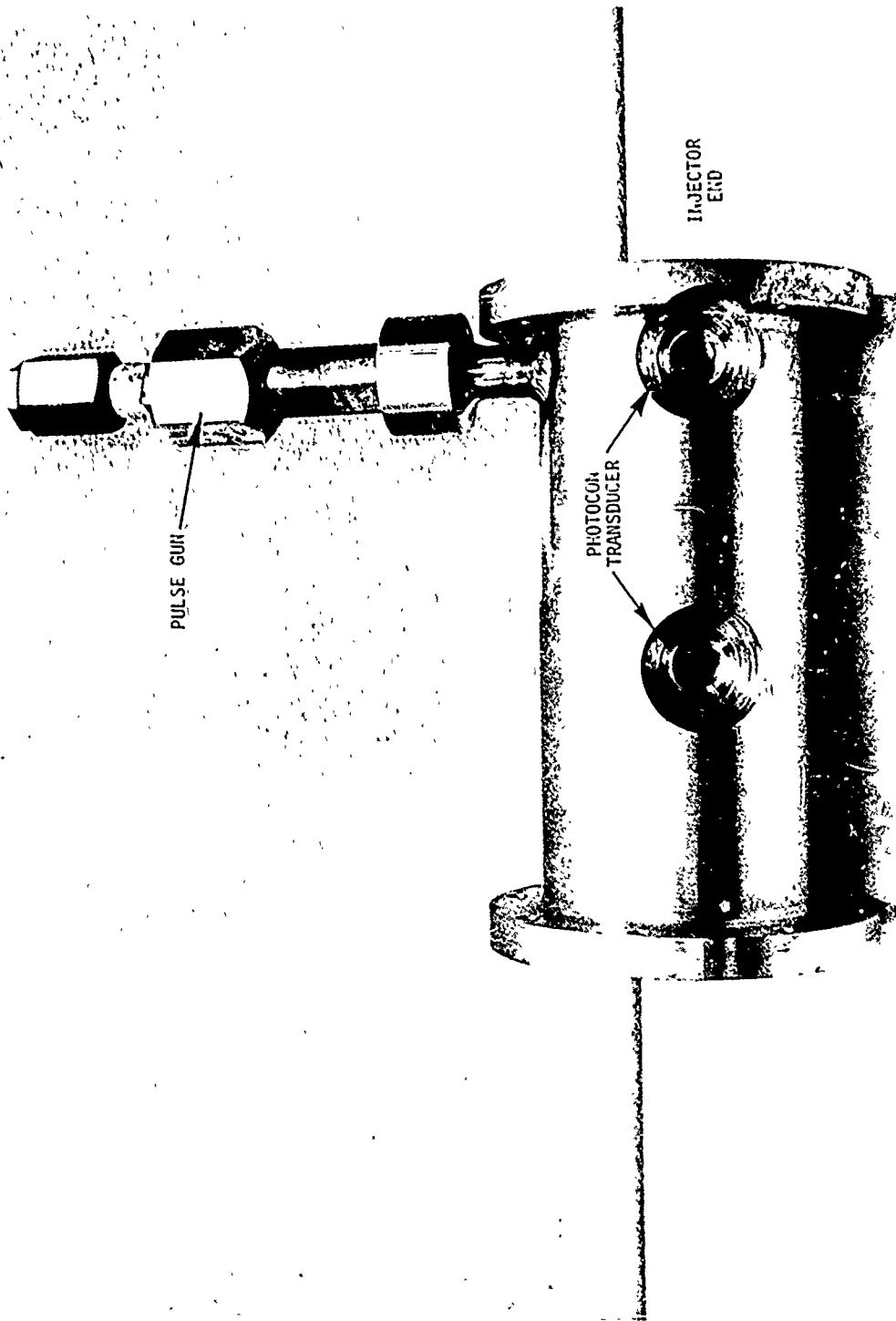
Figure 23. 13 Inch L* Steel Stability Chamber

PULSE GUN

PHOTOCON TRANSDUCER
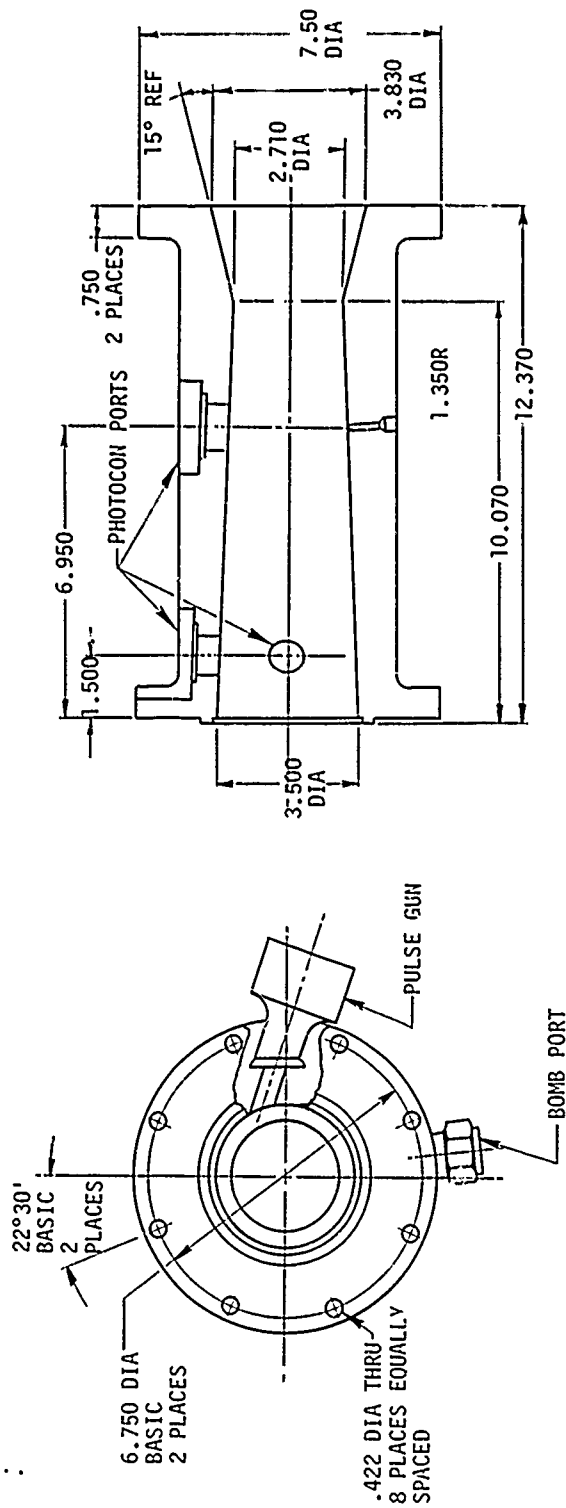
INJECTOR END

Figure 24. Design Details of Stability Chamber

IV, B, Mechanical Design (cont.)

This chamber, made of mild steel, was designed with a long injector-to-throat length (10 in.) to accommodate a full array of stability-evaluating devices. Ports were included for installation of three water-cooled Photocon high-frequency pressure transducers, two of which were coplanar 1.5 in. from the injector in line with an upstream unit. On the side opposite the in-line photocon ports, a pad was provided for installation of an accelerometer. Conventional Tabor pressure transducers were installed for measurement of chamber pressure.

(U)   A tangential pulse gun port and a nondirectional bomb port were included in the steel stability chamber, both located 1.5 in. from the baffle tips. The pulse gun was sized to accommodate Magnum shell casings. The bomb, shown in cross section in Figure 25, was sized to receive 13.5-grain plastic explosive detonators. Since the bomb port was sealed during operation by an external Swage-Loc fitting, it was possible to position the detonator at any point in the chamber from the edge to the injector center. The detonator itself was encased in a Teflon sleeve, the design for which assumed burn-through after 1.5 sec of exposure to the steady-state combustion products. Both the pulse gun and the nondirectional bomb were fired electrically, the pulse being induced normally after 0.5 sec of operation and the bomb at 1.4 sec into the test (thus minimizing possible shrapnel from the Teflon casing).

(U)   Unlike the remaining chambers, the steel stability chamber had a bolt flange at the aft end of the nozzle. This flange was incorporated to allow in-place Photocon calibration through use of a bolt-on nozzle cover plate and to permit attachment of an altitude can for subsequent altitude start tests.
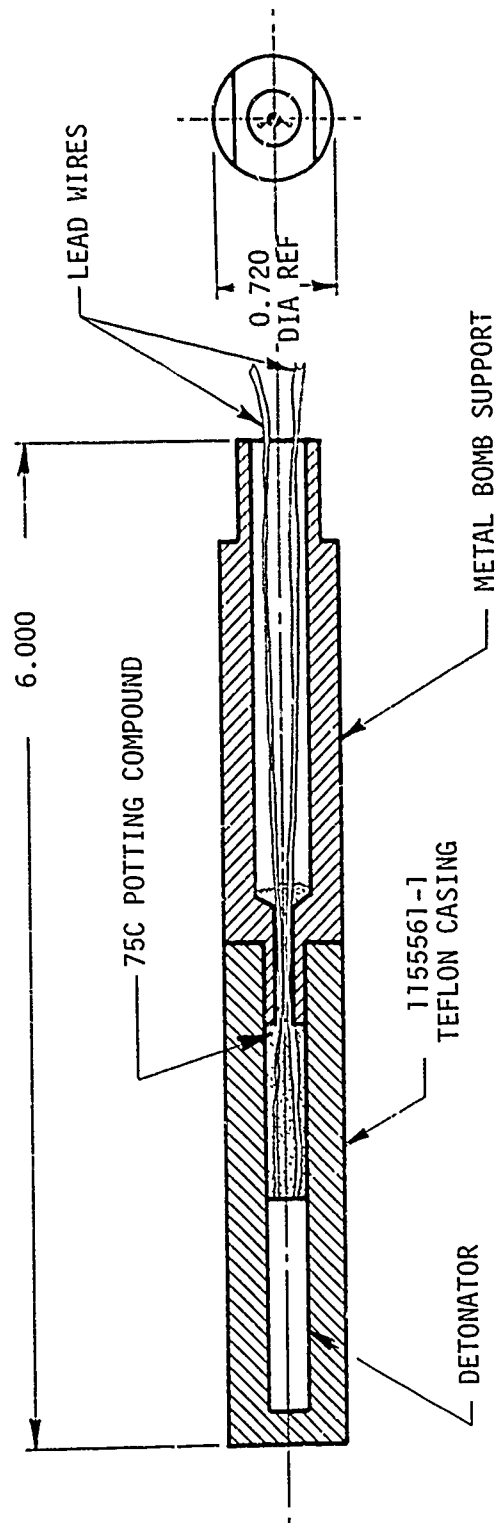
Figure 25. Non-Directional Bomb Design

IV, B, Mechanical Design (cont.)

(U)   A chamber representative of those used in performance analysis is shown in Figure 26. Four chambers were designed for this task. Three were copper; their configuration and dimensions are tabulated in Figure 27. The fourth chamber was of steel and matched the 5-in.-long (injector-to-throat) copper chamber. All performance chambers had provisions for at least two Photocon pressure transducers and one Tabor pressure transducer. The copper chambers were instrumented with 18 gas-side thermocouples; the steel performance chamber was instrumented with six gas-side insulated thermocouples (see Section V,C).

(U)   The performance chambers were used in all tests pertaining to the evaluation of combustion efficiency, characteristic length (L*) effects, or wall temperatures as a function of boundary cooling parameters. The Photocon transducers were monitored; however, the performance tests were not pulsed or bombed.

(U)   The remaining program task--injector/chamber compatibility--was accomplished through use of phenolic streak chambers, one of which is shown in Figure 28. These chambers consisted of conical mild steel shells containing contoured chamber/nozzle liners of WBC 2230 silica phenolic. Provisions were included for monitoring chamber pressure and backside wall temperatures. There were no Photocon ports for evaluation of high-frequency pressure waves, since the injector was fully qualified before the compatibility chambers were designed.

        b.   Bipropellant Valve

(U)   The only remaining design task applicable to this program was the derivation of a thrust chamber valve. Four criteria were used in valve selection: (1) ease of rework, (2) separate and individually controlled valve

Report AFRPL-TR-69-122

Figure 26. 6.5 Inch 1.* Copper Performance Chamber
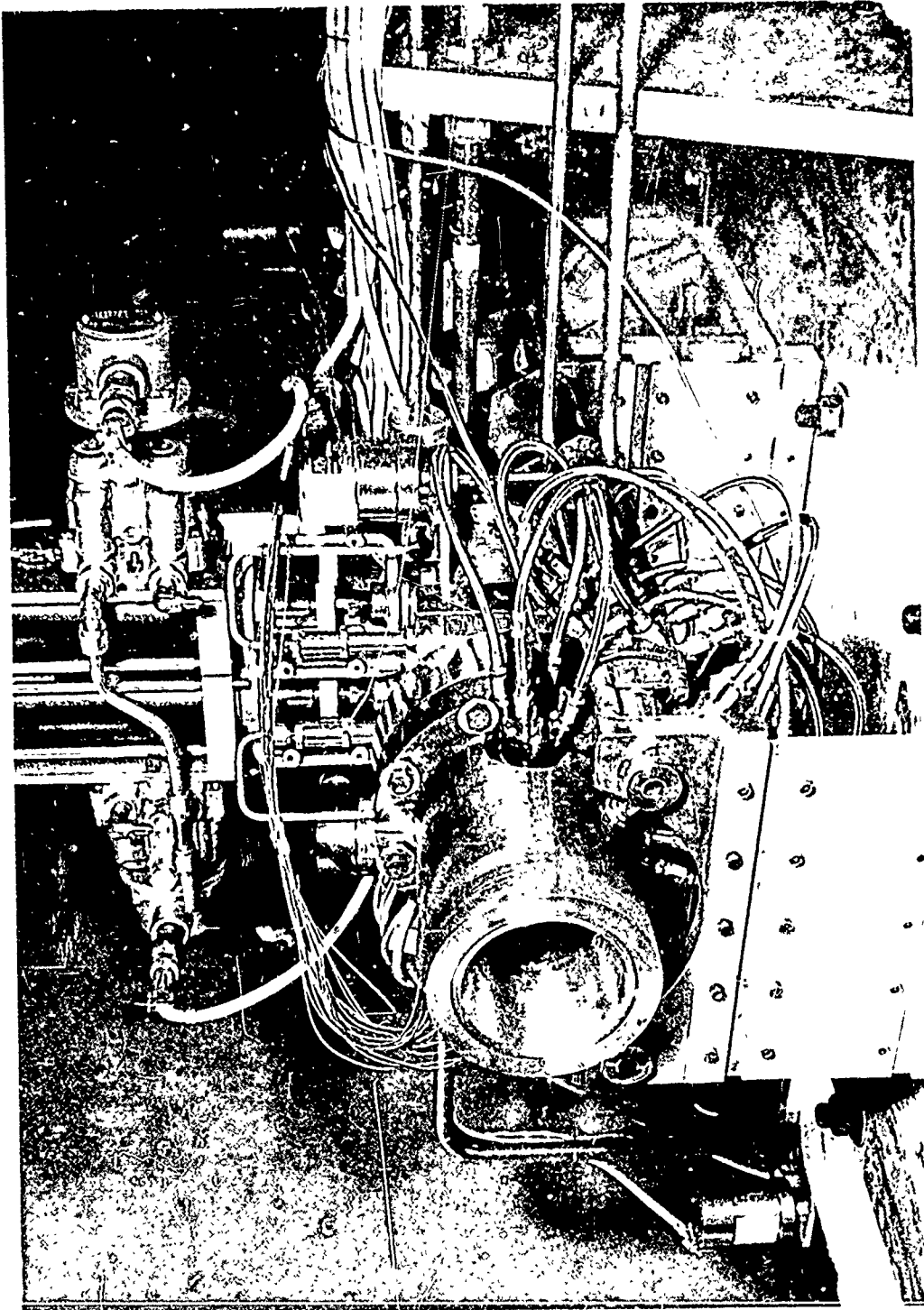
Figure 27. Design Details of Copper Chambers

TABULATION BLOCK					
DASH NO.	L DIM	D ANGLE REF	E ANGLE (±0° 30')	F DIM	G DIM
-1	10.070	2° 16'	2° 16'	6.950	12.370
-2	5.070	4° 30'	4° 30'	3.300	7.370
-3	3.070	7° 30'	7° 30'	-	5.370

THERMOCOUPLE
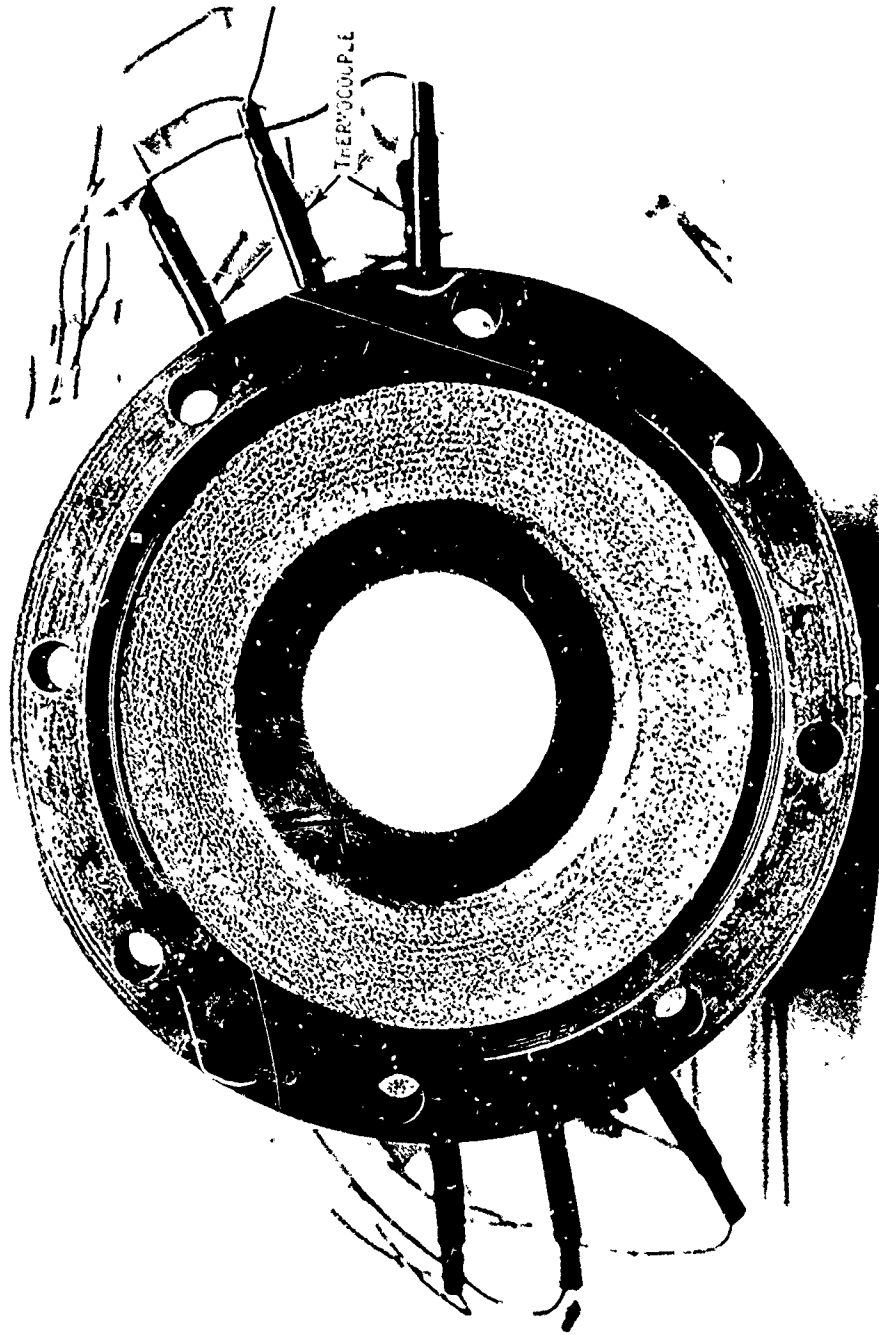
Figure 28. Phenolic Streak Chamber - Forward End

IV, B, Mechanical Design (cont.)

pintles, (3) minimum manifold size, and (4) close coupling between the valve
and the injector. The valve designed and built to satisfy these requirements
is shown in Figure 29. This valve consists of two identical 3/4-in.
pneumatically operated pintle valves. The valve type was selected over the
smaller and lighter conventional bipropellant valves in compliance with the
desire to simplify any required rework or valve modification. Bipropellant
valve characteristics and the associated close coupling with the injector were
achieved by placing both valves in a common body, as shown in Figure 29.
Individual operators were employed on each pintle shaft; provisions were
included, however, for a yoke that could be applied to the shafts, permitting
simultaneous valve actuation should test results deem this feasible.
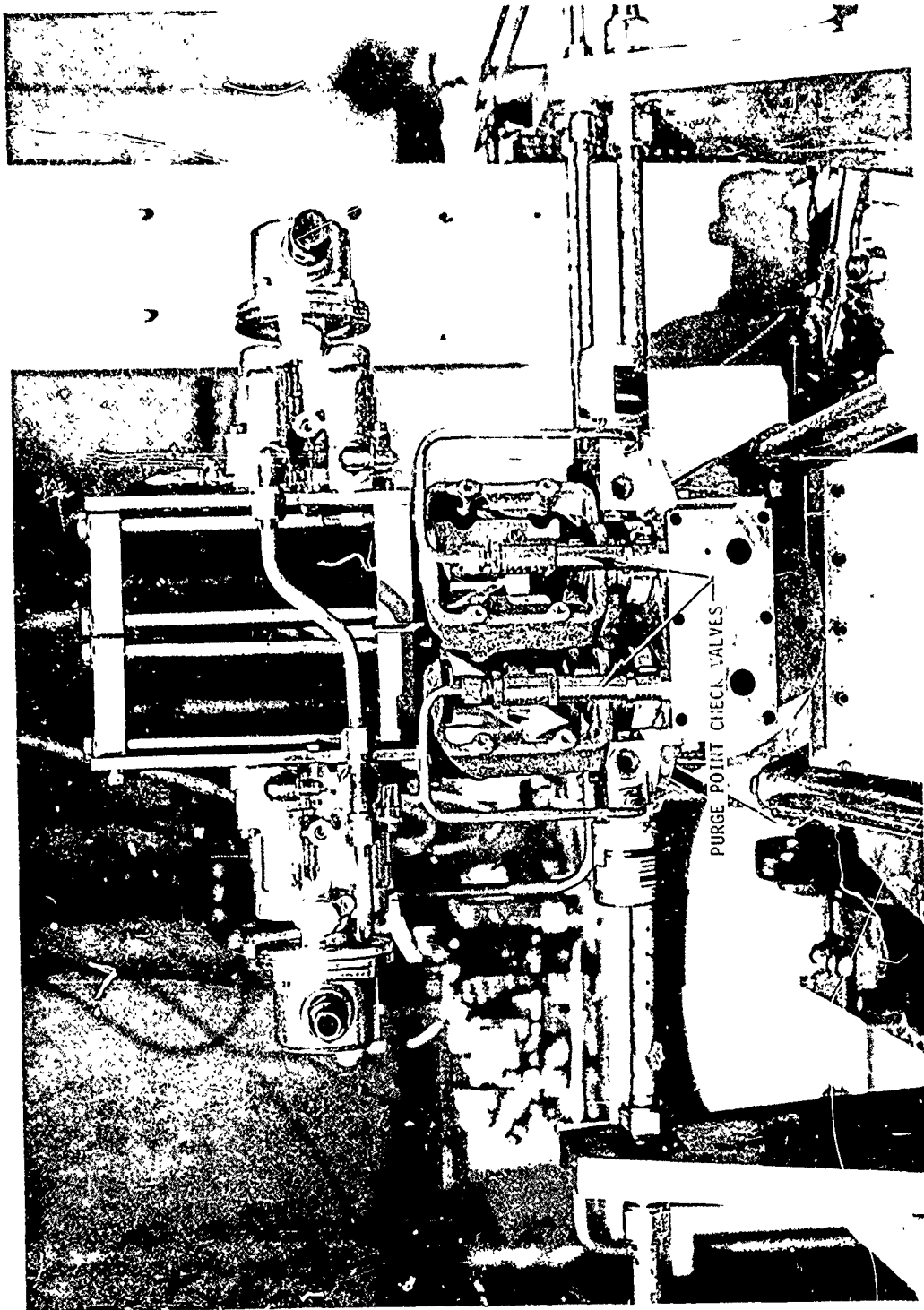
Figure 29. Bipropellant Thrust Chamber Valve

Page 79

SECTION V

FABRICATION

(C)   The primary goal of this program was a demonstration of the operating characteristics of a HIPERTHIN injector when used with the propellants N_2O_4/N_2H_4. Before this demonstration could be accomplished, however, it was first necessary to develop the conceptual hardware. The following paragraphs present a history of the fabrication tasks conducted during the program. The problems encountered in the various areas and their solutions are included.

A.   INJECTOR FABRICATION

(U)   A total of six injectors were completed and tested during this program. Of these, five were impinging units and one was totally showerhead. One showerhead injector and one impinger were lost during the fabrication process. Table II presents a review of the injector fabrication.

(U)   Injector fabrication paralleled injector design in that it progressed through three phases of accomplishment. Assembly of the phase one injector designs was accomplished according to the flow schematic of Figure 30. The problems encountered, both in the design and the manufacturing processes, were influential in formulating the fabrication technique shown in Figure 31. This latter technique, refined in the area of final machining, was employed to produce the final demonstration injector.

1.   Phase One Injector Fabrication

(C)   A view of a completed phase one injector is shown in Figure 32. This unit, designated I1-MO*, was fabricated according to the process schematic of Figure 30. The details of step 1, Figure 30, are more clearly presented in Figure 33. The HIPERTHIN platelet stack consists of alternating fuel and

---

*I1-MO: First impinging injector, no modifications.

TABLE II

INJECTOR FABRICATION RESULTS

Injector SN	Injector Type	Designation	Fabrication Status
001	Impinging	I1	Completed and tested
002	Impinging	I2	Lost in initial braze cycle due to retort failure
003	Impinging	I3	Completed and tested
010	Showerhead	S1	Completed and tested
020	Showerhead	S2	Lost during secondary braze due to interpropellant leaks
004	Impinging	I4	Completed and tested
005	Impinging	I5	Completed and tested
006	Impinging	I6	Completed and tested
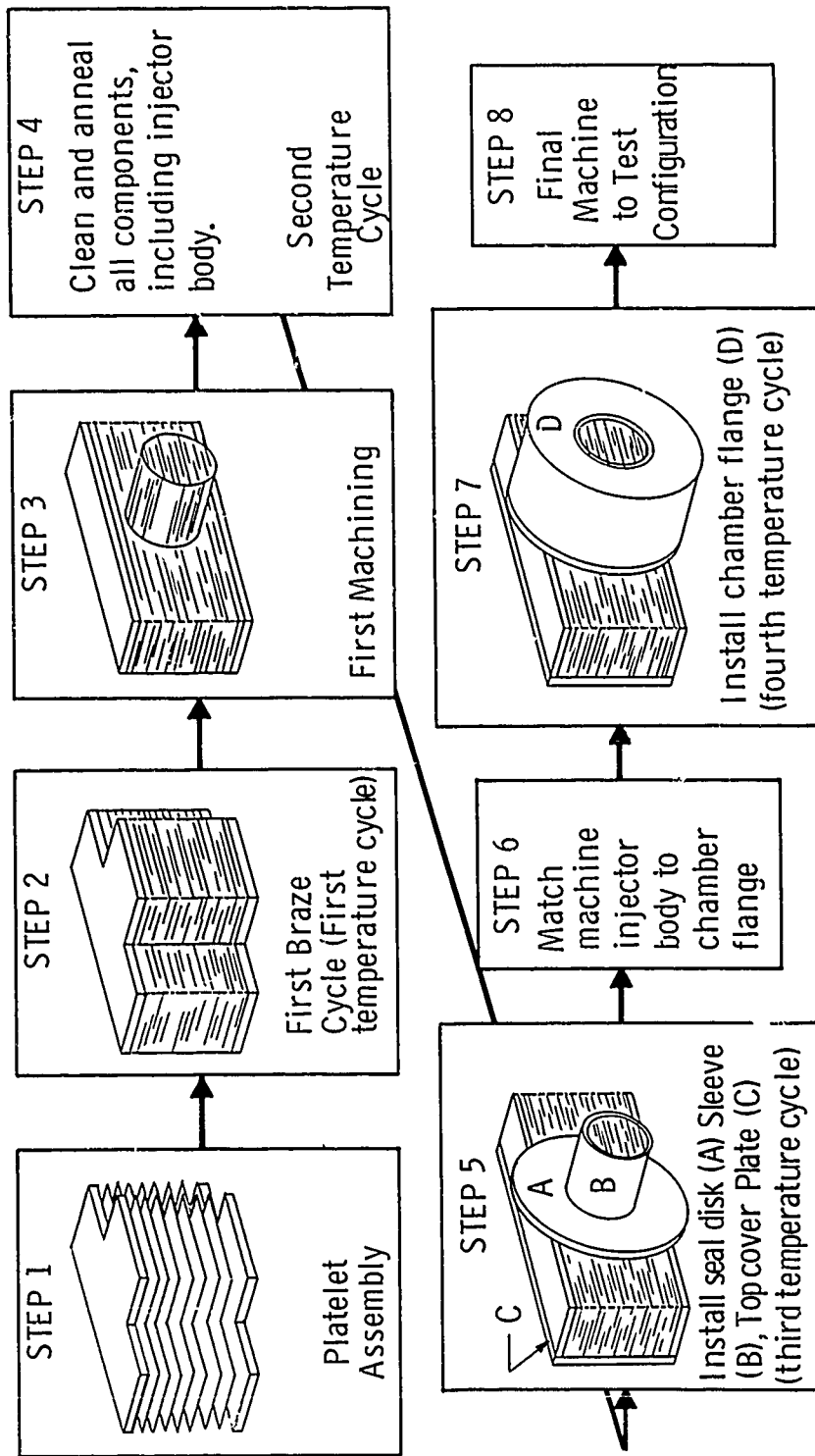
Figure 30. Injector Fabrication Sequence – Phase I Design (u)

Report AFRPL-TR-69-122

FINAL MACHINE
TO TEST
CONFIGURATION

FINAL INJECTOR

PLATELET ASSEMBLY
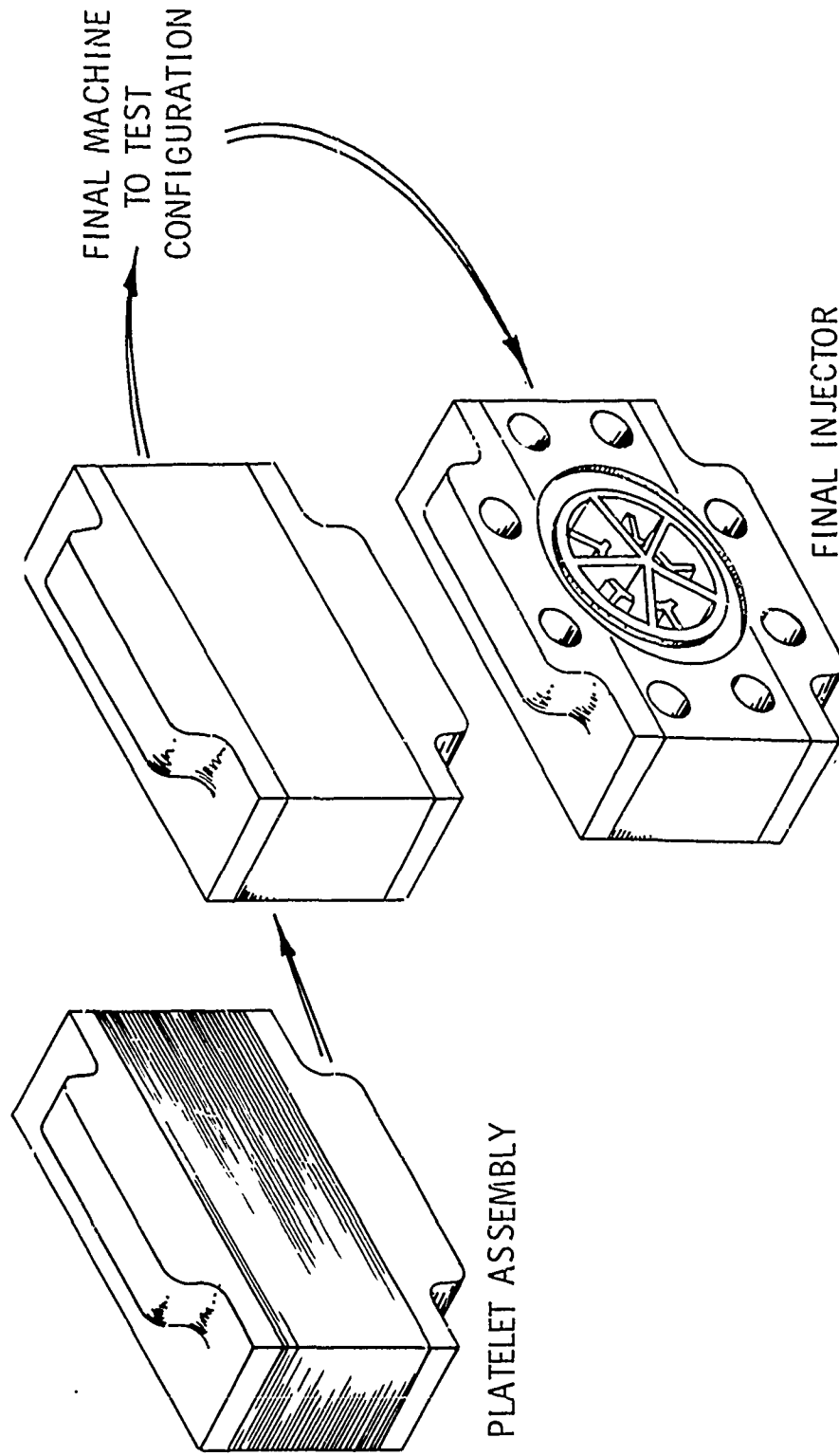
Figure 31.   Injector Fabrication Sequence - Phase II Design (u)

Page 83
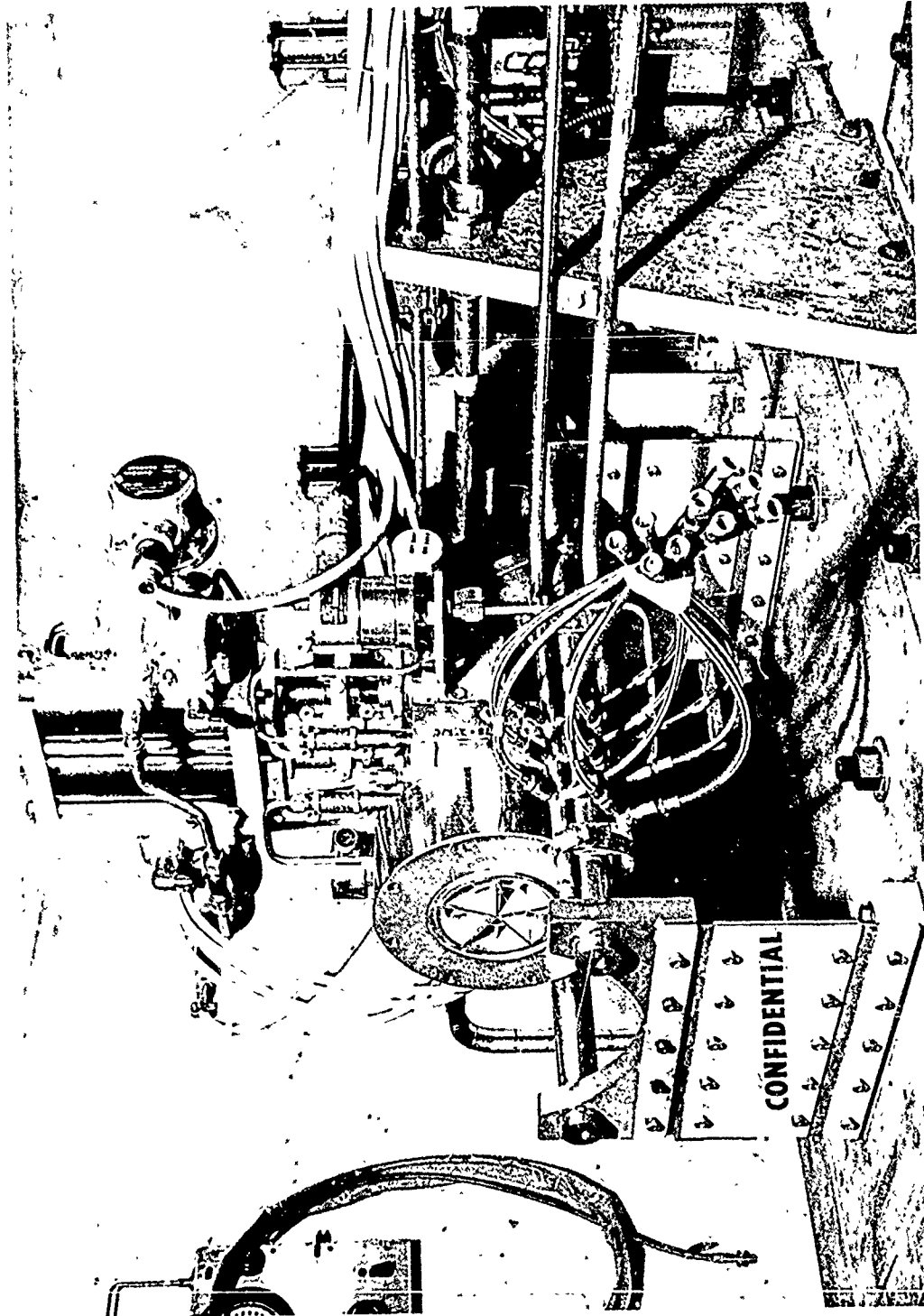
Figure 32. Phase One Injector – I1-MO (u)
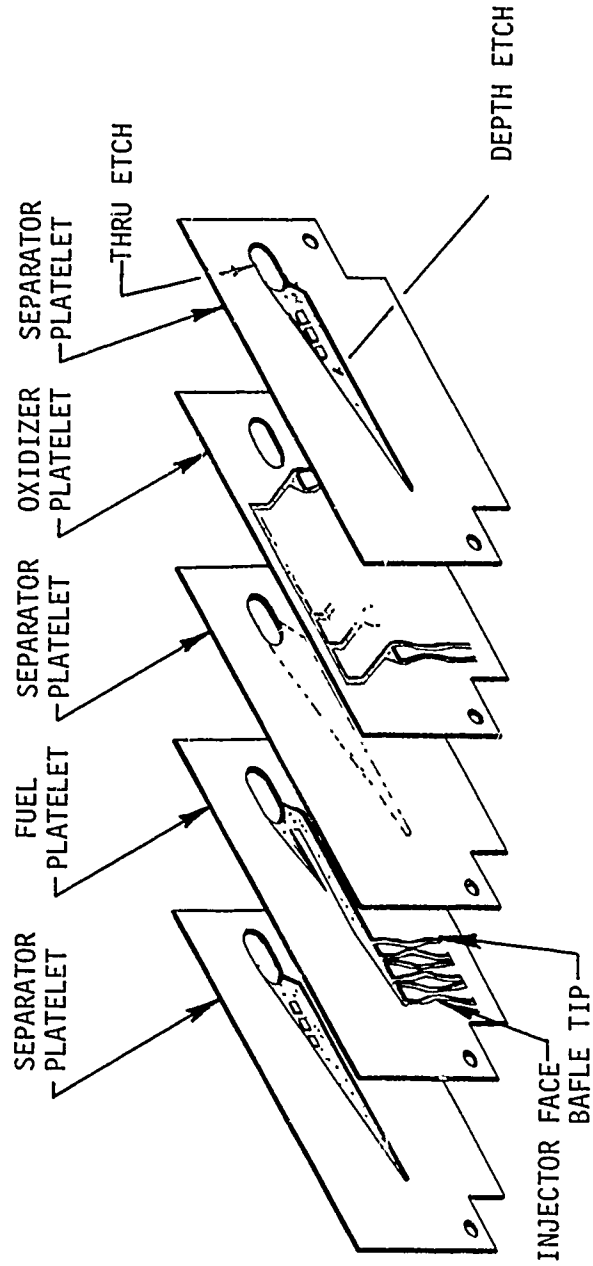
Figure 33. Assembly Sequence (u)

V, A, Injector Fabrication (cont.)

oxidizer metering platelets sandwiched between thicker separator platelets.
The platelet stack itself is sandwiched between end plates, thick in this case
to provide manifold flange material. Blank platelets and braze foil were used
at the platelet stack-to-end plate interface (Section IV,A,5) to prevent
external propellant leaks should unequal postbraze cooldown cause cracks in
this area. Care was taken during the stacking process to eliminate those
platelets possessing either excessive pitting (due to breakdown of the etchant
resist during platelet fabrication) or excessive curl (due to platelet manufac-
ture from rolled sheet stock). As a result of these precautions, there were
no injector failures due to the step 1 process.

(C)   Once stacked, the platelet assembly was strapped and positioned
in a braze retort. Weights and thermocouples were applied, the retort lid was
welded in place, a vacuum was drawn followed by a hydrogen purge, and the unit
was subjected to a time-temperature cycle during which platelet bonding occurred.
This process was completed successfully with one exception. During the brazing
of the second impinging injector (I2-MO), the braze retort burned through,
resulting in the loss of the reducing hydrogen atmosphere and complete oxidation
of the platelet stack. It was subsequently determined that the retort lid had
been improperly welded in place. Future recurrences of this failure were pre-
vented by setting minimum standards on the retorts used for such braze cycles.

(C)   Steps 3 through 7 in Figure 30 were unique in this contract
to the phase one injectors. Identical techniques had been used in previous
injectors of similar diameter, most notably in the fabrication of the larger
preproposal injector for this program. The platelets of the phase one contract
injectors, however, incorporated two changes that were found to be incompatible
with the assembly techniques: a greater face length due to the three-in-one-
design and depth-etched pockets in the separator platelets.

V, A, Injector Fabrication (cont.)

(C)   Both of these changes in platelet design made step 5 of
Figure 30 difficult. Circular machining (step 3) of the impinging injectors
opened direct propellant leak paths to the outside by cutting through the deep
pockets etched into the separator platelets. Injectors I1 and I3 were found
to have bipropellant leaks at the sleeve-to-platelet stack interface after the
first attempt at completing step 5. Both were salvaged by remachining the
round platelet "barrel", thus smearing the braze material over the separator
pockets, and repeating the braze installation of a sleeve and disk. The
resulting double application of braze alloy sealed the leaks but tended to
plug the outer channels.

(C)   Circular machining of the showerhead platelets produced
similar propellant leak paths. In this case, however, the gaps were a result
of the long platelet length and the thin platelet material. Injector S1-MO
was salvaged after step 5 in a manner similar to that used with the impinging
units. Injector S2-MO was scrapped when repeated attempts at completing step 5
were unsuccessful in stopping interpropellant leaks.

(C)   The initial pattern machining, as well as subsequent baffle
modifications, were accomplished using the electric-discharge machining (EDM)
process. Phase two injector fabrication experience identified contamination
problems which were the result of procedures used during the EDM process. It
is suspected, for reasons discussed below, that the phase one units may have
suffered a degree of circuit plugging due to the machining techniques.

(C)   In the transition from the phase one to the phase two injector
designs, the fabrication shortcomings identified were reviewed. It was con-
cluded that (1) the number of braze cycles should be minimized to avoid repeated
thermal stress buildup in the injectors, (2) the use of separate, brazed-on
flanges should be eliminated to remove the requirement for circular machining,

V, A, Injector Fabrication (cont.)

and (3) the platelets should be made as small as possible. The platelets were thus redesigned to the phase two configuration and the assembly procedure shown in Figure 31 was adopted.

2. Phase Two Injector Fabrication

(C)   It may be seen from Figure 31 that the phase two injectors were manufactured with a minimum of steps. The procedures of secondary machining and brazing were eliminated. Two injectors were built to this design: injectors I4 and I5. Both were assembled, brazed, and final machined with no apparent difficulty. Flow tests conducted on the first of these injectors revealed that the oxidizer circuit was partially plugged.

(C)   HIPERTHIN injectors are final machined using the EDM process. This technique consists of removing metal by passing a high-intensity arc between the part and an electrode containing whatever pattern the final unit is to possess. The injectors have been aligned on a base plate, submerged in oil, and machined by bringing the electrode spindle down to meet the injector. It is normal practice to pump oil up through the part to lift from the injector chips of metal and carbon (electrode material) resulting from the machining operation. Because this flushing oil flow is stopped when the electrode is in cutting position, it is necessary to cycle (or lift) the electrode periodically to allow resumption of oil flow and removal of sediment.

(U)   Injector I4 was the first of the phase two injectors to be fabricated. After delivery of the completed unit, water flushes and hydrotests showed the oxidizer circuit to be approximately 80% plugged. Analysis of residue from the circuit showed deposits of carbon and steel inside the injector. Subsequent investigation resulted in the following conclusions. First, final manifold machining had been attempted before the injector face had been fully opened. As a result, there was no oil flow into the majority of oxidizer

V, A, Injector Fabrication (cont.)

orifices during the entire manifold machining process. This fact accounted
for the massive plugging experienced. Second, the machine was set to cut in
60-sec cycles, with flow maintained through the orifices for only 2 to 3 sec.
This cycle was deemed insufficient to remove all the sediment generated in
60-sec of machining. Third, oil pressure to the orifices was held at only
10 to 12 psi. Again, it was felt that increased flush pressure was required.

(U)   Based on these conclusions, a set of machining criteria was
derived and imposed on the machining vendor. In all subsequent operations,
including those conducted on injector I5 and on the final injector (I6), the
injector was mounted on the movable spindle and was lowered to meet a stationary
electrode. This was specified to circumvent particles settling into the injector
due to gravity. Also, it was specified that a maximum cycle time of 30 sec
would be employed, 15 sec of which would consist of orifice flushing. A final
dictate was that, after every 15 min of actual machining time, the injector
would be lifted and subjected to a minimum of 40 psi oil flow. Injectors I5
and I6 were assembled and machined with no anomalies.

(C)   The conclusions pertaining to the current reproducibility of
this hardware are presented later in the report (Sections VIII,A and IX). It
will suffice to say at this point that the ability to successfully fabricate
any number of similar HIPERTHIN injectors has reached a one-for-one basis.
The definition of brazing limitations, platelet characteristic effects, and
machining requirements pertaining to injector cleanliness has resulted already
in the completely successful fabrication of two units, the last of which was
processed from initial design to hydrotest in eleven days.

V, Fabrication (cont.)

B. ANCILLARY HARDWARE

(U)   All ancillary hardware employed on this program was fabricated
according to standard procedures and with no difficulty. The steel stability
chamber and the short steel performance chamber were turned from a billet of
1020 mild steel. The copper performance chambers were similarly turned from
billets of OFHC copper. All fittings applicable to the steel chambers were
welded in place. Instruments were applied to the copper chambers through
tapped ports.

(U)   The retaining can of the phenolic streak chamber was fabricated
of mild steel. The insert itself was tape wrapped and molded with a 45° (to
the centerline) tape orientation. Exterior and interior contours were machined
from the molded billet.

(U)   The calorimetric instrumentation applied to the copper chambers
consisted of 0.020-in.-dia sheathed chromel-alumel thermocouples that were
brazed at the gas-side surface of the heat sink copper chamber. The thermo-
couple installation was accomplished by inserting the 0.020-in.-dia grounded
junction probe in a 0.022-in. hole that had been eloxed through the chamber
wall. The junctions were then positioned flush with the gas-side surface and
furnace brazed using a commercial braze alloy. The above procedure minimized
the disturbance to both gas flow and the wall heat conduction paths.

(U)   The adiabatic wall probes shown in Figure 34 were made from
0.040-in.-dia tungsten-rhenium alloy wire with a tantalum sheath. These were
mounted in a zirconia sleeve and inserted through the chamber wall such that
the top of the probe extended along the wall and slightly into the low-
temperature film barrier. The use of the zirconia plug simulated the behavior
of a refractory wall chamber.

(This page is Unclassified)
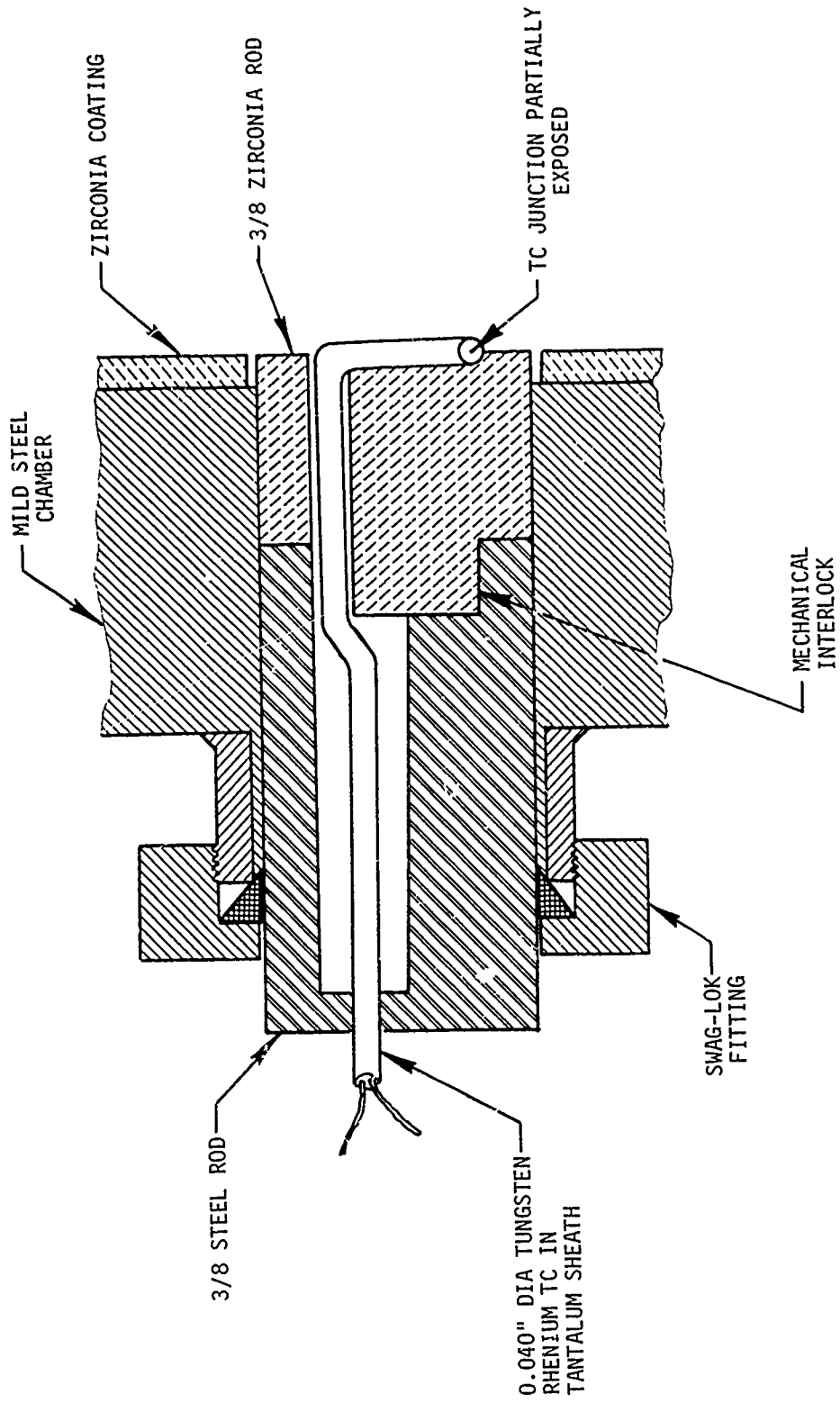
Figure 34. Design Detail of Insulated Tungsten-Rhenium Thermocouples

V, B, Ancillary Hardware (cont.)

(U)   Phenolic chamber instrumentation consisted of twelve depth thermo-
couples. Of these twelve, eight were 20-mil chromel/alumel and four were 40-mil
tungsten/rhenium thermocouples. Holes were drilled into the phenolic liner
material from the can exterior. The thermocouples were then inserted and sealed
in place with welded-on Swage-Loc fittings. X-rays were taken of the chamber
to allow exact determination of the thermocouple junction location.

SECTION VI

EXPERIMENTATION

A. EQUIPMENT AND HARDWARE

1. Thrust Stand

(U)   The thrust stand employed during the entire experimental test phase is shown in Figure 35. Details of the engine mount are also shown in Figure 35. The engine rested on a flexure-mounted table, which in turn was connected to the thrust take-out structural through a 2000-lb load cell. The engine was cantilevered from the valve-injector support; the short chamber lengths precluded the need for additional support. The injector was flush mounted to the valve body, which in turn was fixed on the cradle. This fixed-valve arrangement allowed removal of the chamber or injector/chamber assembly without disconnecting and draining propellant feed lines after each test.

(U)   A schematic of the propellant feed system is shown in Figure 36. All feed lines were 3/4-in. stainless tubing. Propellant was filtered through dual (10 and 2 micron absolute) filters during fill procedures and during the tests by a 10 micron filter located upstream of the dual turbine-type flow meters. A 500 psi GN_2 purge was plumbed into the valve body immediately down-stream of each pintle. Check valves located at the purge inlet points provided automatic purge control during the tests.

(U)   There were no hardening orifices or cavitating flow control venturis employed during the test series. Propellants were pressure fed to the engine, with flow control being derived through consideration of flow rates, line drop, and injector drop.

Report AFRPL-TR-69-122
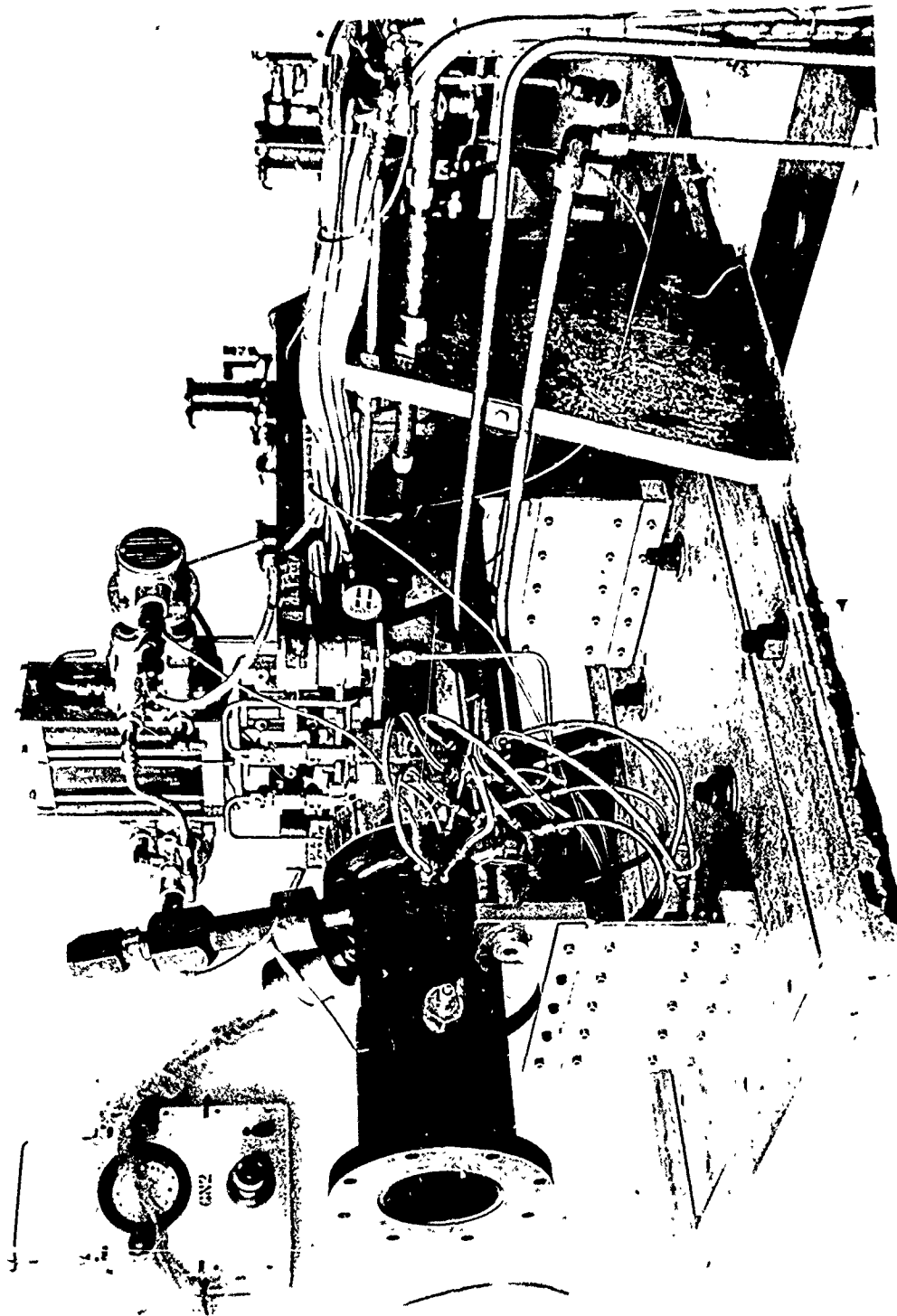
Figure 35. Engine Test Facility

Page 94

Report AFRPL-TR-69-122
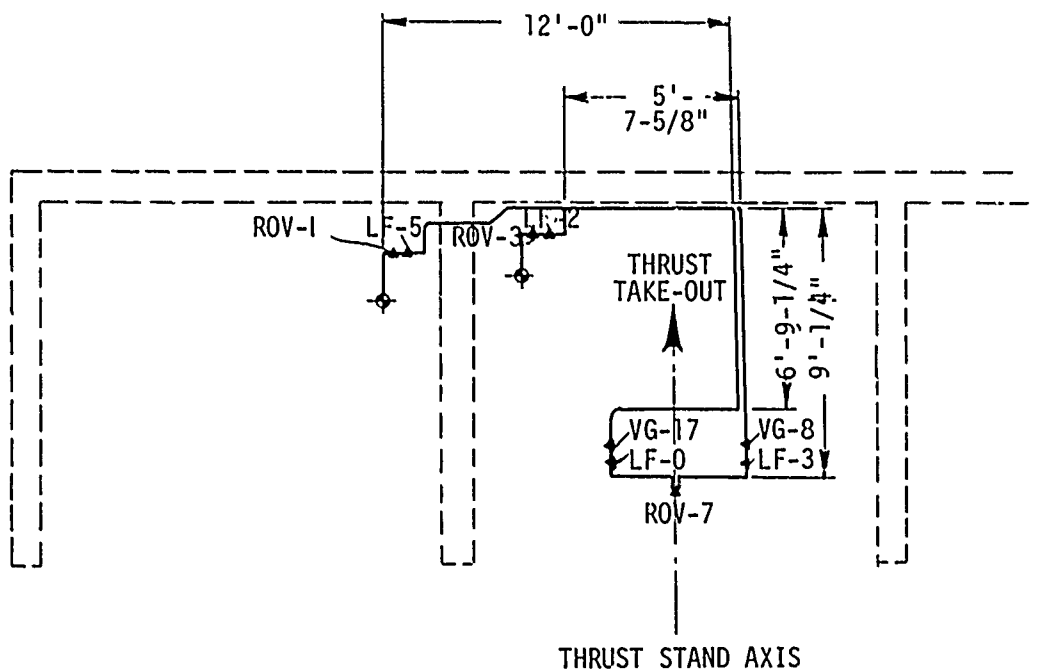
PLAN VIEW
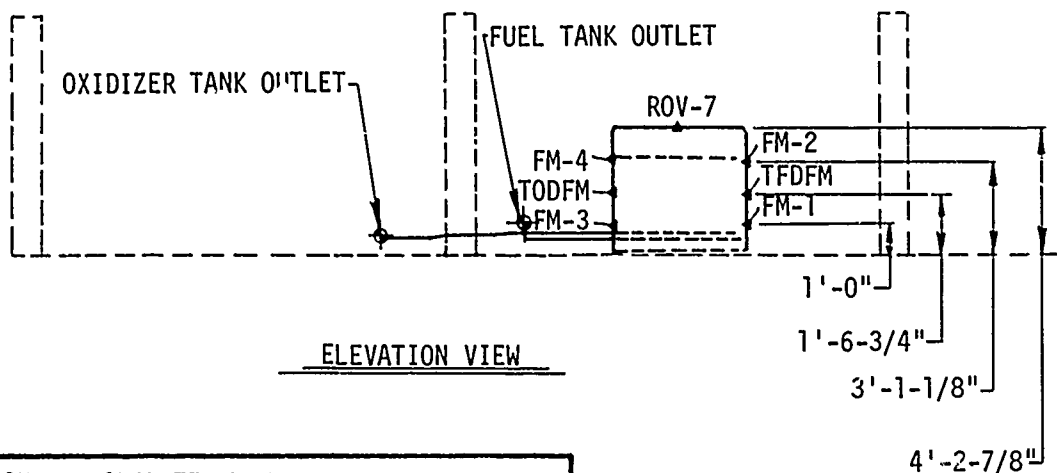
ELEVATION VIEW

OX	– OXIDIZER LINE
F	– FUEL LINE
ROV	– REMOTE OPERATED VALVE
LF	– LINE FILTER
VG	– GATE VALVE (HAND)
FM	– FLOW METER
TODFM–	OXIDIZER TEMPERATURE TRANSDUCER
TFDFM–	FUEL TEMPERATURE TRANSDUCER

Figure 36.   Propellant Feed System Schematic

Page 95

VI, A, Equipment and Hardware (cont.)

2. Instrumentation

(U)   The only thermal instrumentation applicable to the test
facility itself was the thermocouple assembly in each propellant feed line.
These thermocouples, mounted at the downstream (or exit) side of the flow meters,
were used to measure propellant temperature to the injector. No temperature
readings were obtained on the ambient propellant in the run tanks.

(U)   It may be seen from Figure 36 that Tabor pressure transducers
were employed to measure propellant tank pressures, flow meter discharge pres-
sures, injector manifold pressures, and chamber pressure. The pressure data so
obtained were used to determine the system drop as a function of flow rate.
This information was then employed to finalize, or balance, the tank pressures
required to give desired flow rates and chamber pressures.

(U)   High-frequency pressure transducers, or Photocons, were
employed in all but the phenolic streak chambers. The pressure waves picked up
by these transducers were recorded using a Sangamo 3500 FM tape recorder. The
tapes were subsequently played out through either a Hybrid analyzer system (in
which case plots of amplitude versus frequency were obtained) or a galvanometer
to obtain a permanent printed record of the pressure traces.

(U)   All low-frequency pressure data, flow meter data, thrust, and
temperature data were recorded and processed through an IBM 360 (Model 40)
computer. This unit received the digital input and converted it into engineering
units for subsequent analysis.

VI, Experimentation (cont.)

B.   TEST PROGRAM

1.   Test Plan

(U)   The experimental engine firings conducted during this program
were made in a sequence amenable to evaluation of the basic parameters:
stability, performance, altitude start capability, and compatibility. The
majority of tests conducted dealt with stability demonstration since, in the
absence of smooth combustion, all other parameters become academic.

(U)   In all, 100 engine firings were conducted. A tabulated summary
of the tests is presented in Table III. All tests were conducted in the test
facilities located in the Physics Laboratory complex at the Aerojet-General
Corporation in Sacramento. The test phase ranged in time from August 1968
through March 1969.

2.   Test Summaries

(U)   The purpose of this section is to briefly describe the objective
and the results of each of the test conducted. It shall be seen that not all
tests were amenable to complete theoretical evaluation. Reasons for the deletion
of these tests from the analyses described in Section VII will be presented.

a.   Tests 3K-1-101 through 3K-1-105

(U)   The first tests to be conducted on the program employed
an impinging injector designated I1-MO (first impinger, no modifications). The
baffle pattern (Figure 32), located in the first baffle zone (see Section IV,B,1),
consisted of five major radial blades 0.80 in. high, five minor radial blades
0.35 in. high, and a circumferential hub on the half-radius, also of the

TABLE III

HYDRAZINE INJECTOR TEST SUMMARY (u)

Common Engine Data:

Chamber pressure	= 300 psia nominal
Weight flow	= 10.0 lb/sec nominal
Thrust	= 2300 lbf nominal at sea level conditions
Contraction ratio	= 1.67:1
Expansion ratio	= 2:1
High-frequency instrumentation	= 2 Photocon transducers
Line orifices	= None
Line venturis	= None
Cooling parameters at nominal MR	= 1.4

Test No. 3K-1-	Test Date	Duration (sec)	Injector	Chamber	Pulse* (grain-psia)	Bomb (grain)	Mixture Ratio (overall)	Boundary MR	% Coolant Flow	% Coolant Area	Remarks
101	8-23-68	0.5	I1-M0	13 L* Stl	None	None	0.99	None	--	--	--	Stable, no spikes, performance low - contaminated N_2O_4
102	8-23-68	1.1	I1-M0	13 L* Stl	None	None	1.23	None	--	--	--	Performance low - contaminated N_2O_4, no spikes
103	9-19-68	1.5	I1-M0	13 L* Stl	None	None	1.13	None	--	--	--	Pressure spikes, recovery <20 msec
104	9-19-68	1.2	I1-M0	13 L* Stl	None	None	1.28	None	--	--	--	Pressure spikes, recovery <20 msec, started simultaneous propellant shutdown to soften tailoff
105	9-19-68	2.1	I1-M0	13 L* Stl	None	7	1.13	None	--	--	--	Pressure spikes, recovery <20 msec - bomb too small for $\Delta P/P_c = 1.75$ criterion
106	9-20-68	0.5	S1-M0	13 L* Stl	None	None	1.21	None	--	--	--	Rough operation, evidence of intermanifold leak
107	9-20-68	1.0	S1-M0	13 L* Stl	None	None	1.19	None	--	--	--	Intermanifold leak confirmed
108	9-27-68	1.0	I1-M1	13 L* Stl	None	None	1.10	None	--	--	--	No spikes, unstable entire run 7200 Hz ±95 psi
109	9-27-68	1.0	I1-M1	13 L* Stl	10-10K	None	0.82	None	--	--	--	Spikes decay in 100-200 msec, pulse √ $\Delta P/P_c = 1.75$
110	9-27-68	1.0	I1-M1	13 L* Stl	10-10K	None	1.32	None	--	--	--	Decay time in excess of 40 msec, 0.705 in. baffles too short
111	10-5-68	1.0	I1-M2	13 L* Stl	20-10K	None	1.16	None	--	--	--	Stable, no spikes, noise ±25 psi, pulse marginal
112	10-5-68	1.0	I1-M2	13 L* Stl	15-0K	None	1.10	None	--	--	--	Stable, no spikes, noise ±25 psi, pulse unsatisfactory
113	10-5-68	1.0	I1-M2	13 L* Stl	20-10K	None	1.27	None	--	--	--	Stable, noise ±25 psi, pulse marginal

*The figures listed for the pulse tests indicate first the grain size and then the burst pressure rating (in psia) of the burst diaphragm.

TABLE III (cont.)

Test No. 3K-1-	Test Date	Duration (sec)	Injector	Chamber	Pulse (grain-psia)	Bomb (grain)	Mixture Ratio (overall)	Boundary MR	% Coolant Flow	% Coolant Area	Remarks
114	10-5-68	1.0	I1-M2	13 L* Stl	20-10K	None	0.80	None	--	--	Stable, no spikes at low MR, pulse marginal
115	10-10-68	0.75	I1-M2	6.5 L* Cu	None	None	1.35	None	--	--	Stable, no spikes, noise ±25 psi
116	10-10-68	3.0	I1-M2	6.5 L* Cu	None	None	1.36	None	--	--	Stable, no spikes, noise ±25 psi, recovery temperature approximately 5000°F
117	10-10-68	0.75	I1-M2	6.5 L* Cu	None	None	1.16	0.2	17.0	34	Stable, no spikes, noise ±25 psi
118	10-10-68	3.0	I1-M2	6.5 L* Cu	None	None	1.16	0.2	17.0	34	Stable, no spikes, noise ±25 psi, recovery temperature approximately 3700°F
119	10-24-68	3.0	I1-M2	6.5 L* Cu	None	None	1.24	0.5	21.2	34	Stable, recovery temperature approximately 4000-4500°F
120	10-24-68	3.0	I1-M2	6.5 L* Cu	None	None	1.40	0.5	10.0	16	Stable, no spikes
121	10-24-68	3.0	I1-M2	6.5 L* Cu	None	None	1.39	0.5	12.5	20	Stable, no spikes
122	10-24-68	3.0	I1-M2	6.5 L* Cu	None	None	1.35	0.5	14.4	23	Stable, spikes, terminated tests due to baffle splitting
	10-31-68	0.75	I3-MO	13 L* Stl	None	None	1.30	None	--	--	No spikes, 35 msec oxidizer lead, simultaneous shutdown, 600 psi overpressure on start
124	10-31-68	0.75	I3-MO	13 L* Stl	None	None	1.29	None	--	--	Simultaneous valve opening, closing - 1200 psi spike on start
125	10-31-68	0.75	I3-MO	13 L* Stl	None	None	1.18	None	--	--	35 msec fuel lead, simultaneous shutdown - audibly hard start
126	10-31-68	0.75	I3-MO	13 L* Stl	15-20K	13.5	1.18	None	--	--	Test invalid, bomb blew out of chamber on start
127	11-1-68	1.1	I1-M3	13 L* Stl	20-20K	None	1.23	None	--	--	No spikes, roughness increased due to absence of center, minor radial blades
128	11-1-68	1.1	I1-M3	13 L* Stl	20-20K	None	0.79	None	--	--	No spikes, decay <40 msec, noise ±40 psi
129	11-7-68	0.5	I3-M1	13 L* Stl	None	None	1.18	None	--	--	No spikes, noise level ±35-40 psi
130	11-7-68	0.5	I3-M1	13 L* Cu	None	None	1.13	None	--	--	Same as previous test: chamber ineffective in reducing noise
131	11-7-68	1.6	I1-M3	13 L* Stl	None	13.5	1.24	None	--	--	Bomb satisfactory, CF/F_c = 1.96, no shrapnel damage to injector
132	11-13-68	0.5	I3-M2	13 L* Stl	None	None	1.08	None	--	--	Center blades, no minor radial blades, spikes, noise ±40 psi
133	11-13-68	0.5	I3-M2	13 L* Stl	None	None	1.08	None	--	--	Same as -132

TABLE III (cont.)

Test No. 3K-1-	Test Date	Duration (sec)	Injector	Chamber	Pulse (grain-psia)	Bomb (grain)	Mixture Ratio (overall)	Boundary MR	% Coolant Flow	% Coolant Area	Remarks
134	11-20-68	1.0	11-M4	13 L* Stl	None	None	1.07	None	--	--	Spikes, decay <40 msec, noise ±30 psi
135	11-21-68	0.5	11-M5	13 L* Cu	None	None	1.12	None	--	--	Removed baffle tip pockets, spikes, noise ±30 psi, T_{fuel} = 58°F
136	11-21-68	0.5	11-M5	13 L* Cu	None	None	1.13	None	--	--	Same as -13', T_{fuel} = 90°F
137	11-22-68	0.5	11-M6	13 L* Stl	None	None	1.23	None	--	--	No spikes, noise ±25 psi (same as 11-M2)
138	11-22-68	0.5	11-M6	13 L* Stl	20-20K	None	1.22	None	--	--	Same as -137, dynamical stable
139	11-26-68	1.6	11-M6	13 L* Stl	20-20K	None	1.22	None	--	--	No spikes, pulse decay <40 msec, noise ±25 psi
140	11-26-68	1.6	11-M6	13 L* Stl	None	13.5	1.23	None	--	--	Same as -139
141	12-1-68	0.3	11-M6	4 L* Cu	None	None	--	--	--	--	Checkout test - no data taken
142	12-12-68	3.1	11-M6	4 L* Cu	None	None	1.44	None	--	--	No spikes, stable, noise ±25 psi
143	12-12-68	3.1	11-M6	4 L* Cu	None	None	1.29	0.2	17.0	34	Unstable 7000 Hz, ±70 psi
144	12-12-68	3.1	11-M6	4 L* Cu	None	None	1.34	0.5	21.2	34	Unstable 7000 Hz, ±65 psi
145	12-12-68	3.1	11-M6	4 L* Cu	None	None	1.47	0.5	14.4	23	Unstable 7000 Hz, ±80 psi
146	12-12-68	3.1	11-M6	4 L* Cu	None	None	1.49	0.5	12.5	20	Unstable 7000 Hz, ±60 psi
147	12-12-68	3.1	11-M6	4 L* Cu	None	None	1.44	None	--	--	Stable, No spikes, noise ±35 psi
148	12-12-68	3.1	11-M6	6.5 L* Cu	None	None	1.38	0.5	14.4	23	Unstable 7000 Hz, ±70 psi
149	12-16-68	1.5	11-M6	6.5 L* Cu	None	None	1.33	0.5	21.2	34	Unstable 7000 Hz, ±60 psi - insulated T/Cs - T_{throat} = 3500°F
150	12-16-68	1.5	11-M6	13 L* Stl	None	None	1.35	0.5	21.2	34	Unstable 7000 Hz, ±50 psi
151	1-13-69	0.3	11-M6	13 L* Stl	None	None	1.20	None	--	--	Stable, noise ±30 psi, simulated altitude start
152	1-13-69	0.3	11-M6	13 L* Stl	None	None	1.18	None	--	--	Simulated altitude start
153	1-14-69	0.3	11-M6	1, L* Stl	None	None	1.18	None	--	--	Simulated altitude start, vacuum can added
154	1-15-69	0.5	15-M2	6.5 L* Cu	None	None	1.14	None	--	--	First test Phase II injector design, stable spike on start, no roughness after start
155	1-15-69	3.0	15-M0	6.5 L* Cu	None	None	1.10	None	--	--	Rough operation with spikes
156	1-15-69	1.0	15-MC	6.5 L* Cu	None	None	1.10	None	--	--	Rough with spikes. Postfire examination sawed injector split under seal serrations Ground serrations off, with epoxy

TABLE III (cont.)

Test No. 3K-1-	Test Date	Duration (sec)	Injector	Chamber	Pulse (grain-psia)	Bomb (grain)	Mixture Ratio (overall)	Boundary MR	Z Coolant Flow	Z Coolant Area	Remarks
157	1-21-69	1.0	15-M0	6.5 L* Cu	None	None	1.08	None	--	--	Rough with spikes, noise ±30 psi
158	1-28-69	1.0	15-M1	6.5 L* Cu	None	None	1.21	None	--	--	Reduced number of spikes, noise between spikes ±15 psi
159	1-28-69	1.0	15-M1	6.5 L* Cu	None	None	1.21	None	--	--	No spikes, rough operation, ±30 psi
160	1-30-69	1.0	15-M2	6.5 L* Cu	None	None	1.20	None	--	--	No spikes, noise level ±40 psi
161	2-7-69	0.8	15-M3	6.5 L* Cu	None	None	1.19	None	--	--	Spikes, noise level ±50 psi, hub diameter = 1.1 in.
162	2-7-69	0.8	15-M3	6.5 L* Cu	None	None	1.20	None	--	--	Rough with intermittent spikes
163	2-11-69	1.0	15-M3	6.5 L* Cu	None	None	1.01	None	--	--	Unstable 7500 Hz, ±150 psi N_2O_4/MMH
164	2-11-69	1.0	15-M3	6.5 L* Cu	None	None	1.10	None	--	--	Same as -163
165	2-11-69	0.5	13-M3	6.5 L* Ca	None	None	1.18	None	--	--	Flat-faced injector, unstable 8000 Hz, ±150 psi, N_2O_4/MMH
166	2-14-69	0.5	14-M1	13 L* Stl	None	None	1.21	None	--	--	Stable, no spikes, noise ±6 psi
167	2-14-69	0.5	14-M1	13 L* Stl	None	None	1.21	None	--	--	Same as -166
168	2-14-69	0.5	14-M1	13 L* Stl	None	None	1.21	None	--	--	Attempted vacuum start, purges left on prefire
169	2-14-69	0.5	14-M1	13 L* Stl	None	None	1.21	None	--	--	Same as -168, attempted fuel start
170	2-14-69	0.5	14-M1	13 L* Stl	None	None	1.21	None	--	--	Oxidizer lead altitude start, no over-pressure, noise ±6 psi
171	2-14-69	0.5	14-M1	13 L* Stl	None	None	1.21	None	--	--	Attempted fuel lead altitude start, blew bomb plug from chamber
172	2-18-69	0.5	14-M1	6.5 L* Cu	None	None	1.23	None	--	--	No spikes, ±6 psi noise level
173	2-18-69	0.5	14-M1	6.5 L* Cu	None	None	1.49	None	--	--	One spike, smooth otherwise
174	2-18-69	0.5	14-M1	6.5 L* Cu	None	None	0.86	None	--	--	Smooth, no spikes
175	2-18-69	4.0	14-M1	6.5 L* Cu	None	None	1.18	0.5	21.2	34	Six spikes, smooth between, T_{fuel} = 49 to 101°F
176	2-18-69	4.0	14-M1	6.5 L* Cu	None	None	1.18	0.5	21.2	34	One spike, T_{fuel} = 60 to 105°F
177	2-18-69	4.0	14-M1	6.5 L* Cu	None	None	0.98	0.5	21.2	34	Twelve spikes, T_{fuel} = 75 to 108°F
178	2-18-69	4.0	14-M1	6.5 L* Cu	None	None	0.93	0.5	21.2	34	Two spikes, T_{fuel} = 80 to 109°F
179	2-26-69	4.0	14-M1	6.5 L* Cu	None	None	1.20	0.5	21.2	34	Two spikes last second, decay 20 msec, T_{fuel} = 53 to 97°F

TABLE III (cont.)

Test No. BK-1-	Test Date	Duration (sec)	Injector	Chamber	Pulse (grain-psia)	Bomb (grain)	Mixture Ratio (overall)	Boundary MR	% Coolant Flow	% Coolant Area	Remarks
180	2-26-69	0.5	15-M4	6.5 L* Cu	None	None	1.07	0.5	21.2	34	Spikes, noise level ±30 psi
181	2-26-69	0.5	11-M7	6.5 L* Cu	None	None	1.21	0.5	21.2	34	Resonator included - test invalid, Unstable 7000 Hz
182	3-14-69	4.0	14-M2	6.5 L* Cu	None	None	1.19	0.5	21.2	34	Four spikes, noise level ±6 psi
183	3-18-69	4.0	14-M2	6.5 L* Cu	None	None	1.23	0.5	21.2	34	Spikes during first second, noise level ±6 psi
184	3-20-69	0.5	16-M0	6.5 L* Cu	None	None	--	--	--	--	Checkout test final injector, no data taken
185	3-20-69	4.0	16-M0	6.5 L* Cu	None	None	1.04	0.5	21.2	34	No spikes, noise ±6 psi, performance test
186	3-20-69	4.0	16-M0	6.5 L* Cu	None	None	0.86	0.5	21.2	34	Same as -185, performance test
187	3-20-69	4.0	16-M0	6.5 L* Cu	None	None	1.40	0.5	21.2	34	Same as -185, performance test
188	3-20-69	5.0	16-M0	6.5 L* Cu	None	None	1.16	0.5	21.2	34	Same as -185, shutdown on thermocouple trip (1920°F)
189	3-21-69	1.5	16-M0	13 L* Cu	None	None	1.23	0.5	21.2	34	Stable, no spikes, compatibility test with rubber liner
190	3-21-69	1.0	16-M0	13 L* Stl	20-20K	None	1.17	0.5	21.2	34	No spikes, smooth, pulse test at nominal MR
191	3-21-69	1.0	16-M0	13 L* Stl	20-20K	None	0.85	0.5	21.2	34	No spikes, pulse test at low MR
192	3-21-69	1.0	16-M0	13 L* Stl	20-20K	None	1.36	0.5	21.2	34	Pulse test at high MR, no spikes, noise ±6 psi
193	3-21-69	1.5	16-M0	13 L* Stl	None	13.5	1.16	0.5	21.2	34	Bomb test at nominal MR, no spikes
194	3-21-69	0.5	16-M0	13 L* Stl	None	None	1.19	0.5	21.2	34	Altitude start demonstration, oxidizer lead no overpressure
195	3-24-69	1.5	16-M0	13 L* Stl	None	13.5	1.30	0.5	21.2	34	Bomb test at high MR, no spikes
196	3-24-69	1.5	16-M0	13 L* Stl	None	13.5	0.81	0.5	21.2	34	Bomb test at low MR, bomb misfired, no spikes
197	3-25-69	1.0	16-M0	6.5 L* Si-Ph	None	None	1.13	0.5	21.2	34	Phenolic chamber checkout test
198	3-25-69	22.0	16-M0	4.5 L* Si-Ph	None	None	1.13	0.5	21.2	34	Injector durability demonstration, no spikes, noise ±6 psi
199	3-27-69	1.0	16-M0	6.5 L* Si-Ph	None	None	1.14	0.5	21.2	34	Checkout test
200	3-27-69	21.0	16-M0	6.5 L* Si-Ph	None	None	1.13	0.5	21.2	34	Injector durability demonstration, no spikes, noise ±6 psi

VI, B, Test Program (cont.)

low height. The major blades radiated from a common center; the minor blades subdivided the outer pockets bordered by the outside diameter, the hub, and the major blades.

(U)   Tests 3K-1-101 and 3K-1-102 showed low performance. Posttest evaluation revealed that the oxidizer was contaminated with an equivalent water content of 14%. These tests were not used in performance analyses.

(U)   Two items of significance were accomplished prior to the third test. The oxidizer propellant line and tank were drained and the system refilled with certified propellant, and the injector purge system was converted from 120 psi pressure to 500 psi pressure. This latter task was performed to eliminate very hard transients observed on the first two tests. During the system conversion, provisions were made for venting the fuel circuit purge line to ambient after ignition. In subsequent tests, the fuel purge valve was closed after achievement of steady state. As a result, 500 psi GN_2 automatically flushed the oxidizer circuit upon shutdown. After the oxidizer was gone, the fuel purge was manually operated and residual propellant was flushed from the injector. These procedures, in addition to shortening the oxidizer lead and eliminating oxidizer lag, were successful in stopping the hard transients.

(C)   Tests 3K-1-103 through 105 were found to have high performance; chamber pressure showed several random spikes. In all cases, the spikes damped within 20 milliseconds. They were influential, however, in promoting orifice spreading and platelet splitting. The decision was made to machine an identical pattern into the next face level; a 15° rotation of the pattern was also planned to remove the structurally weak baffle running parallel with platelet orientation.

(U)   Upon postfire injector disassembly, approximately two ounces of sand-like residue was found in the oxidizer manifold plenum.

VI, B, Test Program (cont.)

This material, formed in the feed line by the contaminated propellant, had been building up in the manifold during the latter three tests. It was possible that oxidizer orifice plugging by the material had caused fuel rich zones to occur in the chamber and, thus, spiking. The lines were again cleaned prior to the next test series.

b. Tests 3K-1-106 through 3K-1-107

(U)   These tests, the only ones conducted using a showerhead injector, demonstrated rough combustion. Posttest evaluation showed inter-manifold leaks of fuel into the oxidizer. The rough operation precluded the acquisition of performance data.

c. Tests 3K-1-108 through 3K-1-110

(C)   These three tests were conducted using injector I1-M1 (first modification). The baffle pattern, located in the second face level, was identical to that of -M0, except for a 15° rotation and a reduced major baffle height to 0.705 in. This latter change was incorporated to avoid having depth-etched separator pockets at all major baffle tips.

(C)   Test 3K-1-108 was entirely unstable in a first tangential mode. Tests 3K-1-109 and -110 had periods of smooth operation; however, there were spikes that failed to damp within 40 milliseconds. Representative Photocon data are shown in Figure 37. It was thus concluded that the major baffles had to be increased in height to regain stable operation. To accomplish this, an interface level change was designed that (1) cut into the impinging level, thus adding 0.035 in. to baffle height and increasing the impinging distance; (2) removed all baffles within the hub to provide a greater number of impinging orifices; and (3) cut vertically through the depth-etched separator pockets
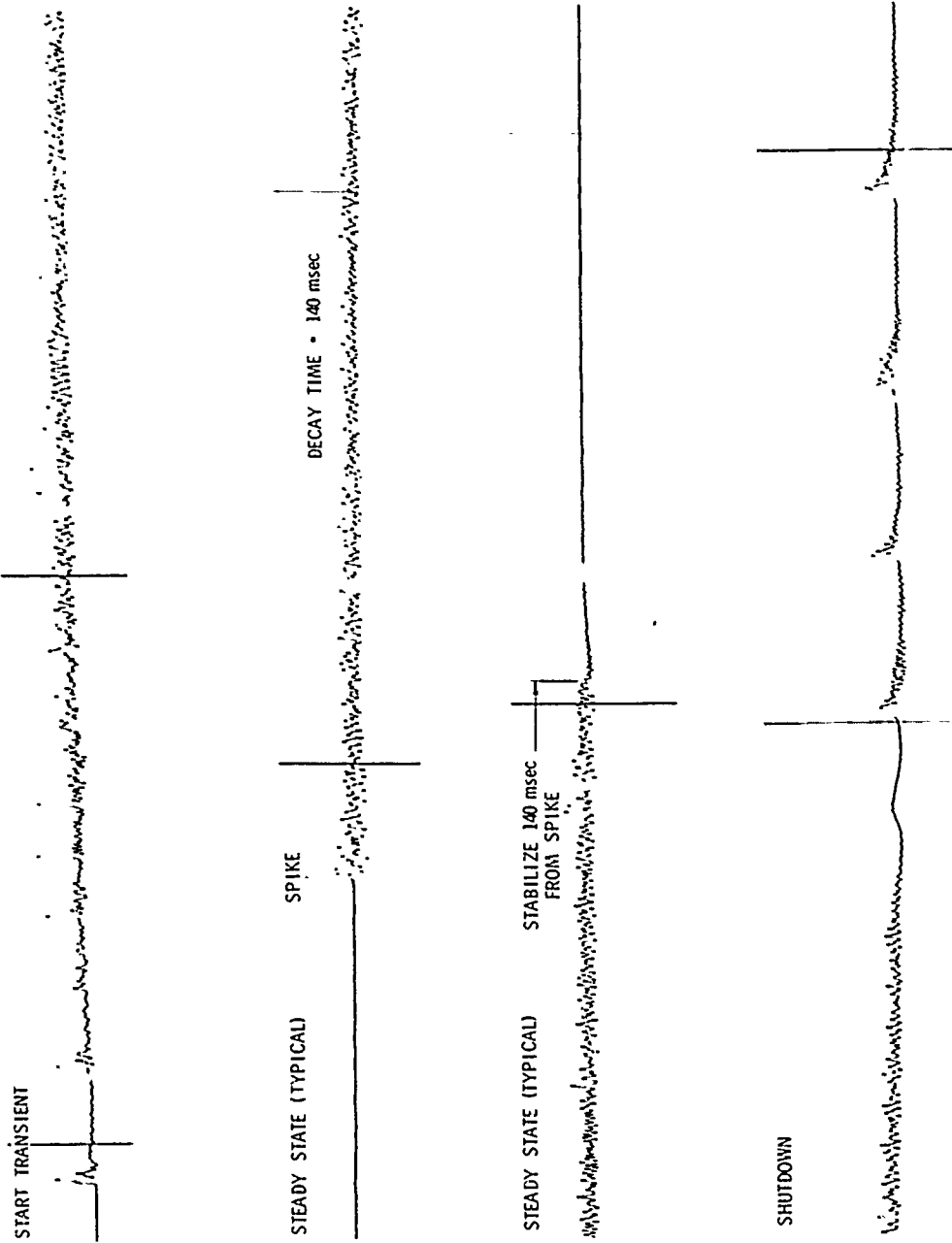
Figure 37. High-Frequency Pressure Trace – Test 3K-1-109

VI, B, Test Program (cont.)

formed at the baffle roots. It was felt that this latter step would reduce the pocket size and, thus, the volume of potential hydrazine traps that could promote hydrazine accumulation and popping.

      d.   Tests 3K-1-111 through 3K-1-114

(U)   These tests were conducted with injector I1-M2, which incorporated the changes discussed above. The major baffles were 0.740 in.; the minor blades were 0.385 in. There were no baffles in the center and all baffle roots had been cut vertically, as shown in Figure 38.

(C)   Tests 3K-1-111 through -114 showed no self-induced pops or instability. The only anomalies noted were a combustion noise level of $\pm 8\%$ (3% over specification) and burning in the area of the vertical cuts. Subsequent testing showed that the face burning progressed until all narrow platelet walls had been removed; the burning then stabilized and progressed no further.

(U)   These tests were all conducted on the 13-in. L* steel stability chamber. Pulses were fired during all tests in an evaluation of pulse size as a function of charge and burst diaphragm size. The combinations tested were: a 15-grain 0.38 special charge with a 10,000 psi diaphragm, a 20-grain magnum charge with a 10,000 psi diaphragm, and a 20-grain magnum charge with a 20,000 psi nonfragmenting diaphragm. The latter combination was found to produce pulses equaling or exceeding the $\Delta P/P_c = 1.75$ criterion. In all cases, the pulses damped within 20 milliseconds. A representative high-frequency pressure trace is shown in Figure 39.

      e.   Tests 3K-1-115 through 3K-1-122

(U)   These tests, all of which employed injector I1-M2, were conducted on the 6.5-in. L* copper chamber. Their objective was to evaluate
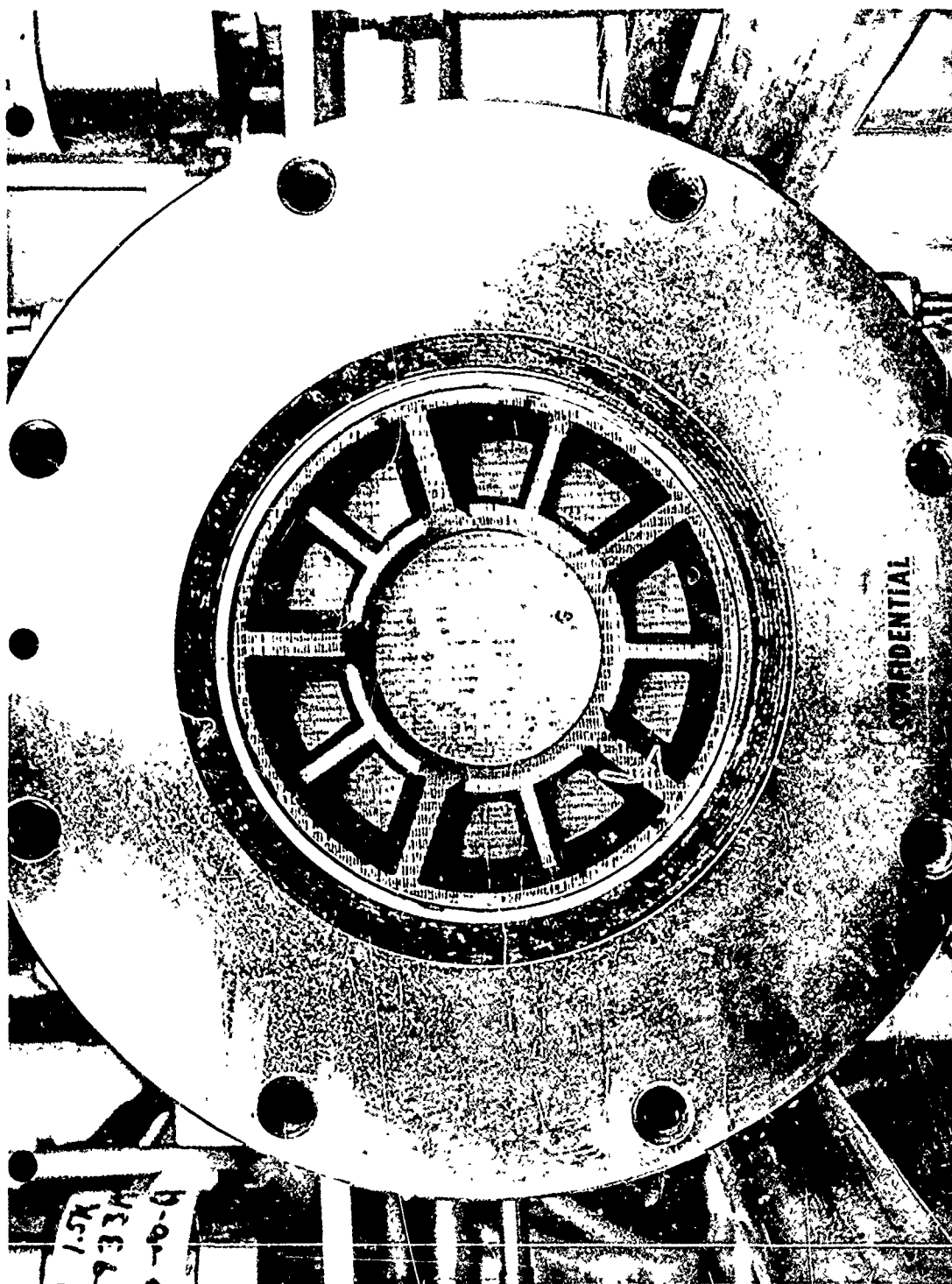
Rep tt AERPL IF 69 t

Figure 38. Injector I1-M2 (Prefire) (u)
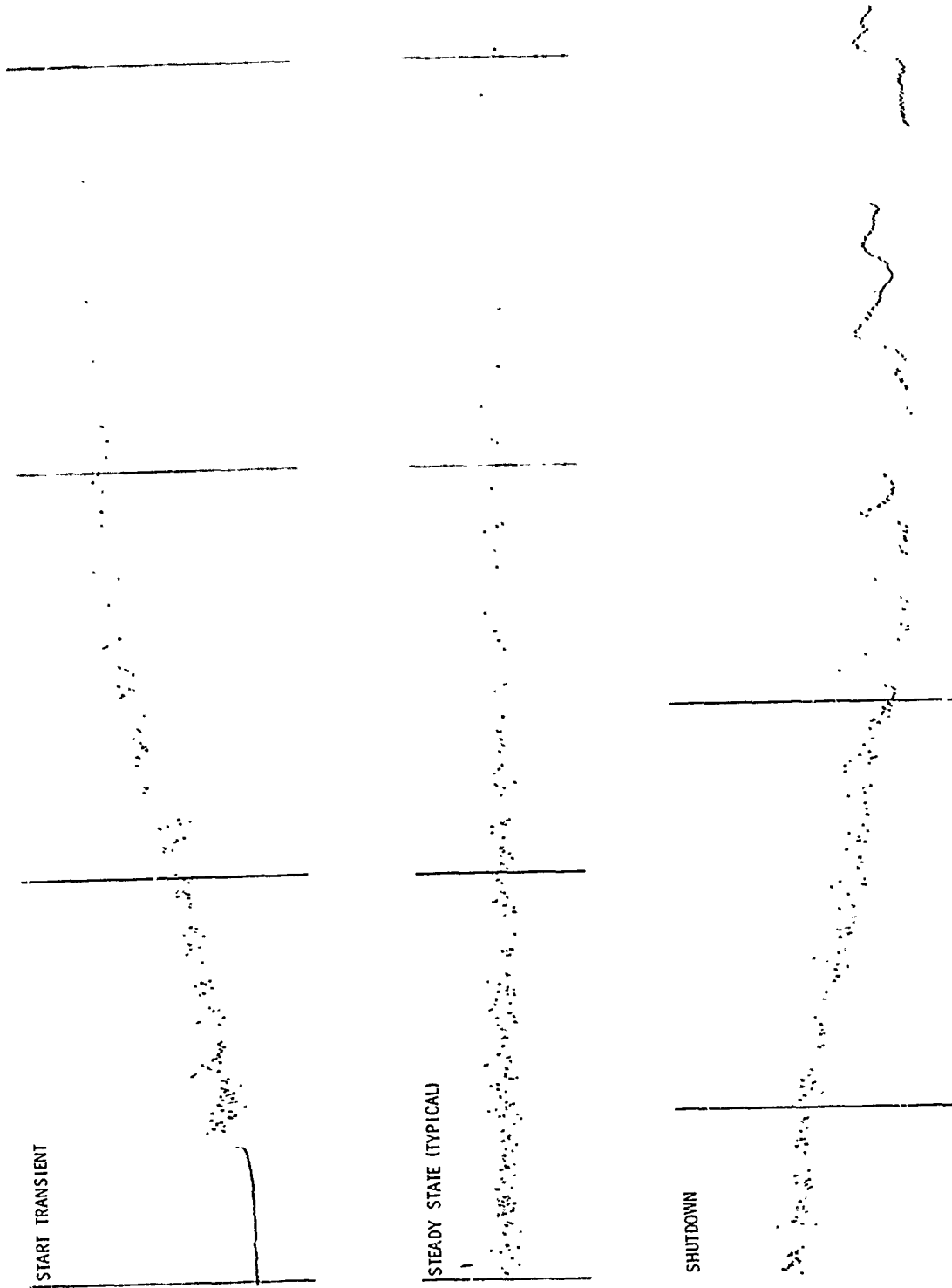
Figure 39. High-Frequency Pressure Trace -- Test 3K-1-114

PHOTOCON #1 - 159.3 psi/in. P-P

START TRANSIENT

STEADY STATE (TYPICAL)

SHUTDOWN

VI, B, Test Program (cont.)

the cooling effectiveness of the off-mixture ratio boundary combustion and to obtain parametric data relating boundary mixture ratio and percent cooling with chamber wall temperature. All tests except 3K-1-115 and -117 were run for 3 seconds. In all cases, there were no pressure spikes nor noise exceeding $\pm 8\%$.

(C)   Injector I1-M2 is shown in Figure 40 after approximately 24 seconds of operation. The platelet burning shown at the baffle roots was essentially unchanged since Test 3K-1-114. The baffles revealed definite structural weakness. The platelet splitting and orifice deformation was progressive. The decision was made to remachine the injector after Test 122 to obtain a new face condition.

f.   Tests 3K-1-123 through 3K-1-126

(U)   The next series of tests employed the third impinging injector, I3-M0. Its pattern (shown in Figure 41) was identical to that of I1-M2 with the exception of increased blade height. The major baffles were 0.80 in. high and the minor blades and hub were 0.435 in. high.

(U)   These tests were conducted to evaluate propellant lead relationships during the start transient. A simultaneous shutdown had been proven effective after the first two tests. Test 3K-1-123 was started with a 35 msec oxidizer lead. Subsequent tests employed simultaneous valve opening and a 35 msec fuel lead. Of these sequences, the 35 msec oxidizer lead gave the best sea level ignition results (minimum spikes) and offered the most potential for altitude starts. This sequence--a 35 millisecond oxidizer lead and a simultaneous shutdown--was thus selected for future tests.

(U)   The tests with injector I3-M0 were slightly rougher than had been observed with injector I1-M2. The peak-to-peak amplitude of the combustion noise was approximately 60 to 65 psi. There were no pressure spikes in any of the tests.

Report AFRPL-TR-69-122
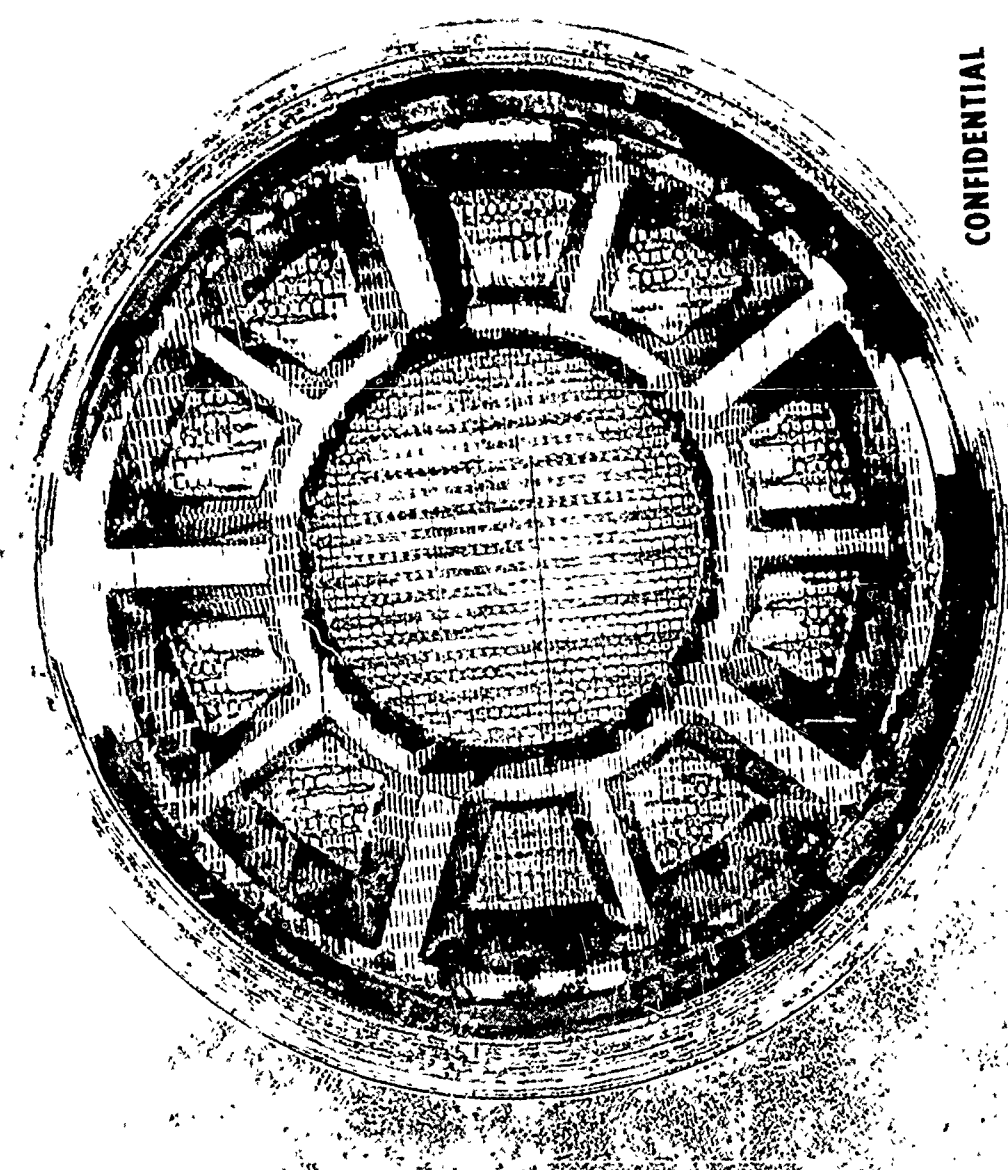
CONFIDENTIAL

Figure 40. Injector 11-M2 Postfire 24 Seconds (u)

Report AFRPL-TR-69-1

Figure 41. Injector 13-90 (u)

Page 111

VI, B, Test Program (cont.)

g.   Tests 3K-1-127 through 3K-1-138

(U)   These tests were conducted in an evaluation of the effect
of baffle reduction on combustion noise level. Previous injectors with a full
star pattern and all minor blades had exhibited very smooth operation; there
had been spikes, however, which had invalidated the data. Injector I1-M2 had
shown no spikes; however, the noise level had increased to ±25 psi. Spectral
density analysis of the high-frequency data showed a predominant first tangen-
tial mode in the noise constituents.

(U)   Three primary patterns were tested in this series. The
first, which constituted injector I1-M3 (Figure 42), contained five major blades
0.740 in. high and a 0.400 in. hub. There were no minor radial blades. This
same pattern was repeated in injector I3-M1 (Figure 43) with the exception that
all blades were 0.740 in. high.

(U)   The second major pattern variation is shown in Figure 44.
This injector (I3-M2) contained 0.740 in. major baffles intersecting at the
center and a 0.400 in. hub at the half radius. Again, the outer pockets were
left undivided. The third pattern, incorporated in injector I1-M6, was an
identical repeat of I1-M2. This was done to determine repeatability of
injector operation.

(U)   Spectral analysis of the high-frequency data generated
with each design revealed three significant facts. First, the combustion noise
produced with a pattern such as that shown in Figure 38 (nothing in center)
contained a dominant first tangential mode. This single mode contributed most
to the ±25 psi amplitude. Second, patterns such as that shown in Figure 44
suppressed the first tangential mode but allowed the higher modes (third
tangential (3T), first radial (1R), and fourth tangential (4T)) to become
effective. The noise level produced with this pattern was measured to be ±35 psi.
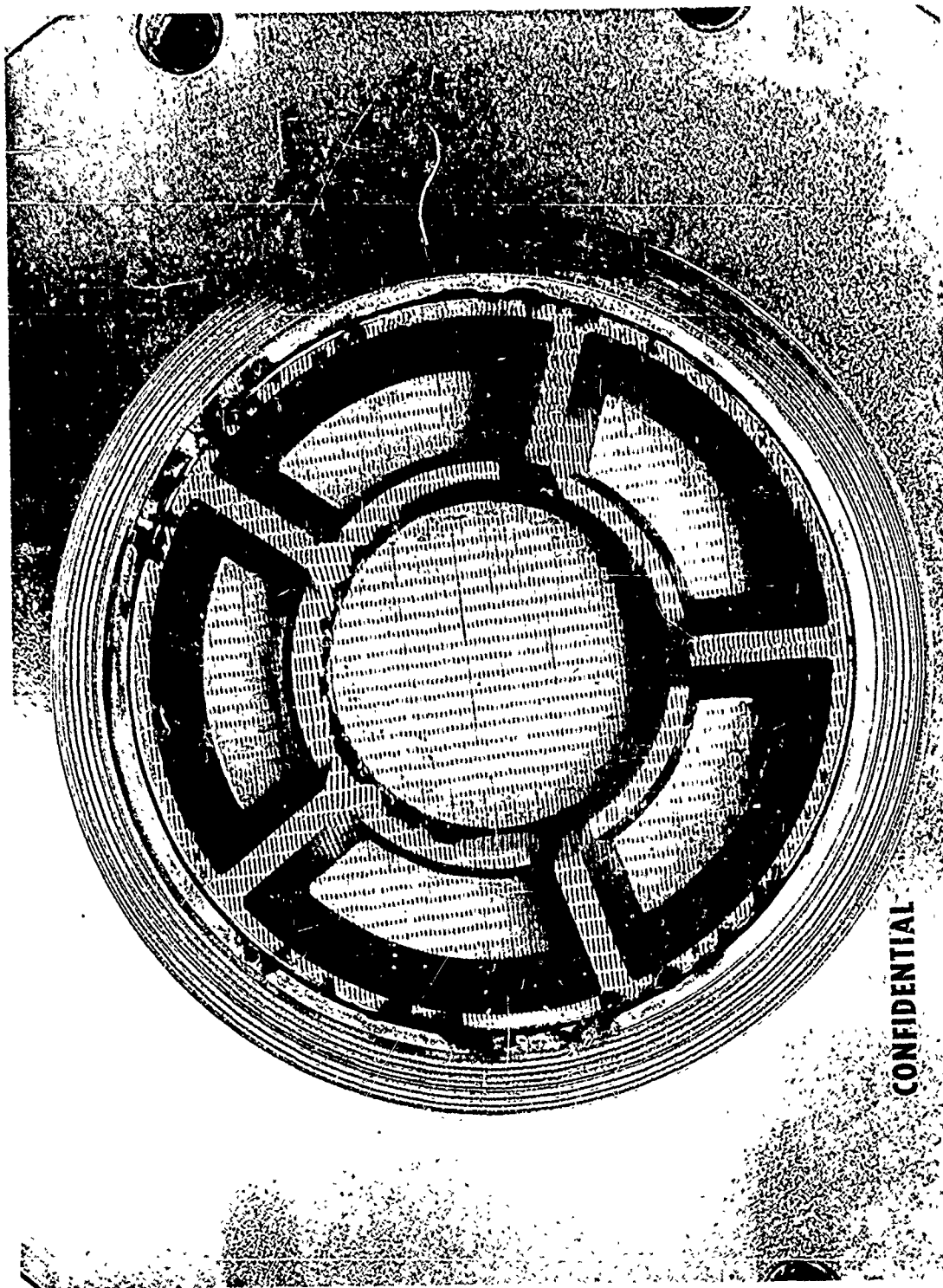
Figure 42. Injector T1-M3 (u)
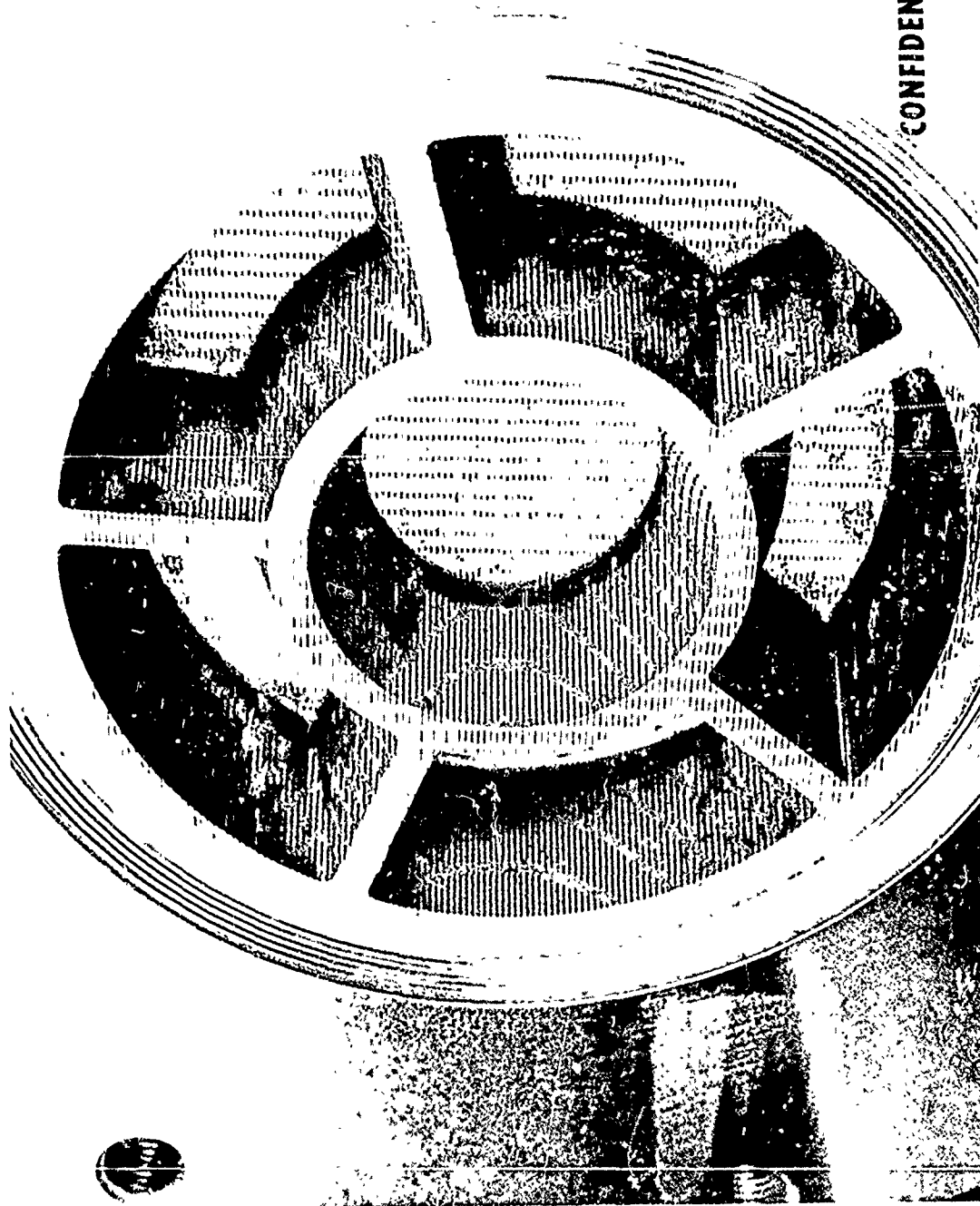
Figure 43. Injector I3-V1 (u)

VI, B, Test Program (cont.)

Third, patterns in which both the center and outer pockets were left open
(Figures 42 and 43) allowed modes 1T, 3T, 1R, and 4T to contribute to a ± 35
to 40 psi oscillation. It was thus concluded that minor blades were needed
in the center if possible and definitely in the outer pockets between the hub
and major baffles.

h.   Tests 3K-1-139 and 3K-1-140

(U)   These tests, conducted on injector I1-M6, were performed
as demonstration tests. In both cases, there were no random spikes, the noise
level was ± 25 psi, and pulse- and bomb-induced spikes of 600 psi were damped
in less than 30 milliseconds.

i.   Tests 3K-1-141 through 3K-1-148

(U)   These tests, all of which employed injector I1-M6, were
conducted on a 4-in. L* (3 in. from injector to throat) copper chamber. The
objective of the tests was to evaluate both cooled and uncooled performance
with the very small chamber.

(U)   The addition of the cooling ring in the oxidizer manifold
was found to produce combustion instability and, thus, invalidate the test data.
It was not immediately apparent why the injector was unstable; in retrospect,
however, it is theorized that previous machining-induced orifice plugging had
sufficiently altered the injector hydraulics to allow instability at off-mixture
ratio conditions.

j.   Test 3K-1-149

(U)   This test, conducted with injector I1-M6 and the short
L* steel chamber, was made to obtain a direct measurement of steady-state
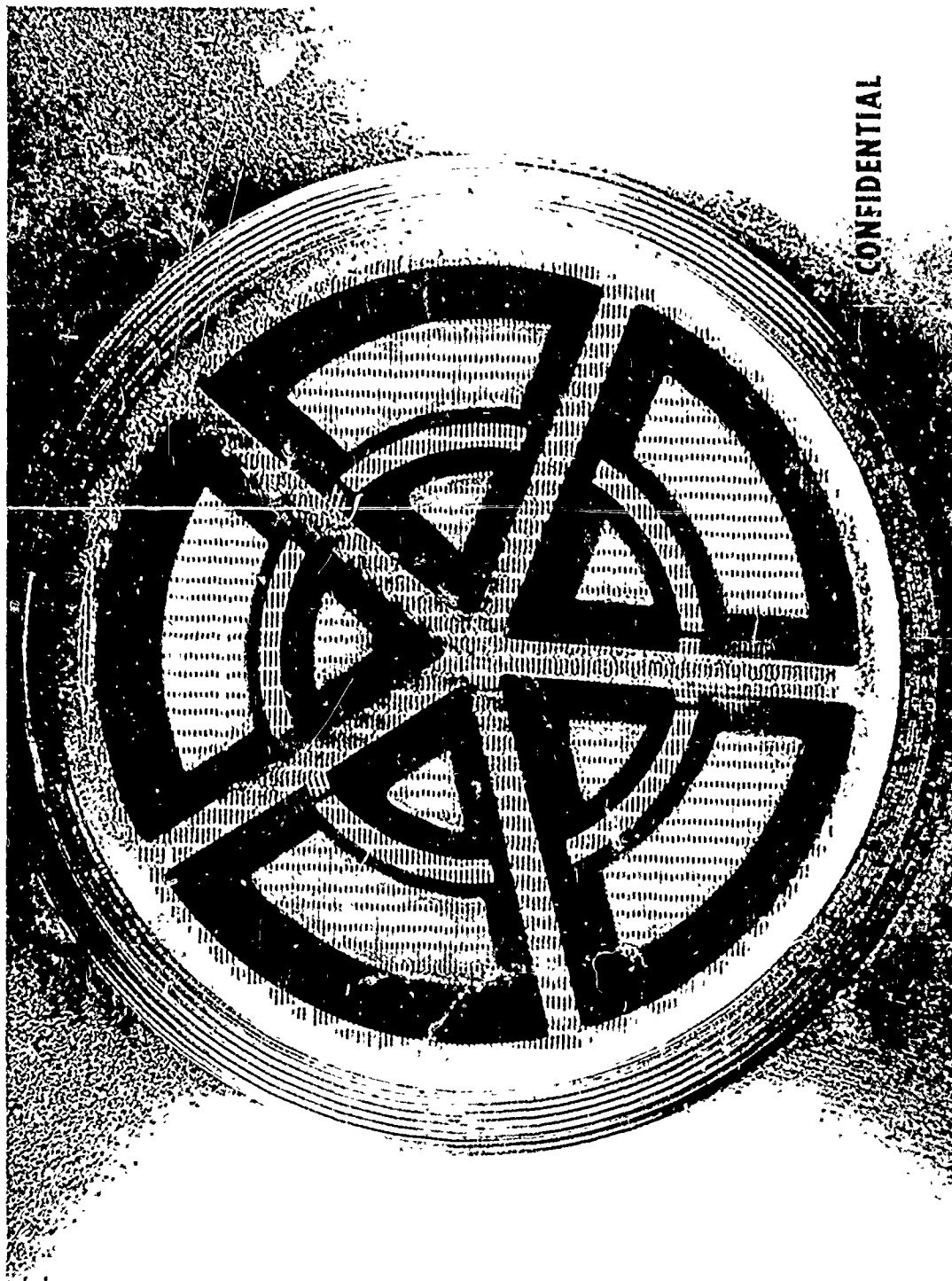
Report AFRPL-TR-69-122

Figure 44. Injector I3-M2 (u)

VI, B, Test Program (cont.)

recovery temperature at the chamber wall. To accomplish this, the insulated tantalum-sheathed tungsten/rhenium thermocouples were employed. A cooling ring designed to provide a boundary mixture ratio of 0.5 and a percent coolant flow of 21.2 over 34% of the injector face was used.

(U)   The test, as were previous cooling tests with this injector, was unstable. The thermocouples, however, recorded steady-state wall temperatures ranging to 4000°F in the throat. It was thus apparent that the boundary cooling was effective even though the combustion process was unstable.

k.   Tests 3K-1-150 through 3K-1-153

(U)   The next four tests were conducted to evaluate the altitude starting characteristics of the injector. To accomplish this task, a 6-ft-long, 10-in.-dia pipe was bolted to the nozzle flange of the 13-in. L* steel chamber. A plate was then placed over the exit of the pipe and sealed in place by pulling a vacuum on the engine assembly. Starting altitude was measured by a 0 to 5 psia Tabor pressure transducer located in the chamber itself. Normal chamber pressure was measured with a standard psig transducer.

(U)   In all cases, the firing sequence was started with an indicated chamber pressure of 0.2 to 0.4 psia. It was found that the absolute pressure transducer overranged before actual ignition. It was subsequently determined that the vacuum pressure readings inside the chamber were invalidated when the throat went sonic. For this reason, altitude testing was stopped until the absolute pressure transducer could be relocated downstream of the throat.

1.   Tests 3K-1-154 through 3K-1-183

(U)   These tests were, with few exceptions, conducted using the phase two injectors I4 and I5 (see Section IV,B). As has been discussed,

VI, B, Test Program (cont.)

I4 was received with a partially plugged oxidizer circuit. The circuit was opened to a fireable condition by flushing the channels with etching solution. It was impossible to completely clean the circuit, however, and test results with this injector were somewhat confounded by spikes caused by hydrazine accumulation in the areas of oxidizer starvation.

(U)   There was one significant difference between injectors I4 and I5, other than the plugging mentioned above. This difference was the inside diameter of the hub. Injector I4, as had all past injectors, had an internal hub diameter of 1.64 in. The corresponding measurement in injector I5 was 1.1 in. The operation of I4 was characterized by extremely smooth operation with interspersed random spikes. I5 was characterized by random noise of ± 30 psi with no spikes. It was thus concluded that the pattern of injector I4, with the larger hub and subdivided center pocket, would, with clean injection circuits, provide the desired level of stability and combustion smoothness. This was later proved to be true with the final injector, I6.

(U)   Two sets of tests were conducted in this series which were directed more toward acquisition of general information than attainment of the specific program goals. The first set consisted of Tests 3K-1-163 through 3K-1-165. These tests employed the propellant combination N_2O_4/MMH. Two tests employed a baffled injector; the third employed a flat-face impinging injector. The objective was to evaluate the stability of the MMH when fired in a high performance, very fine pattern. All three tests had pure instabilities in a first tangential mode (approximately 7000 Hz). This information provided the first experimental data point pertinent to the sensitive frequency relationships between neat hydrazine, AeroZINE 50, and MMH.

(C)   The second test of a generalized nature was Test 3K-1-181. This test, again using N_2O_4/N_2H_4, employed the flat-faced injector/resonator combination shown in Figure 45. This test was conducted to evaluate the potential applicability of a resonator with a platelet injector.
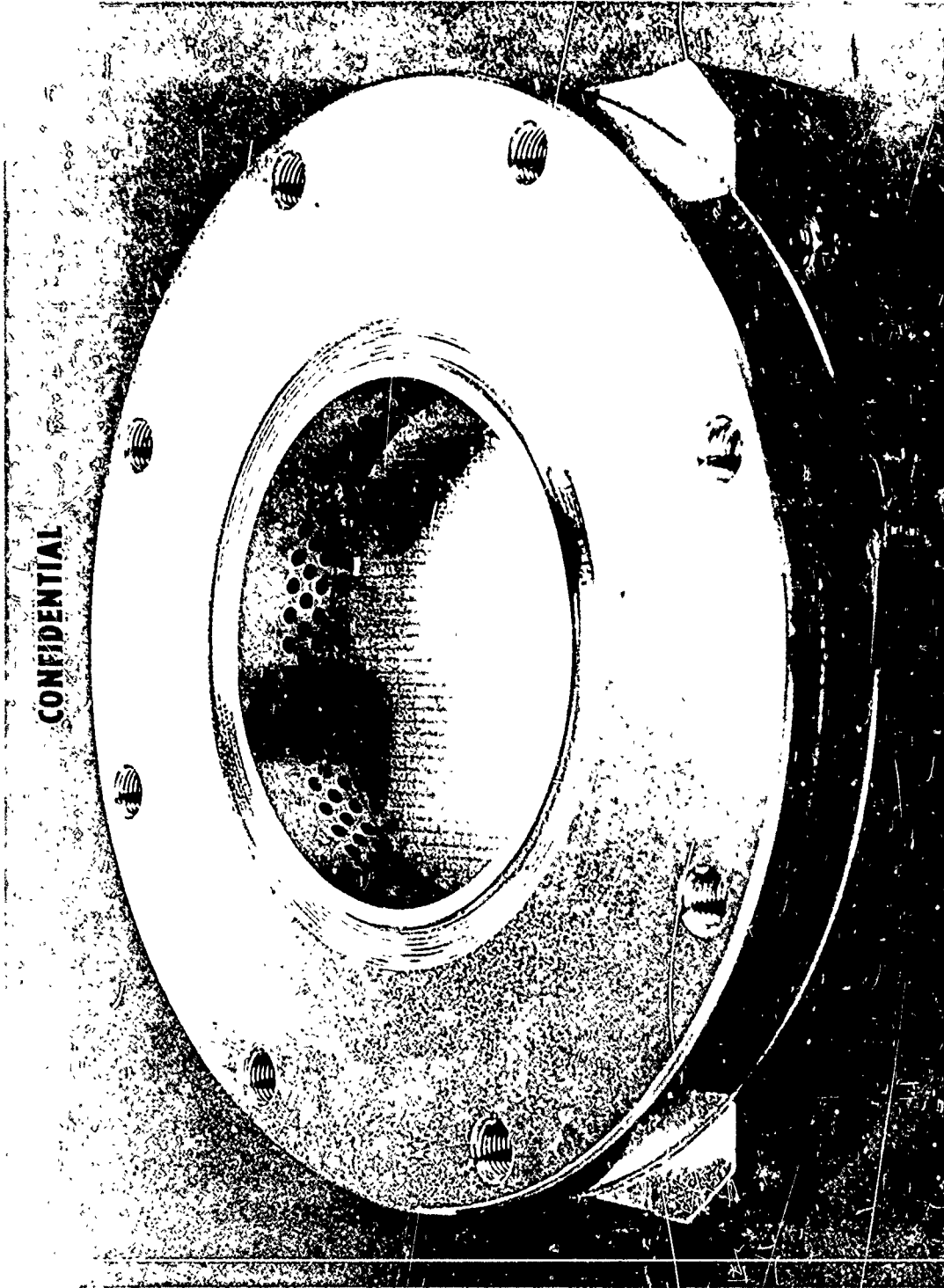
Figure 45. Injector I1-M7 with Resonator (u)

Page 119

VI, B, Test Program (cont.)

(U)   The resonator design was non-optimum in order to use
existing hardware. As a result, the resonator ring was butted to live propel-
lant channels at the injector face. Resulting injection into the resonator
cavity resulted in complete loss of the resonator ring. No further firings
were made with a resonator.

m.   Tests 3K-1-184 through 3K-1-196

(U)   These tests were conducted on the final injector, I6-MO.
This injector, shown in Figure 46, contained the baffle pattern deemed optimum
as a result of all prior test history. The major blades in this pattern were
0.80 in. high with a 16° wall angle. The minor blades, including the hub and
center, were 0.40 in. high.

(C)   This injector was used to complete the program. Tests
3K-1-184 through -196 included performance tests over the full mixture ratio
range, bomb and pulse tests (each over the full mixture ratio range), and alti-
tude start test in which the downstream absolute pressure transducer recorded
no significant pressure spike, and a compatibility test on a coated copper
chamber. In all cases, there were no spikes and the noise level was ± 6 psi
($\pm 2\%$ of chamber pressure). Of significance also was an absence of face burning,
platelet splitting, or significant orifice deformation. Photocon pressure data
illustrative of the smooth operation of this injector is shown in Figure 47.

n.   Tests 3K-1-197 through 3K-1-200

(U)   The final four tests were conducted using injector I6-MO
and 6.5-in. L* phenolic chambers. Tests 3K-1-197 and -199 were each 1 sec
in duration. Tests 3K-1-198 and -200 had 21-sec durations. The main objective
of these tests was an evaluation of the durability of the injector. A secondary
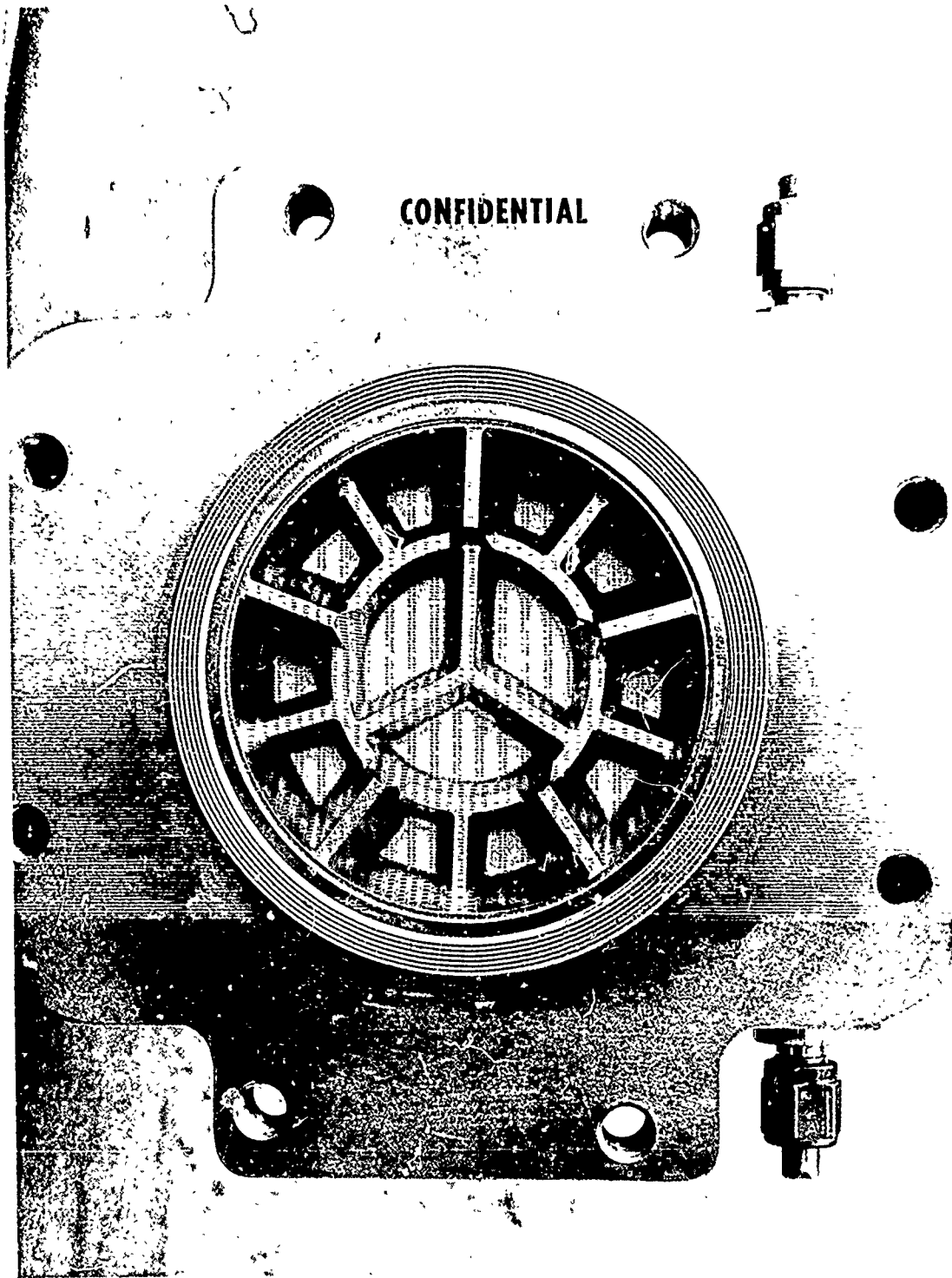
Figure 46. Injector I6-MO (u)

Page 121

PHOTOCON #1 - 563 psi/in. P-P

START TRANSIENT

STEADY STATE (TYPICAL)

.01 SEC

SHUTDOWN
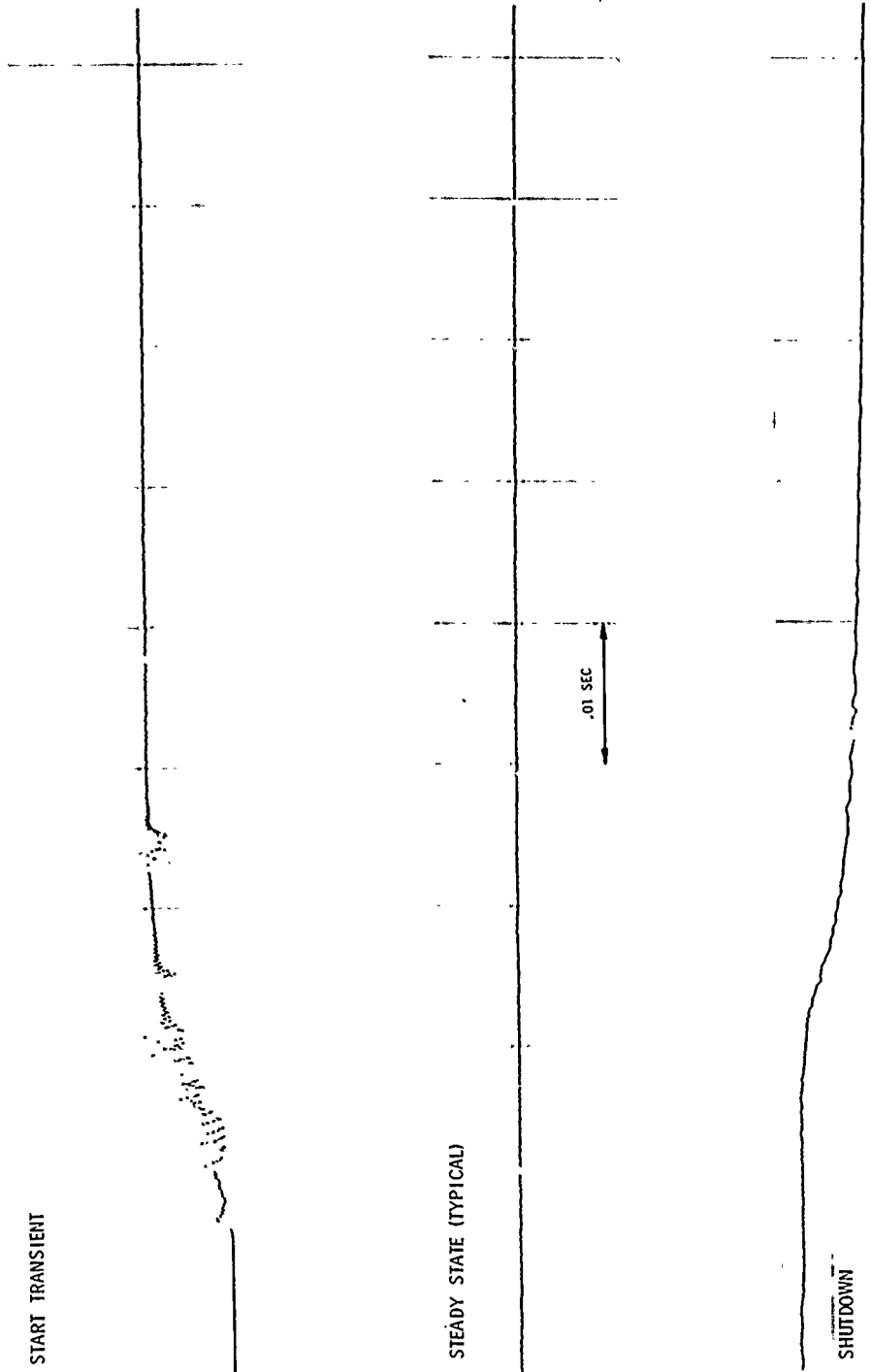
Figure 47. High-Frequency Pressure Trace — Test 3K-1-188

(This Page is Unclassified)

Report AFRPL-TR-69-122

VI, B, Test Program (cont.)

objective was evaluation of the long duration injector/chamber compatibility.
As shall be discussed in subsequent sections, the results of these tests
proved the injector to be very durable and compatibility to be acceptable.

C. PROBLEM AREAS

(U)   The problem areas encountered during this program were almost
exclusively related to injector/baffle operation. These problems, discussed
elsewhere in the report, affected the rate of attainment of the program goals,
rather than the ability to carry on the experimental program. The only excep-
tion was the early discovery of contaminated propellant in the oxidizer feed
system. This problem was solved by emptying and refilling the tank and pre-
vented by sampling the propellant periodically for water content. No further
incidences of out-of-specification propellant were found.

(U)   There were, during the program, no feed system or thrust chamber
valve failures, electrical malfunctions, or instrumentation failures. Conse-
quently, there was no expenditure of effort in tasks unrelated to the primary
objectives of the program.

SECTION VII

EXPERIMENTAL RESULTS

A. PERFORMANCE

1. Data Reduction Techniques

(U)   All engine tests were fired in Bay 2 of Test Area A. Instrumented parameters relevant to the performance analyses included thrust, weight flow rates, chamber pressure, nozzle throat and exit diameters, and propellant temperatures. In addition, tank and manifold pressures were measured as were selected hardware temperatures. The system accuracies (1σ) for thrust, chamber pressure, and weight flow rate are shown below along with the 1σ value for I_{sp}, determined using a root sum square of the thrust and weight flow rate accuracy.

Parameter	1σ, %
Thrust	±0.17
Chamber pressure	±0.25
Oxidizer flow rate	±0.50
Fuel flow rate	±0.50
Specific impulse	±0.53

(U)   As noted above, the system accuracy for I_{sp} was approximately ±0.5%. This is equivalent to approximately ±1.3 lbf-sec/lbm. The calculated 1σ deviation for these parameters during representative data sample periods was within the 0.5% value for I_{sp}. Thus, the pertinent performance parameters were essentially constant, although the data sample times were necessarily short due to the limited test durations. A correction was applied to adjust the short duration copper and steel chamber transient heat losses to the adiabatic wall conditions of the flight type chamber.

VII, A, Performance (cont.)

(U)   During the performance analysis, oscillograph traces were
used for rapid determination of mixture ratio for engine balance, for detection
of significant pressure or thrust fluctuations, and as a guide in selection of
test data sample periods. X-Y plotters were used in conjunction with digital
listings to determine significant thermal trends which might influence perfor-
mance. The digital listings were also used for all final determinations of
system performance.

(U)   Criteria for data sample time selection were that steady-state
flow, thrust and chamber pressure had been attained and that no large fluctua-
tions of these parameters occurred during the sample period. For comparison
of performance among tests on which thermal steady state was not achieved,
data times were selected which corresponded to nearly equal chamber wall
temperature rise rates.

(U)   The only parameters which were difficult to measure accurately
or which contained suspected errors were oxidizer inlet temperature, chamber
stagnation pressure, and nozzle throat and exit areas. Suspected measurement
errors occurred intermittently in oxidizer temperature readings, probably due
to corrosion of the thermocouple. A plot of specific impulse error as a
function of oxidizer temperature error is shown in Figure 48. For tests with
suspected erroneous readings, the oxidizer temperature was assumed to be equal
to the fuel temperature. (The tests on which this assumption was used are
noted in the performance summary table.) The maximum expected temperature
difference between the two propellants was 10°F. Thus from Figure 48, the
maximum I_{sp} error due to these temperature effects was only expected to be
1.2 lbf-sec/lbm.

(U)   The difficulties encountered in accurate measurement of
chamber stagnation pressure and effective throat and exit flow areas are
difficulties inherent in these parameters regardless of the engine system
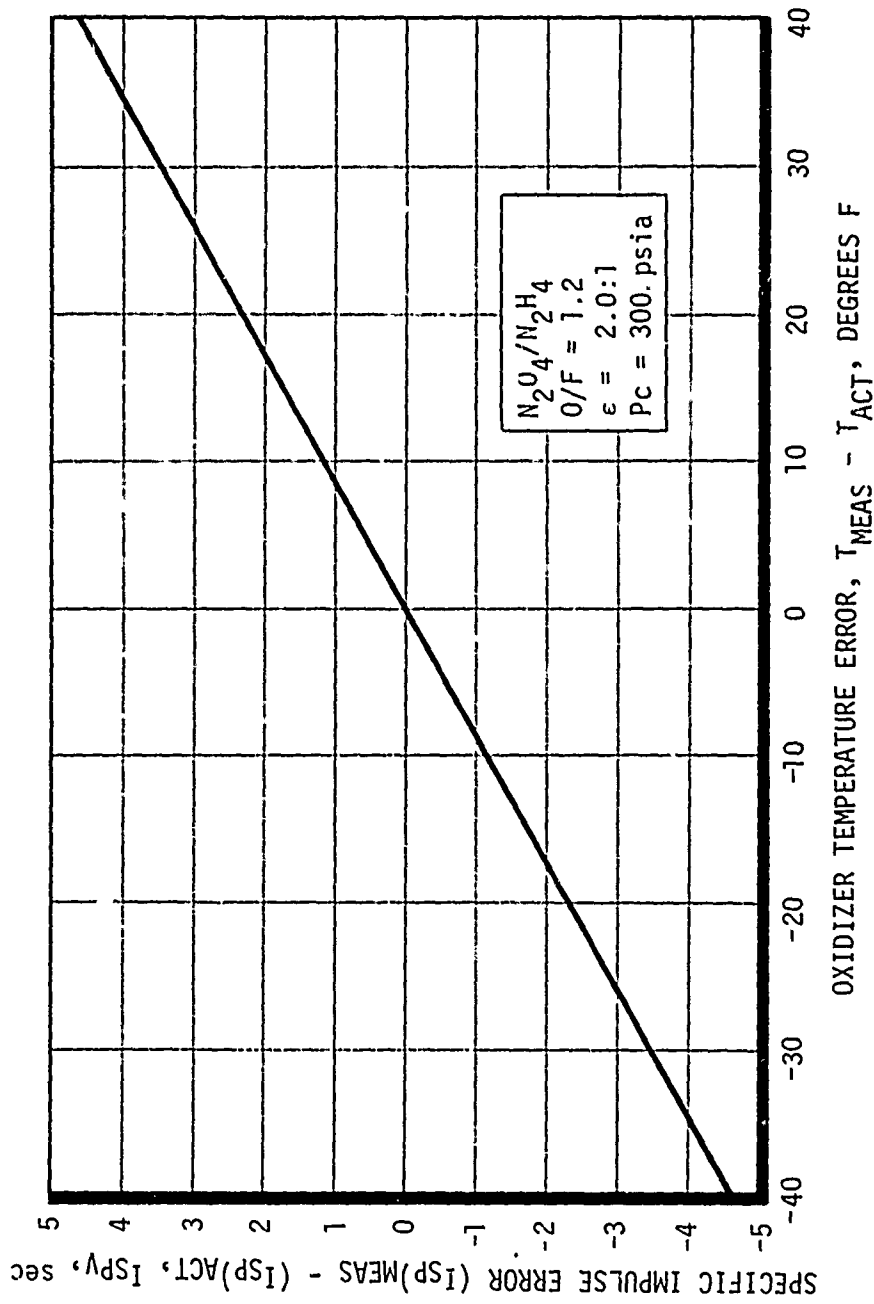
Figure 48. Effect of Oxidizer Temperature Error on Specific
Impulse Error

VII, A, Performance (cont.)

being analyzed. For this reason the energy release efficiency, which is based on measured thrust and calculated nozzle performance losses, is preferable to c* efficiency as a measure of combustion efficiency. Accurate flow area measurements in a rocket engine are difficult due to the effects of thermal expansion and boundary layer growth. True measurement of chamber stagnation pressure is difficult due to contraction ratio and combustion effects. For example, the correction from static to stagnation pressure ranged from 10% to 25%, depending on the location of the pressure tap in the chamber. These corrections were only approximate, since they were made assuming isentropic flow from the P_c tap to the throat, i.e., no heat addition (combustion) or chamber heat loss downstream of the P_c tap.

(U)   Tests 3K-1-185 to 188, conducted with a 5-in. chamber (6.5-in. L*), exhibited low values of measured chamber pressure. The percent c* achieved on these tests was lower than the percent I_{sp}. The I_{sp} data were consistent with previous data generated with similar injectors. No explicit reason can be given for the low chamber pressure readings on these tests. Except for the abnormal oxidizer temperature readings and the low chamber pressure readings on certain tests, no other significant anomalies were apparent in the measured data of the tests evaluated.

2.   Phases I and II Injector Design

a.   Sea Level Performance

(U)   During the Phases I and II injector testing, baffle patterns were evaluated using five injectors. All injector patterns evaluated used like-on-like doublet type elements at the face and showerhead elements on the baffles. Two tests conducted with injectors containing all showerhead elements were not evaluated for performance due to large thrust and chamber pressure oscillations during the firing. A tabulation of operating, design,

VII, A, Performance (cont.)

and performance parameters for tests of the injectors with candidate baffle designs is presented in Table IV. Only those tests for which the performance was considered valid are presented. (The test summary presented in Table III contains information regarding the deletion of tests from this performance summary.)

(C)   In all, 27 tests were evaluated with regard to performance. A breakdown of valid Phases I and II performance tests fired at each chamber length, with and without barrier cooling, are tabulated below.

No. of Tests	No. of Baffle Designs	Chamber Length, in.	Barrier Cooling	O/F Range
18	8	10	No	0.79 - 1.30
2	1	5	No	1.36
1	1	3	No	1.44
6	1	5	Yes	1.16 - 1.41

It is obvious that, even though performance was evaluated on 27 tests, a large number of test parameters was varied. A parametric performance analysis based on the Phases I and II injector designs was considered a useful endeavor as it provided valuable insight with respect to the expected performance characteristics of the final injector design. Only a moderate amount of empirical data was available for such an endeavor, however, due to the large number of variables and relatively small number of tests.

(1) Mixture Ratio Effects

(C)   The specific impulse data from uncooled tests with the Phases I and II injectors are shown in Figure 49 as a function of injector mixture ratio. The one-dimensional equilibrium (ODE) specific impulse and the

TABLE IV

SUMMARY OF PHASE I AND II INJECTOR PERFORMANCE (u)

| Test No. 3K-1-	Injector	Chamber	Chamber* Pressure, psia	Overall Mixture Ratio	Barrier Mixture Ratio	% Coolant Flow	% Coolant Area	Sea Level Thrust, lbf	Weight Flow Rate, lbm/sec	Vacuum** Specific Impulse, lbf-sec/lbm	% I_{sp}	Characteristic Velocity,* ft/sec	% $c*$	η_{ER}	Comments
111	11-M2	13 L* Stl	291	1.16	---	Uncooled	---	2234	9.412	255.4	95.5	5730	98.0	99.5	Valid performance test, no cooling
112	11-M2	13 L* Stl	324	1.10				2435	10.060	258.9	96.9	5976	102.0	100.7	
113	11-M2	13 L* Stl	319	1.27				2431	10.152	256.2	96.1	5826	100.0	100.2	
114	11-M2	13 L* Stl	327	0.81				2510	10.526	254.6	97.0	5762	99.7	100.5	
115	11-M2	6.5 L* Cu	311	1.36				2402	10.165	253.0	95.5	5677	98.2	99.9	
116	11-M2	6.5 L* Cu	307	1.36		Uncooled		2391	10.126	252.8	95.4	5715	98.6	99.7	Valid performance test, no cooling
117	11-M2	6.5 L* Cu	288	1.16	0.2	17.0	34.0	2166	9.708	240.6	89.9	5503	94.0	100.3	Valid performance test, barrier cooling
118	11-M2	6.5 L* Cu	289	1.16	0.2	17.0	34.0	2176	9.723	241.2	90.2	5523	94.4	100.4	
119	11-M2	6.5 L* Cu	297	1.23	0.5	21.2	34.0	2261	9.921	245.0	91.8	5539	95.2	100.4	
120	11-M2	6.5 L* Cu	314	1.41	0.5	10.0	16.0	2398	10.420	246.4	93.4	5599	97.4	106.0	
121	11-M2	6.5 L* Cu	309	1.39	0.5	12.5	20.0	2381	10.368	246.0	93.1	5534	96.0	100.2	
122	11-M2	6.5 L* Cu	310	1.35	0.5	14.4	23.0	2348	10.314	244.1	92.0	5570	96.3	99.5	Valid performance test, barrier cooling
123	13-M0	13 L* Stl	313	1.30	---	Uncooled	---	2349	9.844	255.6	96.3	5903	102.0	100.3	Valid performance, no cooling
124	13-M0	13 L* Stl	317	1.29				2384	9.989	255.4	96.2	5881	101.0	100.2	Valid performance, no cooling
125	13-M0	13 L* Stl	--	--				--	--	--	--	--	--	--	Performance invalid, chamber gas leak
126	13-M0	13 L* Stl	--	--				--	--	--	--	--	--	--	Test invalid, web blew out of chamber on start
127	11-M3	13 L* Stl	314	1.23				2341	9.763	257.0	96.4	5964	102.0	100.4	Valid performance test
128	11-M3	13 L* Stl	327	0.79				2462	10.360	253.8	97.1	5856	102.0	100.5	
129	13-M1	13 L* Stl	343	1.18				2532	10.480	257.8	96.4	6070	104.0	100.4	
130	13-M1	13 L* Cu	337	1.13				2592	10.744	257.0	96.1	5812	99.2	101.0	
131	11-M3	13 L* Stl	322	1.24				2373	9.887	257.1	96.3	6040	104.0	100.3	Valid performance test spikes, performance evaluated during stable period
132	13-M2	13 L* Stl	345	1.08				2549	10.520	258.2	96.6	6086	104.0	100.2	
133	13-M2	13 L* Stl	346	1.08				2557	10.568	257.6	96.4	6073	104.0	100.0	
134	11-M4	13 L* Cu	332	1.07				2557	10.749	253.7	95.0	5727	97.7	100.0	
135	11-M5	13 L* Cu	329	1.12				2551	10.656	255.1	95.4	5723	97.8	100.3	spikes, performance evaluated during stable period
136	11-M5	13 L* Cu	328	1.05				2522	10.671	252.2	94.3	5702	97.0	99.4	
137	11-M6	13 L* Stl	326	1.23				2439	10.259	254.3	95.2	5892	101.0	99.4	Valid performance test, no cooling
138	11-M6	13 L* Stl	326	1.22				2432	10.143	256.5	96.1	5967	102.0	100.2	
139	11-M6	13 L* Stl	323	1.22				2425	10.157	255.4	95.7	5909	101.0	99.8	
140	11-M6	13 L* Stl	328	1.22				2420	10.095	256.5	96.1	6027	103.0	100.2	Valid performance test, no cooling
141	11-M6	4 L* Cu	--	--				--	--	--	--	--	--	--	Balance test, data not reduced
142	11-M6	4 L* Cu	305	1.44	---	Uncooled	---	2351	10.128	248.9	94.6	5594	97.5	98.7	Valid performance, 4 L* chamber

*Corrected to stagnation conditions.
**Area ratio = 2.0:1.
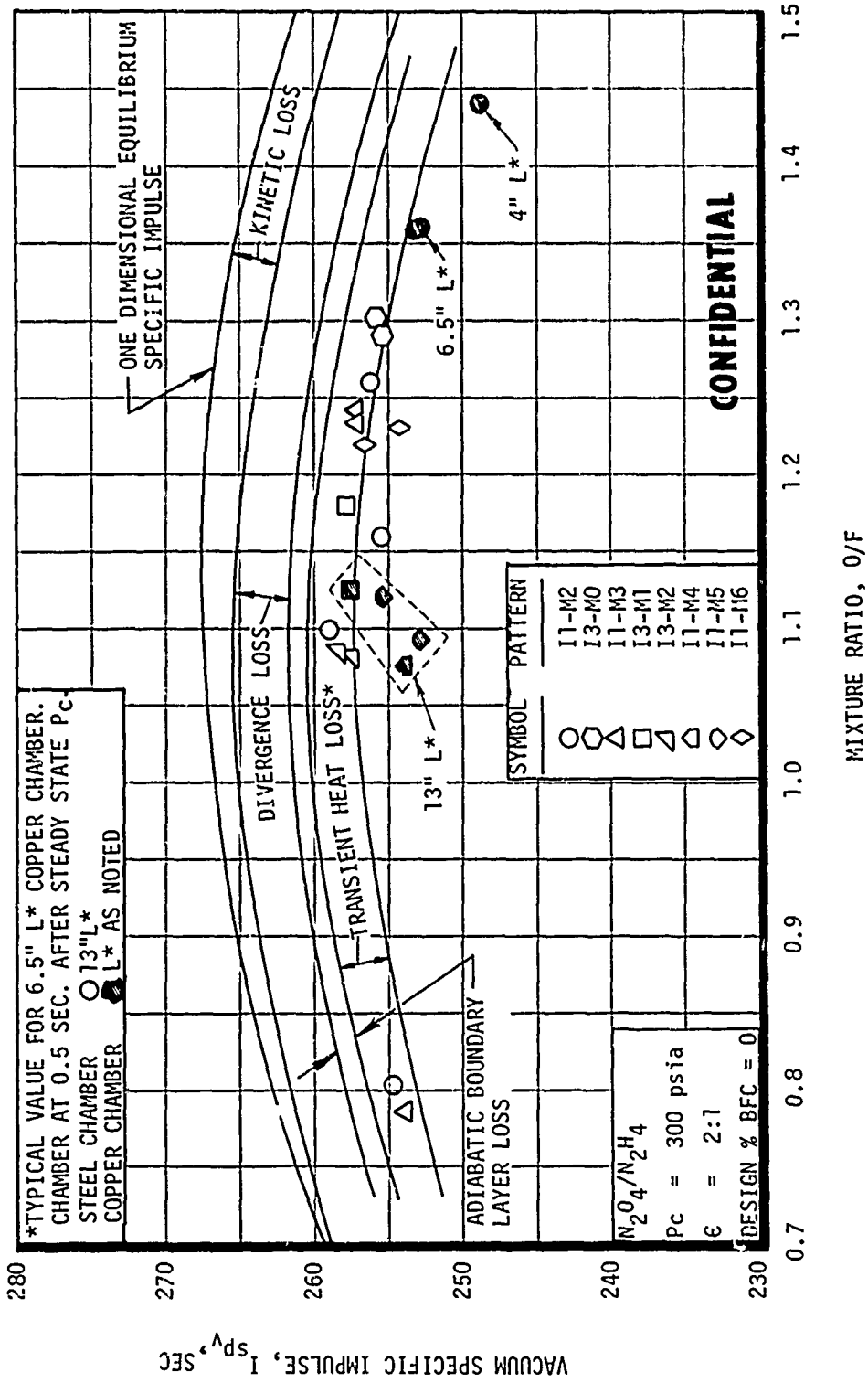
Figure 49. Effect of Mixture Ratio on Specific Impulse for Uncooled Tests – Phase I and II Injector (u)

VII, A, Performance (cont.)

predicted performance losses due to kinetics, boundary layer effects, and
nozzle divergence are also illustrated on the figure. A comparison of the ODE
I_{sp} minus the above losses with the test data indicates that these losses essen-
tially account for the difference between the theoretical (ODE) I_{sp}, and the
measured I_{sp}. That is, energy release losses and mixture ratio maldistribution
losses were essentially zero throughout the range of mixture ratio surveyed for
all candidate injectors. Data from these same tests are presented in Figure 50
with specific impulse efficiency and energy release efficiency as the dependent
parameters and mixture ratio as the independent parameter. It may be seen that
both measures of efficiency for these tests were virtually constant throughout
the mixture ratio range tested, within a value of $\pm 1.0\%$. Variations in baffle
patterns did not appear to influence either the efficiency level of the injectors
or the effect of mixture ratio on the efficiency.

(C)   This constant level of efficiency achieved during
the uncooled tests is not surprising considering the HIPERTHIN injector design.
Neither the efficiencies of the like-on-like impinging elements nor the
showerhead elements are significantly affected by variations in fuel to
oxidizer momentum ratio as a result of mixture ratio changes. In addition,
for the uncooled tests, the HIPERTHIN pattern eliminates any mixture ratio
maldistribution loss which could cause the efficiency to be affected by mixture
ratio. For the low area ratio tests, kinetic losses, which are a function of
mixture ratio, amount to less than 1%. Therefore, the influence of mixture
ratio on kinetic loss is insignificant.

(U)   Insufficient test data were available to determine
the empirical effect of mixture ratio on performance for the tests of the
candidate injectors with barrier zone cooling. However, analytical curves
of performance as a function of mixture ratio can be defined for various
cooling conditions and the test data can be shown in relation to these curves.
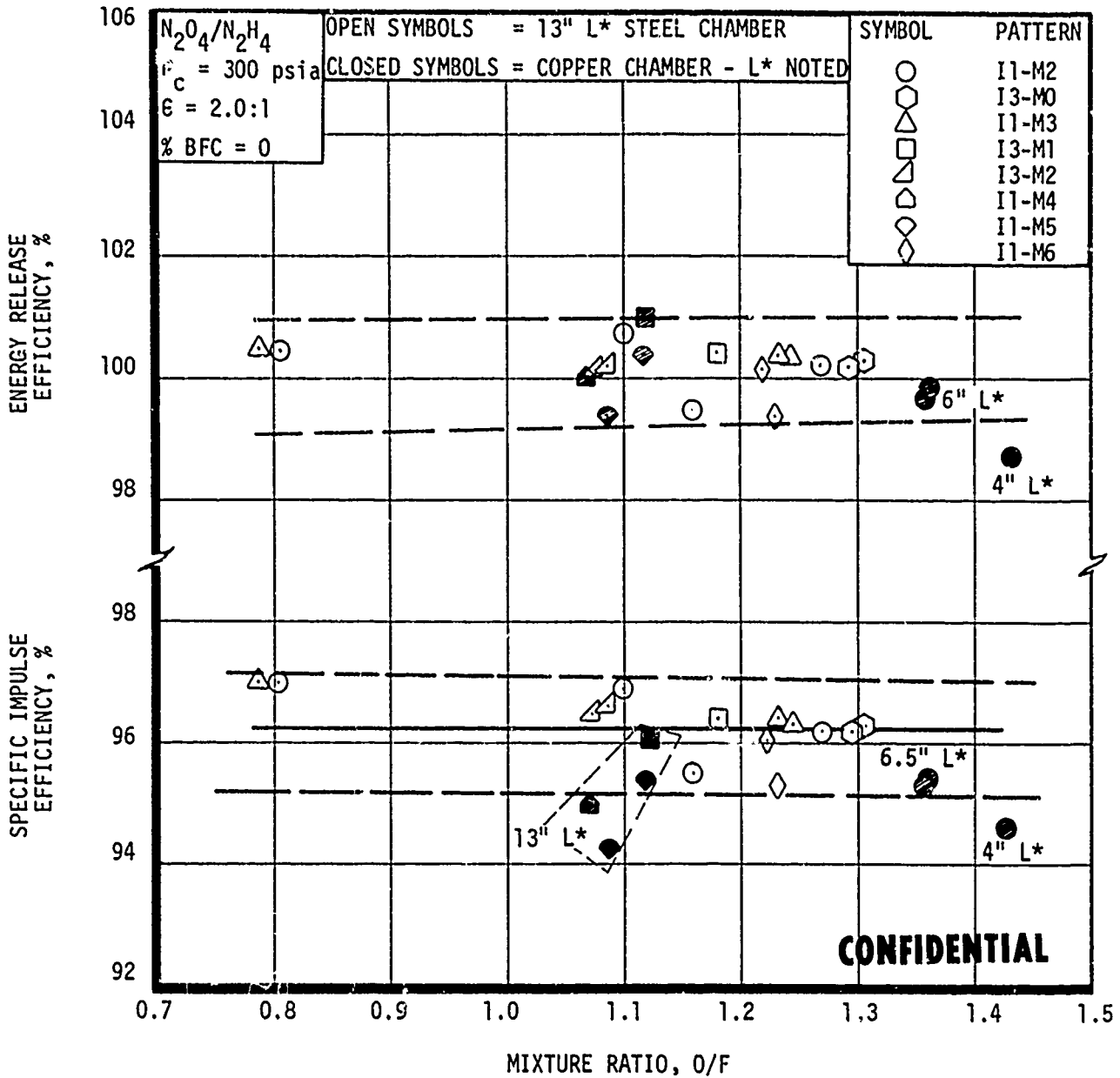
Figure 50. Engine Efficiencies versus Mixture Ratio for
Uncooled Tests - Phase I and II Injectors (u)

VII, A, Performance (cont.)

Such a technique was used to present the data of Figure 51. From these data, it appears that the assumption of no mixing between barrier and core used to generate the analytical prediction is reasonable, since the test data points lie near the proper curves.

(2) Chamber Length Effects

(C)   Uncooled tests of the candidate injectors were conducted using chambers of three different lengths: 10 in. (13-in. L*), 5 in. (6.5-in. L*), and 3 in. (4-in. L*). The performance of representative tests conducted with these three chambers is shown in Figure 52. Both the specific impulse efficiency and the energy release efficiency are shown as functions of chamber length. These data indicate no performance degradation for a chamber length reduction from 10 in. to 5 in. During tests with the 10-in. chamber, P_c taps were located 1.5 and 7.0 in. downstream of the injector/chamber interface. Correction for the flow conditions at these two stations resulted in predicted stagnation pressures which differed by only 2%. The agreement between these pressure readings indicates that most of the combustion probably occurred within 1.5 in. of the injector face since momentum pressure losses would have been noted if significant combustion occurred downstream of the 1.5 in. station. The tests with a 3-in.-long chamber (4-in. L*) tended to verify that the combustion was occurring close to the injector face. The curve defining the energy release efficiency - length relationship has been extrapolated to a chamber length of 1.5 in. using the propellant vaporization model described previously. At this point, the predicted n_{ER} is in excess of 94%. Recent test data from a similar size HIPERTHIN unit using similar propellants (Reference 14) yielded an energy release efficiency of 93 to 96% with a 1-in. chamber. Efficiencies of this magnitude are expected from the N_2O_4/N_2H_4 unit with a 1.5-in. chamber.
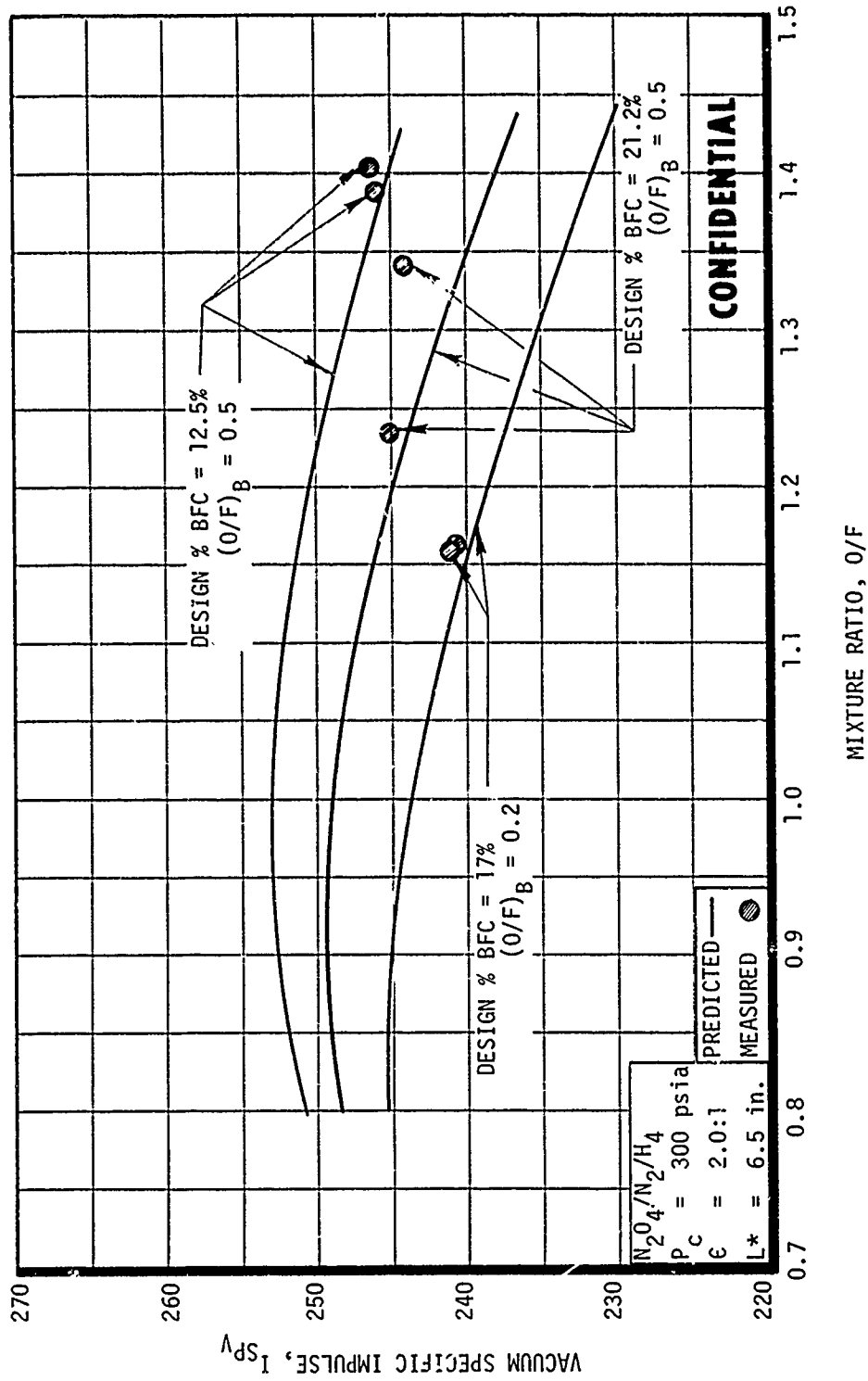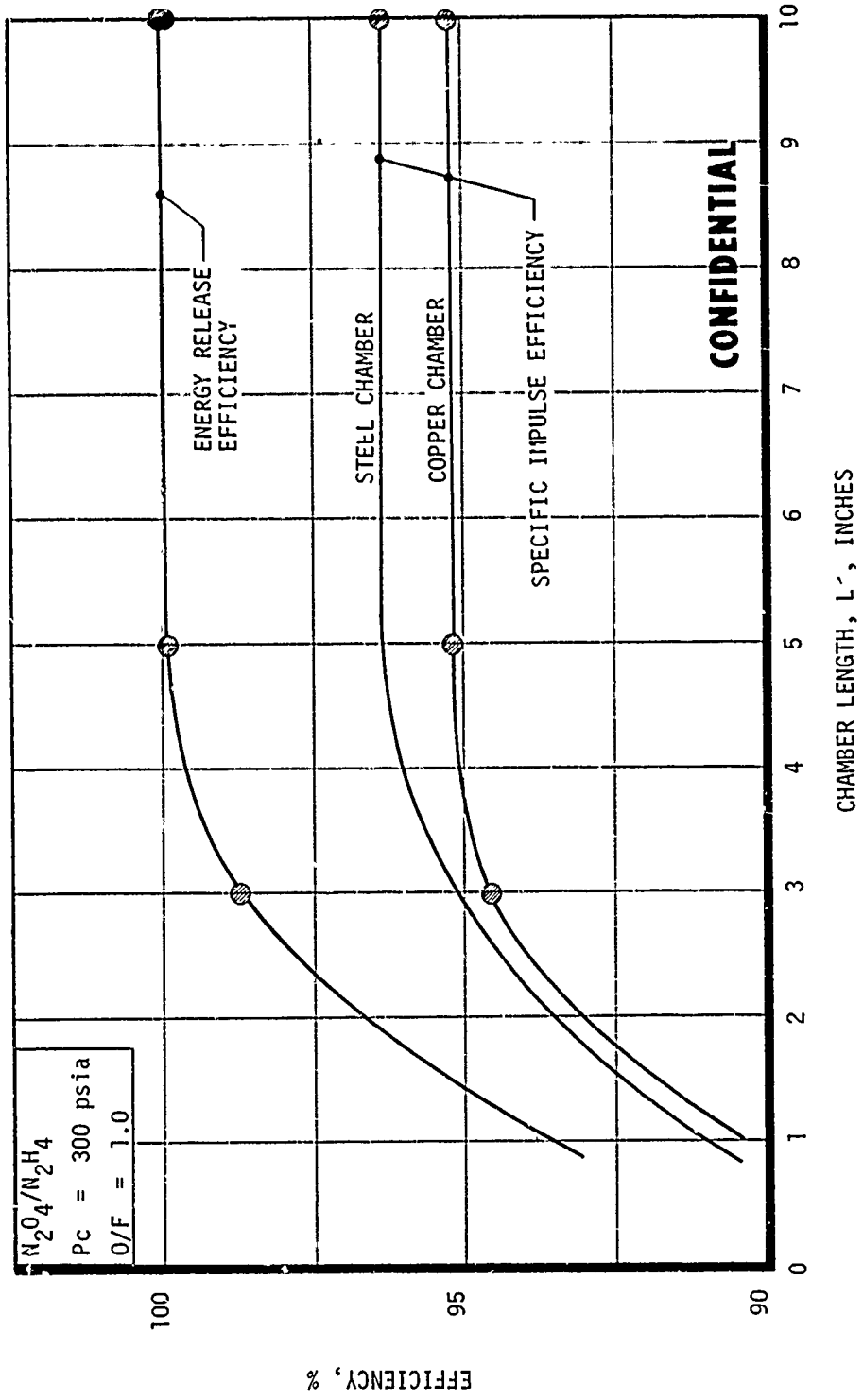
Figure 51. Effect of Mixture Ratio on Specific Impulse for Cooled Tests – Phase I and II Injectors (u)

Figure 52. Effect of Chamber Length on Specific Impulse Phase I and II Injectors (u)

VII, A, Performance (cont.)

(3) Barrier Cooling Effects

(U)   The influence of barrier cooling on performance can
be considered essentially as a mixture ratio maldistribution loss. The loss
due to cooling, assuming no mixing of coolant and core zone, can be estimated
from a stream tube technique which compares the mass flow rate weighted sum
of the coolant and core I_{sp} values to the specific impulse evaluated at the
overall engine mixture ratio. Both the percent barrier flow and the barrier
mixture ratio affect the core mixture ratio. The carpet plots presented in
Figures 53 and 54 illustrate the functional relationship between barrier zone
flow and core flow. Use of these plots allows accurate definition of the
relationship between barrier and core flows.

(U)   Due to the limited amount of test data, the empirical
effect of coolant flow on performance cannot be completely defined without the
use of some analytical curves that were derived from the barrier flow-core
flow relationships of Figures 53 and 54. Also, two assumptions based on the
test data from the uncooled tests are necessary: (1) chamber length variations
between 5 and 10 in. have a negligible effect on performance, and (2) the
various baffle patterns have a negligible effect on performance. An additional
useful condition is that the maximum cooling performance loss would be realized
if the coolant and core stream tubes did not mix but combusted at their
respective mixture ratios. Assumptions (1) and (2) allow all the performance
data from barrier cooled tests to be analyzed as one group. Use of the stream
tube assumption permits minimum limits to be defined for the amount of barrier
flow necessary to effect a measurable performance change. Since two standard
deviations of the system measurement errors for I_{sp} are approximately 2.6 lbf-
sec/lbm, only changes in barrier coolant flow which influence performance by
this amount were considered significant.
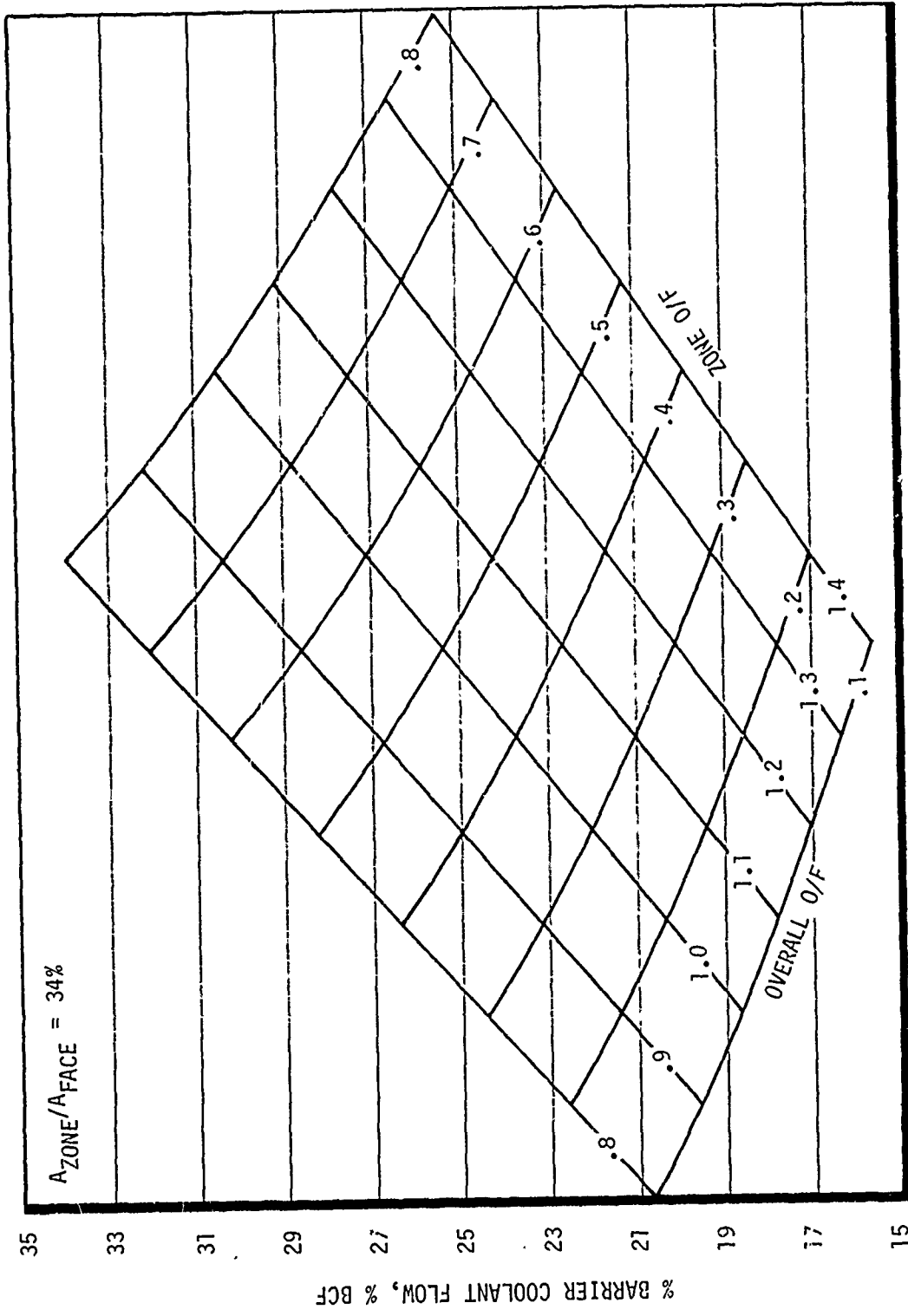
Figure 53. Percent Barrier Cooling as a Function of Barrier and Engine Mixture Ratio
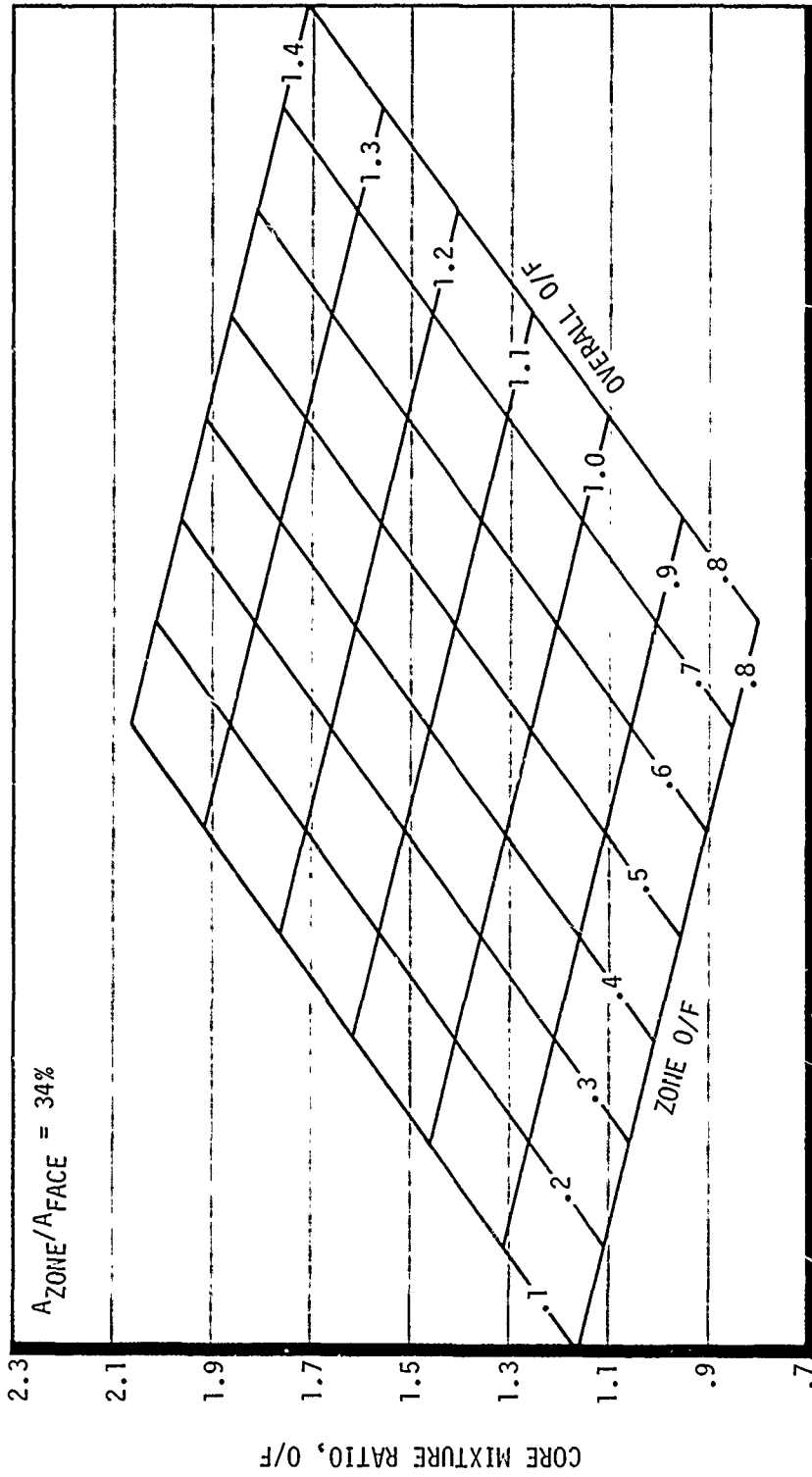
Figure 54. Core Mixture Ratio as a Function of Barrier and Engine Mixture Ratio

VII, A, Performance (cont.)

(C)   The analytically predicted performance loss due to
barrier zone cooling is shown on Figure 55 as a function of percent barrier
flow. Barrier mixture ratios of 0.5 and 0.2 were evaluated at overall mixture
ratios of 1.16 and 1.4. These conditions correspond to the flow conditions
during Tests 3K-1-117, 118, 120, and 121, respectively. The data from these
tests are plotted in the figure. For these tests, the assumption of no mixing
of barrier and core appears to be reasonable.

(4) Performance Conclusions for Phases 1 and II Injectors

(C)   Based on the analysis of test data, the following
conclusions regarding the performance achieved with the Phases I and II
designs may be drawn:

(a) Energy release efficiencies of 99 to 100%
were achieved with all injector configura-
tions on which performance was evaluated.

(b) The effect of engine length on η_{ER} was
negligible in the range of lengths from
5 to 10 in.

(c) The effect of barrier cooling flow on
performance indicates that no appreciable
mixing occurred between barrier and core
zones.

3.   Final Injector Design

a.   Sea Level Performance

(1) Introduction

(C)   The injector design selected for the final test
series was identical to injector I4 except for the use of smaller width
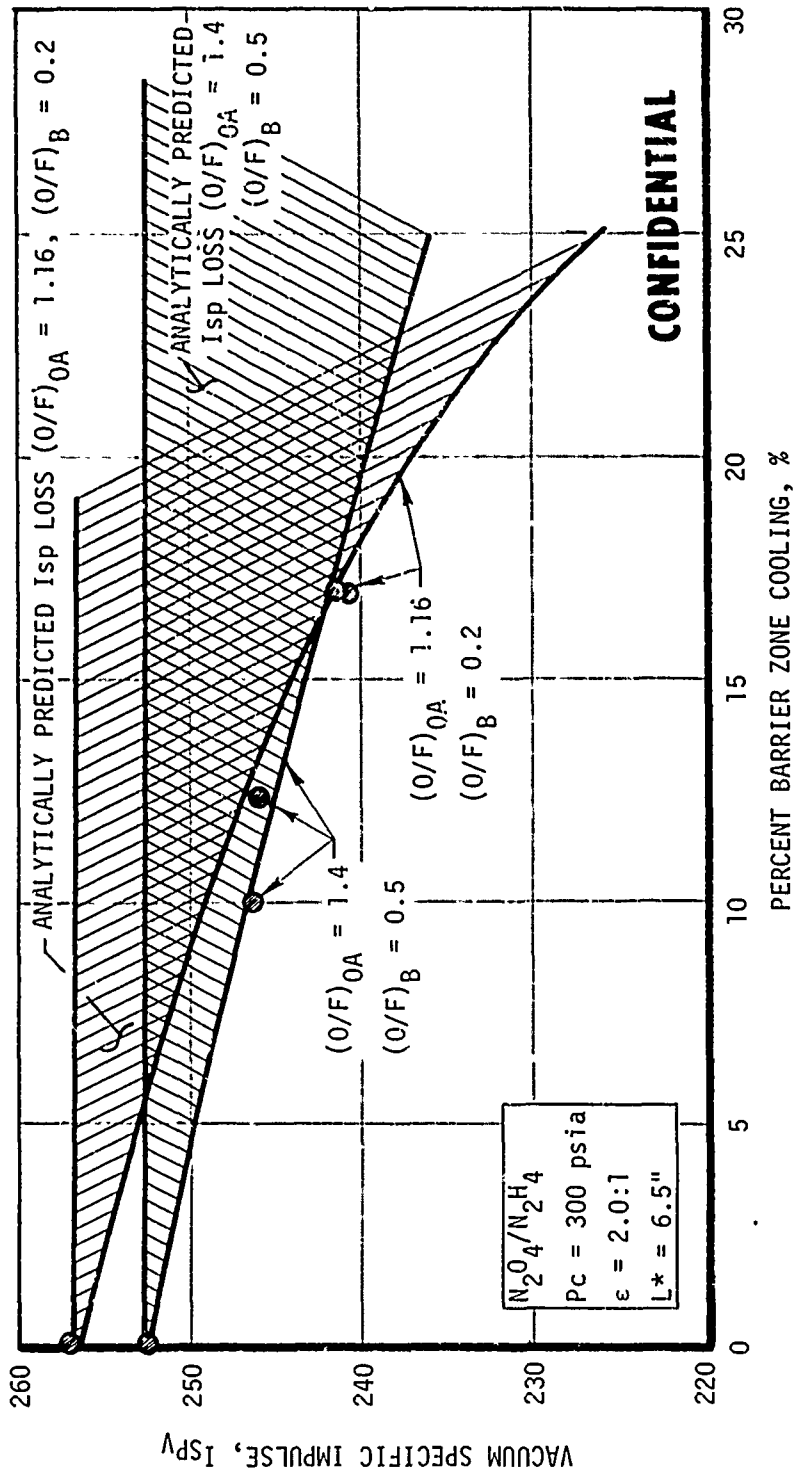
Figure 55. Effect of Cooling Flow on Coolant Performance Loss - Phase I and II Injectors (u)

VII, A, Performance (cont.)

showerhead channels in the baffles. This modification increased the propellant injection velocity at the baffles from 15 ft/sec to 30 ft/sec. The revision to the baffle design was made to eliminate a tendency for platelet separation in the baffle region. The effects of this modification on performance were expected to be small (less than 0.5%) with the 5-in. chamber. Testing of the unit commenced with Test 3K-1-183 (a balance test on which performance parameters were not reduced) and ended with Test 3K-1-200. Chambers tested with this injector included 10-in. and 5-in. copper units, a 10-in. steel chamber, and 5-in. ablative chambers. Performance data from these tests are tabulated in Table V. All tests in this series were with a design intended to provide 21.2% barrier flow with a barrier mixture ratio of 0.5 at a total flow rate of 10 lb/sec and overall injector mixture ratio of 1.4.

> (2) Effect of Design and Operating Variables on Performance

>> (a) Mixture Ratio

(U)   Specific impulse data from Table V are plotted in Figure 56 as a function of engine mixture ratio. Based on these test data, the optimum mixture ratio for specific impulse is approximately 1.0 at an area ratio of 2.0. The data presented in Figure 56 indicate about 1% higher performance with the 13-in. L* steel chamber than with the 6.5-in. L* copper chamber. Based on the data from the preliminary injectors, which achieved complete combustion at all lengths and mixture ratios, it appears unlikely that the performance increase is due to increased energy release efficiency. For the large steel chamber, it is likely that the higher performance was the result of the difference in chamber heat loss and increased mixing between core and barrier gases. Data from tests with the ablative chamber also showed higher performance than was achieved with the identical contour copper chamber. This performance difference was accounted for by the difference in heat loss between the two chambers.

TABLE V

SUMMARY OF FINAL INJECTOR PERFORMANCE (u)

Test No. 3K-1-	Chamber	Overall Mixture Ratio	Chamber* Pressure, psia	Vacuum** Specific Impulse lbf sec/lbm	Characteristic* Velocity, ft/sec c*	% I_{sp} ε=2.0:1	(% c*)*	n_{ER}	Comments
185	6.5 L* Cu	1.04	305.1	250.3	5291	93.7	90.3	~100	Valid performance test, measured P_c low
186	6.5 L* Cu	0.86	283.3	249.7	5274	94.5	90.8	~100	Valid performance test, measured P_c low
187	6.5 L* Cu	1.40	289.9	244.2	5168	92.5	89.7	~100	Valid performance test, measured P_c low
188	6.5 L* Cu	1.16	295.3	248.5	5253	92.9	89.7	~100	Valid performance test, measured P_c low
189	13 L* Cu (insert)	--	--	--	--	--	--	--	Test with ablative boot, performance not evaluated
190	13 L* Stl	1.17	325.7	251.1	5591	94.0	102.0	~100	Valid performance test
191	13 L* Stl	0.848	316.6	250.9	5922	95.0	102.0	~100	Valid performance test
192	13 L* Stl	1.36	324.1	247.9	5875	93.5	102.0	~100	Valid performance test
193	13 L* Stl	1.15	325.4	251.5	5929	94.1	132.0	~100	Valid performance test
194	13 L* Stl	--	--	--	--	--	--	--	Short test, altitude start evaluation thrust oscillation, performance not evaluated
195	13 L* Stl	1.35	324.9	246.7	5039	94.6	103.0	100	Oxidizer temperature error--assumed $T_o = T_f$
196	13 L* Stl	0.839	314.5	250.0	5841	96.6	103.0	100	Oxidizer temperature error--assumed $T_o = T_f$
197	6.5 L* Si-Ph	--	--	--	--	--	--	--	Balance test, performance not evaluated
198	6.5 L* Si-Ph	1.133	339.3	254.3	6207	95.1	106.0	100	Valid performance test
199	6.5 L* Si-Ph	1.140	No P_c	253.1	--	94.6	--	100	Valid performance test
200	6.5 L* Si-Ph	1.131	331.2	252.4	6043	94.4	105.0	100	Valid performance test

*Corrected to stagnation conditions
**Area Ratio = 2.0:1
% BFC = 21.2%
O/F_B = 0.5 at $(O/f)_{o}/A$ = 1.4

Page 142
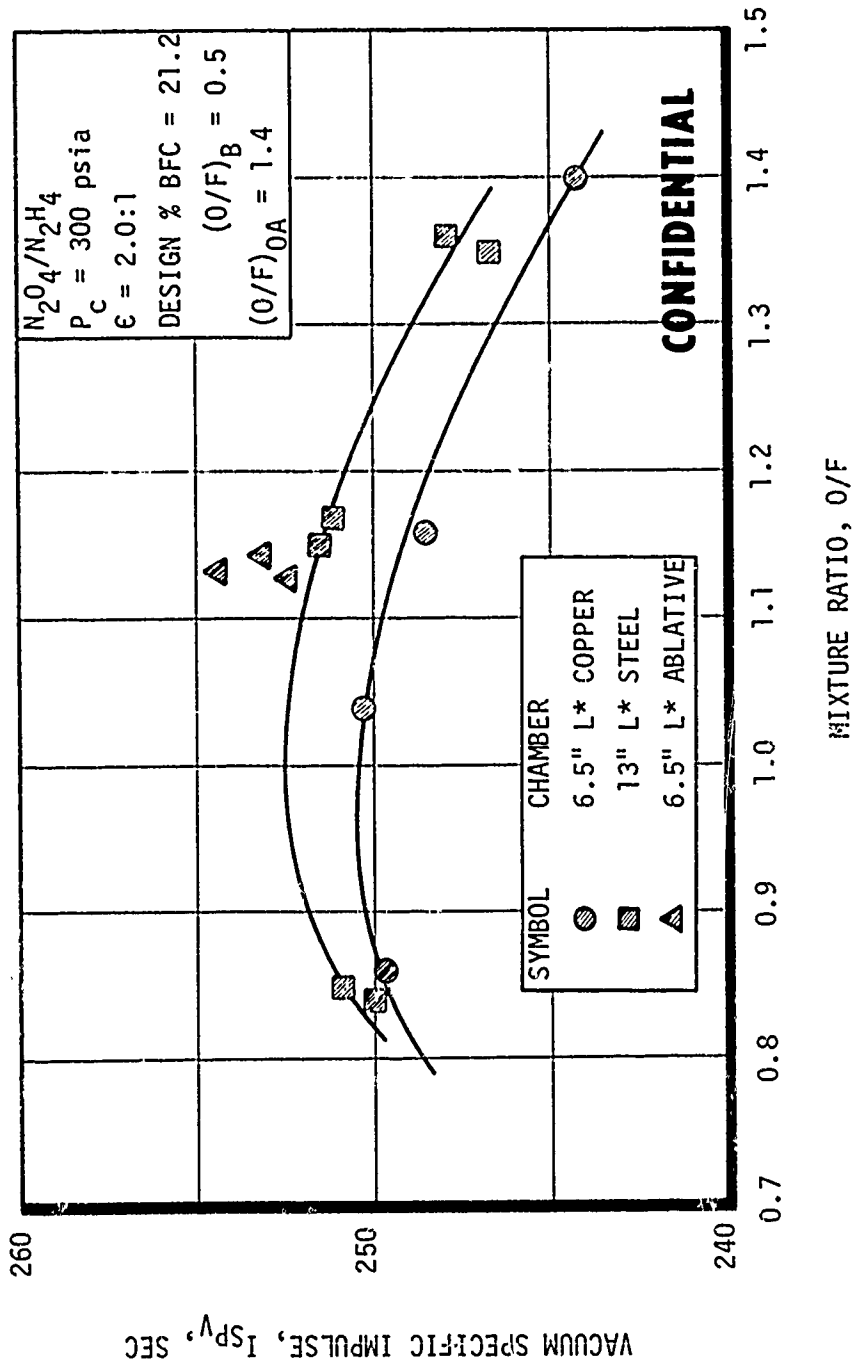
Figure 56. Effect of Mixture Ratio on Measured Specific Impulse – Final Design (u)

VII, A, Performance (cont.)

(U)   An analysis of the performance losses with the
new injector indicates that the barrier and core flows were partially mixed.
The amount of mixing of the two streams is evident from the erosion character-
istics noted after the tests with ablative chambers. The amount of barrier
and core mixing was inferred from the ablative chamber tests by relating the
distinctive areas of erosion to a combustion product temperature and, hence
mixture ratio. Using three stream tubes, an unmixed barrier, a mixed barrier
and core, and an unmixed core, the performance loss analysis technique pre-
dicted the measured performance of the ablative chamber (Test 3K-1-200) within
1 sec of specific impulse. These same stream tubes, adjusted for variations
in overall mixture ratio, were then used to analytically predict specific
impulse over the full test range of O/F. Curves illustrating the magnitude
of the various performance losses for the 6.5-in. L* chamber are shown in
Figure 57. Also shown is a predicted performance curve based on an assumption
of no barrier-core mixing.

(b) Engine Length

(C)   The effect of combustion chamber length on
specific impulse derived from tests using the final injector is shown in
Figure 58. The data in Figure 58 have been corrected to a mixture ratio of
1.0 using the curves of Figure 56. The energy release efficiency, η_{ER}, as a
function of engine length is shown in Figure 59. Energy release efficiencies
were calculated from the test data by adding the "known" losses--barrier
cooling (mixture ratio maldistribution), divergence, and boundary layer--to
the measured specific impulse and comparing this sum to the theoretical ODE
specific impulse. The MRD losses were calculated assuming the three stream
tubes mentioned in the previous section. For comparison, the effect of length
on η_{ER} from a similar HIPERTHIN engine used on Spartan and discussed in Refer-
ence 10 is shown in the figure. The efficiency of the N_2O_4/N_2H_4 engine is
approximately 3% lower than the efficiency of the Spartan unit at a chamber
length of 1.5 in.
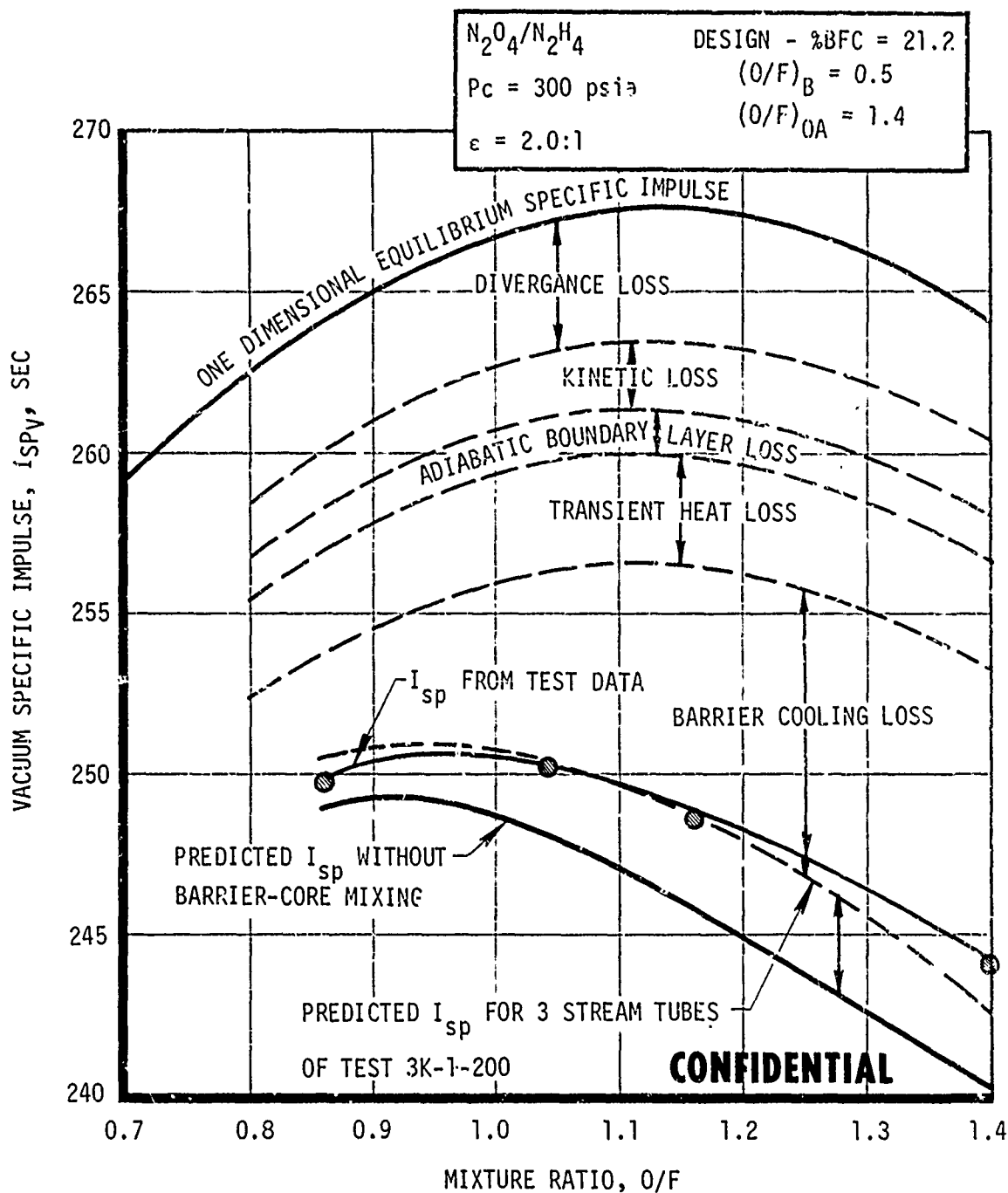
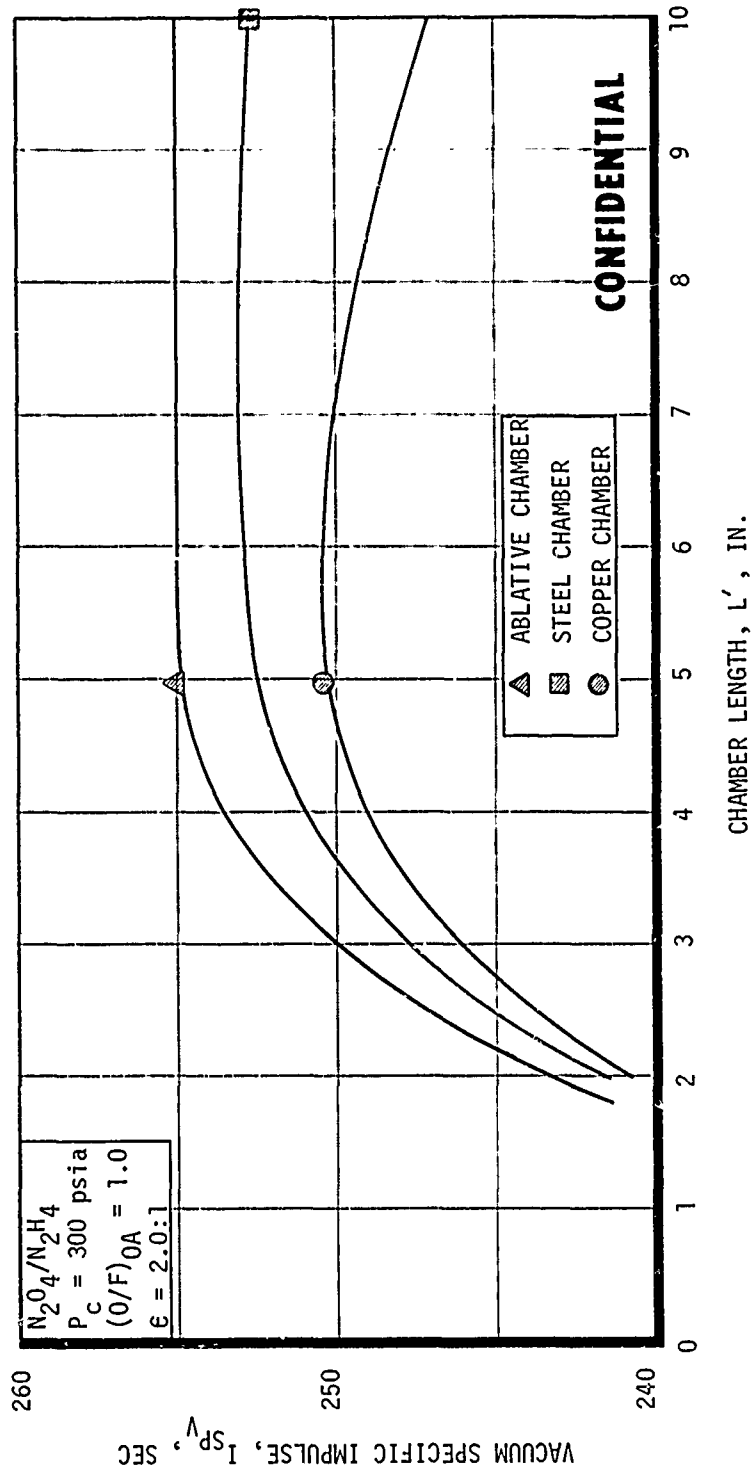Figure 57.   Effect of Mixture Ratio on Performance Losses (u)

Report AFRPL-TR-69-122

Figure 58. Effect of Chamber Length on Specific Impulse – Final Injector (u)

Report AFRPL-TR-69-122
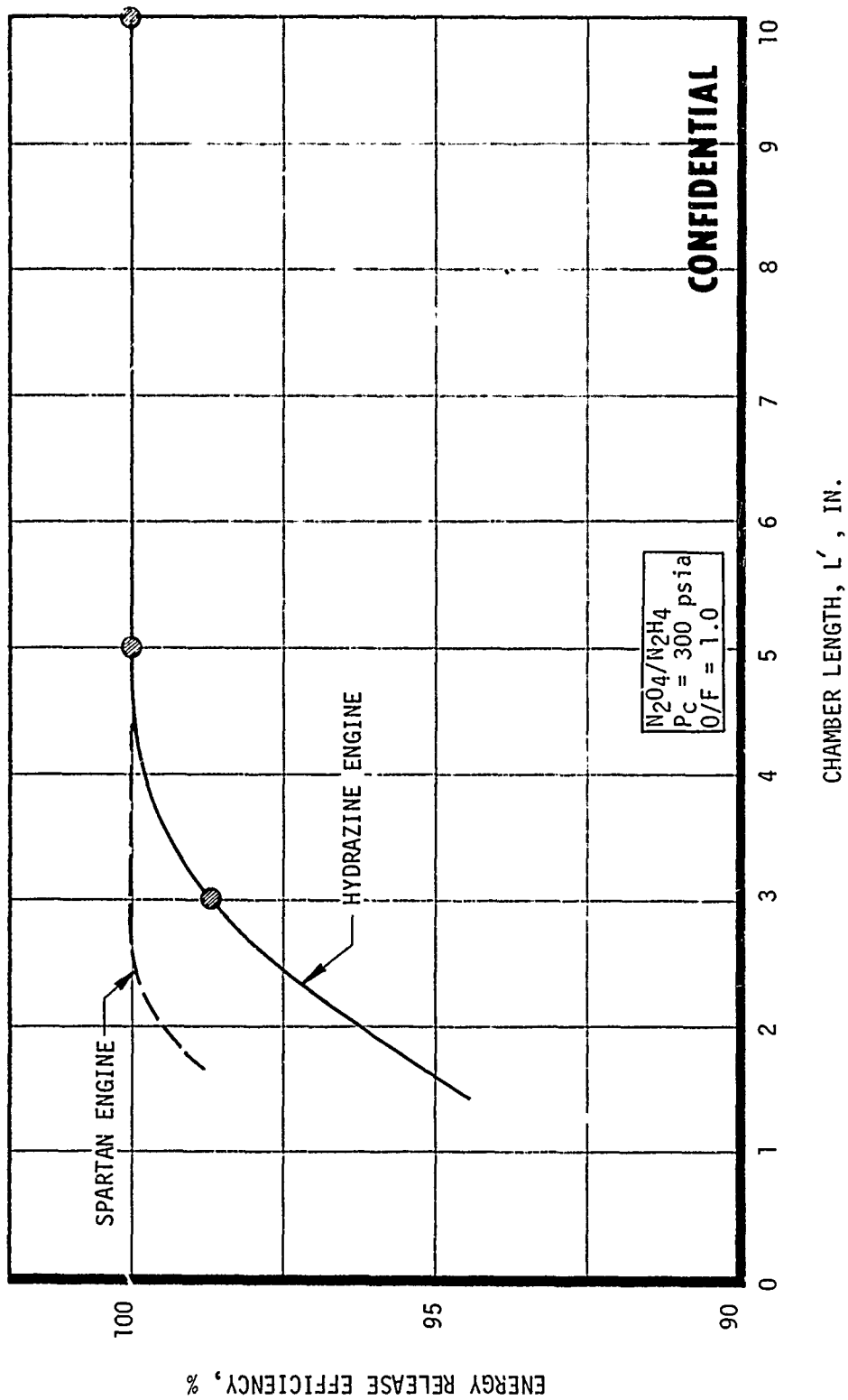
Figure 59. Effect of Chamber Length and Mixture Ratio on Energy
Release Efficiency - Final Injector (u)

VII, A, Performance (cont.)

(c) Barrier Cooling

(U)   The barrier cooling flow produced by the final
injector appeared to mix with the core flow to a much greater degree than that
produced by the Phases I and II injectors. This mixing resulted in higher
performance for the final injector design compared to the preliminary designs
at the same designed cooling flow conditions.

(U)   The barrier flow conditions of the final
design should have provided 21.2% boundary cooling flow at a mixture ratio of
0.5, based on the calculated pressure drop through the coolant ring orifices.
However, modifications to the injector flow circuits may have provided slightly
greater barrier flow and mixture ratio than was calculated based on coolant
orifice flow area. The predicted effect of barrier flow rate on specific
impulse is shown in Figure 60. To define the curve of Figure 60, three stream
tubes were assumed based on core flow conditions, barrier conditions, and
barrier-core mixing.

4.   Extrapolation of Performance to Altitude Conditions

(C)   The altitude performance predictions quoted in this section
rely on loss analyses conducted to determine the cooling and energy release
losses inherent in the measured sea level data. The extrapolation of these
losses to the altitude configuration is usually the least understood phase
of performance extrapolations. The performance losses at altitude due to
nozzle curvature, boundary layer effects, and kinetic effects were calculated
using ICRPG-recommended programs or techniques as set forth in Reference 1.
These losses are fairly well defined and, with the exception of the kinetic
loss, are usually not significantly influenced by injector design parameters.
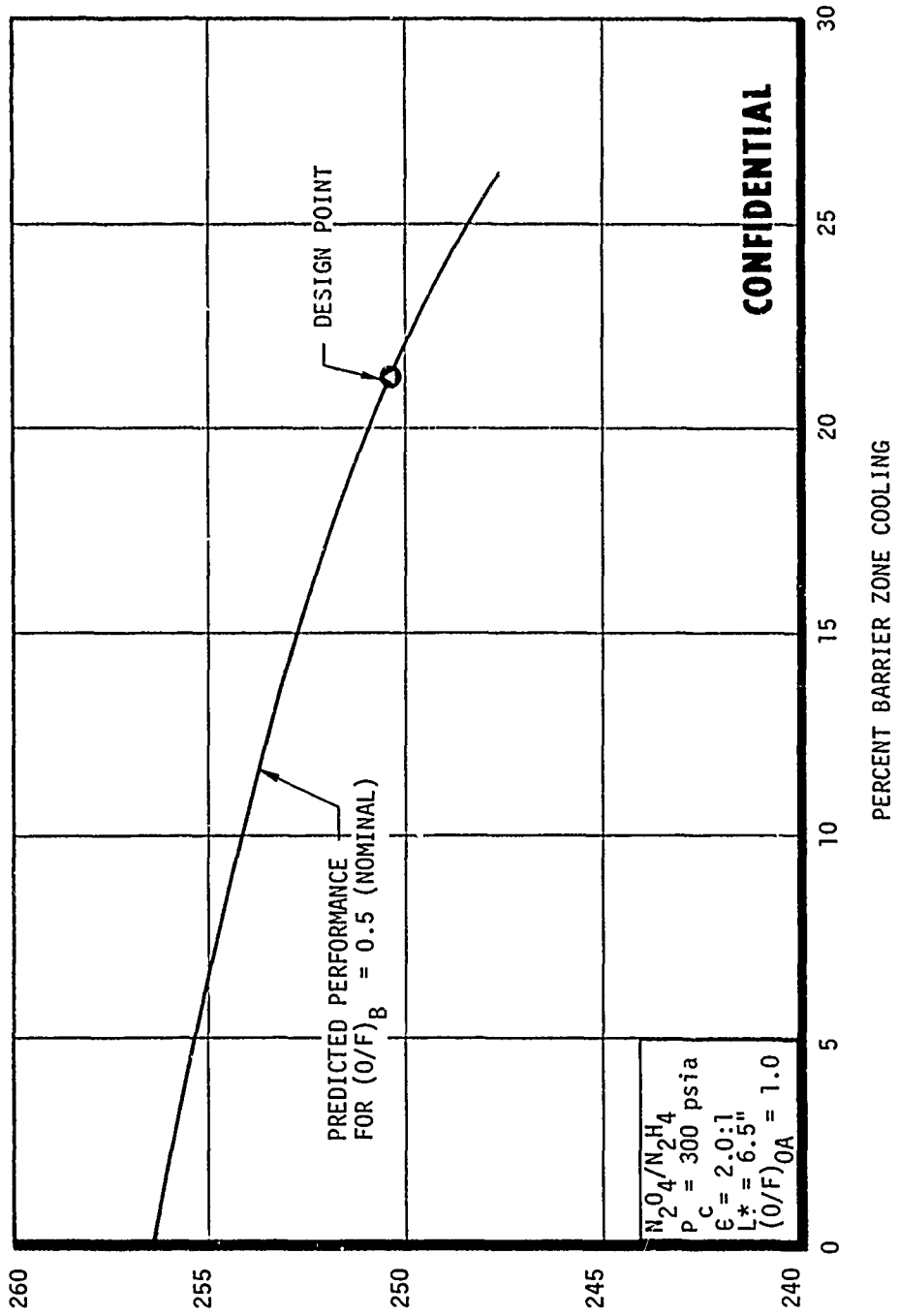
Figure 60. Effect of Barrier Cooling Flow on Specific Impulse (u)

VII, A, Performance (cont.)

(C)   On the other hand, the extrapolation of cooling and energy release losses to altitude is not so well defined and is influenced by the injector design variables. A knowledge of the injector mixture ratio distribution and element energy release efficiency is necessary for accurate performance extrapolation of these losses. This knowledge requires consideration of the injector hydraulics and propellant spray distribution. The propellant vaporization analysis discussed in a preceding section has proven to be a useful tool for the determination of element energy release efficiency. The stream tube analysis, as described in Reference 2, has proven to be useful in determining mixture ratio maldistribution losses such as those caused by barrier cooling requirements. For the N_2O_4/N_2H_4 engine, the energy release efficiencies were essentially 100% and the MRD losses were well characterized by the three-stream-tube model mentioned previously.

(C)   Altitude performance predictions for the hydrazine engine, based on complete combustion (100% η_{ER}) and stream tube flow, are given in the following sections as functions of engine mixture ratio. In addition, an analytical curve of specific impulse as a function of engine length is presented.

a.   Effect of Mixture Ratio on Altitude Specific Impulse

(C)   Extrapolation of sea level data from Tests 3K-1-185 to 188 to an altitude 30:1 area ratio minimum length Rao nozzle configuration results in the specific impulse values shown in Figure 61. The predicted altitude curve based on stream tube data defined by Test 3K-1-200 is also shown in the figure. Comparison between the individual test extrapolations and the predicted curve shows a maximum disparity of less than 1% at a mixture ratio of 1.4. The contract requirement for minimum specific impulse of 300 sec at ε = 30:1 will be exceeded by the engine. A peak value of 309 lbf-sec/lbm at 0/F = 1.0 and an I_{sp} of 300 lbf-sec/lbm or greater will be achieved
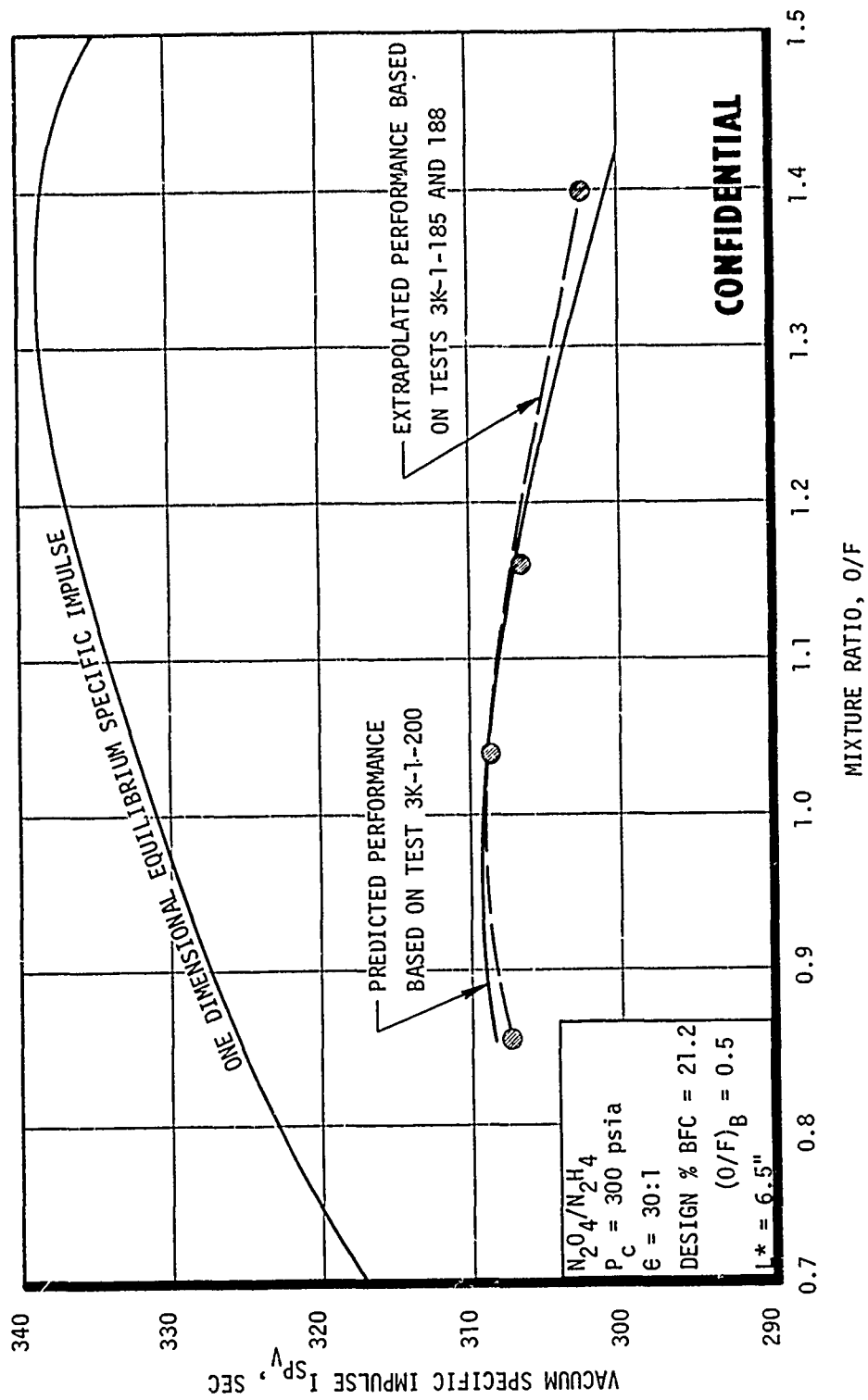
Report AFRPL-TR-69-122

Figure 61. Predicted Effect of Mixture Ratio on Altitude Specific
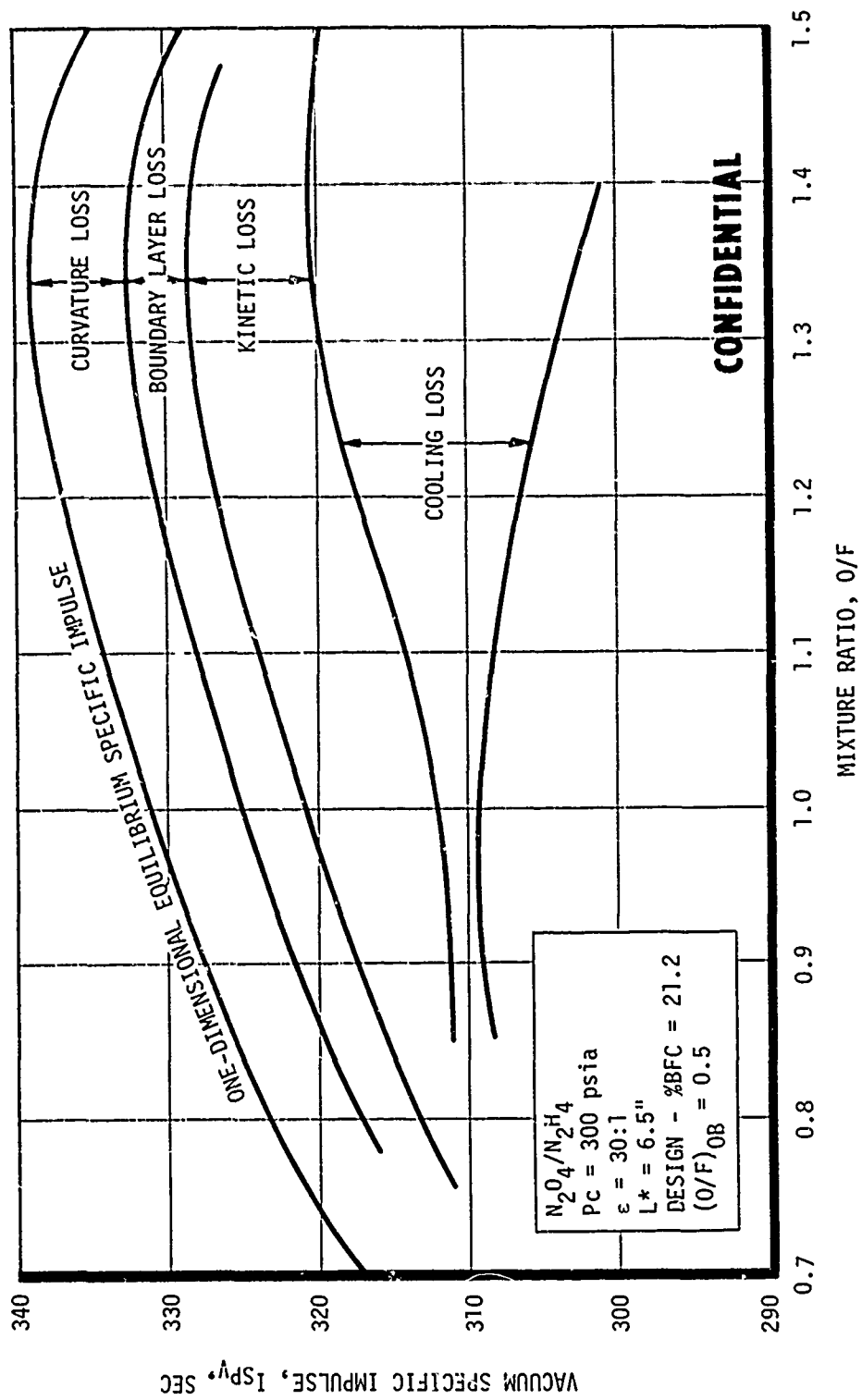Impulse - Final Injector (u)

VII, A, Performance (cont.)

throughout the mixture ratio operating range of 0.95 to 1.40. The minimum
predicted performance of 302 lbf-sec/lbm will occur at O/F = 1.4. For compari-
son, the curve of one-dimensional equilibrium I_{sp} as a function of mixture ratio
for N_2O_4/N_2H_4 at a chamber pressure of 300 psia is shown in the figure. The
difference between the mixture ratio for peak theoretical I_{sp} and the mixture
ratio at maximum predicted I_{sp} is due to the effects of the cooling and kinetic
performance losses. The influence of the performance losses in determining
the shape of the predicted I_{sp}-mixture ratio relationship is illustrated in
Figure 62. The increase in cooling loss at high mixture ratios is the result
of the injector core O/F passing beyond the value for maximum performance.
The data from Figure 62 are presented in Figure 63 in terms of specific impulse
efficiency. Again, the decrease in performance at high mixture ratios, as
shown in the figure, is due to increased cooling and kinetic losses.

b. Effect of Combustion Chamber Length on Altitude
Specific Impulse

(C)   The most significant influence of combustion chamber
length on performance is usually due to combustion efficiency effects caused
by propellant vaporization or atomization limitations. In addition, boundary
layer effects and propellant mixing can also cause performance changes with
length. The length of a chamber usually is a factor in determination of
coolant requirements, so that chamber length has an indirect, but sometimes
significant, influence on coolant performance loss. The predicted effect of
chamber length on energy release efficiency has been shown in Figure 59, along
with the measured effect of η_{ER} for the Spartan engine system. These curves
indicate the possibility of achieving 99 to 100% η_{ER} with chamber lengths down
to 2 in. or less. The energy release curve for the hydrazine engine from
Figure 59 was used to predict the effect of length on altitude specific impulse
as shown by the curve of Figure 64. From this curve, it appears that the

Figure 62. Effect of Mixture Ratio on Altitude Specific Impulse Losses (u)

Report AFRPL-TR-69-122
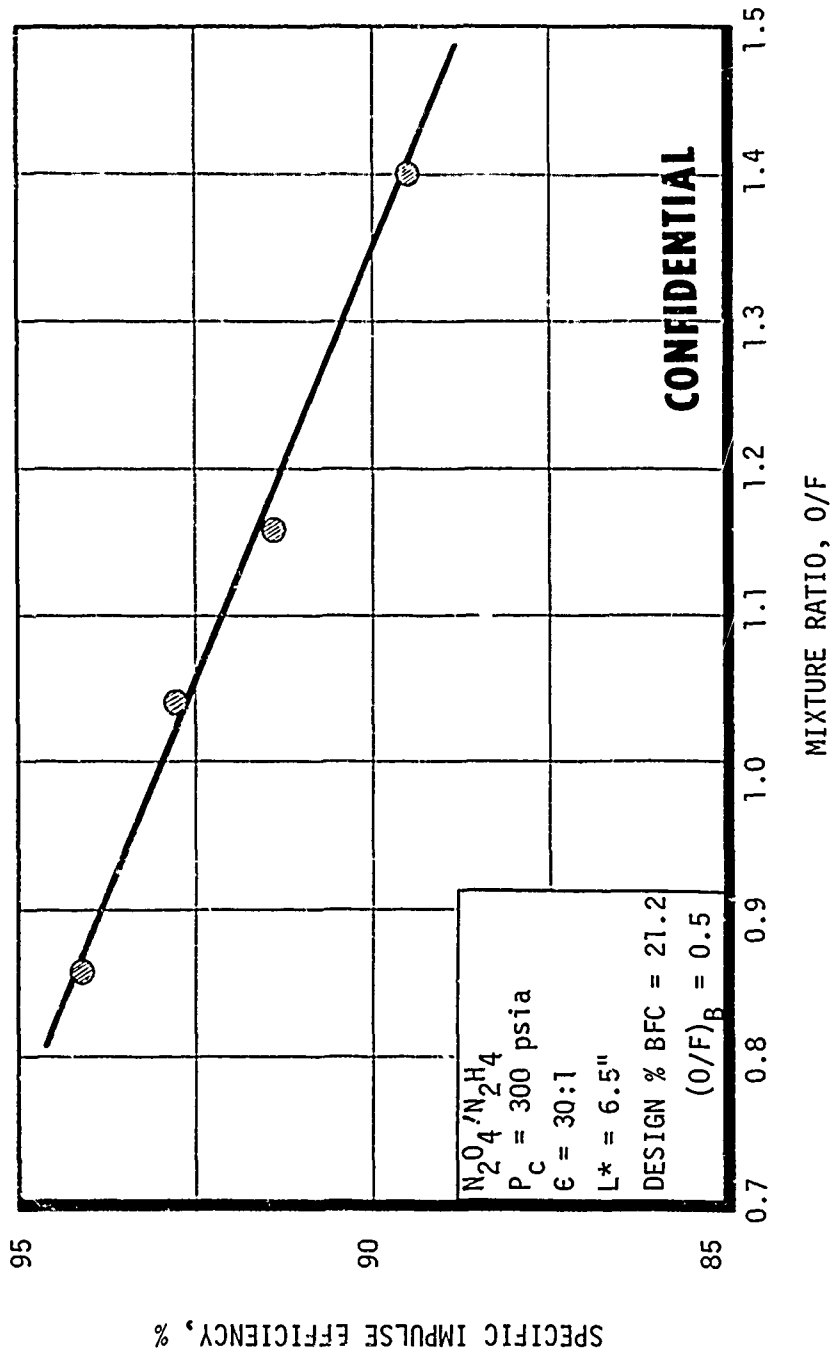
Figure 63. Effect of Mixture Ratio on Predicted Altitude Specific Impulse Efficiency - Final Injector (u)

Page 154
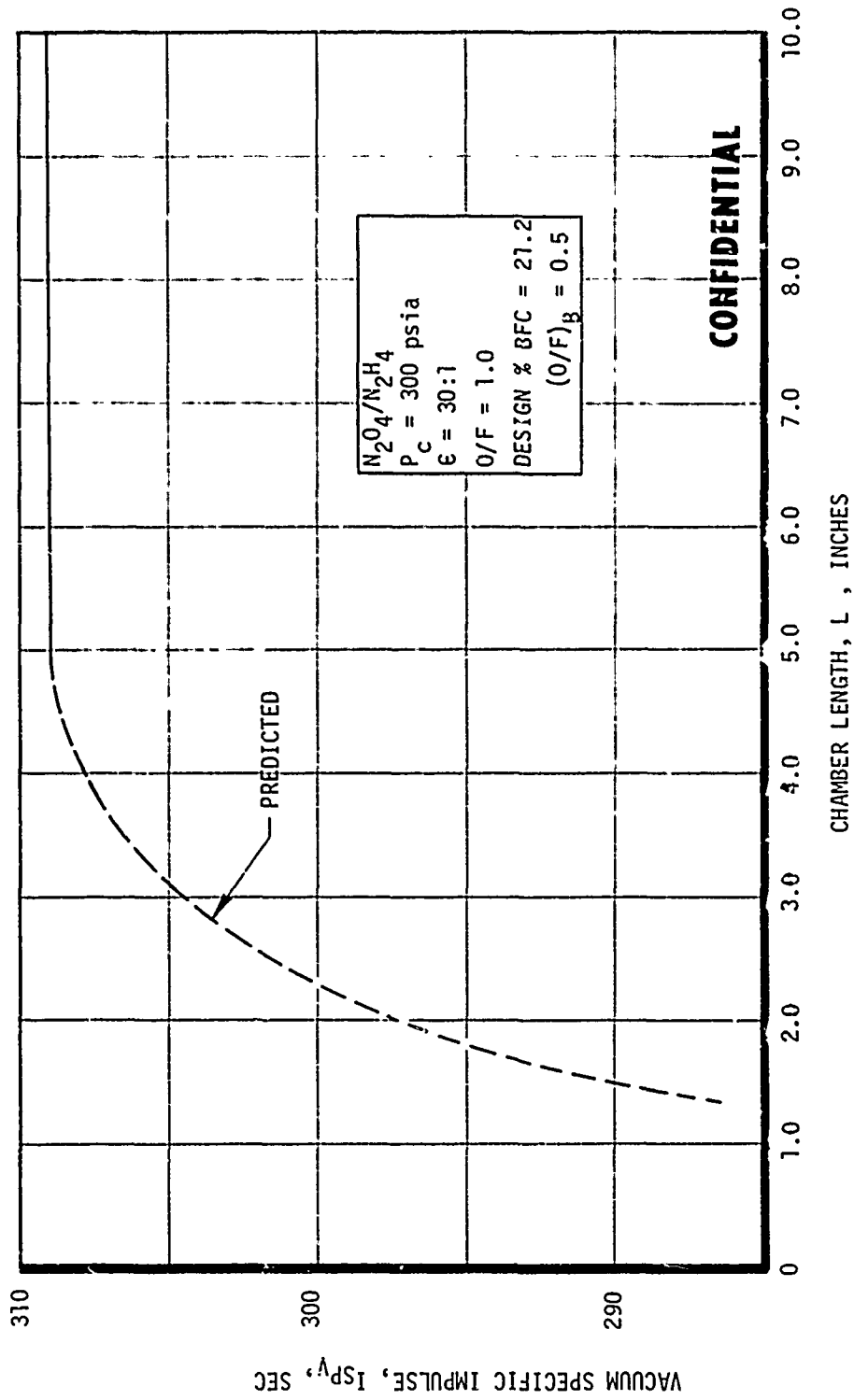
Figure 64. Effect of Chamber Length on Predicted Altitude Specific Impulse - Final Injector (u)

VII, A, Performance (cont.)

required altitude specific impulse of 300 lbf-sec/lbm can be met with a 2.5-in.-long chamber at a mixture ratio of 1.0 and approximately 21.2% boundary cooling flow at a barrier mixture ratio of 0.5. If the barrier flow can be reduced as the chamber is made shorter, the performance at short chamber lengths will be slightly higher than is shown in Figure 64.

5. Performance Conclusions

(C)   The preceding discussion and presentation of test data have led to certain conclusions regarding the performance of the hydrazine injectors. These conclusions are restated in this section in a more explicit and concise form. Data analyses and interpretation of measured sea level performance and predicted altitude performance on the final N_2O_4/N_2H_4 injector design indicate the following:

(C)   a.   The contract requirement for a minimum peak altitude specific impulse of 300 lbf-sec/lbm in the mixture ratio range of 0.95 to 1.40 can be easily achieved with the existing design. With the present design, the unit will exceed the contractually required I_{sp} over the entire mixture ratio range.

(U)   b.   A reduction of combustion chamber length from 5 in. to 3 in. or less will meet contract performance requirements.

(C)   c.   The mixture ratio for maximum sea level and altitude specific impulse is approximately 1.0.

(C)   d.   The sea level data indicate essentially complete energy release efficiency throughout the mixture ratio range of 0.95 to 1.40.

(C)   e.   Reduction in energy release efficiency is not appreciable (<1.0%) down to a chamber length of 3.0 in.

VII, Experimental Results (cont.)

B.   COMPATIBILITY

(U)   Three tests were conducted to evaluate the injector/chamber compatibility of the selected injector design. The first of these employed a 13-inch L* copper chamber that had been lined with a silica-rubber based materi..'. The lining, 0.100 in. thick, extended from the injector through the throat.

(U)   The test in which this liner was used (3K-1-189) was inconclusive due to duration limitations of the liner itself. There was not enough material remaining after the test to allow positive identification of injector streak patterns. Primary emphasis was thus placed on the use of the phenolic streak chambers for compatibility evaluation.

(U)   Two tests (3K-1-198 and 3K-1-200) were conducted using the phenolic chambers. The advantage of this material in compatibility analysis lies in the type of erosion and discoloration that occurs during hot firings. Splashing fuel on the chamber wall will leave virgin material. If the fuel is acting as a monopropellant and combusts next to the chamber wall, the ablative material chars with no significant surface removal. Oxidizer rich but low temperature gases produce a whitish discoloration due to the silica melt. Oxidizer rich and higher temperatures melt the silica and allow surface removal through shear.

(U)   Results of the silica-phenolic ablative chamber tests are summarized below:

1.   Throat erosion was evident at discrete chamber locations following each long-duration test. The result of this erosion was an average radius increase of 0.050 in. and throat area change of 8%.

Report AFRPL-TR-69-122

VII, B, Compatibility (cont.)

2. Chamber streaking occurred in line with both major and minor baffles.

3. Streaking over the minor baffles initiated at the injector/ chamber interface, while major baffle streaks initiated a short distance downstream of the interface. This phenomena implied that a finite mixing distance was required to fill the propellant voids that occur off the baffle tips. These voids, shown graphically in the water flow photographs (Figures 65 and 66) are a result of the sloping baffle walls and the wide, flat, baffle tips.

4. Four locations showing no significant erosion occurred at the 0°, 90°, 180°, and 270° circumferential positions. This was expected, since the 0° and 180° locations have fuel showerhead elements adjacent to the wall. At the 90° and 270° points, the fuel and oxidizer elements alternate, providing uniformly distributed, low mixture ratio flow at the wall.

(U)   Figure 67 shows the erosion pattern in a view looking towards the throat. Observed on the chamber, but not on the photograph, were minute streaks from each fuel and oxidizer circumferential orifice. However, this photograph does illustrate the locations and extent of all major streaking.

(U)   The analytically predicted boundary mixture ratios and gas dynamic distribution at the throat station are shown superimposed over the post-fire throat contour in Figure 68. Good correlation is seen to exist between the predicted higher mixture ratios and actual streaks. Diffusion and mixing between adjacent streams extending from the interface occurred as the combustion gases moved to the throat. Therefore, the initially narrow streaks become broader as the gases progressed downstream.

Report AFRPL-TR-69-122
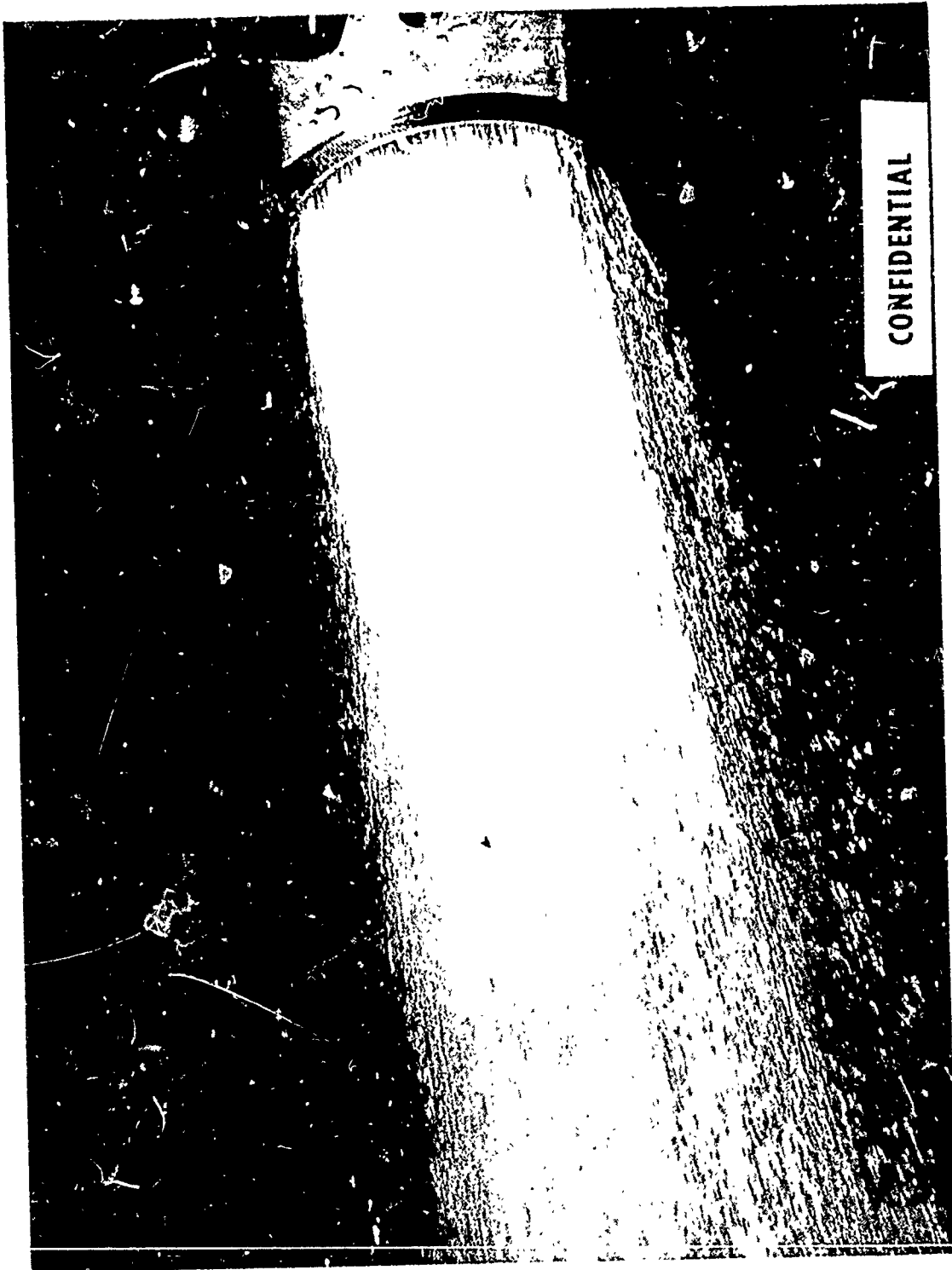
Figure 65. Hydrotest of Injector I6-M0, Fuel Circuit (u)
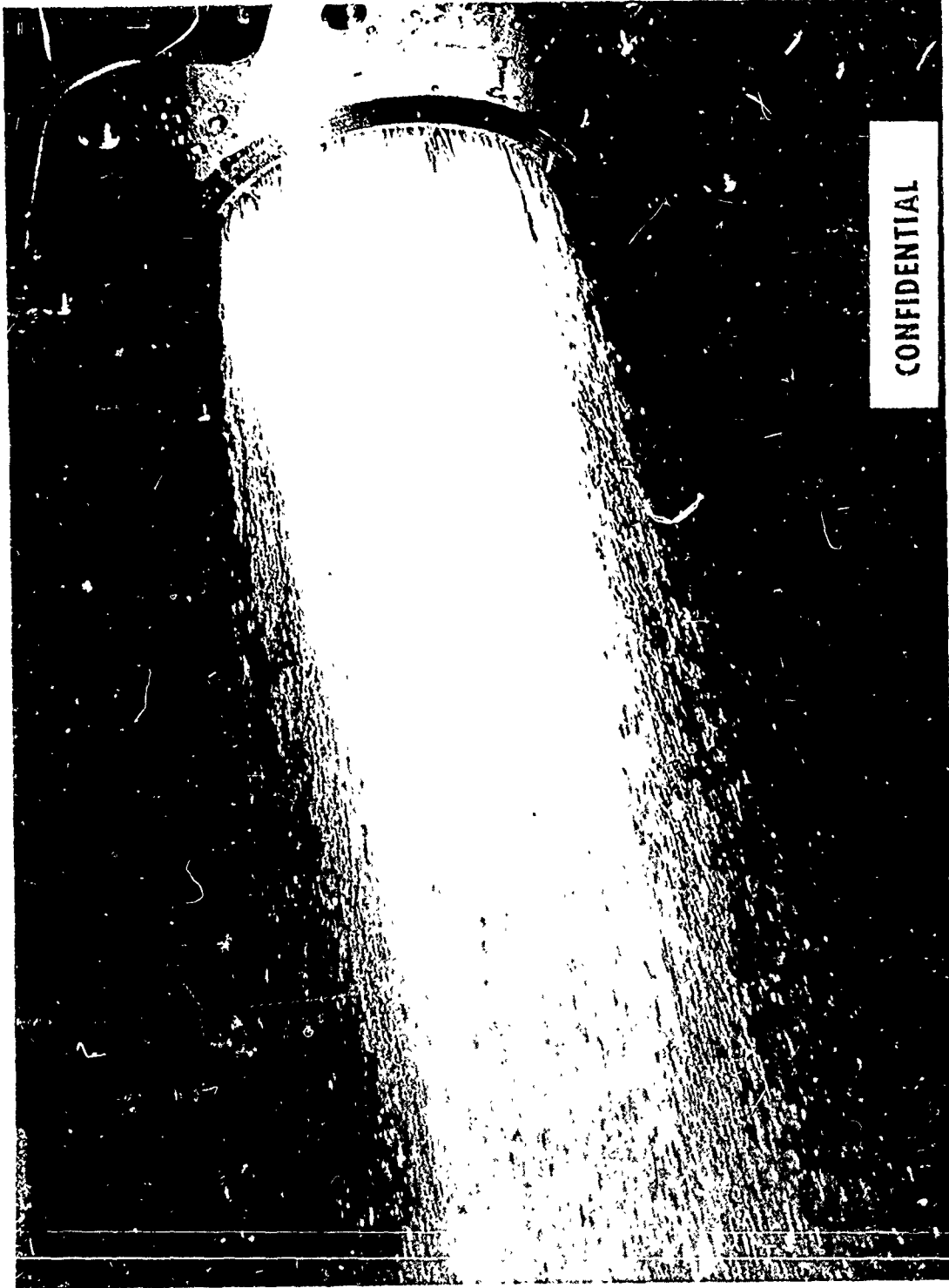
Figure 66. Hydrotest of Injector 16-90, Oxidizer Circuit (u)
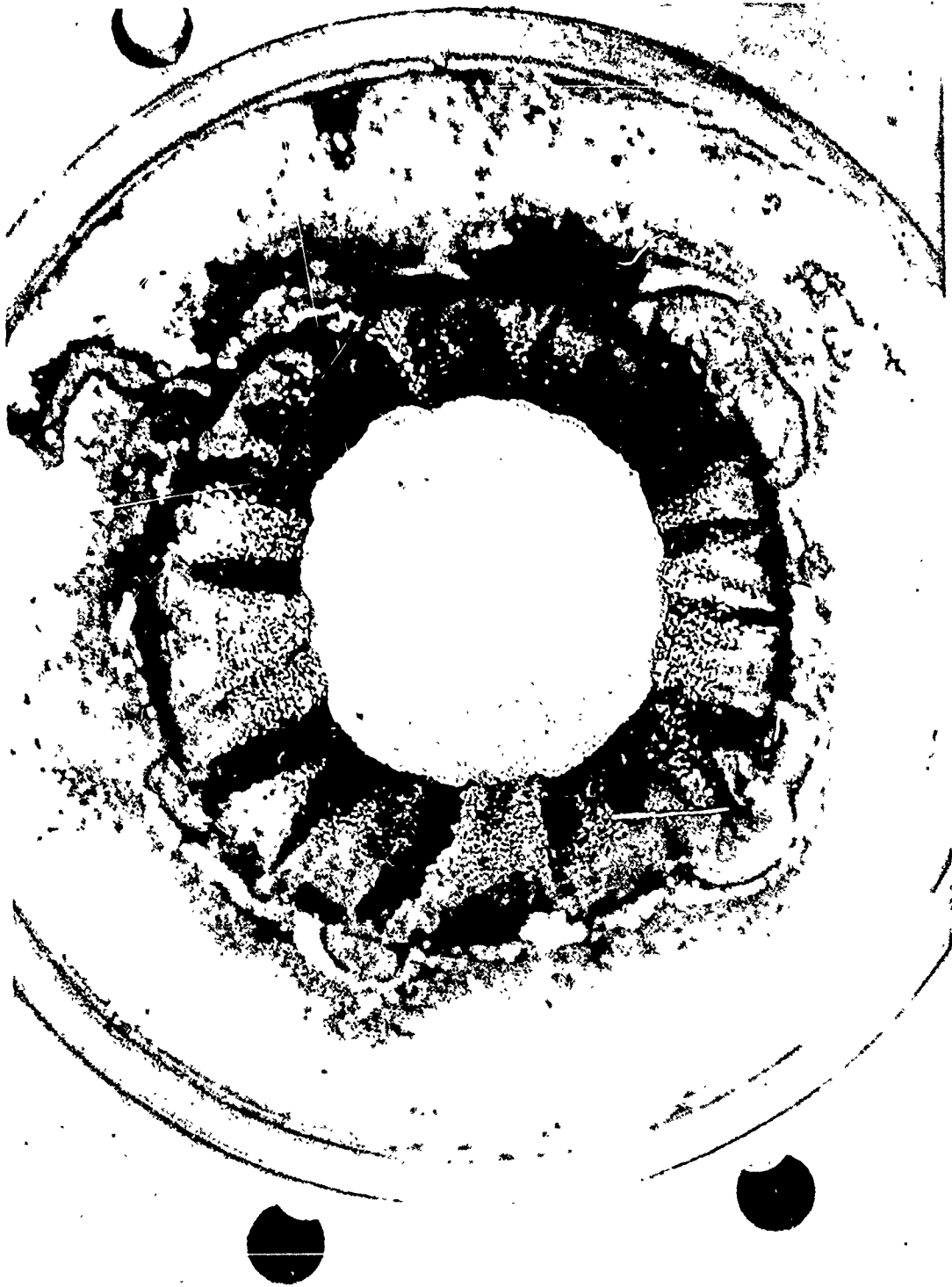
Figure 67. Phenolic Chamber, Postfire
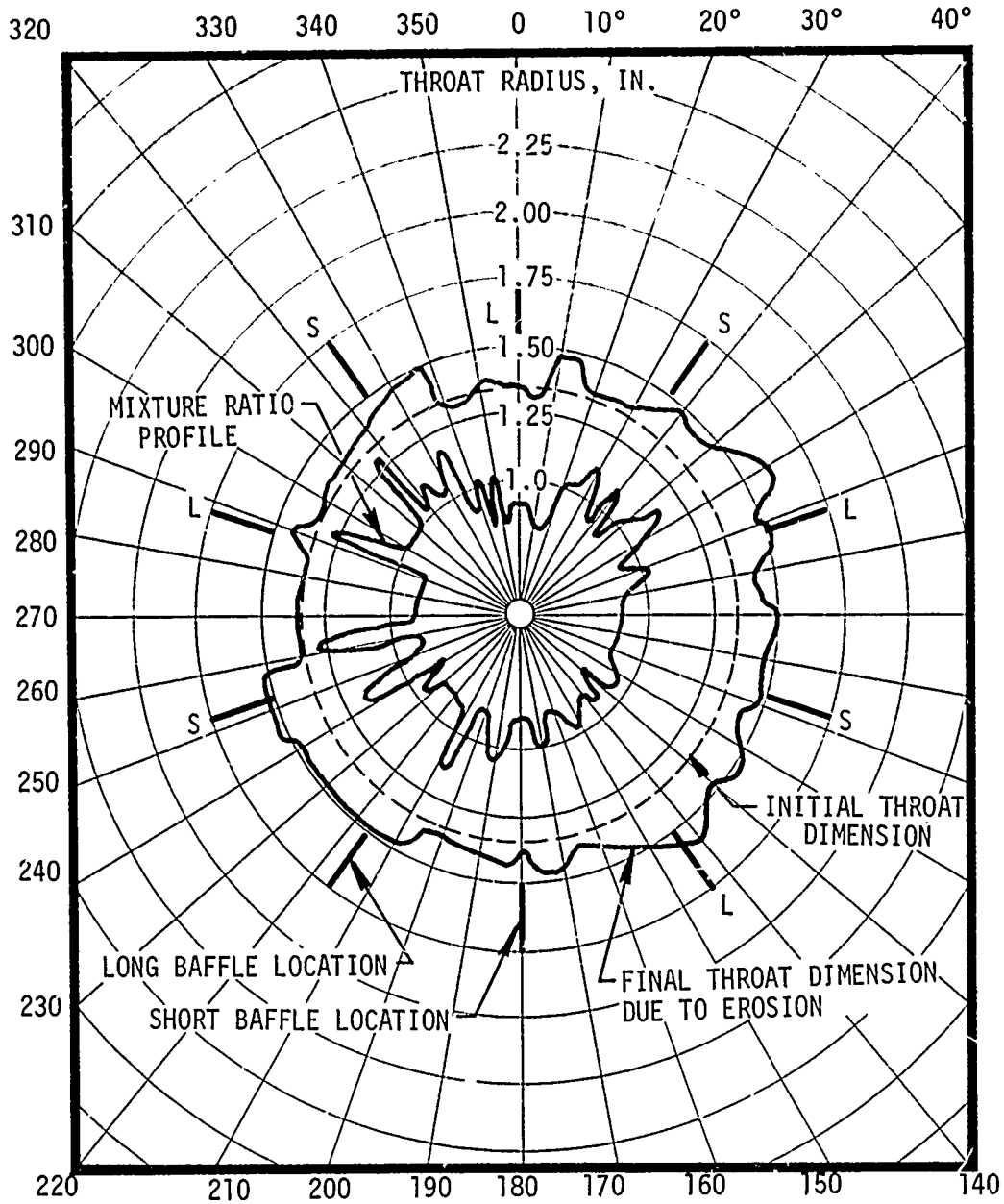
Figure 68. Comparison of Chamber Erosion with Calculated Boundary
Mixture Ratio

VII, B, Compatibility (cont.)

(U)   It is apparent from the posttest condition of the phenolic chamber
that the boundary temperatures exceeded the phenolic melt temperature of
3200°F. This was expected, based upon pre-experimental analyses and tempera-
ture measurements obtained during the experimental phase (see next section).
The compatibility results were extremely beneficial, however, in determining
the applicability of a refractory material, specifically zirconia oxide, as a
chamber insert. A minimum wall side mixture ratio of 0.8 is required to
exceed a combustion temperature of 4700°F, the melting point of zirconia. The
calculated barrier mixture ratios presented in Figure 68 imply lower than 0.8
mixture ratios at the wall. This means that the zirconia material will be
adequately protected from adverse temperature conditions, and injector
compatibility with this material should be ensured.

VII, Experimental Results (cont.)

C. THERMAL

1. Experimental Data Reduction

(U)   Data reduction was accomplished in three phases. Initially, data were reduced by graphical techniques. The great number of data points acquired during testing, however, made it expeditious to automate the approach. A one-dimensional constant properties (DATAP) computer program was thus generated. The final data reduction approach was accomplished on the SINDA 3G thermal program, which included both variable thermal properties of the heat sink and two-dimensional heat conduction effects.

2. Initial Approach

(U)   Figure 69 gives the thrust chamber geometry and thermocouple locations for the 4-in. L* and 6.5-in. L* chamber contours tested. Tests 3K-1-115 through 122 used the 6.5-in. L* copper chamber; Tests 142 through 148 used the 4-in. L* chamber; and Test 149 used the 6.5-in. L* mild steel chamber.

(U)   Chamber gas-side thermocouple data from Tests 3K-1-115 through -122 were initially analyzed by means of temperature response charts to determine the recovery temperature at various axial and circumferential locations. Tests -115 and -116 had no barrier cooling. These tests were used in determining the film coefficients at the thermocouple locations assuming a theoretical recovery temperature. The remaining tests had low mixture ratio barrier cooling. The recovery temperatures were determined by assuming that the film coefficients at the lower mixture ratios varied in proportion to the DB factor calculated by the transport properties computer program.

Report AFRPL-TR-69-122

STATION	13"L*	6.5"L*	4"L*	NO. OF THERMOCOUPLES	COLUMN NO.	L*
1 A-DIM	2.00	0.75	0.75	5	1,2,3,4,5	4 6.5 13
2 B-DIM	4.50	3.00	1.50	3	1,4,5	4 6.5 13
3 C-DIM	7.00	4.50	2.50	3	1,4,5	4 6.5 13
4 D-DIM	10,000	5.00	3.00	3 4 4	1,4,5 1,3,4,5 1,3,4,5	4 6.5 13
5 E-DIM	11,000	5.50	3.50	4 2 2	1,3,4,5 1,5 1,5	4 6.5 13
6 F-DIM	12,000	NONE	NONE	2 0 0	1,5 0 0	4 6.5 13

57°,COL. 4
39°,COL. 3
21°,COL. 2
3°,COL. 1

3° COL. 5

STA. 1 STA. 2 STA. 3 STA. 4 STA. 5 STA. 6

A-DIM B-DIM C-DIM D-DIM E-DIM F-DIM
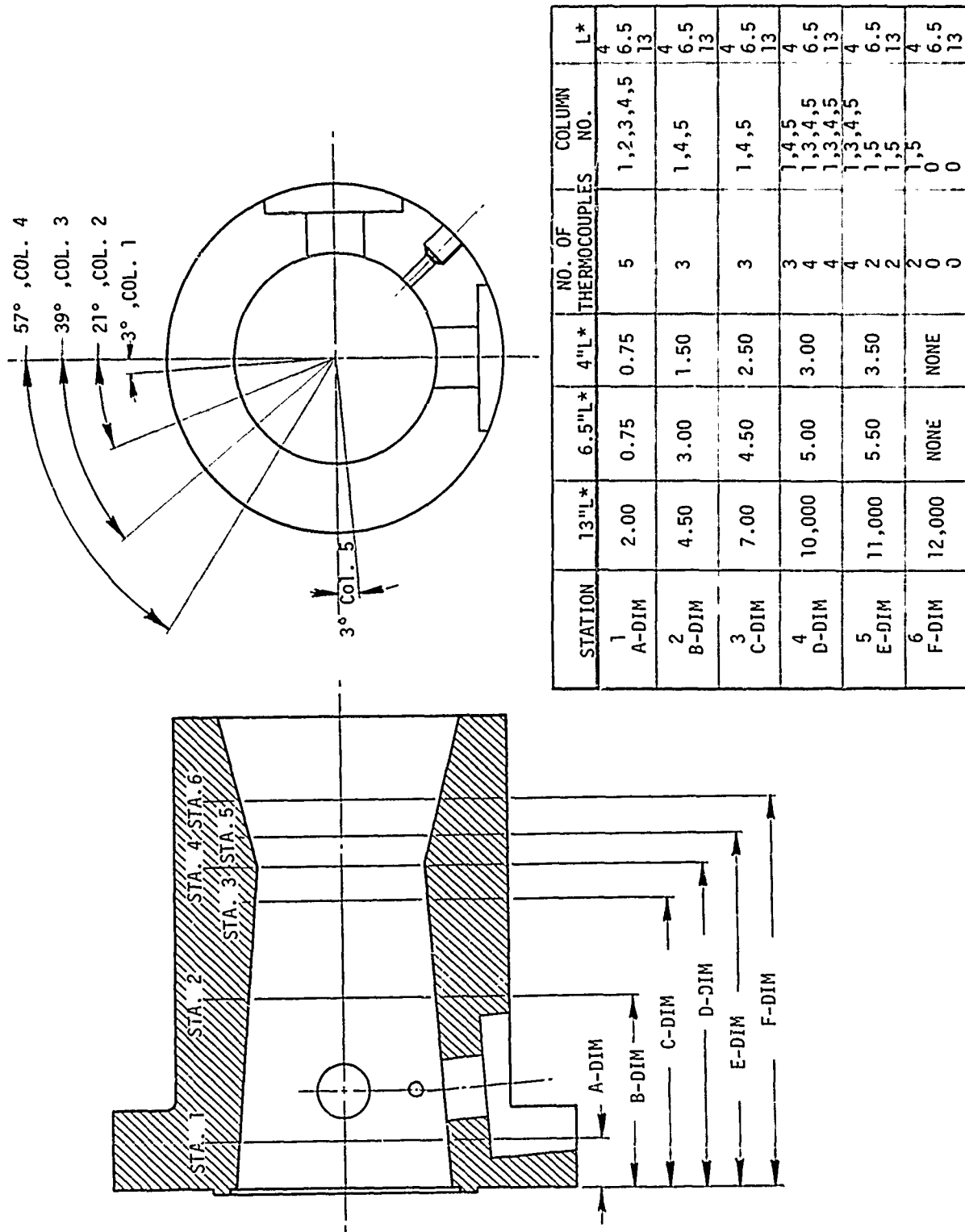
Figure 69. Copper Chamber Thermocouple Locations

Page 165

VII, C, Thermal (cont.)

(U)   The following table presents the average recovery temperatures at each of the three axial locations:

Test	% Flow	% Area	MR_B	$\bar{T}_2$	$\bar{T}_3$	$\bar{T}_4$
117	17	34	0.2	3150	3500	3350
118	17	34	0.2	3200	3600	3550
119	21.2	34	0.5	3750	3750	3600
120	10	16	0.5	4350	4350	4200
121	12.5	20	0.5	4100	4400	4150
122	14.4	23	0.5	4100	4225	4025

In this table, percent flow and percent area refer to the barrier, whose mixture ratio is MR_B. The temperatures are in °F.

(U)   It may be seen that individual thermocouple responses at a particular axial location are different. This is indicative of either injector streaking or instrumentation variabilities such as variations in junction location. The results are not considered especially accurate because of the low final gas-side wall temperatures, the limitations of constant property charts and the inaccuracies of chart interpolations. It is significant to note, however, that gas-side temperature measurements attained using the insulated thermocouples agree closely with the above data. Using this latter technique, direct throat recovery temperatures of approximately 4000°F were observed.

(U)   The FORTRAN program (DATAP) developed on the GE Mk II time sharing system accomplished the task of reducing approximately 240 temperature transients in a fraction of the time it would have taken by conventional means. A second program was written which was designed to correlate the heat

VII, C, Thermal (cont.)

transfer coefficients thus obtained by computing Bartz C_g values, Stanton and Reynolds numbers. Both programs functioned as designed and provided good heat flux data; however, the results were largely inconclusive in determining recovery temperature and coefficient, mainly because of the relatively short run times and low wall temperature rise. Data reduction from the copper chambers was incapable of identifying the effects of varying barrier flow on recovery temperature with any degree of confidence due to the wide range of acceptable h_g and T_r combinations that matched the transients. The reason for this insensitivity is attributed to the small change from the cold wall heat flux, caused by the low wall temperatures measured (typically 1200°F maximum after a three-second burn). For thermocouple T4-1 (Test-142), the cold wall flux was nominally 7.8 Btu/in.^{2}-sec. After a 3-sec firing, the flux was still 6.4 Btu/in.^{2}-sec, or a change of only 18%. Figure 70 is a transient typical of those from which boundary conditions were inferred.

(U)   Because of the difficulties encountered in understanding the temperature measurements, the data reduction entered a third phase during which the SINDA-3G computer program was employed. In addition, some of the earlier assumptions employed in data reduction were further scrutinized.

3. SINDA-3G Model

(U)   In order to evaluate the effect of the start transient, use was made of the SINDA-3G differencing analyzer. In these studies, a one-dimensional model (cyl. coordinates) was driven with the measured wall temperature response. Experimental values of transient heat flux were obtained by attaching a dummy conductance to the gas-side mode and metering the heat flow through the conductor. The conductance was sized to give negligible temperature drop at the peak flux. Network solution was obtained by using forward-backward differencing; thus, the stability of the solution was not affected by the small dummy conductor and computer run times were minimal.
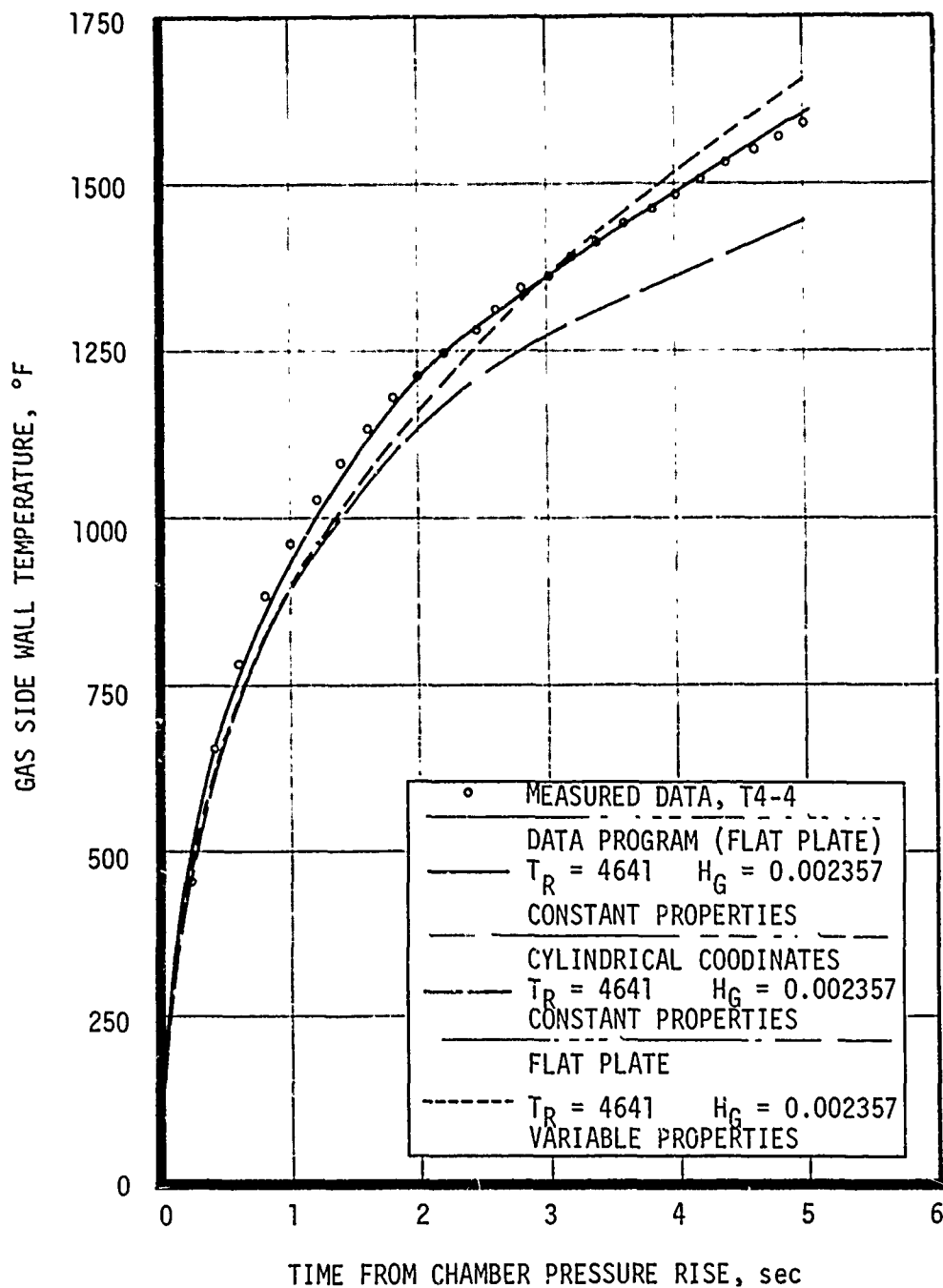
Figure 70. Thermocouple Transient Data – Test 3K-1-188

VII, C, Thermal (cont.)

(U)   Figures 71 and 72 show the experimental plots of heat flux versus time and wall temperature for two of the throat station thermocouples in Test 3K-1-188, which had 30% longer run times and higher wall temperatures than earlier runs. From the plots, it can be seen that after approximately 0.5 sec the heat transfer to the wall has reached steady state. If it is assumed that after this point in time h_g and Tr are constant, then it is theoretically possible to calculate the boundary coefficients according to the following:

$$h_g = - \frac{d(Q/A)}{dT_w/dT} \tag{1}$$

$$Tr = T_w + \frac{Q}{A}/h_g \tag{2}$$

Making use of Equation 1, the transient data $Q/A(t)$, $T_w(t)$ were curve fit by the following equation:

$$Y = X/a + b \ (x) \tag{3}$$

which has as its derivative:

$$Y' = a/(a + bx)^2 \tag{4}$$

(U)   The above equations were then put into a small program which calculated the boundary conditions as a function of time. The results of this calculation for T4-3 are given in Table VI. As can be seen from the table, there is no consistent set of boundary conditions that satisfy the data. Three possible causes are: (1) Tr is not constant with time, (2) h_g is a function of wall temperature, or (3) two- and three-dimensional conduction effects are occurring in the chamber wall. Item (1) would seem unlikely after steady state combustion is achieved. Item (2) can be theoretically shown to exist; however, the range of the correction factor (depending on the assumed value of Tr) varies
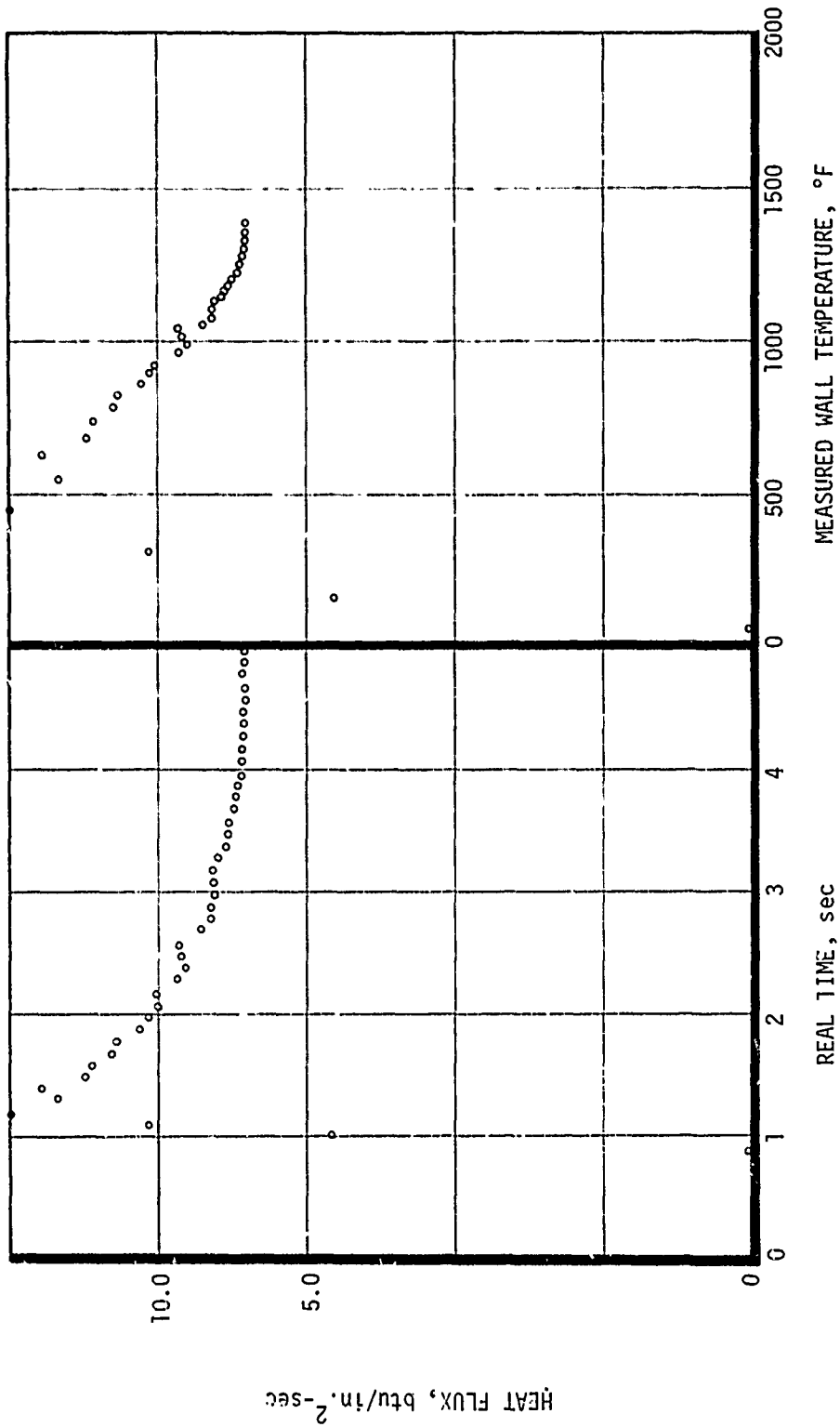
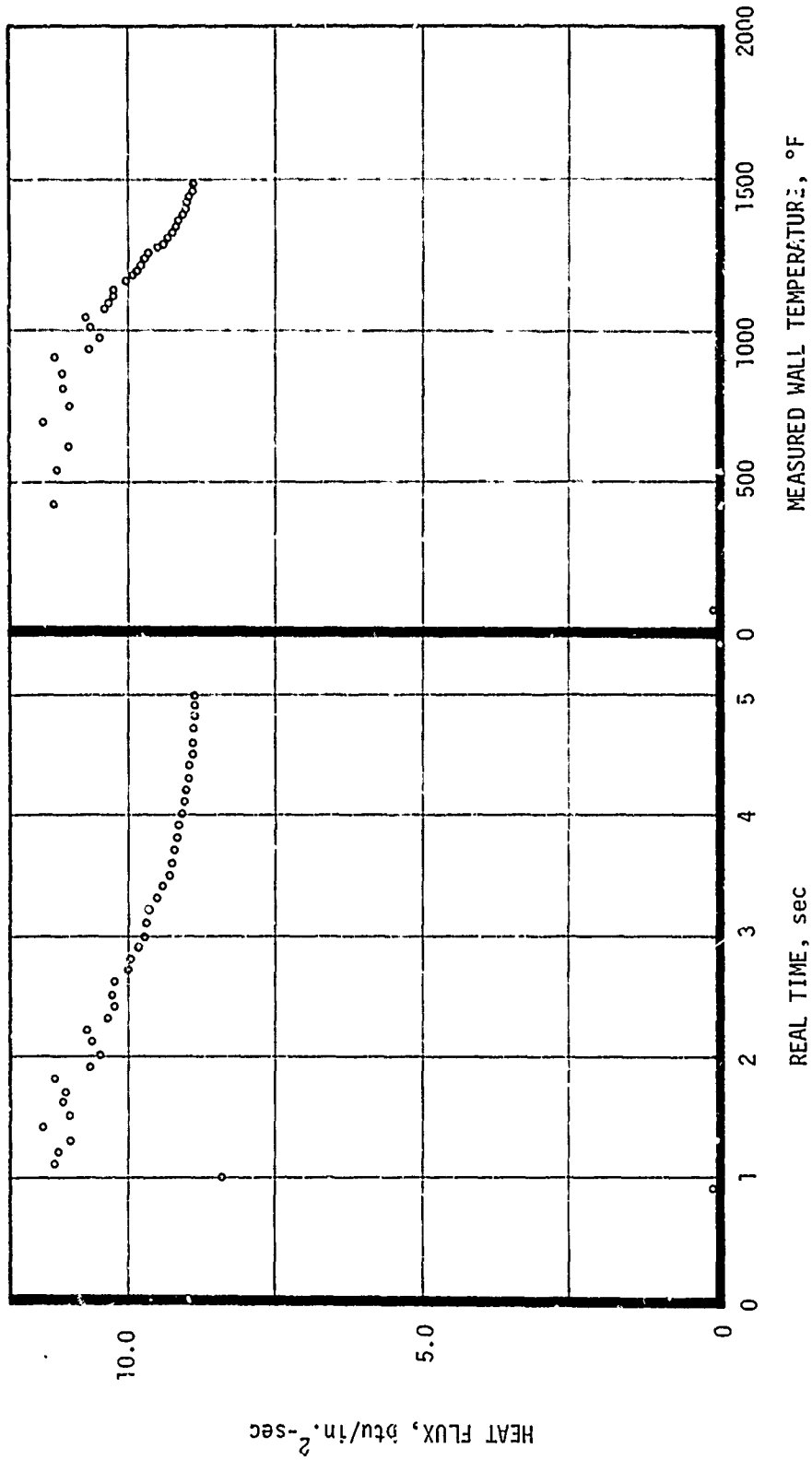Figure 71. Heat Flux Versus Time – Thermocouple T4-3

Report AFRPL-TR-69-122

Figure 72. Heat Flux Versus Time – Thermocouple T4-4

Report 0053-F-1

TABLE VI

CALCULATED RECOVERY TEMPERATURES AND HEAT TRANSFER COEFFICIENTS
TEST 3K-1-188

Time	T_w	Q	Hg	T_r
1.50	743.93544	11.49299	0.01211	1693.15630
1.60	776.35321	11.12879	0.01042	1843.93360
1.70	807.39820	10.92609	0.00912	1994.34850
1.80	837.15292	10.57051	0.00809	2144.05620
1.90	865.69893	10.35186	0.00725	2292.76910
2.00	893.10753	10.16266	0.00657	2440.24850
2.10	919.44538	9.99735	0.00600	2586.29720
2.20	944.77401	9.85166	0.00552	2730.75310
2.30	969.15034	9.72230	0.00511	2873.48460
2.40	992.62709	9.60667	0.00475	3014.38570
2.50	1015.25320	9.50269	0.00444	3153.37240
2.60	1037.07400	9.40869	0.00418	3290.37970
2.70	1058.13170	9.32330	0.00394	3425.35850
2.80	1078.46580	9.24538	0.00373	3558.27330
2.90	1098.11280	9.17400	0.00354	3689.10050
3.00	1117.10710	9.10836	0.00337	3817.82630
3.10	1135.48060	9.04780	0.00322	3944.44560
3.20	1153.26320	8.99175	0.00308	3068.96010
3.30	1170.48310	8.93973	0.00296	4191.37790
3.40	1187.16640	8.89132	0.00285	4311.71220
3.50	1203.33800	8.84615	0.00274	4429.98050
3.60	1219.02090	8.80391	0.00265	4546.20380
3.70	1234.23710	8.76432	0.00256	4660.40620
3.80	1249.00700	8.72715 ·	0.00248	4772.61420
3.90	1263.35000	8.69217	0.00240	4882.85650
4.00	1277.28440	8.65919	0.00233	4991.16320
4.10	1290.82730	8.62806	0.00227	5097.56580
4.20	1303.99500	8.59862	0.00221	5202.09670
4.30	1316.80290	8.57073	0.00215	5304.78930
4.50	1341.39680	8.51916	0.00205	5504.79440
4.60	1353.20960	8.49526	0.00200	5602.17520
4.70	1364.71630	8.47251	0.00196	5697.85 0
4.80	1375.92870	8.45082	0.00191	5791.86500
4.90	1386.85800	8.43012	0.00187	5884.24210
5.00	1397.51460	8.41035	0.00184	5975.01910

VII, C, Thermal (cont.)

by only 20% over the measured wall temperature range. The final item is the most likely candidate, as some streaking has been observed with this injector. The fact that the measured heat flux is becoming constant (Figures 71 and 72) with increasing wall temperature would indicate that heat is flowing by conduction to the thermocouple location. Since the heat flux is becoming flat, there becomes virtually an infinite set of boundary conditions that will match the observed temperature data, particularly those that result in a low ratio of T_w/Tr.

(U) The fact that the data reduction program recreates the observed transient (Figure 70) cannot be questioned and would seem to give confidence in the analysis. If, however, the inferred boundary conditions are imposed on the same solution (integral technique) using cylindrical coordinates as shown also in Figure 70 rather than the flat plate solution assumed earlier, the fit is rather poor. Also shown in Figure 70 is the predicted response using the same boundary conditions but including temperature varying thermal properties in the flat plate solution.

4. Conclusions

(U) The computer program used to infer gas-side boundary conditions demonstrated the ability to match and recreate transient temperature data. From the above analysis, it would seem absolutely necessary to isolate the thermocouple locations from two- and three-dimensional conduction effects if gas-side boundary conditions are to be inferred from thermally instrumented chambers.

VII, C, Thermal (cont.)

(U)   Because of the inability to precisely define h_g and, speci-
fically, recovery temperature through purely analytical means (based on the
data generated with the copper chambers) it was necessary to rely on gross
chamber affects to determine a feasible boundary temperature. Erosion char-
acteristics exhibited by tne phenolic chambers illustrated a boundary tempera-
ture in excess of 3200°F. Compatibility results, however, in conjunction with
recently obtained data generated with a refractory throat material, show the
boundary temperature produced with the final injector to be less than 4700°F.

D.   STABILITY

1.   Stability Data Acquisition and Reduction

(U)   The stability data were acquired by means of two high-
frequency Photocon 352A pressure transducers lccated 90° apart in the chamber
wall 1.5 in. from the injector face. The transducers were originally located
over a baffle tip and between two baffles; later in the program, however, the
baffles were rotated 15°, placing both transducers between baffles. Both a
tangential pulse gun and a nondirectional bomb were used to rate the tability
of the system. When the pulse gun was not in use, it was plugged with a rod
that was flush with the chamber wall to eliminate an unintended source of
damping. The pressure data obtained from the Photocon transducers were
recorded on an FM tape recorder and played back at 160 in. per second in
order to analyze the high frequencies observed on this program. When it was
necessary to determine the amplitude of more than one frequency of oscilla-
tion, a spectral analysis was performed on the entire run. The data were
printed out in a computer tabulation for every 0.0125 sec as a function of
both frequency and time. The frequency bandwidths employed were 800 cps; the
frequency range of interest was from 0 to 40,000 cps. The system frequency
response from the Photocon source through the tape recording and playback

VII, D, Stability (cont.)

amplifiers resulted in final computer printout data that were limited to just below 30,000 cps. This allowed for adequate evaluation of up to the fifth tangential (5T) acoustic mode at about 27,000 cps.

2. Derivation of Baffle Pattern

(U)   The proposed injector baffle patterns were based on the results of the work done in the preproposal phase of this program. This preproposal effort developed an injector baffle pattern which had seven radial baffles 0.7 in. high, a 0.2-in.-high hub baffle, and 0.2-in.-high radial baffles extending from the hub to the chamber wall. This baffle pattern would have resulted in an unacceptably dense pattern for the smaller diameter program chambers. Therefore, it was decided that a fewer number of baffles could be used, which would result in baffle pockets comparable in size to the successful preproposal injector design. To compensate for the use of fewer baffles (five instead of seven), it was necessary to make the remaining baffles slightly longer relative to the chamber diameter. Therefore, the baffle was to remain 0.7 in. high instead of being scaled down to 0.61 in. with the chamber diameter reduction from 4.0 to 3.5 in.

3. Stability Results

a. Baffles

(U)   The six injectors tested during this program were cumulatively tested with twenty different baffle patterns. Of these twenty, thirteen were unique in that the basic pattern was either wholly modified or the blade heights were different. The remaining seven patterns were either identical repeats on different injectors or incorporated minor modifications such as variations in blade wall angle or tip width. The thirteen unique patterns are shown in Figure 73.
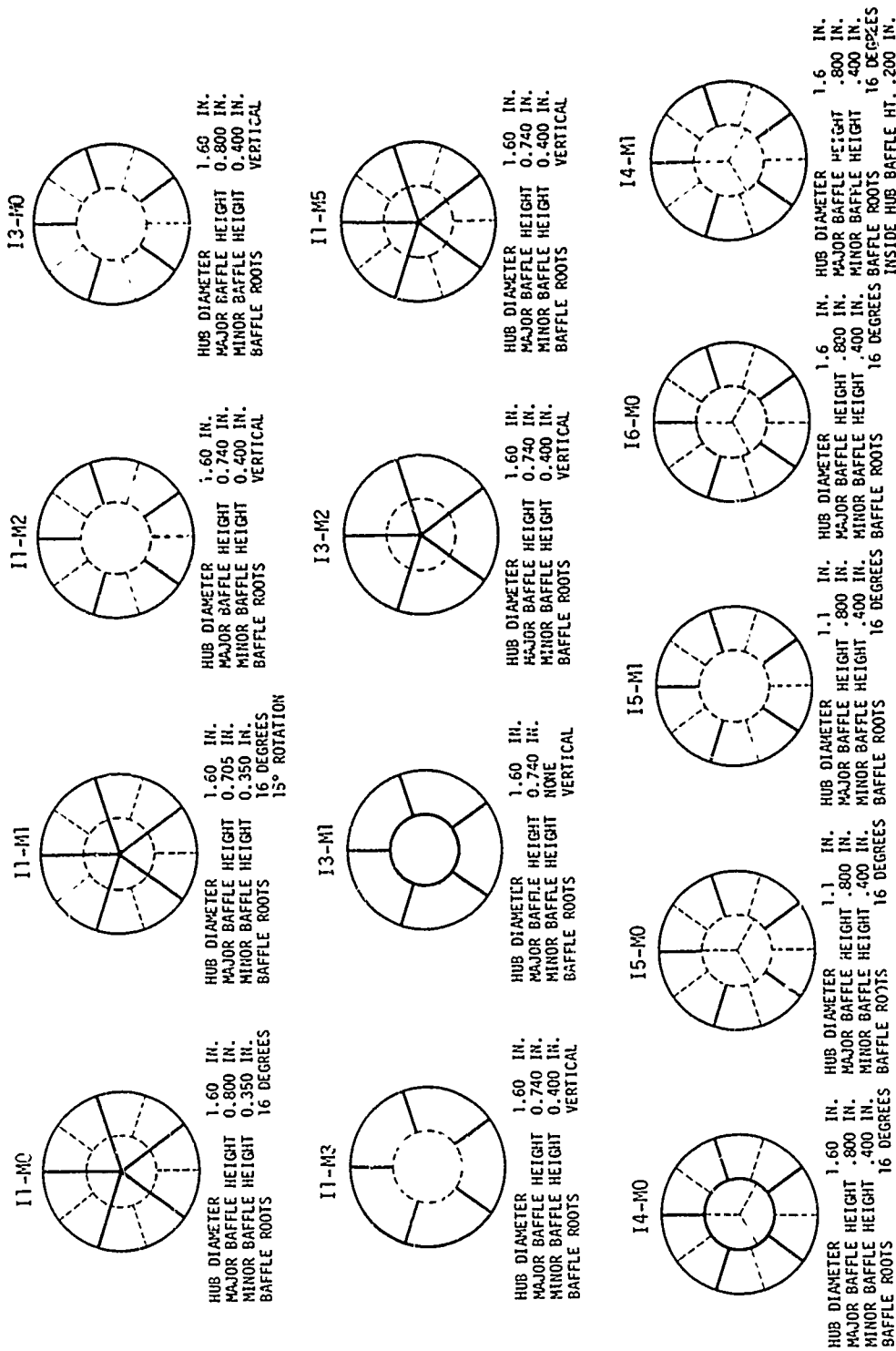
Report AFRPL-TR-69-122

Figure 73. Unique Baffle Configurations

VII, D, Stability (cont.)

(U)   All patterns shown, with the exception of number 12,
were unacceptable in operation. Pattern number 2 was unstable in the first
tangential acoustic mode at 7200 cycles per second. The peak-to-peak oscil-
latory amplitude was 190 psi. It was concluded (and later proved) that
baffles less than 0.740 in. in height were, in this system, inherently
unstable. Patterns 3, 4, 10, and 11 were dynamically stable; however, there
was exhibited a random oscillation noise exceeding the allowable pressure
limitation of $\pm$5% of chamber pressure. The remaining patterns exhibited either
very noisy operation or random pressure spikes of significant amplitude. It
is now believed that random oxidizer circuit plugging during machining was
influential in causing pressure spikes and, thus, possibly unnecessary baffle
pattern rejection. Based on the then current information, however, the
patterns were varied progressively until the successful pattern shown as
number 12 was achieved. This pattern was employed in the final demonstration
injector.

(U)   The significant baffle changes effected during the
program were:

(1) A reduction in major baffle height from 0.800 in
     to 0.705 in.

(2) Removal of the major baffles from inside the hub
     and decreasing the height of remaining blades
     to 0.740 in.

(3) Removal of the minor baffles from outside the hub
     and decreasing major blade height to 0.740 in.

(4) Both (2) and (3) with an increase in hub height
     to 0.800 in.

(5) Removal of the major radial blades from injector
     center and replacing them with three minor blades
     0.400 in. high.

VII, D, Stability (cont.)

(U)   The significant of these changes is shown in Figure 74
in the form of spectrum analyses of the Photocon pressure data. The data
summary time were taken 0.1 sec before shutdown and were averaged over a
0.1-sec inte al. It may be seen that a complete five-bladed major pattern
inhibits the lower, or first tangential, mode. This pattern, in conjunction
with a full array of minor blades, inhibits all modes. Conversely, removal
of the center blades results in a significant increase in 1T susceptibility
and, thus, noisier engine operation. Elimination of the outer minor radial
blades, while maintaining the center pattern, provides suppression of the
first tangential mode but allows higher modes to become dominant. Again,
this results in noisy operation. Removal of all but the outer major blades
and the hub allows all dominant modes to become significant. As was seen
in the test data, this baffle change allowed pressure oscillations of $\pm$40 psi
amplitude.

(U)   It was evident from these results that one of the major
baffle damping mechanisms is the interference of the baffle with the trans-
verse acoustic mode velocity maximums. It was apparent that, for maximum
damping of an acoustic mode, there had to be a baffle interfering with all
the acoustic mode velocity maximums. In the case of the first tangential
acoustic mode and those modes combined with it, there had to be a baffle
across the injector center. Similarly, all the pure tangential modes required
radially oriented baffles near the chamber wall and exceeding in number
(preferably double) the number of acoustic velocity maximums. Thus, main-
tenance of all radial blades between the hub and injector circumference sup-
pressed all modes up to the fifth tangential.

Report AFRPL-TR-69-122

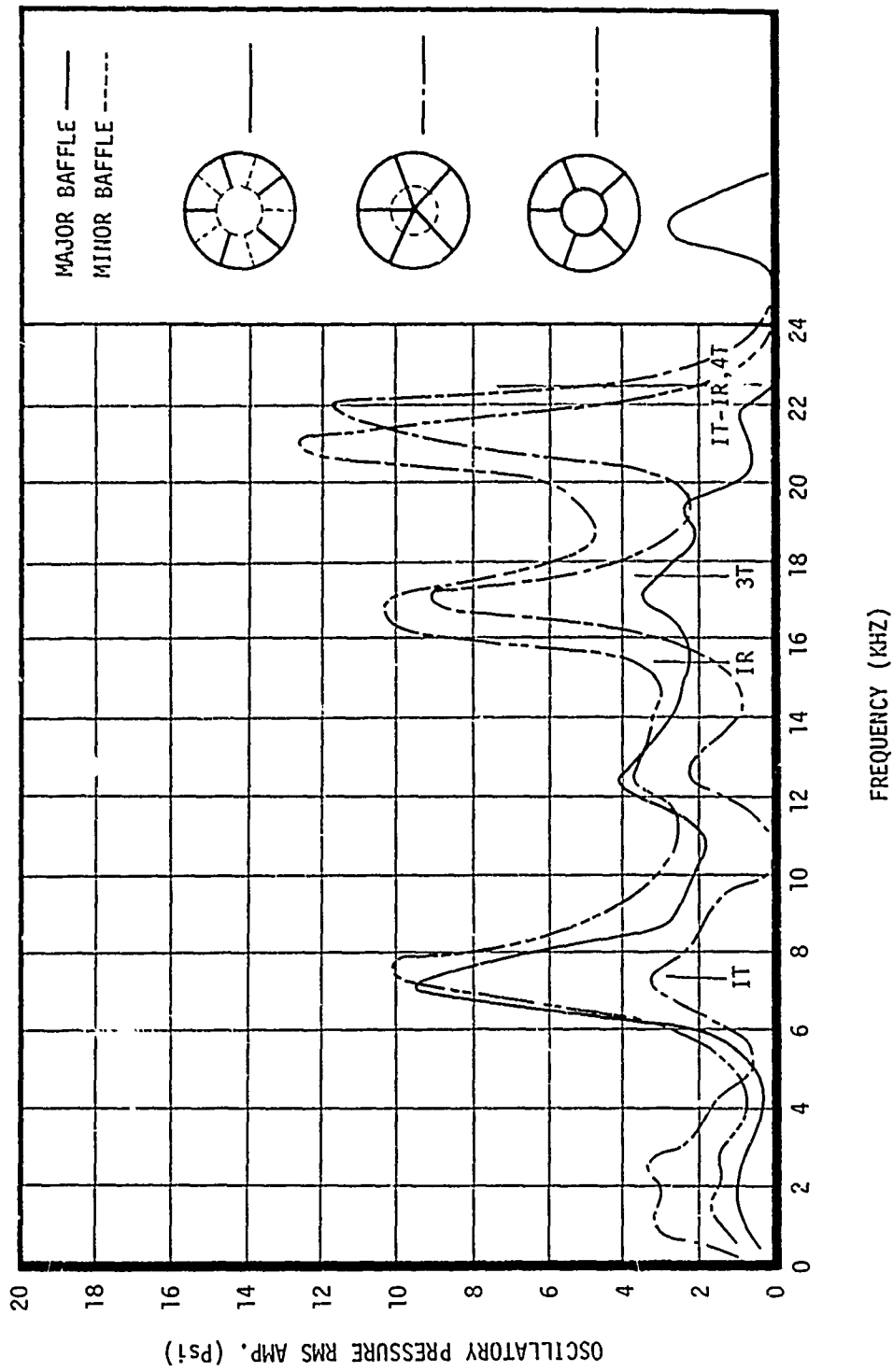Figure 74. Effect of Baffle Pattern on Mode Susceptibility

VII, D, Stability (cont.)

b.   Flow Distribution Effects

(U)   The method chosen to control the barrier cooling mixture
ratio had compensating stability effects for the pure tangential acoustic
modes. By decreasing the oxidizer barrier flow and maintaining a constant
fuel flow, the propellant distribution was, in effect, "humped" toward the
center of the injector. As was discussed in Section IV,A,5, this reduction
in boundary flow relative to the injector center tends to stabilize the pure
tangential modes.

(U)   It is impossible to assess the actual contribution to
stability due to flow distribution on this program because of the overriding
influence of the associated baffle patterns. It can be stated, however, that
there were no deleterious effects due to flow distribution. Stability was
not degraded in those cases in which the pattern was held constant and the
boundary flow was varied.

c.   Chamber Geometry Effects

(U)   The chamber geometry variable for this program consisted
primarily of shortening the chamber from 10 in. (13-in.L*) to 5 in. (6.5-in. L*).
The injector diameter of 3.5 in. and throat size of 2.7 in. remained the same.

(U)   These length changes, as with flow distribution, were
capable of only minor influences on stability in comparison with the baffle
patterns themselves. It would be expected that the longer chamber would be
most prone to exhibit pure longitudinal acoustic modes at frequencies lower
than 8000 cycles per second. The shorter chamber, while not likely to exhibit
longitudinal oscillation, would be more susceptible to instability in the
transverse modes. No results applicable to these theories were conclusively
obtained during this program.

VII, D, Stability (cont.)

   d.   Propellant Combination Effects

(C)   Prior to this program, there was a scarcity of data relative to the sensitive combustion frequency for injectors using HIPERTHIN orifices and for fuels other than AeroZINE 50. This program utilized hydrazine as the fuel for all but three tests (Tests 3K-1-163, 164, and 165). These three tests utilized monomethylhydrazine (MMH) as a fuel in an effort to obtain a reference stability condition.

(C)   Tests 3K-1-163 and 164 utilized an injector with a baffle pattern of the type that had been proven capable of stabilizing all high-frequency acoustic modes up to 18,000 cps using hydrazine as the fuel. Test 3K-1-165 utilized an injector that had a flat face of like impinging injection elements and no baffles or damping devices of any kind. Both injectors were found to be unstable in the first tangential acoustic mode (7500 cps baffled and 8000 cps unbaffled) when tested with MMH. The baffled injector experienced a slightly lower first tangential mode frequency due to the presence of the baffles.

(C)   It was unexpected that the baffled injector using MMH as a fuel would go unstable in the first tangential mode at 7500 cps, if at all, rather than at the higher frequency baffle pocket modes. This result, along with anomalies recently observed with this and other hydrazine systems, has caused a re-evaluation of sensitive time lag correlations with respect to the various fuels.

(C)   At the time the analytical stability evaluation of the injector designs proposed for use in this program was being conducted, the most recent sensitive time lag correlation had just been published. Six months later another correlation was published (Ref. 15) which tended to

Page 181

VII, D, Stability (cont.)

correct the earlier correlation with respect to recent hydrazine test results. The correlating formula of the earlier correlation was as follows:

$$\tau_{fuel} = \frac{0.25\ d_f^{1/2}}{M_c\ \dfrac{P_c^{1/3}}{P_{CRF}}}$$

The latter correlation of Reference 15 did not present a formula, but the ordinate on the curves presented showed the sensitive time lag, τ, to be proportional to identical factors (i.e., fuel orifice diameter, d_f; the chamber Mach number, M_c; and the chamber pressure, P_c) with the exception of the fuel critical pressure, P_{CRF}.

(U)   The critical pressure term was removed when it became apparent from more recent test results that hydrazine (N_2H_4) was sensitive to higher frequencies than AeroZINE 50 (A-50). The critical pressure of N_2H_4 is 2131 psi; for AeroZINE 50 it is 1696 psi. The more recent data indicated that, if the critical pressure was to be correlated with recent test results, it should be a multiplication term with chamber pressure rather than a divisive term. This has been verified by the MMH test results generated during this program. Monomethylhydrazine has a critical pressure of 1195 psi and is sensitive to a much lower frequency than the N_2H_4 under the same conditions.

(U)   The results from this program are plotted in Figure 75 with the same coordinates as used by Reardon in Reference 15. The relative positions of the three propellants and the leveling off of the curves shown in Figure 75 have not been shown before but are clearly indicated by both the N_2H_4 and MMH test results of this program.

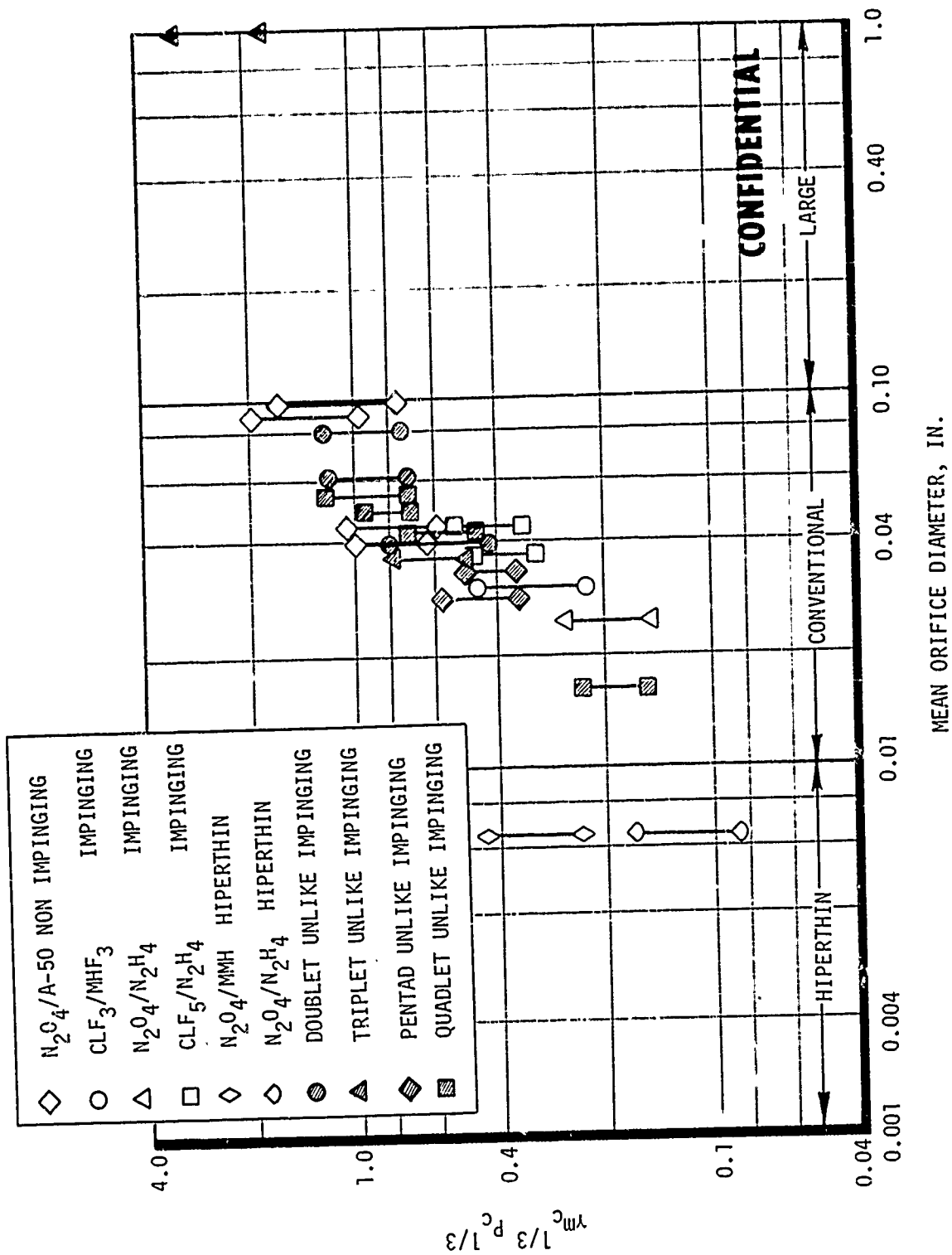Figure 75. Effect of Propellant on Sensitive Frequency (u)

SECTION VIII

INJECTOR RELIABILITY AND MAINTAINABILITY

(U)   The   goals of high performance, stability, and chamber cooling
were met with the injectors fabricated during this program. For complete
development, however, the implicit goals of hardware reproducibility, thermal
reliability, durability, and maintainability must also be met. The following
presents the results of the experimental phase in terms of these latter goals.

A.   REPRODUCIBILITY

(C)   Hardware reproducibility is a measure of the ability to build
sequential units of hardware with minimum component variance and with a maxi-
mum operational repeatability. Low reproducibility was demonstrated with the
phase one hardware, since difficulties were during fabrication of all units.
Conversely, a high degree of reproducibility was demonstrated with the phase
two design. Of three injectors initiated, all three were successfully tested.
All were stacked and brazed with no evidence of internal or external leakage.
One injector experienced circuit plugging during machining; once recognized
the problem was completely rectified. The remaining injectors experienced no
difficulties in machining.

(C)   Insufficient hardware has been built to allow statistical defi-
nition of operational reproducibility. It is significant, however, that the
phase two design, and particularly the final injector, has allowed definition
of successful platelet type, stacking procedures, braze techniques, and final
machining criteria. Knowledge of these parameters, combined with prior
experience in individual platelet selection and plating tolerances, should
prove future components of this type to be nearly 100% reproducible.

VIII, Injector Reliability and Maintainability (cont.)

B.   THERMAL RELIABILITY AND DURABILITY

(C)   The injectors of the phase one design and injectors I4 and I5 of
the phase two design experienced face burning, particularly when vertical
cuts were used at the baffle roots. Also, problems of platelet splitting
and orifice deformation were encountered. Two of these early injectors,
II-M2 and I4-M1, reached cumulative firing durations of approximately 25 sec.
The postfire condition of these units is shown in Figures 40 and 76, respec-
tively. It may be seen that there is little integrity of the platelets,
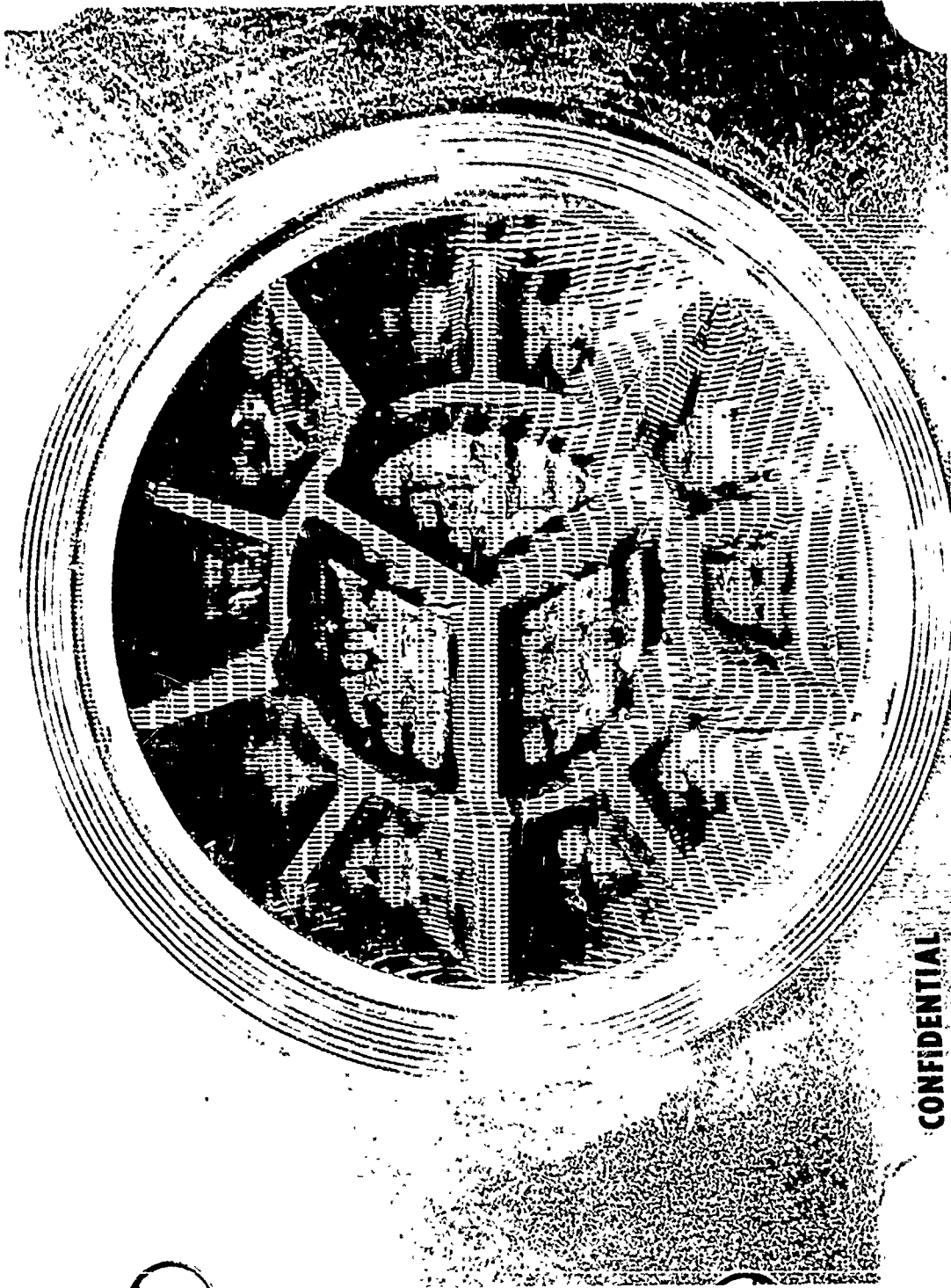especially in the baffles themselves.

(C)   As has been discussed, the showerhead orifice dimensions of the
final injector were reduced from 0.065 in. to 0.040 in. This reduction in
orifice width resulted in a corresponding increase in supporting land width
between orifices. The prefire condition of injector I6-MO was shown in
Figure 46. The postfire condition after 28.5 sec is shown in Figure 77. It
may be seen that there is no metal removal due to thermal effects: there is
no platelet splitting, and the incidence of orifice deformation has been
significantly reduced. The thirteen tests conducted which cumulatively added
28.5 sec to the injector included five pulse and bomb tests during which the
minimum overpressure was 607 psi and the maximum was 967 psi.

(C)   The condition of injector I6-MO after approximately 75 sec is
shown in Figure 78. The added duration was the result of two 1-sec tests
and two tests of greater than 20 sec duration. It may be seen that platelet
splitting has not occurred, nor has there been any major increase in orifice
deformation. Of special significance is the apparent stability of the dark
areas on the face. Direct comparison between the 28-sec and the 75-sec heat
marks shows little, if any, change. It is apparent from these results that
the injector will withstand any duration firing. Also, the structural integ-
rity of the face appears compatible with any pulse operation currently under
consideration.

Report AFRPL-TR-69-122

Figure 76. Injector I4-M1, Postfire 24 Seconds (u)

Page 186

Figure 77. Injector T6-30, Postfire 28.5 Seconds (u)

CONFIDENTIAL

Report AFRPL-TR-69-122

Figure 78. Injector T6-90, Postfire 75 Seconds (u)

VIII, Injector Reliability and Maintainability (cont.)

C.   MAINTAINABILITY

(C)   There are three areas of significance in assessing the maintaina-
bility of the HIPERTHIN injector used in this program. The first is an
evaluation of the plugging sensitivity due to sediment filtration. The second
is a consideration of the nitrogen tetroxide flow decay phenomenon. The last
area pertains to storage requirements and handling limitations.

(U)   The results of this program were illustrative of a high degree
of insensitivity to circuit plugging due to line and tank sediment. Normal
precautions were taken to eliminate propellant contamination. All filling
cycles were conducted with dual 2µ nominal-10µ absolute filters in the fill
line. Also, as is normally the case, two 10µ absolute filters were placed in
series in the propellant run lines. The fact that even these normal precau-
tions may have been unwarranted on this program is evidenced by the results
of Tests 3K-1-103, 104, and 105. Approximately two ounces of line scale were
found in the oxidizer manifold after these three tests (see Section VI,B,2),
yet at no time was there a decrease in performance attributable to mixture
ratio shift (as might be the case if the oxidizer circuit were plugging
uniformly) or increase in injector pressure drop. It appeared from postfire
examination that the sediment was filtered and swept to the manifold periphery,
thus causing no detriment to the system operation.

(C)   Recent test results with HIPERTHIN injectors subjected to particle
laden flow are substantiating these findings. In this study, conducted as
an Aerojet-General independent research investigation, an injector identical
to those used in this program (in terms of channel dimension) is being sub-
jected to several hours of water flow containing particles of known diameter
and concentrations. To date, flow tests have been run with particles ranging
in size from 20µ to 40µ and in concentrations to 180 ppm. Initial results

VIII, C, Maintainability (cont.)

show no change in injector ΔP after two hours of flow. Ultimately, random particles to 200μ in size will be flowed. No problems are anticipated, however, based on the test results previously discussed.

(C)   The second item of significance relative to HIPERTHIN maintainability is flow decay of the oxidizer due to an accumulation of ferric nitrate adduct $(Fe(NO_3)_3 \cdot N_2O_4)$ at orifice inlets. Over the past five years, several instances of N_2O_4 flow decay have been reported. TRW and Rocketdyne (References 16 and 17) have observed flow decay within filters and small-passage valves during temperature cycling N_2O_4 flow experiments. Aerojet has observed flow decay while transferring N_2O_4 from delivery tank cars to storage areas and then to the test area. In all cases, the flow decay has occurred at or near small flow passages such as filters, needle valves, and injector orifices.

(U)   Three common factors have been identified from the various flow decay observations:

- N_2O_4 temperature reduction
- Small flow passages
- Presence of ferric nitrate

On the basis of these observations, the following flow decay mechanism can be hypothesized: (1) flow decay results from the increased pressure drop caused by the precipitation and buildup of ferric nitrate adduct at or within small flow passages, (2) ferric nitrate adduct precipitation results from a reduction in the N_2O_4 temperature which reduces the solubility of $Fe(NO_3)_3$ in N_2O_4, and (3) fluid dynamic variables and flow passage size and geometry influence the precipitation process but their effects are not currently well understood.

VIIl, C, Maintainability (cont.)

(C)   HIPERTHIN, because of the exceptionally small flow passages, could
be susceptible to N_2O_4 flow decay. One common factor in all flow decay
observations was a critical flow constriction which would permit the buildup
of ferric nitrate adduct. On the other hand, because of the extremely large
number of flow passages within HIPERTHIN type hardware, a large quantity of
ferric nitrate must be precipitated in order to cause extensive flow decay.
Since the solubility of ferric nitrate in N_2O_4 is very small (1 to 16 ppm),
large quantities of N_2O_4 and thus very long flow durations would be required.

(C)   Sample calculations to determine plugging potential due to adduct
precipitation were made for the HIPERTHIN injectors used in this program.
The assumption was made, based on the number and size of the oxidizer flow
passages, that six 0.004-in.-dia spherical ferric nitrate particles would
completely block a flow passage and that approximately 10.4 grams of ferric
nitrate would be required to cause flow stoppage. Since the solubility of
ferric nitrate in N_2O_4 decreases from an average of 6 ppm at a temperature
of 100°F to an average of 2.4 ppm at a temperature of 32°F, only 3.6 ppm of
ferric nitrate could be precipitated as the temperature of N_2O_4 decreased by
68°F. Under these conditions it would require approximately 615 lbm or about
51 gallons of N_2O_4 to precipitate 1 gram of ferric nitrate. Therefore, in
order to precipitate 10.4 grams of ferric nitrate in order to stop flow
through the N_2O_4/N_2H_4 injector, flow would have to continue for almost
1200 sec.

(U)   The conditions assumed above are for a very special case which
maximized the probability of flow blockage. For example, a very large
temperature differential (68°F) between the tank and the injector was assumed
in order to maximize the amount of ferric nitrate precipitation. Also, all
precipitating ferric nitrate was assumed to collect at the injector without
any material being forced through the flow passage. Tests with 0.005 and
0.010 in. capillaries have shown that in many cases precipitated ferric

VIII, C, Maintainability (cont.)

nitrate will be forced through the capillary, resulting in flow recovery.
Finally, ferric nitrate accumulation was assumed to be uniform over the entire
injector. Actual posttest observation has shown very little evidence of
precipitate. When the adduct was observed, only a fraction of the oxidizer
orifices was affected. It may thus be stated that the above example has
defined the maximum flow decay rate for this system. The actual decay rate
is in all probability many times smaller.

(C)   The third area of significance to injector maintainability is that
of storage and handling. Results applicable to this area are available from
a recently concluded program during which a HIPERTHIN injector was developed
and qualified for flight tests. Procedures were established which called for
water flush, freon flush, vacuum dehydration, and final packaging. Injectors
subjected to this procedure, stored, and subsequently retested were found to
have no evidence of plugging.

(U)   Similar procedures were followed in this program. After each
test, the injector was removed from the stand and flushed with water. Alcohol
or freon was passed through each circuit. The injector was then blown dry
with GN_2. Normal practice called for storage in a vacuum dehydrator until
the next test. This procedure was followed with all but the final injector.
Following the last test, injector I6 was flushed, blown dry, and then stored
for two weeks under ambient conditions. No flow degradation was observed
following the two week storage.

(U)   There has been insufficient time to achieve a true measure of
storability limitations with the program injectors. While the latter results
indicated no plugging due to failure to dehydrate the injector, it is recom-
mended that the units be dehydrated before long-term storage. The best
practice would be to follow the procedures established for the qualified

VIII, C, Maintainability (cont.)

injectors, which require 24-hour dehydration followed by packaging in the proximity of a desiccant container. Under these conditions, injector storability should be unlimited.

CONFIDENTIAL
(This page is Unclassified)

SECTION IX

CONCLUSIONS

(U)   On the basis of the work accomplished during this program, the following conclusions are made:

A.   PERFORMANCE DEMONSTRATION

(C)   The HIPERTHIN injector developed for use with N_2O_4/N_2H_4 has been shown to offer in excess of 300 sec vacuum specific impulse (at expansion ratio of 30:1) over the full mixture ratio range 0.8 to 1.4. At a mixture ratio of 1.0, the vacuum specific impulse was found to be 309 sec.

B.   ENERGY RELEASE EFFICIENCY

(C)   The injectors developed during this program have demonstrated energy release efficiencies of 100% with both 10-in.-long and 5-in.-long chambers (injector to throat). Of major significance is the invariance of this value over the full mixture ratio range. It may thus be concluded that a complete system design may be weight and volume optimized within demonstrated mixture ratio limitations with no degradation to injector efficiency.

C.   INJECTOR STABILITY

(C)   The injectors tested have been proven to be dynamically stable over the full mixture ratio range, regardless of perturbation intensity or directional characteristics. Also, the combustion noise level has been demonstrated to be extremely low ($\pm$2% of full chamber pressure) with no spiking or random oscillation. Start transients with a 35 millisecond oxidizer lead can be expected to produce from 20 to 40 milliseconds of rough operation with extremely short-duration overpressures approaching 500 to 700 psi. Simultaneous propellant shutdown will, in most cases, promote spike-free chamber pressure tail-off.

IX, Conclusions (cont.)

D. INJECTOR/CHAMBER COMPATIBILITY

(U)   Chamber cooling with off-mixture ratio boundary combustion products has been proved feasible. The injectors are not compatible with conventional phenolic chambers; mixing between the core and boundary flow produces intermittent boundary temperatures exceeding the melting point of the phenolic. There is evidence, however, that the boundary temperature does not exceed 4500°F, thus making the injector compatible in unlimited durations with chambers containing refractory materials.

E. INJECTOR REPRODUCIBILITY

(C)   The problems of fabrication associated with the hydrazine injector have been defined and solved. Knowledge of these problems, in conjunction with prior experience in initial platelet fabrication and selection, has allowed rapid and completely satisfactory fabrication of the latter program injectors. It is anticipated that future units can be produced on a one-for-one-basis.

F. INJECTOR DURABILITY AND MAINTAINABILITY

(C)   The injectors developed on this program have been proven to be extremely resistive to operating conditions which promote thermal and structural degradation. The duration capabilities are unlimited from a thermal standpoint. Similarly, the structural integrity of the platelets is compatible with either steady-state or pulse-mode operation.

(U)   Maintainability of the injectors requires no more than standard filtering procedures during propellant loading. There is no evidence to indicate channel plugging due either to sustained operation or extended storage periods, although it is recommended that residual propellant be purged and dehydrated from the injector following atmospheric testing and prior to storage.

REFERENCES

1. Pieper, J. L., ICRPG Liquid Propellant Thrust Chamber Performance
    Evaluation Manual, CPIA No. 178, September 1968.

2. Pieper, J. L., Dean, L. E., Valentine, R. S., Mixture Ratio Distribution--
    Its Impact on Rocket Thrust Chamber Performance, Journal of Spacecraft and
    Rockets, Vol. 4, No. 6, June 1967.

3. Priem, R. J., Heidmann, M. F., Propellant Vaporization as a Design
    Criterion for Rocket Engine Combustion Chambers, NASA TR-R-67, 1960.

4. Kors, D. L., Bassham, L. B., and Walker, R. E., A Liquid Rocket Performance
    Model Based on Vaporization Interactions, AIAA 5th Propulsion Joint
    Specialist Conference, 9-13 June 1969.

5. Conn, T. E., Hester, J. N., Valentine, R. S., Environmental Effects Upon
    Rocket Injector/Chamber Compatibility, Journal of Spacecraft and Rockets,
    Vol. 4, No. 12, December 1967.

6. Seban, R. A., Heat Transfer and Effectiveness for a Turbulent Boundary
    Layer with Tangential Fluid Injection, J. Heat Transfer 82, No. 4, 1960,
    pp 303-312.

7. Crocco, L., and Cheng, S. I., Theory of Combustion Instability in Liquid
    Propellant Rocket Motors, AGARDograph No. 8, Butterworth's Scientific
    Publications, Ltd., London, 1956.

8. Crocco, L., Grey, J., and Harrje, D. T., Theory of Liquid Propellant
    Rocket Instability and Its Experimental Verification, ARS Journal,
    Vol. 30, No. 2, February 1960.

9. Crocco, L., Harrje, D. T., and Reardon, F. H., Transverse Combustion
    Instability in Liquid Propellant Rocket Motors, ARS Journal, Vol. 32,
    No. 3, March 1962.

10. Reardon, F. H., Crocco, L., and Harrje, D. T., Velocity Effects in
    Transverse Mode Liquid Propellant Rocket Combustion Instability, AIAA
    Journal, Vol. 2, No. 9, 9 September 1964.

11. Smith, A. J., Jr., Reardon, F. H., The Sensitive Time Lag Theory and Its
    Application to Liquid Rocket Combustion Instability Problems, Vol. 1,
    Technical Report AFRPL-TR-67-314, March 1968.

12. Reardon, F. H., McBride, J. M., and Smith, D. J., Effect of Injection
    Distribution on Combustion Stability, AIAA Paper No. 65-613, AIAA
    Propulsion Joint Specialist Conference, June 1965.

CONFIDENTIAL
(This page is Unclassified) ·

REFERENCES (cont.)

13. Bloomer, H. E., Wanharnen, J. P., and Vincent, D. W., Chamber Shape
    Effects on Combustion Instability, 4th ICRPG Combustion Conference,
    Vol. 1, CPIA Publication No. 162, December 1967.

14. Improved Spartan Monopropellant and Bipropellant Reaction Control System
    Technology Programs (U), Vol. II, Final Report No. AGC-9400-17, Contract
    MDAC-A68-8042, 11 April 1969 (Confidential).

15. Reardon, F. H., Correlation of Sensitive-Time-Lag-Theory Combustion
    Parameters with Thrust Chamber Design and Operating Variables, 5th ICRPG
    Combustion Conference, CPIA Publication No. 183, December 1968.

16. Investigation of the Formation and Behavior of Clogging Material in Earth
    and Space Storable Propellants, TRW Interim Report 08113-6007-R000,
    Contract NAS 7-549, October 1967.

17. Methods for Elimination of Corrosion Products of Nitrogen Tetroxide,
    AFRPL-TR-67-217, Final Report, Contract AF 04(611)-11620, July 1967.

Report AFRPL-TR-69-122

APPENDIX

BARRIER COOLING ANALYSIS FOR THE N_2O_4/N_2H_4 SYSTEM

FIGURE LIST

ii

Report AFRPL-TR-69-122, Appendix

LIST OF ABBREVIATIONS AND SYMBOLS

X	barrier cooled length, in.
$\overline{X}$	dimensionless cooled length
X'	adjusted barrier cooled length, in.
S	slot height, in.
χ	equivalent (X/S) value
R	injector face radius, in.
r	local nozzle radius, in.
A	injector face area, square inch
ε	ratio of barrier flow area to total flow area
T	temperature, °R
β	combustion efficiency
η	barrier cooling effectiveness
MR	mixture ratio
$\overline{MR}$	overall mixture ratio
W_T	total propellant flow rate, lb/sec
m	mass velocity ratio (barrier/core)
FFC	barrier coolant fraction of total flow
f	ratio of fuel flow is barrier to total fuel flow
μ	viscosity, lb/ft sec
ρV	mass velocity, $lb/ft^2 sec$
Re	Reynolds number
n	transverse turbulence parameter
α	angle of convergence in nozzle, degrees

Subscripts

o	stagnation conditions
B	barrier conditions
C	core conditions
AW	adiabatic wall conditions
S	slot conditions

(C)   Chemical composition data indicate densities of the barrier and of the core are reasonably close for the range of barrier mixture ratios being considered (0.2 to 0.5). The overall mixture ratio is required to be in the range of 0.9 to 1.4. Thus, it is appropriate to use existing barrier cooling data from air-to-air systems with small temperature differentials. Data by Seban have been utilized in this analysis because of the wide range of velocity ratios investigated and the relatively short core flow development length provided during the experiment. Correlation of the data of Hatch and Papell compare with Seban's data for effectiveness values above 0.7.

(U)   In order to scale the data, it was assumed that a dimensionless cooled length parameter similar to the one suggested by both Seban and Chin, could be used to correlate the data. This parameter is given by:

$$\overline{X} = f \left(\frac{(\rho V)_B}{(\rho V)_C} \right) Re_S^{-0.2} \frac{X}{S}$$

(U)   Since the function involving the mass velocity ratio was not explicitly defined, the data showing cooling effectiveness directly as a function of cooled length/slot height (X/S) were utilized by entering the data for a given mass velocity ratio at an equivalent (X/S) defined by:

$$\chi = (X/S)_{equivalent} = (X/S)_{actual} \left(\frac{Re_{actual}}{Re_{data}} \right)^{-0.2}$$

The actual Reynolds number is related to an injection slot height and is defined by:

$$Re = \frac{\left(\frac{FFC\ W_T}{\varepsilon\ A} \right) S}{\mu_c}$$

Report AFRPL-TR-69-122, Appendix

Where the injection slot height (S) is related to the barrier flow area fraction (ϵ) by,

$$\epsilon = S/R \ (2 - S/R)$$

The experimental Reynolds number was near 6000 in most cases. For the case of uniform fuel distribution;

$$\epsilon = f = \frac{1 + \overline{MR}}{1 + MR_B} \ FFC$$

Thus the Reynolds number, which can be written as

$$Re = \frac{R}{\mu_C} \ \frac{W_T}{A} \ FFC \ \frac{1 - \sqrt{1-\epsilon}}{\epsilon}$$

reduces for the case of uniform fuel distribution to,

$$Re = \frac{R}{\mu_C} \ \frac{W_T}{A} \ \frac{1 - \sqrt{1 - FFC \ \frac{1 + \overline{MR}}{1 + MR_B}}}{(1 + \overline{MR})/(1 + MR_B)}$$

and the equivalent (X/S) is then;

$$\chi = \frac{X}{R} \ (Re_{data})^{0.2} \ \left(\frac{\mu_C A}{R \ W_T}\right)^{0.2} \ \frac{(1 + \overline{MR})/(1 + MR_B)^{0.2}}{\left(1 - \sqrt{1 - FFC \ \frac{1 + \overline{MR}}{1 + MR_B}}\right)}$$

This equation was used to generate a family of χ vs FFC curves (see Figure 1) for various barrier mixture ratios ($MR_B = 0.2, 0.3, 0.4,$ and 0.5).

(This page is Unclassified)

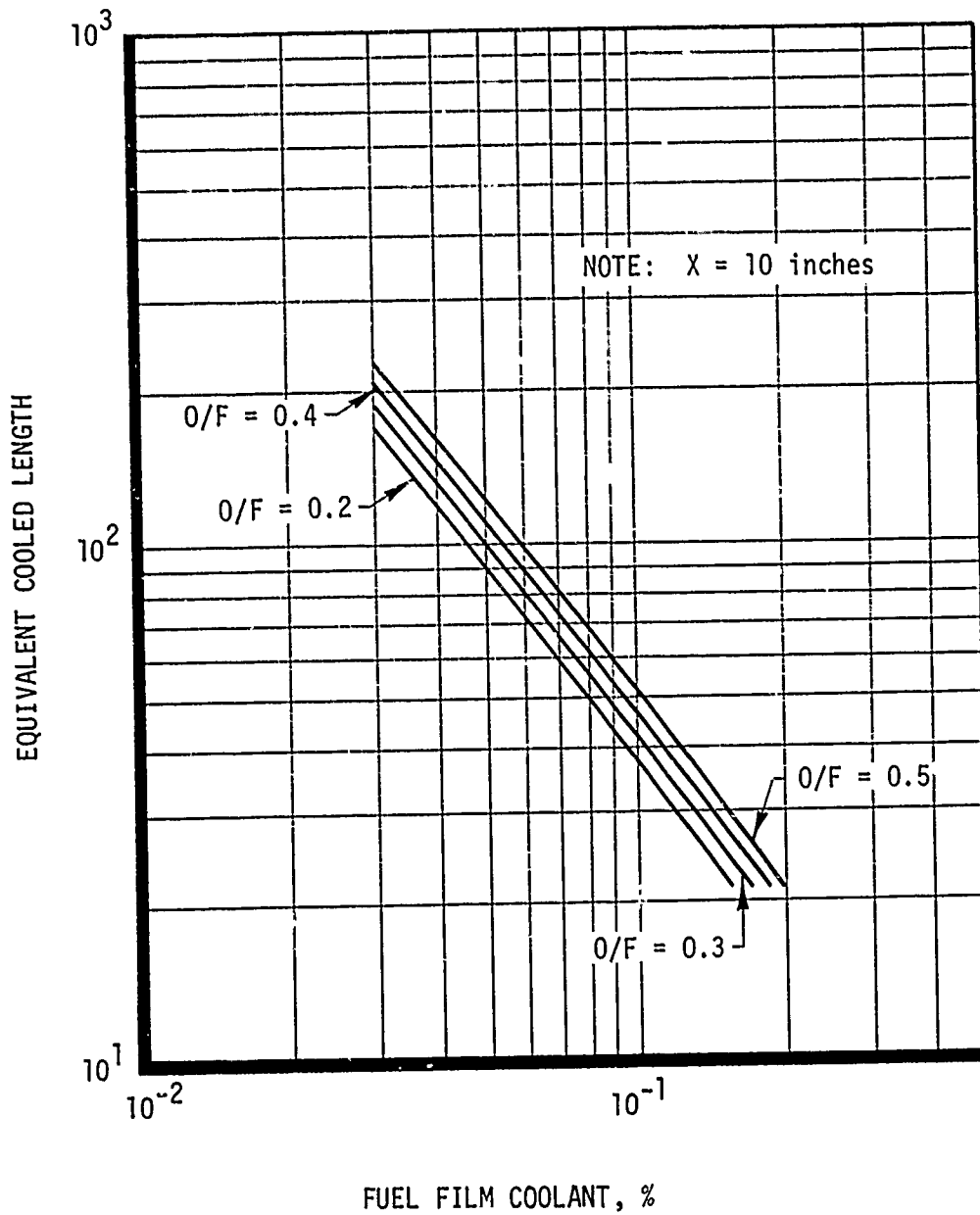Report AFRPL-TR-69-122, Appendix

Figure 1. Equivalent Cooled Length vs Percent Coolant Flow

UNCLASSIFIED
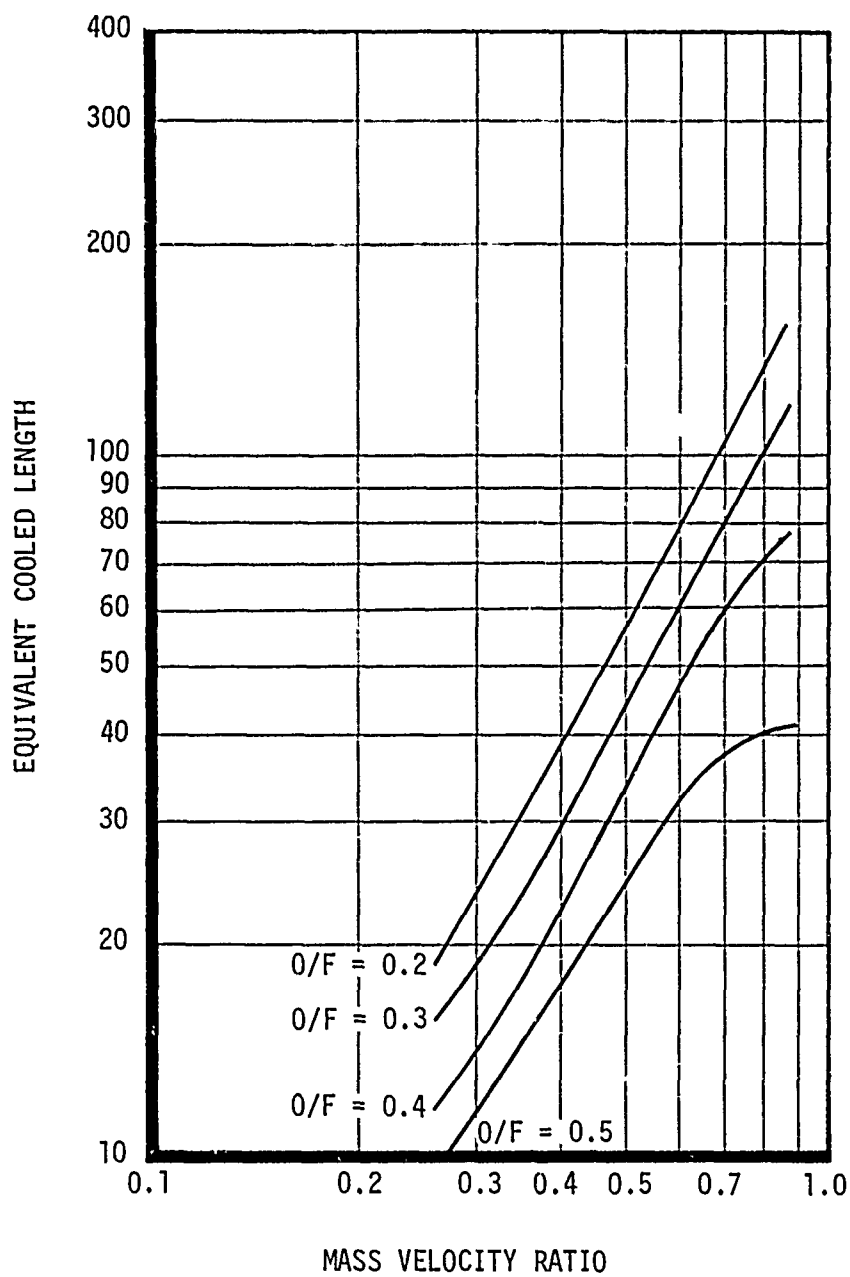
Report AFRPL-TR-69-122, Appendix

Figure 2. Equivalent Cooled Length vs Mass Velocity Ratio

Page 202
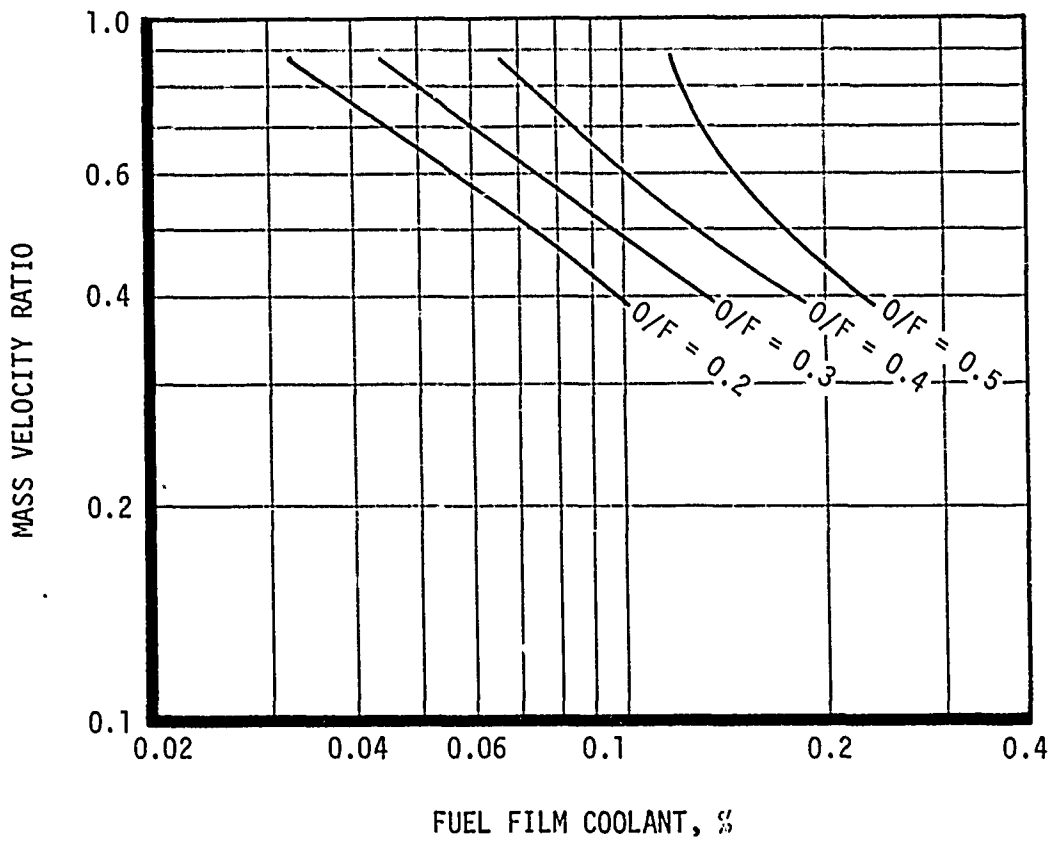
UNCLASSIFIED

Figure 3. Mass Velocity Ratio vs Percent Coolant Flow
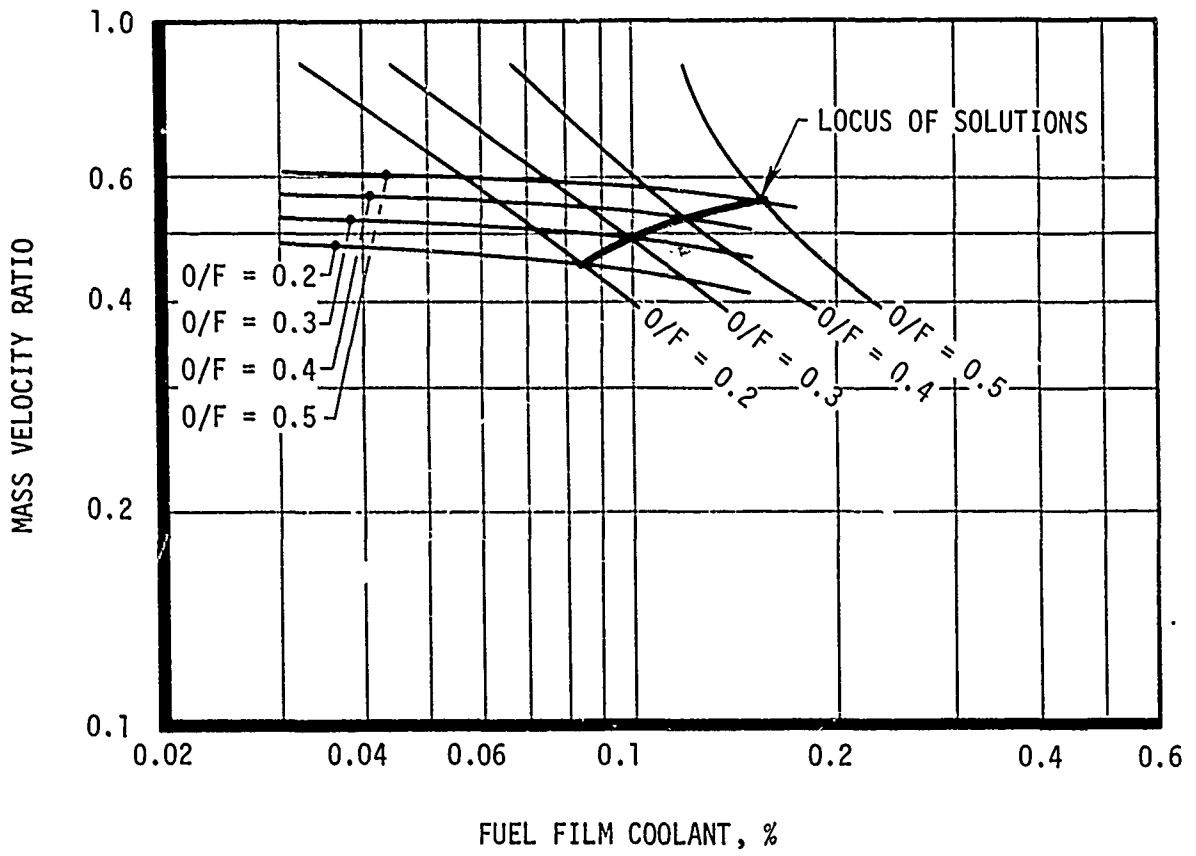
Figure 4. Solutions for Uniform Fuel Distribution

FUEL FILM COOLANT, %

AREA RATIO, A_e/A_t, ε
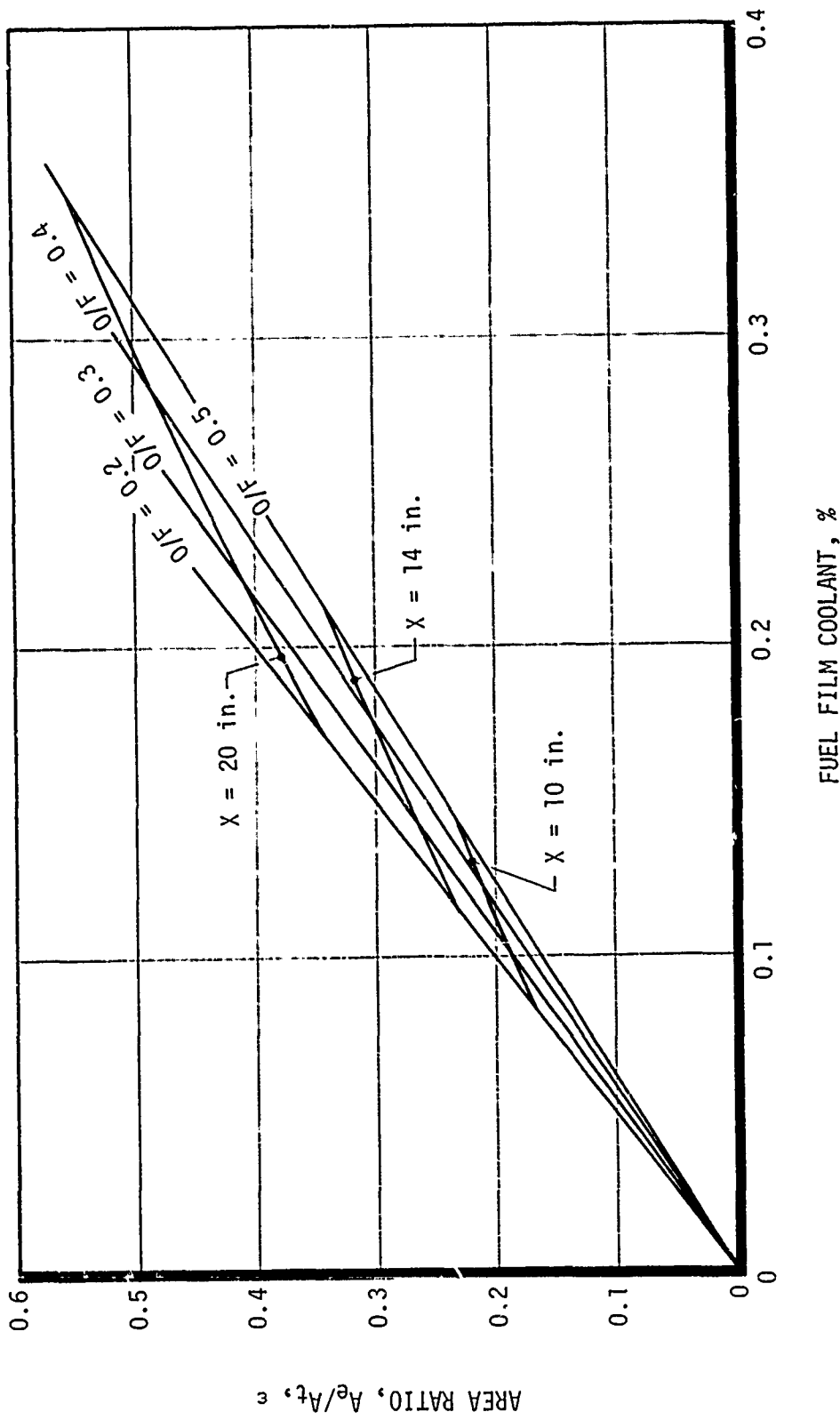
Figure 5. Barrier Design Plane

(U)   In order to account for the effect of acceleration on the mixing between the barrier and the core the following equation for accelerated turbulent flow over a flat plate was employed;

$$X' = \int_0^X \left(\frac{R}{r}\right)^{2(1-n)} dx$$

where n = 0.59 was assumed based on Reference (d)

For a conical chamber design this reduces to;

$$X' = \int_0^X \left(\frac{1}{1 - \frac{X \sin\alpha}{R}}\right)^{0.82} dx$$

For the 10 in. chamber design in Figure 6 the value for X' is 11.1 in. Thus, in order to adequately cool the throat in the 10 in. chamber design, the design plane must be entered at a cooled length of 11.1 in. Defining a safety margin as the ratio of design length/required length, a design length of 14 in. results in a safety margin of;

$$\text{Safety Margin} = \frac{14.0}{11.1} = 1.26$$
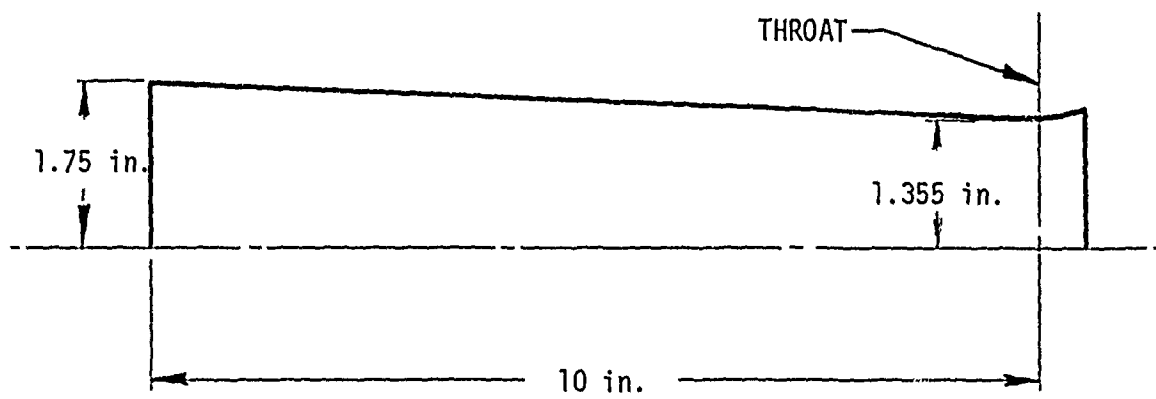
Figure 6. Chamber Contour

Page 207

DOCUMENT CONTROL DATA - R&D

(Security classification of title body of abstract and indexing annotation must be entered when the overall report is classified)

1. ORIGINATING ACTIVITY (Corporate author)	2a. REPORT SECURITY CLASSIFICATION
Aerojet-General Corporation	Confidential
	2b GROUP
	4

3. REPORT TITLE

Development and Demonstration of a N_2O_4/N_2H_4 Injector

4. DESCRIPTIVE NOTES *(Type of report and inclusive dates)*

Final Report – 11 July 1969

5. AUTHOR(S) *(Last name, first name, initial)*

Hartsell, James O.

6. REPORT DATE	7a. TOTAL NO. OF PAGES	7b. NO. OF REFS
11 July 1969	215	17

8a. CONTRACT OR GRANT NO.	9a. ORIGINATOR'S REPORT NUMBER(S)
F04611-68-C-0053	
b. PROJECT NO.	
AFSC Project 3058	
c.	9b. OTHER REPORT NO(S) *(Any other numbers that may be assigned this report)*
d.	AFRPL-TR-69-122

10. AVAILABILITY/LIMITATION NOTICES

In addition to Security Requirements which must be met, this document is subject to special export controls and each transmittal to foreign governments or foreign nationals may be made only with prior approval of AFRPL (RPOR/STINFO) Edwards, California 93523

11. SUPPLEMENTARY NOTES	12. SPONSORING MILITARY ACTIVITY
	Rocket Propulsion Laboratory
	Air Force Systems Command
	Edwards, California

13. ABSTRACT

(U) A twelve-month program was conducted to develop and demonstrate an advanced injector to be used with the propellants N_2O_4/N_2H_4 at a thrust level of 3000 lbf. Five injectors were tested in 13 unique configurations to establish the parameters necessary to the optimization of performance, dynamic stability, chamber cooling capability, and injector/chamber compatibility. Once established, the optimized parameters were incorporated into a final injector. This last unit was employed in performance and stability demonstration tests and in long-duration durability tests. All contract design goals were met or exceeded by the final optimized injector.

DD FORM 1473
1 JAN 64

14.	LINK A		LINK B		LINK C	
KEY WORDS	ROLE	WT	ROLE	WT	ROLE	WT
N_2O_4/N_2H_4 Injector						
Hydrazine Performance						
Post-Boost Propulsion						

INSTRUCTIONS

1. ORIGINATING ACTIVITY: Enter the name and address of the contractor, subcontractor, grantee, Department of Defense activity or other organization (corporate author) issuing the report.

2a. REPORT SECURITY CLASSIFICATION: Enter the over-all security classification of the report. Indicate whether "Restricted Data" is included. Marking is to be in accordance with appropriate security regulations.

2b. GROUP: Automatic downgrading is specified in DoD Directive 5200.10 and Armed Forces Industrial Manual. Enter the group number. Also, when applicable, show that optional markings have been used for Group 3 and Group 4 as authorized.

3. REPORT TITLE: Enter the complete report title in all capital letters. Titles in all cases should be unclassified. If a meaningful title cannot be selected without classification, show title classification in all capitals in parenthesis immediately following the title.

4. DESCRIPTIVE NOTES: If appropriate, enter the type of report, e.g., interim, progress, summary, annual, or final. Give the inclusive dates when a specific reporting period is covered.

5. AUTHOR(S): Enter the name(s) of author(s) as shown on or in the report. Enter last name, first name, middle initial. If military, show rank and branch of service. The name of the principal author is an absolute minimum requirement.

6. REPORT DATE: Enter the date of the report as day, month, year; or month, year. If more than one date appears on the report, use date of publication.

7a. TOTAL NUMBER OF PAGES: The total page count should follow normal pagination procedures, i.e., enter the number of pages containing information.

7b. NUMBER OF REFERENCES: Enter the total number of references cited in the report.

8a. CONTRACT OR GRANT NUMBER: If appropriate, enter the applicable number of the contract or grant under which the report was written.

8b, 8c, & 8d. PROJECT NUMBER: Enter the appropriate military department identification, such as project number, subproject number, system numbers, task number, etc.

9a. ORIGINATOR'S REPORT NUMBER(S): Enter the official report number by which the document will be identified and controlled by the originating activity. This number must be unique to this report.

9b. OTHER REPORT NUMBER(S): If the report has been assigned any other report numbers (either by the originator or by the sponsor), also enter this number(s).

10. AVAILABILITY/LIMITATION NOTICES: Enter any limitations on further dissemination of the report, other than those imposed by security classification, using standard statements such as:

(1) "Qualified requesters may obtain copies of this report from DDC."

(2) "Foreign announcement and dissemination of this report by DDC is not authorized."

(3) "U. S. Government agencies may obtain copies of this report directly from DDC. Other qualified DDC users shall request through

                             ."

(4) "U. S. military agencies may obtain copies of this report directly from DDC. Other qualified users shall request through

                             ."

(5) "All distribution of this report is controlled. Qualified DDC users shall request through

                             ."

If the report has been furnished to the Office of Technical Services, Department of Commerce, for sale to the public, indicate this fact and enter the price, if known.

11. SUPPLEMENTARY NOTES: Use for additional explanatory notes.

12. SPONSORING MILITARY ACTIVITY: Enter the name of the departmental project office or laboratory sponsoring (paying for) the research and development. Include address.

13. ABSTRACT: Enter an abstract giving a brief and factual summary of the document indicative of the report, even though it may also appear elsewhere in the body of the technical report. If additional space is required, a continuation sheet shall be attached.

It is highly desirable that the abstract of classified reports be unclassified. Each paragraph of the abstract shall end with an indication of the military security classification of the information in the paragraph, represented as (TS), (S), (C), or (U)

There is no limitation on the length of the abstract. However, the suggested length is from 150 to 225 words.

14. KEY WORDS: Key words are technically meaningful terms or short phrases that characterize a report and may be used as index entries for cataloging the report. Key words must be selected so that no security classification is required. Identifiers, such as equipment model designation, trade name, military project code name, geographic location, may be used as key words but will be followed by an indication of technical context. The assignment of links, rules, and weights is optional